UNIVERSITY OF CALIFORNIA
RIVERSIDE

Hydrocarbon Seeps of the Mesozoic Great Valley Group Forearc Strata and Franciscan Complex, Northern and Central California, U.S.A.

A Dissertation submitted in partial satisfaction
of the requirements for the degree of

Doctor of Philosophy

in

Geological Sciences

by

Kristin Euphrat Keenan

August 2010

Dissertation Committee:
Dr. Mary L. Droser, Chairperson
Dr. Nigel C. Hughes
Dr. Gordon Love

The Dissertation of Kristin Euphrat Keenan is approved:

_____

_____

_____
Committee Chairperson

University of California, Riverside

To all of you who helped me through this process, I say thank you. Words cannot fully express how indebted to you I am. I will never forget all that you have done.

I dedicate this work to the two most important people in my life. First, to my husband. Jimmy, I couldn't have done this without you. You have always believed in me and have encouraged me to reach for the stars, for this I thank you from the bottom of my heart. I love you so much. Second, to my mother. Mom, you have stood by me through thick and thin and supported me every step of the way. Thank you so much, I will always be grateful. I love you.

ABSTRACT OF THE DISSERTATION

Hydrocarbon Seeps of the Mesozoic Great Valley Group Forearc Strata and Franciscan Complex, Northern and Central California, U.S.A.

by

Kristin Euphrat Keenan

Doctor of Philosophy, Graduate Program in Geological Sciences
University of California, Riverside, August 2010
Dr. Mary L. Droser, Chairperson

Hydrocarbon seeps and their associated chemosymbiosis-based communities have been documented throughout modern oceans, as well as in Neoproterozoic through Pleistocene aged rocks in the stratigraphic record. A particularly good record of ancient hydrocarbon seeps occurs in Mesozoic strata (Tithonian-Maastrichtian) along the western North American continental margin, cropping out throughout the Great Valley Group forearc strata and the Franciscan Complex. This extensive record allows for the comparison of the paleoecological signatures of stratigraphically and spatially related hydrocarbon seeps, which are geotectonically, petrographically, and isotopically consistent with each other.

Ten hydrocarbon seeps were located throughout this region and their physical, morphological, and paleoecological signatures were documented. Analyses indicate that their chemical signatures are petrographically and

paragenetically similar and their geochemical values are consistently anomalous, however, their physical and biological signatures are surprisingly variable. The localities are strikingly different from each other in regards to faunal composition and morphological characteristics. The deposits include variably sized lenses, pods, mounds, and continuous outcrops. Eighteen taxa were identified, the most common being vestimentiferan worm tubes. Gastropods are the most abundant clade, while bivalves are the most diverse. No taxon is found at all ten localities and each locality is dominated by a different taxon that is commonly only a minor constituent of another localities faunal assemblage. This variability indicates that, as with modern seeps, heterogeneity is driven largely by the ephemeral nature of the seep environment, including ebullition volume, rate, and area, rather than by the duration of fluid advection.

These ancient seep deposits cropping out in the GVG forearc strata and the Franciscan Complex preserve the physical, chemical, and biological signatures of a group of tectonically related ancient hydrocarbon seeps and are a record of 80 m.y. of intermittent fluid seepage, occurring over geologically short intervals along the western North American continental margin. As the abundance of recognized hydrocarbon seeps in this area continues to increase, they can be viewed collectively as a quasi-continuous, dynamic fluid-sediment-biotic system, with the potential to reveal larger evolutionary, biogeographic, geotectonic, and geochemical patterns of hydrocarbon seep processes and associated faunas through geologic time.

Table of Contents

List of Figures

Chapter 1

Chapter 2

Chapter 3

List of Tables

Chapter 1

Chapter 2

Chapter 3

Chapter 1

New Findings on Hydrocarbon Seeps of the Mesozoic Great Valley Group Forearc Strata and Franciscan Complex, Northern and Central California, U.S.A.

Abstract

During the Late Mesozoic the western North American continental margin was a dynamically evolving fluid-tectonic-biotic system that consisted of an eastward migrating volcanic arc, a westward migrating subduction complex, and a forearc basin that opened in between the two. Over this 80 m.y. period (Tithonian—Maastrichtian), hydrocarbon seeps formed in the accumulating accretionary prism and forearc basin via the transformation of organic matter into hydrocarbons. Today, these ancient hydrocarbon seep deposits are exposed in northern and central California and crop out in both the Great Valley Group (GVG) forearc strata and Franciscan Complex.

Hydrocarbon seep research has largely focused on individual locality characterization, taxonomic composition and identification of the essential biota, geochemistry, and molecular biomarkers. To date there have only been a limited number of systematic comparative studies of ancient hydrocarbon seeps and their associated faunas, in a similar tectonic setting, through time. Here we describe and compare the morphologic, petrographic, paragenetic, paleontologic, and geochemical signatures of 11 hydrocarbon seeps, deposited over this 80

m.y. interval. The deposits are nearly identical petrographically and paragenetically and in comparison to seawater, are consistently anomalous geochemically, although at outcrop scale, are morphologically variable, with the variability being unrelated to deposit size or location. The most significant results to arise from these data include (1) evidence of methane seepage supporting chemosynthetic hydrocarbon seep communities occurring for a protracted stratigraphic interval, (2) the degree heterogeneity in deposit size, age, and location, and (3) the degree of temporal and spatial heterogeneity and relative abundance between the taxonomic compositions of these 11 deposits.

1. Introduction

Modern offshore hydrocarbon seeps with chemosynthetic communities were first discovered in 1984 on the Florida Escarpment (Paull et al. 1984) and are now commonly recognized where dissolved methane and hydrogen sulfide are advecting from continental margin sediments at ambient seawater temperatures. Locally, anaerobic oxidation of methane (AOM) coupled with sulfate reduction increases alkalinity, enhancing the precipitation of authigenic calcium carbonate (Ritger et al. 1987, Greinert et al. 2002). The methane and sulfide of seep fluids also attracts a community of invertebrates living symbiotically with chemosynthetic microbes (Jannasch 1984, Fisher 1990). These unusual seafloor environments are of particular interest as they may have been crucibles for early life on Earth, they have been significant sites of methane

release to the atmosphere from clathrate destabilization, they may have served as refugia during global environmental crisis, and because of the highly specialized adaptations (e.g. symbiosis) that have evolved in the faunas that inhabit them (Kauffman and Howe 1990, McArthur and Tunnicliffe 1998, Little and Vrijenhoek 2003, Campbell 2006, Duperron et al. 2009).

Hydrocarbon seep deposits have been identified in the stratigraphic record using a series of predictable physical, chemical, and paleontological attributes that are the product of the unusual physical and chemical conditions under which they formed (e.g., Campbell and Bottjer 1993, Cavagna et al. 1999, Kaufmann and Wednt 2000, Peckmann et al. 2001, Campbell et al. 2002, Hepper 2004). These attributes characterize all modern and ancient hydrocarbon seeps, regardless of the location, size, or age of the deposit and they form the basis for their identification in the stratigraphic record. These distinctive characteristics include: (1) a context conducive to the production, migration, accumulation, and discharge of hydrocarbons; (2) deposits of stratigraphically restricted, anomalous, authigenic carbonates; (3) predictable cements, textures, and microbial fabrics, recognized in thin section, distinct from surrounding clastic sediments and which were deposited in a standard sequence of paragenesis (e.g., Beauchamp and Savard 1992, Cavagna et al. 1999, Goedert et al. 2000, Campbell et al. 2002, Peckmann et al. 2002, Schwartz et al. 2003); (4) moderately to strongly depleted $\delta^{13}C$ values, typically ranging from -10‰ to -80‰ PDB (Ritger et al. 1987, Paull et al. 1992, Cavagna et al. 1999, Campbell 2006);

and (5) faunal assemblages associated with endemic and/or chemosymbiotic biota (Hickman 1984).

Based on these criteria, hydrocarbon seeps have been recognized in the stratigraphic record from the Neoproterozoic (Jiang et al. 2003) through the Pleistocene (Little and Vrijenhoek 2003). A particularly good record of spatially discrete and stratigraphically extensive hydrocarbon seeps occurs in Mesozoic strata of the western United States (Campbell and Bottjer 1993, 1995, Campbell et al. 2002, Hepper et al. 2003, Hepper 2004, Kiel and Campbell 2005, Birgel et al. 2006, Campbell 2006, Hepper 2006, Hepper and Droser 2007, Keenan et al. 2008, Kiel et al. 2008), although most localities have not been studied in detail or formally described as hydrocarbon seeps. These deposits formed on the floor of an actively evolving forearc basin along the western North American continental margin, which at this time, was bounded by an eastward migrating volcanic arc and a westward migrating subduction zone (Godfrey et al. 1997, Dickinson 2008). Today, these hydrocarbon seep deposits are exposed in the Great Valley Group (GVG) forearc strata (deposited in the forearc basin) and the Franciscan Complex (deposited during subduction), both of which extend from Red Bluff to Santa Barbara, in northern and central California.

To date, there have been a limited number of studies comparing multiple coeval hydrocarbon seep deposits, such as the thousands of Late Cretaceous Tepee Buttes deposits, cropping out from New Mexico to Montana (Kauffman et al. 1996), the numerous seep carbonates in the Oligocene Lincoln Creek

Formation (LCF), in western Washington state (Peckmann et al. 2002), as well as a small number of studies including four seeps from the GVG forearc strata (Campbell 1995, Campbell et al. 2002, Hepper 2004, Birgel et al. 2006). Although these studies have variably included petrographic, paleontological, geochemical, and molecular biomarker analyses (Campbell 1995, Kauffman et al. 1996, Campbell et al. 2002, Peckmann et al. 2002, Hepper 2004, Birgel et al. 2006), few studies have examined the physical (deposit morphology), petrographic, paleontological, and geochemical signatures of ancient hydrocarbon seeps through an extended stratigraphic interval and in a broadly similar tectonic setting (e.g., Majima et al. 2005).

In this paper we present data on 11 Tithonian through Maastrichtian aged hydrocarbon seep deposits cropping out throughout the GVG forearc strata and the Franciscan Complex, in northern and central California (Figure 1A, 2A). Four of these deposits were documented during previous studies (see Campbell 1995, Campbell et al. 2002, Hepper 2004, Kiel et al. 2008, and references therein), while seven are described here for the first time. All 11 were evaluated and compared using paleontological, sedimentological, geochemical, and taphonomic data in order to compare the spatial and stratigraphic variability among sites during a protracted interval of hydrocarbon seepage along the active tectonic margin.

2. Geological Setting

The geologic evolution of the Mesozoic western North American continental margin has been classically interpreted as an Andean-style arc and trench system, which resulted in the formation of the Franciscan Accretionary Complex of the Coast Ranges, the GVG forearc strata, and the Sierra Nevada batholith, injected into the roots of the Cordilleran magmatic arc (Godfrey et al. 1997, Dickinson 2008). The relative timing of formation includes the coeval deposition of GVG forearc strata, the Franciscan Complex (Ingersoll 1978a, Blake and Jones 1981), and the approximately 20 known hydrocarbon seep deposits (Campbell 2006), the latter of which occur in a variety of geologic formations, as well as in some units that have yet to be formally described (Figure 2B).

The Franciscan Complex is the most westerly of the three tectonic provinces, forming as an accretionary prism when the Farallon plate subducted eastward beneath the western margin of the North American craton (Hamilton 1969, Dickinson 2008, Ernst et al. 2008). It is subdivided into three terranes, which are comprised of basaltic pillow flows, pillow breccias, and tuffs intruded by diabase sills, mudstone and sandstone, with thick lenses of polymict conglomerate and minor shale, greenstone, bedded chert, and limestone, commonly separated by zones of mélange (Swe and Dickinson 1970, Blake and Jones 1981, Blake and McLaughlin 1989). Today, the Franciscan trends NNW and forms a complexly deformed region that structurally underlies a less-

deformed upper plate of GVG forearc strata (Hamilton 1969, Swe and Dickinson 1970), bounded by the San Andreas Fault to the east and by the Coast Range Fault to the west.

In the Late Jurassic, while the Franciscan Complex accumulated in the west through accretion, GVG forearc sediments were concurrently deposited in the forearc basin adjacent to the active Klamath-Sierran arc complex and Sierra Nevada batholith, above the Coast Range Ophiolite (Swe and Dickinson 1970, Blake and Jones 1981, Dickinson 1981, Blake and McLaughlin 1989). Sediment deposition continued until the end of the Cretaceous, with the forearc basin filling nearly to sea level, during which time the subduction complex migrated westward and the magmatic arc migrated eastward (Ingersoll 1978a, Dickinson and Seely 1979, Ingersoll 1982, Dickinson 2008).

Recent studies offer alternative views on the Late Jurassic to Latest Cretaceous geologic history of this region, although these new data are still poorly resolved. Using detrital zircon age signatures, Surpless et al. (2006) suggest that GVG deposition largely occurred in the Cretaceous, creating a discrepancy between regional biostratigraphy based on *Buchia* zones and chronostratigraphy based on radiometric age dates, both of which suggest GVG deposition occurred from the Late Jurassic through the latest Cretaceous. In contrast, using detrital zircon evidence, Wright and Wyld (2007) confirm, as previously reported, that GVG strata were originally deposited during the Late Jurassic through the Early Cretaceous, however, that were deposited in a basin

that was translated parallel to the convergent margin as a forearc sliver. They assert that this forearc sliver originated ~500 km south of its current location, with the southwest Cordillera initially serving as the sediment source and the Sierra Nevada and Klamath regions serving as a sediment source throughout the remainder of the Mesozoic. Although both studies offer alternative views to the formation of the Jurassic through the Cretaceous strata of northern and central California, neither is conclusive and further work in the region is needed. Due to this remaining uncertainty, each hydrocarbon seep deposit included in this study, was dated using previously documented ages for enclosing strata of the GVG forearc strata and Franciscan Complex (e.g. Ojakangas 1964, McLaughlin et al. 1989, and others) or were assigned using ammonites or *Buchia* collected during the course of this study (e.g. Gabb 1869, Anderson 1938, Jones et al. 1969, Elder 1999, and others).

Today, Upper Jurassic through Lower Cretaceous strata of the GVG are exposed along the west side of the Sacramento Valley and predominantly consist of basin plain and outer fan deposits (Ingersoll 1978b, Constenius et al. 2000). Upper Cretaceous strata crop out nearly continuously along the length of the Sacramento and San Joaquin Valleys (Ingersoll 1978b), comprising sediments that were principally sub-sea fan turbidites that prograded into the forearc trough from eastern sources in the arc massif (Bailey and Jones 1973, Dickinson 1981). The 12,000 m succession of GVG sediments consist of well-bedded mudstone, siltstone, sandstone, and conglomerate derived from granitic basement of the

Sierran and Klamath regions (Blake and Jones 1981) and interspersed within it are deposits of variably fossiliferous hydrocarbon-derived carbonate.

Included in this study are new data on four previously described GVG hydrocarbon seep sites (Campbell 1995, Birgel et al. 2006), including Cold Fork of Cottonwood Creek (CFCC), Wilbur Springs (WS), Paskenta (Pa), and Guenoc Ranch (GR), in addition to seven deposits from both the GVG forearc strata and the Franciscan Complex, which are described for the first time, including Bear Creek (BC), Romero Creek (RmC), Harrington Flat Road (HFR), Rocky Creek (RC), Little Indian Valley (LIV), Wide Awake Mine (WAM) and Rice Valley (RV).

3. Materials and Methods

Samples were collected from 10 carbonate deposits cropping out in GVG and Franciscan rocks. The eleventh, Paskenta, is no longer accessible, but was included in the petrographic and isotopic portions of this paper using analyses published in Campbell (1995) and Campbell et al. (2002). Standard sedimentological (e.g., clastic texture, degree of sorting, rounding of grains, fabric, diagenetic features, etc), stratigraphic (e.g., beds and bedding, grading of turbidites, depositional bed forms and structures, etc), and paleontologic (e.g., species richness, abundance, etc) data were recorded in the field, with an emphasis on facies criteria (e.g., lithology, rock colors, grain size and shape, particle types, bedding and lamination, sedimentary structures and textures, fossil content, stratigraphic and structural relationships, geometry of carbonate

bodies, etc; Flügel 1982). Samples of all major lithologies were collected for petrographic, paleontologic, and geochemical analyses, with special attention paid to collecting samples representative of all cements, microbial fabrics, and textures, for later laboratory microfacies analyses. Replicate bulk samples were collected throughout each locality for later fossil identification, with each sample filling one sample bag (~4,500 cm^3).

In the laboratory, hand-samples were cut and polished to reveal cross-sectional views. Twenty-five to 30 thin sections (30 to 70 microns thick), representative of sedimentary surfaces, cements, textures, microbial fabrics, matrix material, and shell material were made for each locality (~300 thin sections in total). Thin sections were used for both petrographic and isotopic analyses and were analyzed on a Boreal Polarizing Microscope using plane-polarized and cross-polarized light. ^{13}C and ^{18}O isotopic analyses of carbonates were performed at the University of California, Riverside, on a Thermo Electron Corporation Delta V Plus Isotope Ratio Mass Spectrometer using ISODAT 2.5 software. Between 10 and 15 samples (excepting Bear Creek for which 57 samples were processed) of detrital-rich microcrystalline carbonate (micarb), clotted (microbial) micrite, fibrous calcite, yellow calcite, and/or sparry calcite were collected per deposit (175 samples total), using a hand-held microdrill, from the surfaces of cut and polished thin section chips. Between ~0.150 and ~0.200 micrograms of material was collected into sample vials. The $\delta^{13}C$ and the $\delta^{18}O$ results are here reported relative to the PDB standard and appropriate correction

factors were applied (Craig 1957). The average precision for $\delta^{13}C$ and $\delta^{18}O$ are ± 0.06‰ and ± 0.1‰, respectively.

Over a six-month period, ~2,500 lbs of carbonate from the 10 localities was processed. Processing included performing fossil crack-outs with a rock hammer, followed by the use of a hand lens or dissecting microscope to locate and identify the smallest fossils and the naked eye to locate and identify the larger fossils. Abundance data was collected concurrently (Table 1) and all faunal material was identified to the finest possible taxonomic level (Table 2). Material preserved as steinkerns or identifiable only to class or ordinal level was also counted. Identifications were made primarily on the basis of descriptions and figures in Stanton (1895), Anderson (1938), Kiel and Campbell (2005), Campbell et al. (2008), and Kiel et al. (2008).

4. Hydrocarbon Seep Descriptions

Hydrocarbon seep deposits of northern and central California occur as heavily weathered, variably sized, discrete, fossiliferous units eroding out of the marine siliciclastics of the GVG and Franciscan Complex (Table 3). The 11 study deposits reveal variable outcrop morphologies, some of which are illustrated in Figure 3 and which include three primary morphologies:

(1) individual carbonate cobbles (≤ 15.25 cm across), boulders (≥ 15.26 cm), pods (clusters of cobbles and boulders), and/or lenses (10 to 40 cm thick and 20 to ≥ 300 cm long);

(2) as discrete, roughly circular to elliptical carbonate mounds (ranging from 142.1 m^2 to a minimum of 5.57 m^2); and

(3) as vertical or linear carbonate outcrops that extend continuously or discontinuously, from a few meters to hundreds of meters in length.

RC, RmC, LIV, WS, and WAM are each characterized by (1) and their margins were defined by the lateral extent of the discrete carbonate outcrops, varying considerably in size and in the quantity of available outcrop. The HFR deposit is characterized by (2) and its margins were defined by the lateral extent of the mounds found in the vicinity. BC, GR, and CFCC are characterized by (3), however, BC crops out over a 32 m interval that includes multiple stratigraphically relatable carbonate outcrops, GR crops out as rare, discontinuous lenses cropping out over a 2 x 4 km area, and CFCC crops out in a nearly continuous lens for 300 m.

In all three styles of seep preservation, the local stratigraphic context is rarely preserved, thus, the deposits occur as topographic highs on the landscape, surrounded by Cenozoic alluvium, although during deposition, they likely displayed little to no relief above the seafloor. BC, GR, Pa, and CFCC also occur as topographic highs on the landscape, likely attaining little to no relief above the seafloor during deposition, however, unlike the other seven deposits, have significant local geologic context preserved.

4.1 *Petrographic Signatures*

The unique nature of the hydrocarbon seep depositional environment produces a distinct suite of petrographic features that occur in a predictable paragenetic sequence, reflecting the changing chemistry of the depositional to burial environments (cf. Harris et al. 1985). Relevant seep-related petrographic features are present throughout most samples in this study and demonstrate that, despite stratigraphic and spatial segregation, as well as variable local conditions, remarkably similar petrographic and paragenetic signatures developed throughout (cf. Beauchamp and Savard 1992, Godfrey et al. 1997, Campbell et al. 2002, Barbieri and Cavalazzi 2005, Peckmann et al. 2007).

The typical sequence of paragenesis of the GVG and Franciscan hydrocarbon seep carbonates can be divided into early seafloor and late diagenetic phases, with the earliest phases precipitating in conjunction with macrofaunal activity (Figure 4). The early phases include deposition of (1) detrital-rich micarb, including (1a) peloids, (1b) calcispheres, and (1c) pyrite framboids; followed by (2) a corrosion event (CE1), producing pyrite coated corrosion surfaces, (3) worm tube activity, deposition of (4) yellow calcite, (5) fibrous calcite, including (5a) fibrous, (5b) botryoidal, and (5c) dentate habits, and (6) microbial fabrics. The late phases include (7) a second corrosion event (CE2), lacking concurrent deposition of pyrite, (8) deposition of siliciclastic silt-clay fill, (9) a fracturing event creating veins, (10) the deposition of equant calcite spar in the remaining open pore space, vugs, and veins, and (11) the *in situ*

replacement of earlier phase cements by neomorphosed microspar. Additionally in the later phases, there is a transformation of calcite crystals to dolomite crystals, although the timing of this transformation varies from deposit to deposit. The evolution of these 11 phases is depicted schematically in Figure 5.

While there is some variability within the sampled thin sections, the earliest phases are relatively consistent for each of the 11 localities. In the later stages, however, this consistency diminishes and some differences in the sequences arise. These late phase events are identified by a noticeable lack of pyrite, including pyrite framboids and pyrite coated corrosion surfaces. For example, sparry calcite crystals are clear, occasionally displaying polysynthetic twinning, while lacking inclusions or pyrite framboids. Additionally, these late stage events can be identified with the aid of cathodoluminescence microscopy, which uses streams of electrons to delineate late stage events that are not visible under plane-polarized or cross-polarized light (Boggs Jr. and Krinsley 2006). Since this was outside of the scope of this project, the differences in each localities later stage events could be due to the difficulty in discerning them using only plane-polarized or cross-polarized light. Therefore, with these data, these differences cannot be conclusively attributed to differences in depositional environment. After examining close to 300 thin sections, however, there is enough overlap in the early phases of the paragenetic sequences, as well as some overlap of the later phases, to consider them as having similar origins and following similar evolutionary pathways.

4.1.1 *Early Phase Events*

At all 11 seep deposits, detrital-rich micarb (Figure 6A, B, F, G, H) was the earliest component of the paragenetic sequence deposited and which, subsequent to deposition, experienced some degree of corrosion, dissolution, and/or recrystallization. It forms the bulk of the GVG and Franciscan hydrocarbon seep carbonate matrix and is the most common cement visible at outcrop/hand sample scale; although, in thin section, the prevalence of detrital-rich micarb can be highly variable. In some cases, it is the most common feature present in thin section (e.g., GR, HFR), while in others, its pervasiveness was decreased by subsequent corrosion events, which created irregular vugs (e.g., RC, RV) that were filled by later phase cements, microbial fabrics, and textures (e.g., fibrous and sparry calcite, peloids, etc.). In thin section, micarb is commonly associated with organic detritus such as microfossils and plant material (e.g., HFR, BC), as well as peloids, calcispheres, pyrite framboids, and *in situ* seep faunas (bivalves, brachiopods, gastropods, worm tubes, and ammonites).

Peloids (Figure 6C, D, H) encompass all grains that are constructed of an aggregate of cryptocrystalline carbonate, regardless of their size or origin (McKee and Gutschick 1969, Bathurst 1975). They are common in most of the GVG and Franciscan seep thin sections, especially in those from Little Indian Valley (Figure 6D). Their shapes range from spherical to ellipsoidal; however, some are occasionally irregular and filled with pyrite framboids, calcispheres,

and/or detrital-rich micarb. There are a few that have a well-developed anhedral to subhedral rim of sparry microcrystalline calcite surrounding a tightly interlocking microcrystalline nucleus. They vary considerably in size, ranging from ~226 μm to ~1.026 mm and are infrequently offset by calcite-filled veins, indicating that at least some of the peloids formed prior to late stage fracturing events. They lack internal structure and their outer edges form a thin dark line that clearly demarcates them from the enclosing detrital-rich micarb, fibrous calcite, or other surrounding material.

Calcispheres were first described by Williamson (1883) as spheres constructed of a calcite wall enclosing a spherical chamber. One suggestion for their origin links the non-spinose calcispheres to the reproductive cysts of the modern dasycladacian *Acetabularia*, but at one time or another they have been linked to a number of plant and animal taxa, with no concrete conclusions drawn (Rupp 1968, Bathurst 1975). Although a common constituent within the GVG and Franciscan thin sections, they vary in size, shape, and distribution. In all cases, they are silt- to sand-sized spherules filled with clear to cloudy sparry calcite cement, micarb, and occasionally, a small number of pyrite framboids. They generally range in size from ~76 μm to ~114 μm and are most commonly round, although their shape can also be elliptical to highly irregular. They do not have the internal concentric layers that calcispheres from other environments have, although some appear to have clearly defined outer walls and/or spines.

Many of the GVG and Franciscan calcispheres appear diffuse, a possible indication of post-depositional diagenetic alteration (i.e., Bathurst, 1975).

Pyrite is common at seafloor seeps because H_2S is a ubiquitous seepage fluid. A local increase in H_2S seepage results in the formation of an acidic reducing environment, which forms metastable iron monosulphides and which during early diagenesis, readily transform to pyrite under most conditions (Berner 1984, Beauchamp et al. 1989). Therefore, the presence of pyrite in thin section is an indication that sulfide-rich fluids were periodically present throughout deposition (Goedert and Campbell 1995). Pyrite is present in all of the GVG and Franciscan thin sections as robust framboids, as discontinuous horizons lining corrosion surfaces etched out of the matrix micarb, or as the material replacing the organic walls of worm tubes (Figure 6A, C, D, G). Framboids are extremely common, although vary considerably in size and density from deposit to deposit. They appear as black clusters of framboids ranging from <38 μm to >190 μm in size and are found as detritus in the detrital-rich micarb, within peloids and calcispheres, in the neomorphosed microspar, and rarely in the clotted microbial fabrics.

In the GVG and Franciscan seeps, following the deposition of detrital-rich micarb, H_2S seeping out of seafloor sediments resulted in localized acidic conditions causing corrosion, which produced irregularly shaped vugs and remnant micarb islands that are often coated with incomplete horizons of pyrite and which were subsequently engulfed by younger cements (Figure 6B, E;

Beauchamp et al. 1989). Vugs are present at all of the localities and are commonly lined with later phase horizons of fibrous or botryoidal calcite and then filled with equant calcite spar (Figure 6A, B, H). They vary in diameter from ~1.0 mm to ~9.0 mm, although due to their irregular shape, their diameter can vary considerably. Their walls are generally rounded to subrounded or wavy and, in places, cut through remnant micarb islands, peloids, unusually large pyrite framboids, or calcispheres. The internal walls of the smaller vugs are typically lined with a thin crust of fibrous calcite with the remaining cavity space filled with sparry calcite. The internal walls of the larger vugs are often lined with a thin horizon of yellow calcite followed by an extensive growth of fibrous, botryoidal, or dentate calcite, which grows into and fills vacant pore space (Figure 6A, B). Vugs are almost always bounded by detrital-rich micarb, but are also in places surrounded by pyrite framboid-rich microspar. Remnant micarb islands, surfaces, and irregular horizons are usually all that remain of the early micarb phase.

The next major early cement phase consists of a variety of calcite cements, including both yellow and fibrous calcite (fibrous, botryoidal, and dentate habits). Deposition of yellow calcite occurred first (Figure 6B), followed by the deposition of the three habits of fibrous calcite, in apparently random order. Yellow calcite grew as anhedral crystals from corroded detrital-rich micarb regions, partially filling pre-existing voids and vugs, and irregularly coating all available surfaces. Its thickness generally varies over short distances and most

likely formed as an aggrading *in situ* replacement of early detrital-rich micarb, possibly related to dissolution associated with corrosion. This irregular thickness is especially obvious at HFR where it inconsistently lines or completely replaces the walls of worm tubes; however, it can also precipitate as very thin horizons coating vugs or macrofaunal shells (e.g., GR, LIV, CFCC, Figure 6C).

The three habits of fibrous calcite follow the precipitation of yellow calcite and include: (1) fibrous calcite cement (Figure 6A, D, E, F, G, H), (2) large botryoidal calcite cement fans (Figure 6B) precipitated in vugs, and/or (3) clear, transparent, dentate calcite cement. The fibrous habit forms as serrated crystals growing by the addition of ions perpendicular to boundaries of pore walls or particle surfaces; first to suitable crystalline nuclei embedded in the surface, followed by normal accretion on crystal facies (Bathurst 1975) and the dentate habit fills small voids with inwardly stellate subhedral rhombs and crystals of calcite. Both the fibrous and botryoidal forms have undulating extinction, while the dentate does not. The three types are commonly found lining vugs and cavities, surrounding peloids or macrofossils, filling pore spaces, and/or radiating outward as fans from thin horizons of yellow calcite. All three types are typically white or buff in color, but can also have a brownish hue, indicative of submicroscopic contaminants. They can also encase varying quantities of dark inclusions that appear as black to reddish streaks or extremely small globules, which may be trapped hydrocarbons (see Campbell et al. 2002). The content of these inclusions reflects the composition of the fluids during precipitation

provided there have been no significant pressure and temperature changes between the time of formation of the inclusion and the time of sampling (Roedder and Bodnar 1980, Burruss 1981). The fibrous crystals typically show rhombic terminations as outlined by submicrometric calcite inclusions and measure from ~38 μm to ~5.0 mm in length and ~19 μm to ~1.52 mm in width. The fibrous horizons commonly fill pore spaces (LIV) or replace large areas of detrital-rich micarb (RV), occasionally extending for the length of an entire thin section (2.5 x 5 cm). Yellow calcite and the three habits of fibrous calcite are present in all GVG and Franciscan seep thin sections.

Deposition of clotted microbial fabrics followed the precipitation of the fibrous cements, appearing in thin section, as described by Campbell et al. (2002), as finely laminated micarb horizons, micarb peloids with indistinct edges filled with unidentifiable detritus, and/or as finely clotted/cloudy micarb fabrics lining vugs and filling small voids. Under plane-polarized light, the microbial micarb has a clotted texture and is generally detritus-free, although, occasionally a small number of irregular to round pyrite framboids measuring ≤ ~76 μm in diameter and a small quantity of medium to fine-grained equant sparry calcite crystals are present. Clotted micarb forms small clumps ≤ ~5.0 mm across and is often irregularly bordered by fine-grained sparry calcite, medium to fine-grained equant sparry calcite, or neomorphosed microspar. Microbial fabrics were only observed at seven of the GVG and Franciscan seep localities (e.g.,

GR, Pa, CFCC, WS, WAM, BC, RC); however, not being present at all 11 localities is likely due to the general rarity of microbial fabrics.

4.1.2 *Late Phase Events*

A second, nonferroan (corrosion surfaces not pyrite coated) corrosion event (CE2) ± deposition of siliciclastic silt-clay fill marks the beginning of the late phase of precipitation. This was followed by a fracturing event (Figure 6E, G), which was subsequently filled with sparry calcite and the precipitation of sparry calcite in the vugs and other available pore spaces (Figure 6C, E, F, G). In these deposits, sparry calcite is a cavity-filling spar cement that forms aggregates of fine to medium grained, anhedral to subhedral crystals that increase in size as they grow from the cavity wall into the center of the void. The crystals are clear to cloudy with rare rhombohedral cleavage and polysynthetic twinning.

Neomorphosed micarb (Figure 6F) variably replaces detrital-rich micarb, yellow calcite, and/or fibrous calcite (all three habits), via aggrading neomorphism. This is an *in situ* process whereby a mosaic of finely crystalline carbonate is replaced by a coarser (sparry) patchy mosaic (Folk 1965, Flügel 2004) and is a process that includes polymorphic transformation and recrystallization (Bathurst 1975). Its formation begins in the partly consolidated sediment and can change an entire mass of micarb into a coarser sparry mosaic (Bathurst 1975). In the GVG and Franciscan seeps, the patches of microspar commonly incompletely engulf the cements, microbial fabrics, and textures, although rarely exceed more than ~4 cm^2. Neomorphosed micarb is commonly

found lining small regions of partially dolomitized micarb, which selectively replaces small regions of detrital-rich micarb. In general, dolomite crystals are rare in the GVG and Franciscan thin sections and unless associated with neomorphosed micarb, their timing of formation is difficult to ascertain, since they can form at any stage of diagenesis (Scholle and Ulmer-Scholle 2003). Where present however, the dolomite crystals are nonplanar and subhedral, with mostly curved crystal boundaries, ranging from densely to poorly packed. Dolomite crystals are present in the BC, HFR, WS, and WAM thin sections.

4.1.3 *Paragenesis*

Methane and hydrogen sulfide are the two most common sources of energy utilized by the microbes in hydrocarbon seeps (Gaillard et al. 1992). These fluids form via diagenesis of organic matter shed from neighboring continents or mountain chains or through primary productivity in the sediment column (Cavagna et al. 1999). The fluids can migrate from their zones of genesis along permeable fault zones, stratigraphic layers, or via mud and serpentinite diapirs (Orange and Campbell 1997, Conti and Fontana 1999, Van Dover et al. 2002) and can be captured in rising pore water being driven out of the sedimentary unit by compression, compaction, or cementation, and/or by the deformation that is common in tectonically active areas (Ritger et al. 1987, Campbell and Bottjer 1993).

The earliest phases of the paragenetic sequence were initiated by the consumption of reduced gases (biogenic methane or hydrogen sulfide) by a

consortium of archaea and sulfate-reducing bacteria. This caused a localized increase in alkalinity, resulting in the precipitation of calcium carbonate either above the seafloor or below the oxic layer in the sediment column, probably no deeper than several centimeters to a few meters below the seabed, depending on the location of the oxic/anoxic boundary (Ritger et al. 1987, Beauchamp and Savard 1992, Aharon 2000).

Based on the presence of organic matter and pyrite, the earlist phase events, including micarb and yellow calcite, precipitated in anoxic sediments below the sediment-water interface, linked to AOM and sulfate reduction (Reeburgh 1976, Hoehler et al. 1994). These events culminated in CE1 and its associated pyrite corrosion surfaces, which suggest an increased influx of hydrogen sulfide into the system. Once advecting methane reached the oxic portion of the sediment column, above the zone of sulfate reduction (Beauchamp and Savard 1992), the precipitation of later phase events began, including fibrous (all three habits) and sparry calcite. The lack of organic matter and pyrite in these phases suggests their precipitation occurred under aerobic conditions. The macrofaunal fossils are restricted to the earliest diagenetic stages in all 11 deposits and are associated with detrital-rich micarb, except for worm tubes, which are variably encrusted with yellow calcite. The presence of the macrofauna suggests that the anoxic conditions and precipitation of carbonate occurred just below the sediment-water interface, with the faunas living at or

directly above the oxic/anoxic boundary, which would have been either at or just below the seafloor.

Despite deposition occurring over millions of years and their variable sizes and morphologies, petrographic observations show that 10 of the 11 deposits have all five major phases or events (as defined by Campbell et al. 2002) present in their paragenetic sequences, including detrital-rich micarb, CE1, yellow calcite, fibrous calcite, and sparry calcite, with the late phase events being characterized by some variability. Not only are the 11 deposits petrographically consistent with each other and with earlier studies of GVG and Franciscan hydrocarbon seeps (e.g., Campbell et al. 2002, Hepper 2004), but they are also consistent with seeps of the Canadian Arctic (e.g., Beauchamp and Savard 1992), the LCF seeps in western Washington state (e.g., Peckmann et al. 2002), the Hollard Mound seeps in Germany (e.g., Peckmann et al. 1999), the Italian Apennine seeps in Italy (e.g., Conti and Fontana 2005), and the Tepee Buttes in Colorado (e.g., Kauffman et al. 1996).

4.2 *Geochemistry*

The five volumetrically dominant carbonate phases (detrital-rich micarb, yellow calcite, fibrous calcite (all three habits), microbial fabrics, and sparry calcite) of the GVG and Franciscan seeps were sampled for stable carbon and oxygen isotope analysis in order to reconstruct the conditions that resulted in mineral formation (Figure 7). The primary carbonate phases are characterized by variable, but depleted, carbon isotope ratios ranging from -43.7‰ PDB at Pa,

to -3.42‰ PDB at GR and oxygen isotope ratios ranging from -13.9‰ PDB at Pa, to 1.54‰ PDB at WS.

The isotope values are significantly more negative than typical seawater DIC or typical Mesozoic marine carbonates, suggesting a carbon source derived from seep fluids and enriched in reduced organic compounds; although some values are not negative enough to indicate carbonate precipitation occurring solely from a methane-enriched fluid source. The $\delta^{13}C$ values generated for these localities indicate a significant contribution of biogenic methane derived from diagenetic decomposition of thermally immature organic matter that was subsequently mixed to an indeterminable degree with marine bicarbonate present in seawater, with a $\delta^{13}C$ value of ~0‰ (Peckmann et al. 1999, Peckmann et al. 2001) and are consistent with biomarker analyses performed by Birgel et al. (2006) at the Cold Fork of Cottonwood Creek, Wilbur Springs, and the Paskenta localities.

Although seep carbonates tend to yield carbon isotope values ranging from -10‰ to -80‰ PDB, depending on the origin of the methane (Ritger et al. 1987, Paull et al. 1992, Cavagna et al. 1999), heavier values such as those of the GVG and Franciscan seeps have also been documented (e.g., Kiel and Peckmann 2008). These ^{13}C-depleted values are the product of AOM occurring in sediment porewaters, which consumes methane and sulfate and produces hydrogen sulfide and dissolved inorganic carbon (DIC), according to the generalized net reaction: $SO_4^{2-} + CH_4 \rightarrow HS^- + HCO_3^- + H_2O$, as originally

proposed by Reeburgh (1976), and readdressed later by Zehnder and Brock (1979), and Hoehler et al. (1994). This process produces ^{13}C-depleted DIC and alkalinity, which diffuses upward along a concentration gradient and is consumed by carbonate precipitation, resulting in $\delta^{13}C$-depleted carbonate (Werne et al. 2004). The resulting hydrogen sulfide is partially trapped within the carbonate in pyrite framboids and partially mobilized into the overlying pore fluids, fueling chemosynthesis of the sulfide-oxidizing bacteria found living in various symbiotic associations with benthic macrofauna or forming mats at the seafloor (Cavagna et al. 1999, Stakes et al. 1999).

In addition the variable, although depleted $\delta^{13}C$ values recorded at all 11 localities, positive $\delta^{13}C$ values were also recorded, however, only at the Bear Creek deposit. These unusual values are likely the result of *in situ* methanogenesis by archaeal methanogens, a process that enriches the CO_2 pool in ^{13}C, the heavier isotope (Irwin et al. 1977, Boehme et al. 1996). During AOM, advecting methane was trapped in the zone of sulfate reduction, where it was used for energy synthesis, along with seawater sulfate that diffused down into the sediment column, by a syntrophic consortium of methane oxidizers and sulfate reducers (Joye et al. 2004, Orcutt et al. 2005). This consortium preferentially used ^{12}C over ^{13}C, enriching the pore water in heavy carbon and depleting the newly produced bicarbonate in light carbon (Joye et al. 2004). This process continued until pore water sulfate concentrations were depleted, which caused the zone of AOM and sulfate reduction to shallow. Fluid advection rates

could also have increased at this time and as a result, the zone of AOM was less capable of trapping the higher rates of advecting methane, which resulted in more fluid venting at the seafloor and mixing with seawater. If the isotopically depleted bicarbonate vented and mixed with seawater, the available carbon pool shifted to that produced by methanogenesis, a process that results in the production of isotopically heavy carbon dioxide (Irwin et al. 1977). This carbon dioxide readily dissolved in pore water and increased bicarbonate concentrations, resulting in the precipitation of calcium carbonate with a heavy isotopic signature.

4.3 *Paleontology*

Many macrofauna inhabiting the modern hydrocarbon seep setting live symbiotically with a chemoautotrophic microbial consortium that consists of methane-oxidizing archaea and sulfate-reducing bacteria, which create energy for carbohydrate production by consuming discharging methane and sulfate during AOM (Reeburgh 1976, Fisher 1990, Cavagna et al. 1999, Peckmann et al. 2001, Peckmann et al. 2002, Werne et al. 2004). Ancient hydrocarbon seep faunal assemblages typically include a variety of recurring taxa, belonging to the mollusk families Lucinidae, Mytilidae, Solemyidae, Thyasiridae, and Vesicomyidae and the annelid family Siboglinidae (frenulate and vestimentiferan worm tubes; Fisher 1990, Callender and Powell 1997, Peckmann et al. 2005, Pleijel et al. 2009). Based on shell morphology and preserved life positions, the Lucinidae are the only family with evidence for chemosymbiosis preserved in the

stratigraphic record (Cobabe 1998, Taylor and Glover 2000). Although evidence has not been found in the stratigraphic record for symbiosis in the other four families, since their living representatives are known to have symbionts, it is likely that they did as well.

The GVG and Franciscan hydrocarbon seep deposits preserve typical and endemic hydrocarbon seep taxa, as well as opportunistic species (Tables 1 and 2). At these deposits, the typical seep taxa comprise those common to, although not exclusive to, both modern and ancient hydrocarbon seeps, including lucinid (e.g. Taylor and Glover 1997, Conti and Fontana 1998, Taylor and Glover 2000, 2006, and others) and thyasirid bivalves (e.g. Dufour 2005, Taylor et al. 2007, and others). The endemic taxa include those found only in modern or ancient hydrocarbon seeps, such as the gastropods *Lithomphalus enderlini* (Figure 8E, G) and *Paskentana paskentaensis* (Figure 8B, K), among others, both of which were collected during the course of this study. Finally, the opportunistic taxa, which are those that inhabit marginal environmental settings to escape from predation pressures and which flourish under low-oxygen conditions (Fürsich and Thomsen 2005), include the bivalve *Pecten complexicosta* and both the inoceramid and buchiid bivalves, all of which were collected during the course of this study.

With the exception of Paskenta, fossils were collected at all localities and the faunal assemblages are populated by eighteen taxa (Table 1 and 2), including five clades: brachiopods (at WS, WAM, Pa), gastropods (at BC, Pa,

HFR, WS, WAM, GR, LIV, RC, CFCC), bivalves (at BC, Pa, HFR, RV, RmC, LIV, GR), ammonites (at GR, BC, Pa, HFR), and siboglinid worm tubes (at BC, CFCC, HFR, LIV, GR), in addition to indeterminate bivalves, gastropods, and ammonites. These deposits are characterized by spatial and temporal heterogeneity in faunal composition and relative abundance, which is illustrated in Figure 9. Of the 10 fossil-bearing seeps, three are dominated by steinkerns of bivalves and gastropods that are not identifiable below class level, including HFR (bivalves), LIV (bivalves), and RC (gastropods). Five of the deposits are dominated by different identifiable species, including BC, CFCC, RV, RmC, and GR. Each of these dominating taxa are also minor components of other faunal assemblages. For example, the gastropod *P. paskentaensis* comprises 62% of the BC assemblage, while it only comprises 1% of the WAM assemblage and the gastropod *Retiskenea*? *kieli* (Figure 8O, P) comprises 49% of the CFCC assemblage, but only 4% of the RC assemblage. The remaining two deposits, WS and WAM, are both dominated by *Peregrinella whitneyi* (Figure 9V, W), which comprises 91% and 93% of the two assemblages, respectively. However, WS and WAM are the same age, and are in close proximity to each other, and it is possible that they represent a single coeval seep system, rather than discrete seepage events, but exposure precludes testing this relationship. The bivalve (Figure 8T, AA) and gastropod (Figure 8Q, F, H) steinkerns at HFR and RC, respectively, are better preserved than the bivalve steinkerns at LIV, which are completely unidentifiable. Those at HFR are most likely thyasirids (Figure 8Y,

BB) or *Astarte trapezoidalis* (Figure 8S) and at RC are most likely *Atresius liratus* (Figure 8C). There are no taxa common to *all* 10 localities and although worm tubes are found at 6 of the 10 localities; they are never dominant in an assemblage.

4.3.2 *Taphonomy*

Fossil preservation is variable both from deposit to deposit, as well as within a single deposit (Figure 8). Although original shell material is preserved at some localities, gastropods and bivalves are commonly preserved as molds or steinkerns. Some specimens are pristine and are identifiable to the species level, such as *P. paskentaensis* at LIV (Figure 8B) and *A. trapezoidalis* at BC (Figure 8S). Other specimens are preserved only as fragments, although are still identifiable to the genus or species level, such as *P. complexicosta* at RC and inoceramid bivalves at GR, HFR, BC, RmC (Figure 8X), while some are too degraded to identify beyond clade or ordinal level, including the gastropod and bivalve steinkerns present at all 10 localities (Figure 8F, H, Q, T, AA). There is no evidence of predatory boring of gastropods, bioerosion, or biofragmentation or abrasion of shells due to mechanical degradation or chemical dissolution.

The brachiopod (*P. whitneyi* at WS and WAM, Figure 8V, W) and bivalve shells (lucinid bivalves at BC, Figure 8N, *A. trapezoidalis* at BC, Figure 8S; thyasirid bivalves at HFR, Figure 8Y, BB; *A. trapezoidalis* at HFR) are commonly articulated, the worm tubes are typically clustered (CFCC, GR, BC, HFR, RC, LIV), and all specimens from all localities lack significant signs of transport or of a

long residence time before burial, suggesting that the deposits represent *in situ* populations. Disarticulated specimens and horizons of shell hash are found in 3 deposits, including WS, WAM, and LIV, although are generally localized and only minor components of each deposit as a whole.

It is important to consider that these results could have been skewed by the large number of steinkerns collected and by sampling issues related to the sizes and accessibility of some of the outcrops. The rarefied species richness curves indicate that further sampling at LIV, GR, BC, and WAM would likely have recovered more taxa, while the reverse is true for CFCC, HFR, RC, and WS, all of which reach an asymptote (Figure 10).

5. Temporal and Spatial Variance

There are three significant aspects to the temporal and spatial record of the GVG seeps. First, are their remarkably similar petrographic and paragenetic signatures, specifically in the early phases of paragenesis, as well as their consistently anomalous geochemical values in comparison to seawater carbon. This indicates that there was intermittent methane seepage throughout the forearc basin and accretionary prism for ~80 m.y. and that throughout this entire period, the chemistry of the advecting fluids remained relatively consistent. Of the 11 localities, Romero Creek is the only outlier and likely lacks phases beyond the precipitation of detrital-rich micarb due to the complete consumption of methane prior to reaching the oxic zone, above the zone of sulfate reduction,

where the aerobic oxidation of methane and the precipitation of later phase events occur.

The second significant aspect is the variability of the sizes and shapes of the seeps, which is regardless of age or location. This variability is likely related to the ephemeral nature of the hydrocarbon seep setting, including localized temporal, spatial, and chemical variations in the seeping fluids, including fluid volume, rate, origin, and composition, which would have varied from one area of active seepage to the next. These physical characteristics are consistent with fluid advection at modern seeps, which has been documented varying in rate and volume over short distances and which produces variably sized and shaped deposits. Emissions have been recorded ranging from slow and diffuse, resulting in deposits characterized by precipitation of carbonate below, at, or directly above the seafloor and inhabited by chemosynthesis-based faunas; to fast and vigorous, forming unpopulated chimneys and mud volcanoes (Ritger et al. 1987, Aharon 1994).

These 11 seeps indicate not only that seepage was intermittent, but also that methane release likely occurred over geologically short time scales. Even CFCC, which has the longest and most continuous exposure of the GVG and Franciscan seep deposits is considerably smaller than many of those recorded in the stratigraphic record or in modern oceans. For example, the Panoche Hills (Maastrichtian–Danian) seep deposit is approximately 800 m thick (Schwartz et al. 2003), while each of the thousands of Tepee Buttes mounds can be up to 60

m wide and 30 m tall (Kauffman et al. 1996). These large sizes are also characteristic of modern seeps, which in the Gulf of Mexico have been documented extending over areas of several hundred meters (Jollivet et al. 1990) and on the Blake Ridge extending over areas of several tens of meters (Van Dover et al. 2003).

The third aspect of these assemblages is the spatial and temporal heterogeneity of taxonomic composition and relative abundance from site to site. This heterogeneity is interesting in light of the continuity of the geochemically-based characteristics through time. This is similar to the Oligocene LCF seeps, although is in stark contrast to the Campanian—Maastrichtian Tepee Buttes, which are largely physically and faunally consistent from New Mexico to Montana. The variability in the GVG and Franciscan seeps is the product of the dynamic interactions between organism habitat preferences and the fluctuating geochemical and physical parameters of fluid expulsion, geographic and geotectonic position, variations in the origin and composition of venting fluids, as well as the rate of fluid flow (Carney 1994, Bergquist et al. 2003, Campbell 2006). Since chemoautotrophy is dependent on reduced chemical compounds, the chemical environment influences biological productivity and species distribution (Sahling et al. 2002). This is confirmed by observing modern hydrocarbon seeps, where both the physical characteristics of a given site and the abundance of a faunal community have been found to be proportional to both the volume and rate of advecting seep fluids.

6. Conclusions

The 11 ancient hydrocarbon seep deposits cropping out in the GVG forearc strata and the Franciscan Complex preserve the physical, chemical, and biological signatures of a group of tectonically related ancient hydrocarbon seeps and are a record of 80 m.y. of intermittent fluid seepage, occurring over geologically short intervals, along the western North American continental margin. The chemical signatures of the 11 seeps are similar petrographically and paragenetically and their geochemical values are consistently anomalous, however, their physical and biological signatures are surprisingly variable.

The 11 seeps included in this study that occur in the GVG forearc strata and the Franciscan Complex and the additional 8 mentioned by Kiel et al. (2008), indicate that there are likely many more to be discovered throughout this region. As the abundance of recognized hydrocarbon seeps in this area continues to increase, they can be viewed collectively as a quasi-continuous, dynamic fluid-sediment-biotic system, with the potential to reveal larger evolutionary, biogeographic, geotectonic, and geochemical patterns of hydrocarbon seep processes and associated faunas through geologic time.

References Cited

Aharon, P. 1994. Geology and biology of modern and ancient submarine hydrocarbon seeps and vents: An introduction. Geo-Marine Letters 14:69-73.

Aharon, P. 2000. Microbial Processes and Products Fueled by Hydrocarbons at Submarine Seeps. Pp. 270-281. *In* R. E. Riding, and S. M. Awramik, eds. Microbial Sediments. Springer-Verlag, Berlin.

Anderson, F. M. 1938. Lower Cretaceous Deposits in California and Oregon. Geological Society of America, Baltimore.

Bailey, E. H., and D. L. Jones. 1973. Preliminary lithologic map, Colyear Springs quadrangle, California. *In* U. S. Geological Survey Miscellaneous Field Studies, MF-516.

Barbieri, R., and B. Cavalazzi. 2005. Microbial fabrics from Neogene cold seep carbonates, Northern Apennine, Italy. Palaeogeography, Palaeoclimatology, Palaeoecology 227:143-155.

Bathurst, R. G. C. 1975. Carbonate Sediments and Their Diagenesis. Elsevier Scientific Publishing Company, Amsterdam.

Beauchamp, B., H. R. Krouse, J. C. Harrison, W. W. Nassichuk, and L. S. Eliuk. 1989. Cretaceous Cold-Seep communities and Methane-Derived carbonates in the Canadian Arctic. Science 244:53-56.

Beauchamp, B., and M. Savard. 1992. Cretaceous Chemosynthetic Carbonate Mounds in the Canadian Arctic. Palaios 7:434-450.

Bergquist, D. C., T. Ward, E. E. Cordes, T. McNelis, S. Howlett, R. Kosoff, S. Hourdez, R. Carney, and C. R. Fisher. 2003. Community structure of vestimentiferan-generated habitat islands from Gulf of Mexico cold seeps. Journal of Experimental Marine Biology and Ecology 289:197-222.

Berner, R. A. 1984. Sedimentary pyrite formation: An update. Geochimica et Cosmochimica Acta 48:605-615.

Birgel, D., V. Thiel, K.-U. Hinrichs, M. Elvert, K. A. Campbell, J. Reitner, J. D. Farmer, and J. Peckmann. 2006. Lipid biomarker patterns of methane-seep microbialites from the Mesozoic convergent margin of California. Organic Geochemistry 37:1289-1302.

Blake, M. C., Jr., and D. L. Jones. 1981. The Franciscan Assemblage and Related Rocks in Northern California: A Reinterpretation. Pp. 307-328. *In* W. R. Ernst, ed. The Geotectonic Development of California. Prentice Hall, New Jersey.

Blake, M. C., Jr., and R. J. McLaughlin. 1989. Terranes of the Northern Coast Ranges. P. 75. *In* M. C. Blake, and D. S. Harwood, eds. Tectonic Evolution of Northern California. American Geophysical Union, Washington D.C.

Boehme, S. E., N. E. Blair, J. P. Chanton, and C. S. Martens. 1996. A Mass Balance of ^{13}C and ^{12}C in an Organic-rich Methane-producing Marine Sediment. Geochimica et Cosmochimica Acta 60(20):3835-3848.

Boggs Jr., S., and D. Krinsley. 2006. Application of Cathodoluminescence Imaging to the Study of Sedimentary Rocks. Cambridge University Press, Cambridge.

Burruss, R. C. 1981. Analysis of fluid inclusions; phase equilibria at constant volume. The American Journal of Science 281(8):1104-1126.

Callender, W. R., and E. N. Powell. 1997. Autochthonous Death Assemblages from Chemoautotrophic Communities at Petroleum Seeps: Palaeoproduction, Energy Flow, and Implications for the Fossil Record. Historical Biology 12:165-198.

Campbell, K. A., and D. J. Bottjer. 1993. Fossil Cold Seeps. National Geographic Research and Exploration 9(3):326-343.

Campbell, K. A. 1995. Dynamic Development of Jurassic-Pliocene Cold-Seeps, Convergent Margin of Western North America. PhD. University of Southern California, Los Angeles.

Campbell, K. A., and D. J. Bottjer. 1995. Peregrinella: An Early Cretaceous Cold-Seep-Restricted Brachiopod. Paleobiology 21(4):461-478.

Campbell, K. A., J. D. Farmer, and D. Des Marais. 2002. Ancient hydrocarbon seeps from the Mesozoic convergent margin of California: carbonate geochemistry, fluids and palaeoenvironments. Geofluids 2:63-94.

Campbell, K. A. 2006. Hydrocarbon seep and hydrothermal vent paleoenvironments and paleontology: Past developments and future research directions. Palaeogeography, Palaeoclimatology, Palaeoecology 232:362-407.

Campbell, K. A., D. E. Peterson, and A. C. Alfaro. 2008. Two New Species of *Retiskenea*? (Gastropoda: Neomphalidae) from Lower Cretaceous Hydrocarbon-Seep Carbonates of Northern California. Journal of Paleontology 82(1):140-153.

Carney, R. S. 1994. Consideration of the oasis analogy for chemosynthetic communities at Gulf of Mexico hydrocarbon vents. Geo-Marine Letters 14:149-159.

Cavagna, S., P. Clari, and L. Martire. 1999. The role of bacteria in the formation of cold seep carbonates: geological evidence from Monferrato (Tertiary, NW Italy). Sedimentary Geology 126:253-270.

Cobabe, E. A. 1998. Chemosynthesis and Chemosymbiosis in the Fossil Record: Detecting Unusual Communities Using Isotope Geochemistry. Pp. 255-285. *In* W. L. Manger, and L. K. Meeks, eds. Isotope Paleobiology and Paleoecology. The Paleontological Society Papers, Pittsburgh.

Constenius, K. N., R. A. Johnson, W. R. Dickinson, and T. A. Williams. 2000. Tectonic Evolution of the Jurassic-Cretaceous Great Valley forearc; California: Implications for the Franciscan Thrust-Wedge Hypothesis. Geological Society of America Bulletin 112(11):1703-1723.

Conti, S., and D. Fontana. 1998. Recognition of Primary and Secondary Miocene Lucinid Deposits in the Apennine Chain. Estratto da Memorie Di Scienze Geologiche 50:101-131.

Conti, S., and D. Fontana. 1999. Miocene chemoherms of the northern Apennines, Italy. Geology 27(10):927-930.

Conti, S., and D. Fontana. 2005. Anatomy of seep-carbonates: Ancient examples from the Miocene of the northern Apennines (Italy). Palaeogeography, Palaeoclimatology, Palaeoecology 227:156-175.

Craig, H. 1957. Isotopic standards for carbon and oxygen and correction factors for mass-spectrometric analysis of carbon dioxide. Geochimica et Cosmochimica Acta 12:133-149.

Dickinson, W. R., and D. R. Seely. 1979. Structure and Stratigraphy of Forearc Regions. American Association of Petroleum Geologists Bulletin 63(1):2-31.

Dickinson, W. R. 1981. Plate Tectonics and the Continental Margin of California. Pp. 1-28. *In* W. R. Ernst, ed. The Geotectonic Development of California. Prentice Hall, New Jersey.

Dickinson, W. R. 2008. Accretionary Mesozoic-Cenozoic Expansion of the Cordilleran Continental Margin in California and Adjacent Oregon. Geosphere 4(2):329-353.

Dufour, S. C. 2005. Gill Anatomy and the Evolution of Symbiosis in the Bivalve Family Thyasiridae. The Biological Bulletin 208:200-212.

Duperron, S., J. Lorion, S. Samadi, Olivier, Gros, and F. Gaill. 2009. Symbiosis Between Deep-Sea Mussels (Mytilidae: Bathymodiolinae) and Chemosynthetic Bacteria: Diversity, Function, and Evolution. C. R. Biologies 332:298-310.

Elder, W. P. 1999. Mesozoic Molluscan Fossils from the Golden Gate National Recreation Area and Their Significance to Franciscan Complex Terrane Reconstructions, San Francisco Bay Area, California. National Park Service Paleontological Research 3:7.

Ernst, W. G., C. A. Snow, and H. H. Scherer. 2008. Mesozoic Transpression, Transtension, Subduction and Metallogenesis in Northern and Central California. Terra Nova 20(5):394-413.

Fisher, C. R. 1990. Chemoautotrophic and Methanotrophic Symbiosis in Marine Invertebrates. Aquatic Sciences 2(3,4):399-436.

Flügel, E. 1982. Microfacies Analysis of Limestones. Springer-Verlag, Berlin.

Flügel, E. 2004. Microfacies of Carbonate Rocks. Springer, Berlin.

Folk, R. L. 1965. Some Aspects of Recrystallization in Ancient Limestones. Pp. 14-48. *In* L. C. Pray, and R. C. Murray, eds. Dolomitization and Limestone Diagenesis. Society of Economic Paleontologists and Mineralogists, Special Publication, Tulsa.

Fürsich, F. T., and E. Thomsen. 2005. Jurassic biota and biofacies in erratics from the Sortland area,Vesterålen, northern Norway. Norges Geologiske Undersøkelse 443:37-53.

Gabb, W. M. 1869. Cretaceous and Tertiary Fossils. Palaeontology 2:128-205.

Gaillard, C., M. Rio, and Y. Rolin. 1992. Fossil Chemosynthetic Communities Related to Vents or Seeps in Sedimentary Basins: The Pseudobioherms of Southeastern France Compared to Other World Examples. Palaios 7:451-465.

Godfrey, N. J., B. C. Beaudoin, and S. L. Klemperer. 1997. Ophiolitic basement to the Great Valley forearc basin, California, from seismic and gravity data: Implications for crustal growth at the North American continental margin. GSA Bulletin 109(12):1536-1562.

Goedert, J. L., and K. A. Campbell. 1995. An Early Oligocene Chemosynthetic Community from the Makah Formation, Northwestern Olympic Peninsula, Washington. The Veliger 38(1):22-29.

Goedert, J. L., J. Peckmann, and J. Reitner. 2000. Worm Tubes in an Allochthonous Cold-seep Carbonate From Lower Oligocene Rocks of Western Washington. Journal of Paleontology 74(6):992-999.

Greinert, J., S. M. Bollwerk, A. Derkachev, G. Bohrmann, and E. Suess. 2002. Massive barite deposits and carbonate mineralization in the Derugin Basin, Sea of Okhotsk: Precipitation processes at cold seep sites. Earth and Planetary Science Letters 203(1):165-180.

Hamilton, W. 1969. Mesozoic California and the Underflow of Pacific Mantle. Geological Society of America Bulletin 80:2409-2430.

Harris, P. M., C. G. S. C. Kendall, and I. Lerche. 1985. Carbonate Cementation—A Brief Review. Pp. 79-95. *In* N. Schneidermann, and P. M. Harris, eds. Carbonate Cements. Society of Economic Paleontologists and Mineralogists Special Publication 36, Tulsa.

Hepper, K., L. White, and K. A. Campbell. 2003. Isotopic Analyses of a new Cold Seep locality, Guenoc Ranch, Great Valley Group, northern California. Eos. Transactions American Geophysical Union, Fall Meeting Supplement 84(46):F310.

Hepper, K. 2004. A New Hydrocarbon Seep Locality in the Mesozoic Great Valley Group, Guenoc Ranch, northern California. MS. San Francisco State University, San Francisco.

Hepper, K. 2006. Paleoecological Analysis of Mesozoic Hydrocarbon Seep Faunal Communities, Great Valley Group, Northern California, USA. P. 216. GSA Annual Meeting and Exposition. The Geological Society of America, Philadelphia.

Hepper, K., and M. L. Droser. 2007. Paleoecological Analysis of New Great Valley Group Hydrocarbon Seep Localities. Pp. 30-6. Geological Society of America Annual Meeting. Denver.

Hickman, C. S. 1984. Composition, Structure, Ecology, and Evolution of Six Cenozoic Deep-Water Mollusk
Communities. Journal of Paleontology 58(5):1215-1234.

Hoehler, T. M., M. J. Alperin, D. B. Alpert, and C. S. Martens. 1994. Field and laboratory studies of methane oxidation in an anoxic marine sediment: Evidence for a methanogen-sulfate reducer consortium. Global Biogeochemical Cycles 8(4):451-463.

Ingersoll, R. V. 1978a. Paleogeography and Paleotectonics of the Late Mesozoic Forearc Basin of Northern and Central California. Pp. 471-482. *In* D. G. Howell, and K. A. McDougall, eds. Mesozoic Paleogeography of the Western United States. SEPM Pacific Section, Los Angeles.

Ingersoll, R. V. 1978b. Submarine Fan Facies of the Upper Cretaceous Great Valley Sequence, northern and central California. Sedimentary Geology 21:205-230.

Ingersoll, R. V. 1982. Initiation and evolution of the Great Valley forearc basin of northern and central California, U.S.A. Pp. 459-467. *In* J. K. Leggett, ed. Trench-Forearc Geology; Sedimentation and Tectonics on Modern and Ancient Active Plate Margins. Special Publication-Geological Society of London, London.

Irwin, H., C. Curtis, and M. Coleman. 1977. Isotopic evidence for source of diagenetic carbonates formed during burial of organic-rich sediments. Nature 269(5625):209-213.

Jannasch, H. W. 1984. The Nutritional Basis for Life at Deep-Sea Vents. Oceanus 27(3):73-78.

Jiang, G., M. J. Kennedy, and N. Christie-Blick. 2003. Stable isotopic evidence for methane seeps in Neoproterozoic postglacial cap carbonates. Nature 426(6968):822-826.

Jollivet, D., J.-C. Faugeres, R. Griboulard, D. Desbryuyeres, and G. Blanc. 1990. Composition and spatial organization of a cold seep community on the South Barbados accretionary prism: tectonic, geochemical and sedimentary context. Progress in Oceanography 24:25-45.

Jones, D. L., E. H. Bailey, and R. W. Imlay. 1969. Structural and Stratigraphic Significance of the *Buchia* Zones in the Colyear Springs-Paskenta Area, California. United States Geological Survey Professional Paper 647-A:21.

Joye, S. B., A. Boetius, B. N. Orcutt, J. P. Montoya, H. N. Schulz, M. J. Erickson, and S. K. Lugo. 2004. The anaerobic oxidation of methane and sulfate reduction in sediments from Gulf of Mexico cold seeps. Chemical Geology 205:219-238.

Kauffman, E. G., and B. M. Howe. 1990. Evolutionary and ecological significance of Cretaceous submarine spring communities in Colorado: refugia taxa or new adaptations? P. 15:A68. Geological Society of Canada - Mineralogical Association of Canada Program with Abstracts.

Kauffman, E. G., M. A. Arthur, B. Howe, and P. A. Scholle. 1996. Widespread venting of methane-rich fluids in Late Cretaceous (Campanian) submarine springs (Tepee Buttes), Western Interior seaway, USA. Geology 24(9):799-802.

Kaufmann, B., and J. Wednt. 2000. Calcite Cement Successions in Middle Devonian (Givetian) Carbonate Mud Buildups of the Southern Ahnet Basin (Algerian Sahara). Carbonates and Evaporites 15(2):149-161.

Keenan, K. E., M. L. Droser, and K. A. Campbell. 2008. Hydrocarbon Seeps of the Mesozoic Great Valley Group Forearc Strata, Northern and Central California. Pp. 261-10. Joint Meeting of The Geological Society of America, Soil Science Society of America, American Society of Agronomy, Crop Science Society of America, Gulf Coast Association of Geological Societies with the Gulf Coast Section of SEPM. Houston.

Kiel, S., and K. A. Campbell. 2005. *Lithomphalus enderlini* gen. et sp. nov. from cold-seep carbonates in California-Cretaceous neomphalid gastropod? Palaeogeography, Palaeoclimatology, Palaeoecology 227:232-241.

Kiel, S., K. A. Campbell, W. P. Elder, and C. T. S. Little. 2008. Jurassic and Cretaceous Gastropods from Hydrocarbon Seeps in Forearc Basin and Accretionary Prism Settings, California. Acta Palaeontologica Polonica 53(4):679-703.

Kiel, S., and J. Peckmann. 2008. Paleoecology and Evolutionary Significance of an Early Cretaceous Peregrinella-Dominated Hydrocarbon-Seep Deposit on the Crimean Peninsula. Palaios 23(11):751-759.

Little, C. T. S., and R. C. Vrijenhoek. 2003. Are hydrothermal vent animals living fossils? Trends in Ecology & Evolution 18(11):582-588.

Majima, R., T. Nobuhara, and T. Kitazaki. 2005. Review of fossil chemosynthetic assemblages in Japan. Palaeogeography, Palaeoclimatology, Palaeoecology 227:86-123.

McArthur, A. G., and V. Tunnicliffe. 1998. Modern Ocean Floor Processes and the Geological Record. Pp. 271-291. *In* R. A. Mills, and K. Harrison, eds. Modern Ocean Floor Processes and the Geological Record. Geological Society Special Publication 148, Geological Society, London.

McKee, E. D., and R. C. Gutschick. 1969. History of the Redwall Limestone of Northern Arizona. The Geological Society of America, Memoir 114, Boulder.

McLaughlin, R. J., H. N. Ohlin, D. J. Thormahlen, D. L. Jones, J. W. Miller, and C. D. Blome. 1989. Geologic Map and Structure Sections of the Little Indian Valley-Wilbur Springs Geothermal Area, Northern Coast Ranges, California. *In* United States Geological Survey Miscellaneous Investigations Series Map I-1706.

Ojakangas, R. W. 1964. Petrology and Sedimentation of the Cretaceous Sacramento Valley Sequence, Cache Creek, California. Dissertation. Stanford University, Palo Alto.

Orange, D. L., and K. A. Campbell. 1997. Modern and Ancient Cold Seeps on the Pacific Coast-Monterey Bay, California, and Offshore Oregon as Modern-Day Analogs to the Hoh Accrectionary Complex and Quinault Formation, Washington. Washington Geology 25(4):3-13.

Orcutt, B., A. Boetius, M. Elvert, V. Samarkin, and S. B. Joye. 2005. Molecular biogeochemistry of sulfate reduction, methanogenesis and the anaerobic oxidation of methane at Gulf of Mexico cold seeps. Geochimica et Cosmochimica Acta 69(17):4267-4281.

Paull, C. K., B. Hecker, R. Commeau, R. P. Freeman-Lynde, C. Neumann, W. P. Corso, S. Golubic, J. E. Hook, E. Sikes, and J. Curray. 1984. Biological Communities at the Florida Escarpment Resemble Hydrothermal Vent Taxa. Science 226(4677):965-967.

Paull, C. K., J. P. Chanton, A. C. Neumann, J. A. Coston, C. S. Martens, and W. Showers. 1992. Indicators of Methane-Derived Carbonates and Chemosynthetic Organic Carbon Deposits: Examples from the Florida Escarpment. Palaios 7:361-375.

Peckmann, J., O. H. Walliser, W. Riegel, and J. Reitner. 1999. Signatures of Hydrocarbon Venting in a Middle Devonian Carbonate Mound (Hollard Mound) at the Hamar Laghad (Antiatlas, Morocco). Facies 40:281-296.

Peckmann, J., E. Gischler, W. Oschmann, and J. Reitner. 2001. An Early Carboniferous seep community and hydrocarbon-derived carbonates from the Harz Mountains, Germany. Geology 29(3):271-274.

Peckmann, J., J. L. Goedert, V. Thiel, W. Michaelis, and J. Reitner. 2002. A comprehensive approach to the study of methane-seep deposits from the Lincoln Creek Formation, western Washington State, USA. Sedimentology 49:855-873.

Peckmann, J., C. T. S. Little, F. Gill, and J. Reitner. 2005. Worm tube fossils from the Hollard Mound hydrocarbon-seep deposit, Middle Devonian, Morocco: Palaeozoic seep-related vestimentiferans? Palaeogeography, Palaeoclimatology, Palaeoecology 227(1-3):242-257.

Peckmann, J., K. A. Campbell, O. H. Walliser, and J. Reitner. 2007. A Late Devonian Hydrocarbon-Seep Deposit Dominated by Dimerelloid Brachiopods, Morocco. Palaios 22:114-122.

Pleijel, F., T. G. Dahlgren, and G. W. Rouse. 2009. Progress in systematics: from Siboglinidae to Pogonophora and Vestimentifera and back to Siboglinidae. Comptes rendus. Biologies 332:140-148.

Reeburgh, W. S. 1976. Methane Consumption in Cariaco Trench Waters and Sediments. Earth and Planetary Science Letters 28:337-344.

Ritger, S., B. Carson, and E. Suess. 1987. Methane-derived authigenic carbonates formed by subduction-induced pore-water expulsion along the Oregon/Washington margin. Geological Society of America Bulletin 98:147-156.

Roedder, E., and R. J. Bodnar. 1980. Geologic Pressure Determinations from Fluid Inclusion Studies. Annual Review of Earth and Planetary Sciences 8:263-301.

Rupp, A. W. 1968. Origin, structure, and environmental significance of recent and fossil calcispheres. P. 186. Geological Society of America Special Paper. Geological Society of America, Boulder.

Sahling, H., D. Rickert, R. W. Lee, P. Linke, and E. Suess. 2002. Macrofaunal community structure and sulfide flux at gas hydrate deposits from the Cascadia convergent margin, NE Pacific. Marine Ecology Progress Series 231:121-138.

Scholle, P. A., and D. S. Ulmer-Scholle, eds. 2003. A Color Guide to the Petrography of Carbonate Rocks: Grains, textures, porosity, diagenesis. The American Association of Petroleum Geologists, Tulsa.

Schwartz, H., J. Sample, K. D. Weberling, D. Minisini, and J. C. Moore. 2003. An ancient fluid migration system: cold-seep deposits and sandstone intrusions in the Panoche Hills, California USA. Geo-Marine Letters 23:340-350.

Stakes, D. S., D. Orange, J. B. Paduan, K. A. Salamy, and N. Maher. 1999. Cold-seeps and authigenic carbonate formation in Monterey Bay, California. Marine Geology 159(1-4):93-109.

Stanton, T. W. 1895. Contributions to the Cretaceous Paleontology of the Pacific Coast: The Fauna of the Knoxville Beds. Bulletin of the United States Geological Survey 133:9-132.

Surpless, K. D., S. A. Graham, J. A. Covault, and J. L. Wooden. 2006. Does the Great Valley Group Contain Jurassic Strata? Reevaluation of the Age and Early Evolution of a Classic Forearc Basin. Geology 34(1):21-24.

Swe, W., and W. R. Dickinson. 1970. Sedimentation and Thrusting of Late Mesozoic Rocks in the Coast Ranges near Clear Lake, California. Geological Society of America Bulletin 81:165-188.

Taylor, J. D., and E. A. Glover. 1997. A chemosymbiotic lucinid bivalve (Bivalvia: Lucinoidea) with periostracal pipes: functional morphology and description of a new genus and species. Pp. 335-361. *In* F. E. Wells, ed. The Marine Flora and Fauna of the Houtman Abrolhos Islands, Western Australia. Western Australian Museum, Perth.

Taylor, J. D., and E. A. Glover. 2000. Functional anatomy, chemosymbiosis and evolution of the Lucinidae. Pp. 207-225. *In* E. M. Harper, J. D. Taylor, and J. A. Crame, eds. Evolutionary Biology of the Bivalvia. The Geological Society Special Publications, London.

Taylor, J. D., and E. A. Glover. 2006. Lucinidae (Bivalvia) - the most diverse group of chemosymbiotic molluscs. Zoological Journal of the Linnean Society 148:421-438.

Taylor, J. D., S. T. Williams, and E. A. Glover. 2007. Evolutionary relationships of the bivalve family Thyasiridae (Mollusca: Bivalvia), monophyly and superfamily status. Journal of the Marine Biological Association of the United Kingdom 87:565-574.

Van Dover, C. L., C. R. German, K. G. Speer, L. M. Parson, and R. C. Vrijenhoek. 2002. Evolution and Biogeography of Deep-Sea Vent and Seep Invertebrates. Science 295:1253-1257.

Van Dover, C. L., P. Aharon, J. M. Bernhard, E. Caylor, M. Doerries, W. Flickinger, W. Gilhooly, S. K. Goffredi, K. E. Knick, S. A. Macko, S. Rapoport, E. C. Raulfs, C. Ruppel, J. L. Salerno, R. D. Seitz, B. K. S. Gupta, T. Shank, M. Turnipseed, and R. Vrijenhoek. 2003. Blake Ridge methane seeps: characterization of a soft-sediment, chemosynthetically based ecosystem. Deep-Sea Research I 50:281-300.

Werne, J. P., R. R. Haese, T. Zitter, G. Aloisi, I. Bouloubassi, S. Heijs, A. Fiala-Médioni, R. D. Pancost, J. S. S. Damsté, G. d. Lange, L. J. Forney, J. C. Gottschal, J.-P. Foucher, J. Mascle, and J. Woodside. 2004. Life at cold seeps: a synthesis of biogeochemical and ecological data from Kazan mud volcano, eastern Mediterranean Sea. Chemical Geology 205:367-390.

Williamson, W. C. 1883. The vegetation of the Carboniferous age. Science:529-538.

Wright, J. E., and S. J. Wyld. 2007. Alternative tectonic model for Late Jurassic through Early Cretaceous evolution of the Great Valley Group, California. Geological Society of America Special Paper 419:1-15.

Zehnder, A. J., and T. D. Brock. 1979. Methane formation and methane oxidation by methanogenic bacteria. Journal of Bacteriology 137(1):420-432.

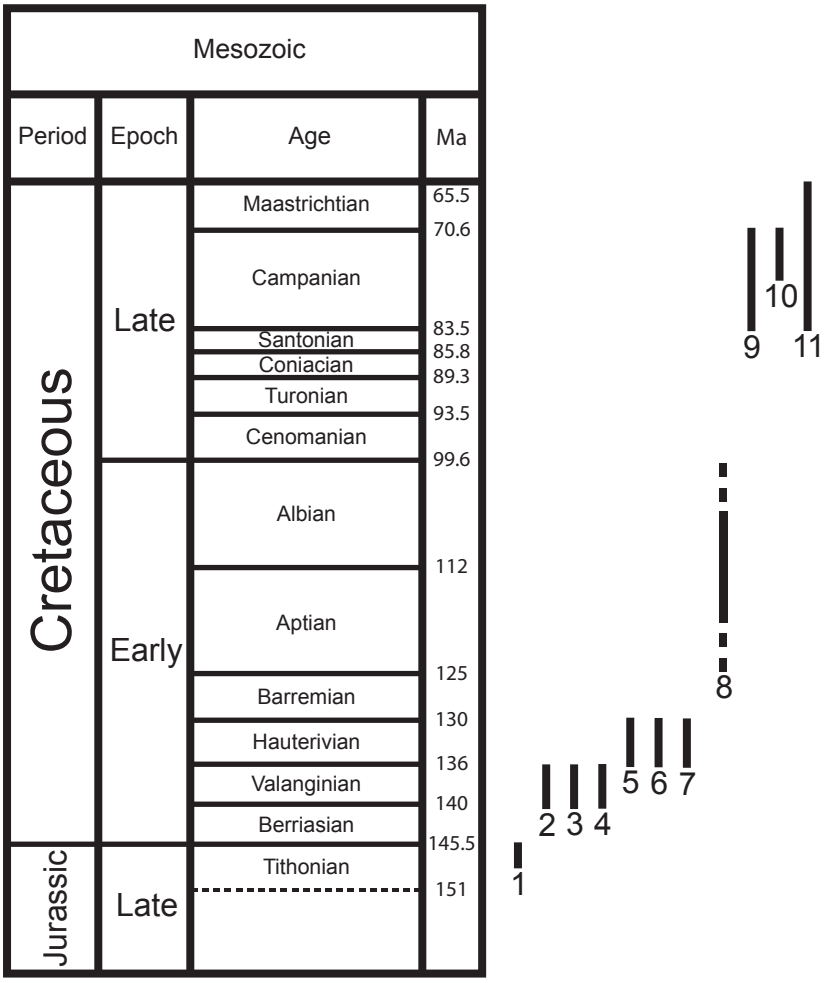

Figure 1. Stratigraphic ranges of the 11 deposits included in this study. The deposits include: (1) Paskenta, (2) Bear Creek, (3) Rocky Creek, (4) Little Indian Valley, (5) Wilbur Springs, (6) Wide Awake Mine, (7) Rice Valley, (8) Cold Fork of Cottonwood Creek, (9) Harrington Flat Road, (10) Romero Creek, and (11) Guenoc Ranch. Stratigraphic ranges are from Campbell (1995), Campbell et al. (2002), Hepper et al. (2004), and Kiel et al. (2008).

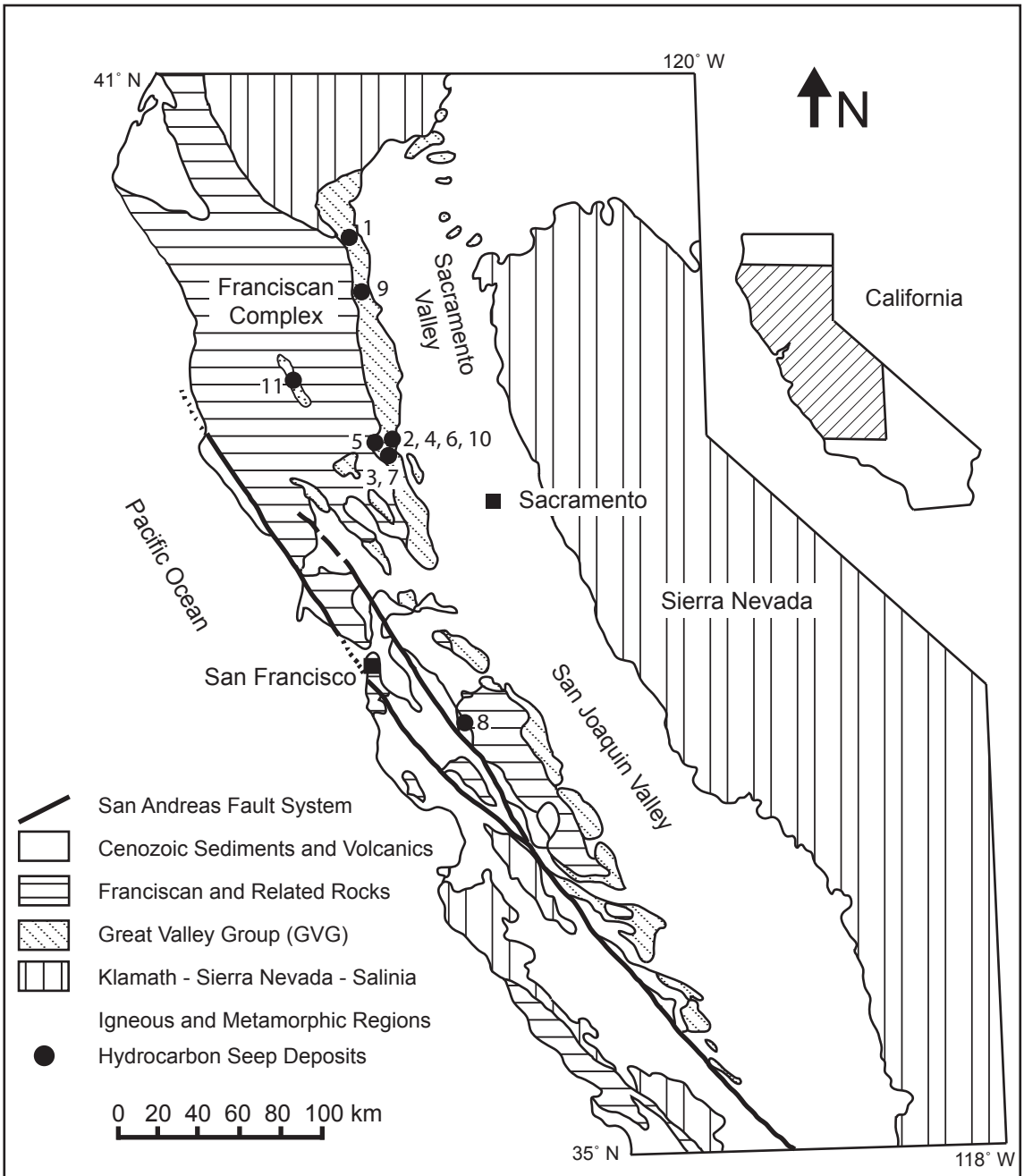

Figure 2A. Locality map for the eleven Mesozoic hydrocarbon seep localities included in this study. The localities include: (1) Cold Fork of Cottonwood Creek, (2) Wilbur Springs, (3) Guenoc Ranch, (4) Bear Creek, (5) Harrington Flat Road, (6) Little Indian Valley, (7) Rocky Creek, (8) Romero Creek, (9) Paskenta, (10) Wide Awake Mine, and (11) Rice Valley. Simplified geology of the western North American Continental margin, including from west to east, the Franciscan Complex, the GVG forearc strata, and the Sierra Nevada batholith. Map after Ingersoll (1978).

Figure 2B. Summary of stratigraphic nomenclature of the GVG forearc strata. Formations the hydrocarbon seeps occur in are in bold. After Lawton (1956), Page (1966), and others.

Period	Epoch	Age (Ma)	Age	Lawton (1956), Page (1966)	Ojakangas (1968)	Dickinson and Rich (1972)	Ingersoll and Dickinson (1981)
Cretaceous	Late	65.5-70.6	Maastrichtian	Not Exposed——Not Exposed——Not Exposed			
		70.6-83.5	Campanian	Forbes Fm. (northern GVG) or **Moreno Fm.** (southern GVG)	Unit VI	Rumsy	Rumsy Fm.
		83.5-85.8	Santonian	Guinda Fm.			
		85.8-89.3	Coniacian	Funks Fm.	Unit V	Cortina	Cortina
		89.3-93.5	Turonian	Sites Fm., Yolo Fm., Venado Fm.			
		93.5-99.6	Cenomanian	Fisk Creek Fm. Brophy Canyon Fm.	Unit IV	Boxer	Boxer
	Early	99.6-112	Albian	Davis Canyon Fm.	Unit III	**Lodoga**	**Lodoga Fm.**
		112-125	Aptian	Little Valley Fm.			
		125-130	Barremian	**Crack Canyon Fm.** / Grizzly Canyon Member		**Stony Creek**	**Stony Creek Fm.**
		130-136	Hauterivian	**Crack Canyon Fm.** / **Blue Ridge Member**			
		136-140	Valanginian		Unit II		
		140-145.5	Berriasian				
Jurassic	Late	145.5-151	Tithonian	Sulphur Cr. Fm. (Knoxville)	Unit I		

= exact contact unconfirmed

= contact variable due to poor/no exposure

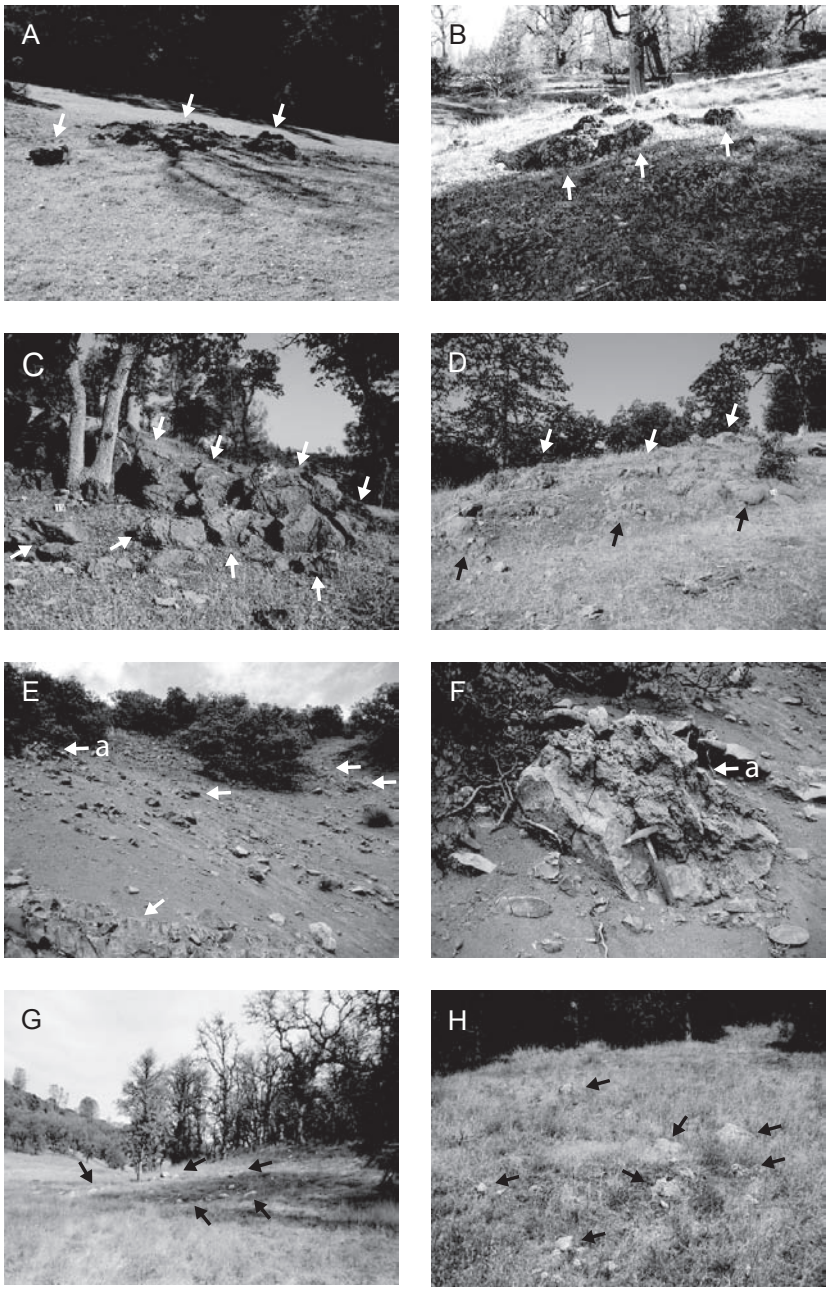

Figure 3. Outcrop variability in some of the hydrocarbon seep localities included in this study. (A-B) Harrington Flat Road, two of twenty roughly circular mounds (morphology type 2). (C-D) Cold Fork of Cottonwood Creek, ~300 m linear outcrop (morphology type 3). (E) Bear Creek, 32 m vertical succession of micarb lenses, pods, etc (morphology type 3). Micarb boulder with (a) and white arrow directed at it are blown up in figure F. (F) Bear Creek, close up of an *in situ* lens of micarb seen in (E) surrounded by GVG turbidites and concretions (morphology type 3). (G-H) Rocky Creek, low lying micarb outcrops (morphology type 1).

Figure 4. The overall paragenesis for the eleven localities. Division between early and late diagenetic stages is shown.

			Paskenta	Bear Creek	Rocky Creek	Little Indian Valley	Wilbur Springs	Wide Awake Ranch	Rice Valley	Cold Fork of Cottonwood Creek	Harrington Flat Road	Romero Creek	Guenoc Ranch
Early	1	Detrital-rich Micrite (Micrite 1), detrital grains ± metazoan activity	●	●	●	●	●	●	●	●	●	●	●
	1a	Peloids		o	o	●	o	●	△	●	●	△	●
	1b	Calcispheres	●	o	o	o	o	o	o	o	●	o	●
	1c	Pyrite framboids	●	●	●	●	●	●	●	●	●	●	●
	2	Corrosion Event 1 (CE1) ± pyrite	●	●	●	●	●	●	●	●	●	△	●
	3	Worm Tube Activity	●	o	o	o	△	△	△	o	o	△	o
	4	Yellow Calcite	●	o	o	●	o	o	△	●	●	△	o
	5a	Fibrous Calcite	●	●	●	●	●	●	●	●	●	△	●
	5b	Botryoidal Calcite		●	o	o	△	△	o	△	△	△	△
	5c	Dentate Calcite	●	●	o	●	●	o	o	●	●	△	△
	6	Clotted Microbial Fabrics		o	△	△	△	o	o	o	o	△	o
Late	7	Corrosion Event 2 (CE2)	●	△	△	△	o	△	△	●	△	△	△
	8	Siliciclastic Silt-Clay Fill	●	o	△	△	●	o	△	●	△	△	△
	9	Fracturing Event		△	△	△	o	o	△	o	o	△	o
	10	Sparry Calcite	●	●	●	●	●	●	●	●	●	△	●
	11	Neomorphosed Micrite	?	o	o	o	△	o	o	o	o	△	o
	12	Corrosion Event 3 (CE3)	△	△	△	●	△	△	△	△	△	△	△
	?	Transformation to dolomite	?	o	△	△	o	o	△	△	o	△	△

Key	
●	Major component
o	Minor component
△	Not present

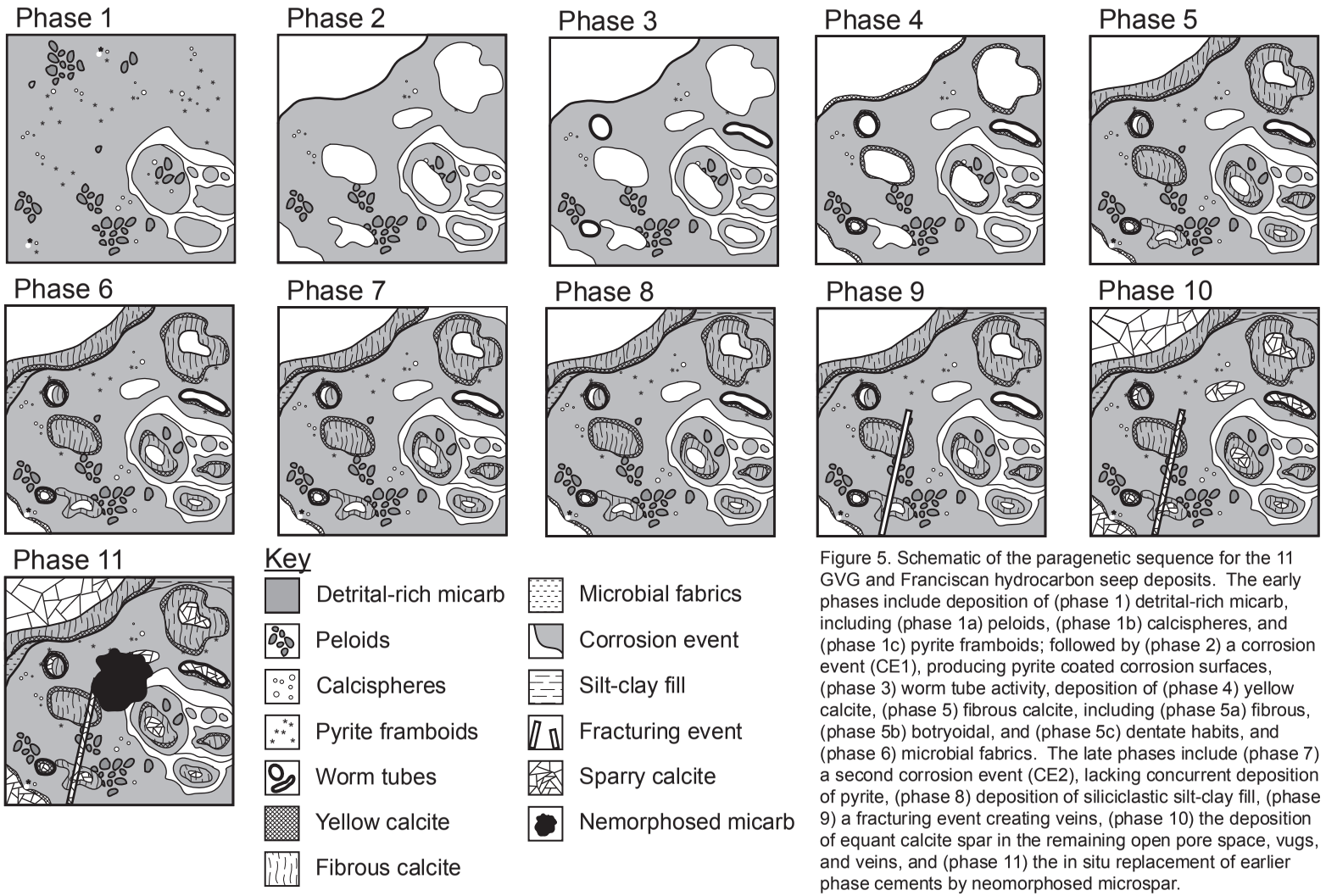

Figure 5. Schematic of the paragenetic sequence for the 11 GVG and Franciscan hydrocarbon seep deposits. The early phases include deposition of (phase 1) detrital-rich micarb, including (phase 1a) peloids, (phase 1b) calcispheres, and (phase 1c) pyrite framboids; followed by (phase 2) a corrosion event (CE1), producing pyrite coated corrosion surfaces, (phase 3) worm tube activity, deposition of (phase 4) yellow calcite, (phase 5) fibrous calcite, including (phase 5a) fibrous, (phase 5b) botryoidal, and (phase 5c) dentate habits, and (phase 6) microbial fabrics. The late phases include (phase 7) a second corrosion event (CE2), lacking concurrent deposition of pyrite, (phase 8) deposition of siliciclastic silt-clay fill, (phase 9) a fracturing event creating veins, (phase 10) the deposition of equant calcite spar in the remaining open pore space, vugs, and veins, and (phase 11) the in situ replacement of earlier phase cements by neomorphosed microspar.

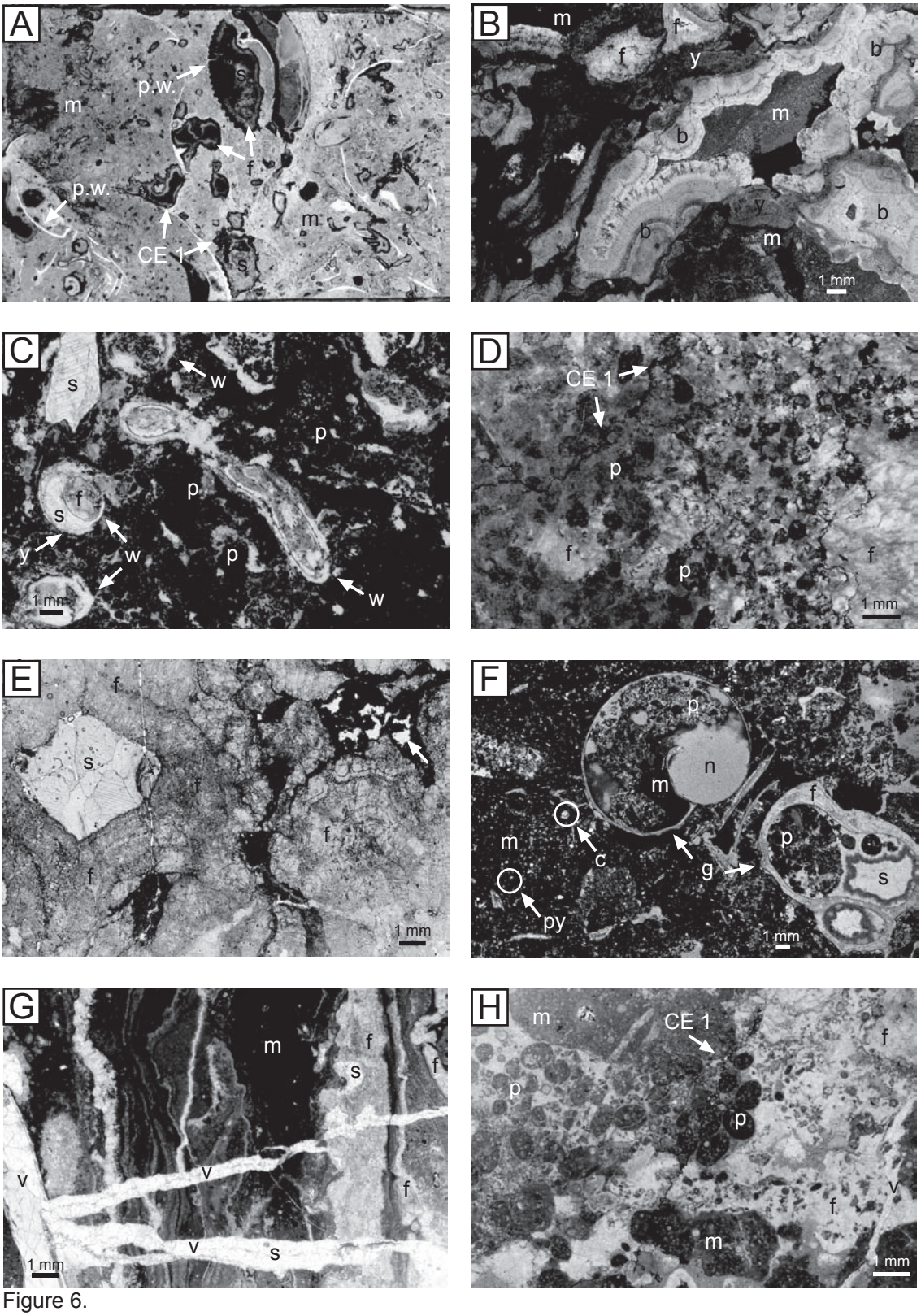
A
p.w.
s
m
f
p.w.
CE 1
s
m
B
m
f
f
y
b
b
m
y
b
b
m
1 mm
C
s
w
p
p
f
s
y
w
p
w
1 mm
D
CE 1
p
f
p
f
1 mm
E
f
s
f
f
f
1 mm
F
p
n
m
f
m
c
g
p
s
py
1 mm
G
m
f
s
f
v
v
f
v
s
1 mm
H
m
CE 1
f
p
p
v
f
m
1 mm
Figure 6.

Figure 6. Illustrations of petrographic textures, fabrics, and cements of the Franciscan and GVG hydrocarbon seeps. (A) White arrows point to fragments of the rhynchonellid brachiopod *Peregrinella whitneyi* (p.w.) encased in detrital-rich micarb (m) and filled with fibrous calcite (f) and sparry calcite (s). White arrows point to evidence of corrosion event 1 (CE1), which was later filled in by fibrous calcite and then by sparry calcite, WAM 3B, 2 x 3 in. (B) Horizons of fibrous calcite, botryoidal calcite (b) and anhedral yellow calcite (y) filling vugs and encrusting remnants of detrital-rich micarb, BC 3A. (C) White arrows point to worm tube fossils (w) in longitudinal and cross section, encased in peloid-rich (p) detrital-rich micarb, and filled with anhedral yellow calcite, fibrous calcite, and sparry calcite (s), HFR 13A. (D) Peloids encased in fibrous calcite and pyrite encrusted corrosion horizons (CE1), note the corrosion event cutting through the peloids (see white arrows), LIV 1DD. (E) Horizons of fibrous calcite filling porosity, followed by the deposition of sparry calcite, RV 2E. (F) Pyrite- and peloid-rich detrital-rich micarb, including pyrite framboids (py), calcispheres (c), peloids, and unidentifiable detritus, encasing gastropods (g, *Paskentana paskentaensis*) incompletely filled with fibrous and sparry calcite and replaced by neomorphosed micrite (n), BC 2A. (G) Successive horizons of detrital-rich micarb and fibrous calcite cross cut by late stage veins (v) filled with sparry calcite, WS 10B. (H) Peloids filled with detrital-rich micarb, with detritus including calcispheres and pyrite framboids, as well as fibrous calcite (dentate), late stage veins, and evidence of CE1, HFR 13B.

Figure 7. Isotope values for GVG and Franciscan seep deposits, N = 175

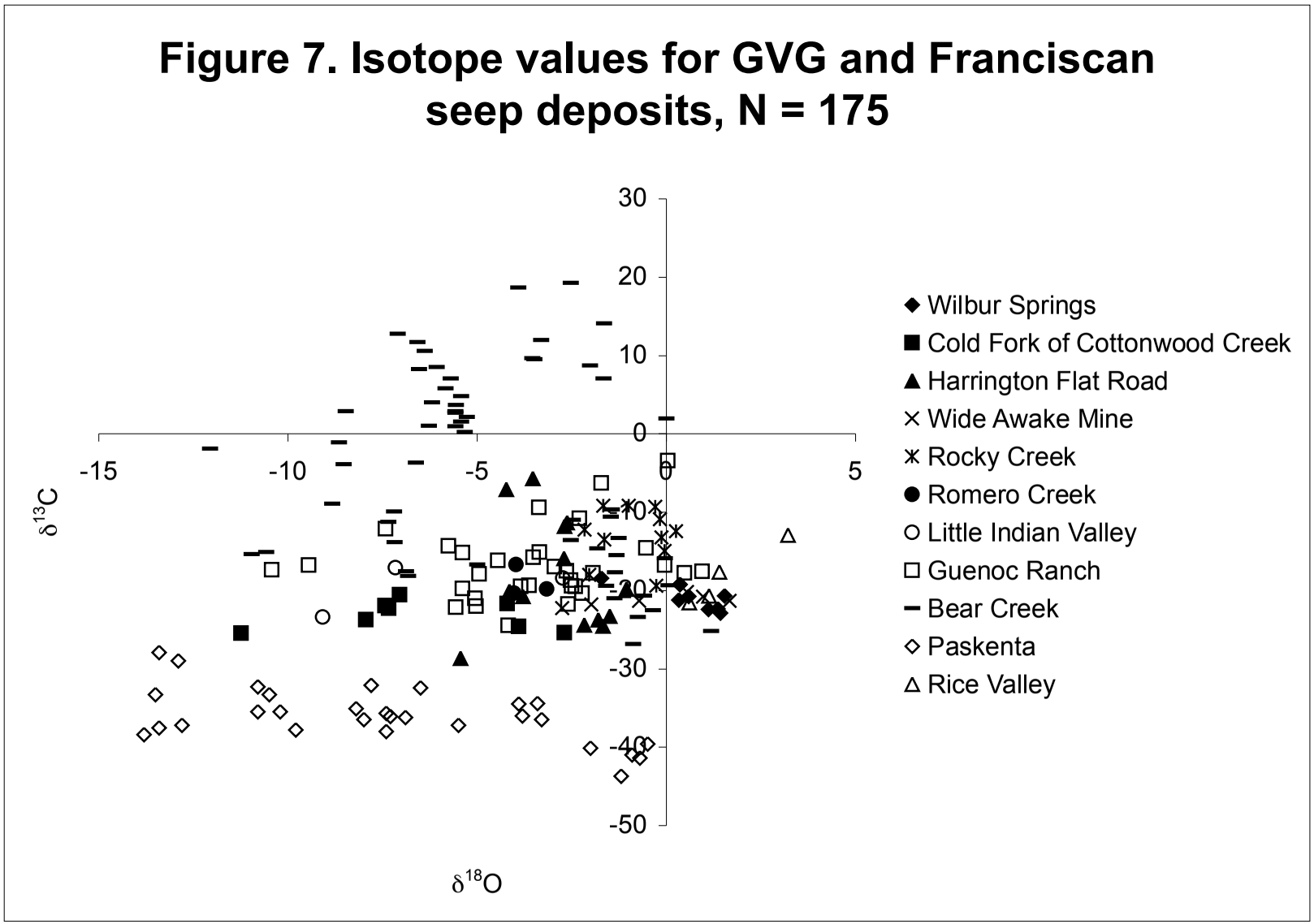

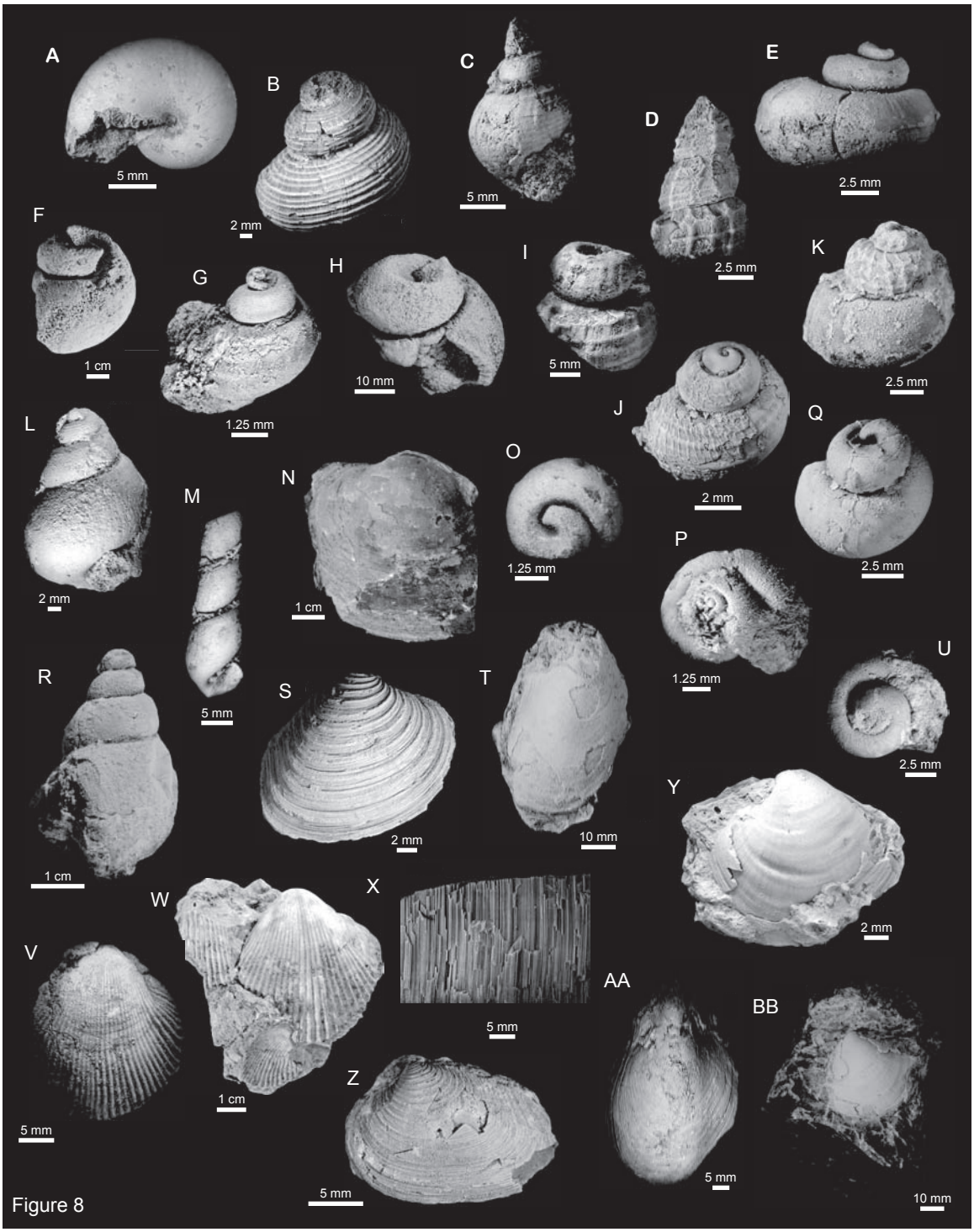
A
5 mm
B
2 mm
C
5 mm
D
2.5 mm
E
2.5 mm
F
1 cm
G
1.25 mm
H
10 mm
I
5 mm
J
2 mm
K
2.5 mm
L
2 mm
M
5 mm
N
1 cm
O
1.25 mm
P
1.25 mm
Q
2.5 mm
R
1 cm
S
2 mm
T
10 mm
U
2.5 mm
V
5 mm
W
1 cm
X
5 mm
Y
2 mm
Z
5 mm
AA
5 mm
BB
10 mm

Figure 8

Figure 8. Figure illustrating the fossils found at all of the localities, except for Paskenta. (A) *Phyllopachyceras*, BC; (B) *Paskentana paskentaensis*, LIV; (C) *Atresius liratus*, RC 9; (D) *Hokkaidoconcha occidentalis*, BC Z; (E) *Lithomphalus enderlini*, RC 1; (F) gastropod steinkern, RC 19; (G) L. enderlini, BC S; (H) gastropod steinkern, RC 19; (I) *A. liratus*, RC 9; (J) *P. paskentaensis*, BC; (K) *P. paskentaensis*, BC; (L) *Bathypurpurinopsis stantoni*, CFCC 12; (M) *Hokkaidoconcha*, HFR 18; (N) lucinid bivalve, BC S; (O) *Retiskenea*? *kieli*, RC; (P) *R.*? *kieli*, CFCC 30; (Q) gastropod steinkern, RC 19; (R) *B. stantoni*, CFCC; (S) *Astarte trapezoidalis*, BC; (T) unidentified long narrow bivalve, WS 16; (U) *Retiskenea*, WS 1; (V) *Peregrinella whitneyi*, WS; (W) *P. whitneyi*, WAM; (X) inoceramid prisms, fragment, HFR 10; (Y) Thyasirid bivalve, HFR 5; (Z) *A. trapezoidalis*, RC 9; (AA) unidentified long narrow bivalve, RC; and (BB) Thyasirid bivalve, HFR 5.

Figure 9. Stacked bar hisotogram illustrating relative abundance of each localities faunal assemblage

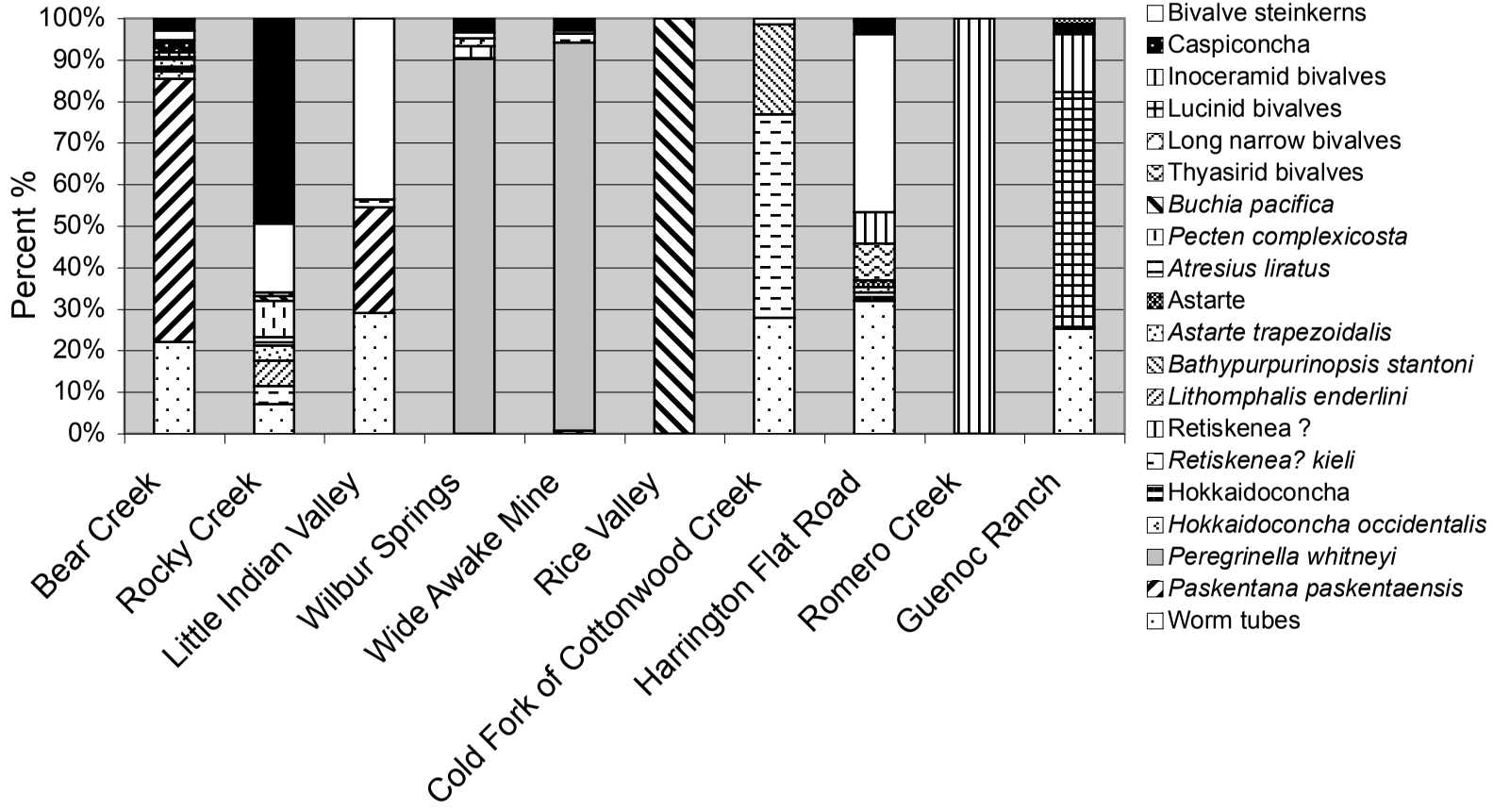

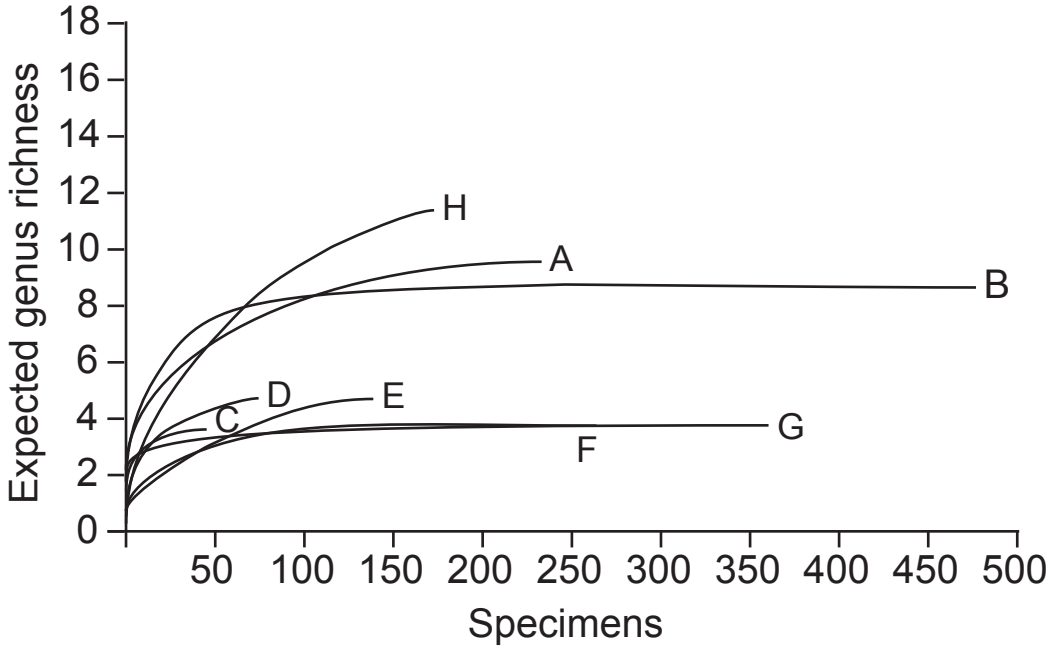

Figure 10. Rarefaction curves for the 8 hydrocarbon seeps with >1 taxon found during the course of this study. A. Harrington Flat Road, B. Rocky Creek, C. Little Indian Valley, D. Guenoc Ranch, E. Wide Awake Mine, F. Wilbur Springs, G. Cold Fork of Cottonwood Creek, H. Bear Creek. A, B, F and G, reach an asymptote indicating further sampling would not have increased the number of taxa recovered, while C, D, E, and H do not reach an asymptote and thus, further sampling would likely have recovered more taxa.

Table 1. Faunal abundance data collected in the laboratory via crack-outs for each of the 10 deposits (excluding Paskenta). Replicate bulk samples were collected throughout each locality, with ~1.3 kg of material processed from each sample bag. The number of samples processed per locality reflects the overall size of the deposit and the number of samples collected. Values included in this table represent the total number of specimens found of a taxon, throughout an entire locality.

Locality Diversity List and Abundances	**Bear Creek**	**Rocky Creek**	**Little Indian Valley**	**Wilbur Springs**	**Wide Awake Mine**	**Rice Valley**	**Cold Fork of Cottonwood Creek**	**Harrington Flat Road**	**Romero Creek**	**Guenoc Ranch**	**Total**
Worm tubes	38	34	16	0	0	0	100	76	0	20	**284**
Paskentana paskentaensis	109	0	14	0	1	0	0	0	0	0	**124**
Peregrinella whitneyi	0	0	0	242	129	0	0	0	0	0	**371**
Hokkaidoconcha occidentalis	3	0	0	0	0	0	0	0	0	0	**3**
Hokkaidoconcha	0	0	0	0	0	0	0	5	0	0	**5**
Retiskenea? kieli	1	21	1	0	3	0	176	0	0	0	**202**
Retiskenea? tuburculata	0	0	0	8	0	0	0	0	0	0	**8**
Lithomphalis enderlini	1	30	0	0	0	0	0	0	0	0	**31**
Bathypurpurinopsis stantoni	0	0	0	0	0	0	78	0	0	0	**78**
Astarte trapezoidalis	3	17	0	0	0	0	0	3	0	0	**23**
Astarte	0	0	0	0	0	0	0	4	0	0	**4**
Atresius liratus	0	10	0	0	0	0	0	0	0	0	**10**
Pecten complexicosta	0	42	0	0	0	0	0	0	0	0	**42**
Buchia pacifica	0	6	0	0	0	2	0	0	0	0	**8**
Thyasirid bivalves	0	0	0	0	0	0	0	21	0	0	**21**
Long narrow bivalve	0	4	0	5	0	0	0	0	0	0	**9**
Lucinid bivalves	1	0	0	0	0	0	0	0	0	45	**46**
Inoceramid bivalves	2	0	0	0	0	0	0	18	5	11	**36**
Caspiconcha	5	0	0	0	0	0	0	0	0	0	**5**
Bivalve steinkerns	4	80	24	4	1	0	5	102	0	0	**220**
Gastropod steinkerns	4	238	0	9	4	0	0	7	0	2	**264**
Phyllopachyceras	1	0	0	0	0	0	0	1	0	0	**2**
Didymoceras* or *Nostoceras	0	0	0	0	0	0	0	0	0	1	**1**
Unidentifiable ammonites	0	0	0	0	0	0	0	1	0	0	**1**
N =	**172**	**482**	**55**	**268**	**138**	**2**	**359**	**238**	**5**	**79**	**1798**

Table 2. Complete faunal list for the 11 GVG and Franciscan hydrocarbon seep localities. Identifications made during the course of this study are denoted with an X. Identifications made by Kiel et al. (2008) are denoted X[1], E.L. Ickes (1910) from the California Academy of Sciences collections by X[2], Stanton (1895) by X[3], Campbell (1995) by X[4], Bailey and Jones (1973) by X[5].

	Paskenta	Bear Creek	Rocky Creek	Little Indian Valley	Wilbur Springs	Wide Awake Mine	Rice Valley	Cold Fork of Cottonwood Creek	Harrington Flat Road	Romero Creek	Guenoc Ranch
Worm tubes	X[4]	X	X	X				X	X		X
Paskentana paskentaensis		X		X		X	X[3]				
Paskentana berryessaensis sp. nov.		X[1]									
Paskentana nov.		X[1]									
Amberleya dilleri Stanton	X[1]										
Amberleya morganensis			X[1]								
Hypsipleura	X[3]										
Cerithium sp.	X[3]										
Peregrinella whitneyi					X	X					
Cooperrhynchia	X[3]										
Hokkaidoconcha occidentalis	X[1]	X			X[1]						
Hokkaidoconcha morenoensis sp. nov.										X[1]	
Hokkaidoconcha bilirata sp. nov.					X[1]			X[1]			
Hokkaidoconcha		X							X		
Fusiform gastropod			X[1]								
Turbo					X[3]						
Retiskenea? *tuburculata*					X		X				
Retiskenea? *kieli*		X	X	X		X		X			
Lithomphalus enderlini		X	X								
Bathypurpurinopsis stantoni								X			
Astarte trapezoidalis		X	X						X		
Astarte									X		
Atresius liratus			X		X						
Pecten complexicosta			X								
Pecten					X[3]						
Modiolid pelecypod							X[3]				
Buchia pacifica		X	X				X				
Buchia inflata		X									
Buchia piochii	X[4]										
Buchia fischeriana	X[4]										
Nucula	X[3]										
Cardinopsis	X[3]										
Corbula	X[3]										
Solemya occidentalis	X[4]				X[3]						
Solemyidae										X[2]	
Thyasiridae									X	X[2]	
Lucinidae		X									X
Lucina colusaensis	X[4]				X[3]						
Lucina ovalis	X[4]										
Inoceramid fragments		X							X	X	X
Caspiconcha		X			X			X[3]			
Phyllopachyceras		X									X
Phylloceras	X[3]										
Leconteites c. *L. deansi*	X[5]										
Didymoceras or *Nostoceras*											X
Belemnites	X[3]						X[3]				

Table 3. Summarized characteristics for the 11 GVG and Franciscan hydrocarbon seep localities included in this study.

Locality Name	ID	Age	GPS Coordinates (UTM, NAD 83/WGS84)	Formation/Description	Litho-stratigraphy	Geotectonic/ Stratigraphic Context	Outcrop Description	Outcrop Size	$\delta^{13}C$ (‰)	$\delta^{18}O$ (‰)	Selected Citations
Paskenta	Pa	Middle to Upper Tithonian	Southeast 1/4 of section 25, T. 24 N., R. 7 W., USGS, 7.5 min., Paskenta Quadrangle	Stony Creek Formation	GVG	Convergent/ syn-sedimentary faults in forearc basin	Crops out in a thick succession of fine-grained GVG turbidites, as two low-relief, light gray carbonate mounds that in total are ~3 m thick and ~30.5 m long (Stanton, 1895; Campbell, 1995)	93 m^2: ~3 m thick and ~30.5 m long	-27.90 to -43.70	-0.10 to -13.90	Campbell (1993, 1995), Campell et al., (2002), Kiel et al., (2008)
Bear Creek	BC	Early Cretaceous (Valanginian)	10 551181E 4322704N	Crack Canyon Formation (informal name of Lawton 1956)	GVG	Convergent/ forearc	The carbonate is discontinuously interbedded with mudstone and fine-grained sandstone turbidites of the GVG forearc strata, characterized by a low sand-to-shale ratio, with each mudstone-sandstone couplet representing a single turbidite event. The individual sandstone layers have distinct bases and tops with no obvious coarsening/fining or thickening/thinning of beds upwards. Sporadically within the turbidites are 14 discontinuous horizons of variably fossiliferous carbonate cobbles, boulders, pods, and lenses that vary from 10 to 40 cm in thickness and 20 to 300 cm in length.	~ 32 m vertical succession	-14.63 to -26.82	-0.88 to -6.73	Kiel and Campbell (2005), Kiel et al., (2008)
Rocky Creek	RC	Early Cretaceous (Valanginian)	See Kiel and Campbell (2005)	Crack Canyon Formation (informal name of Lawton 1956)	GVG	Convergent/ forearc	Comprised of discrete light brownish-gray carbonate cobbles, boulders, and pods.	800 m^2	-19.40 to -12.25	0.26 to -1.66	Kiel and Campbell (2005), Kiel et al., (2008)
Little Indian Valley	LIV	Early Cretaceous (Valanginian?)	10 537222E 4325965N	Occurs in Little Indian Valley terrane	Franciscan	Convergent/ forearc	First noted by McLaughlin et al. (1989) as an isolated occurrence of fossil-rich carbonate surrounded by light-colored argillaceous deposits, and subsequently by Kiel et al. (2008) as a hydrocarbon seep. It crops out in the Little Indian Valley Terrane of the Franciscan Complex and consists of small, gray, cobbles and boulders	100 m^2	-17.12 to -23.40	-2.73 to -9.07	McLaughlin (1989), Kiel et al., (2008)
Wilbur Springs	WS	Early Cretaceous (Hauterivian)	10 550449E 4320227N	Stony Creek Formation	GVG	Convergent/ atop serpentinite diapirs in forearc basin	Crops out in diapir-associated sedimentary serpentinites, within undifferentiated turbidites of the GVG forearc strata (Campbell et al., 1993; Campbell et al., 2002)	2,500 m^2	-18.43 to -24.30	1.42 to -1.79	McLaughlin (1989), Campbell (1993, 1995), Campell et al., (2002), Kiel et al., (2008)
Wide Awake Mine	WAM	Early Cretaceous (Hauterivian)	10 549491E 4320049N	Stony Creek Formation	GVG	Convergent/ forearc	The carbonate crops out as small light gray to dark tan carbonate cobbles dominated by detrital-rich micarb	100 m^2	-20.20 to -22.27	0.98 to -2.74	McLaughlin (1989)
Rice Valley	RV	Early Cretaceous (Hauterivian)	10 512567E 4354487N	Unnamed marine strata (R. J. McLaughlin, pers. comm.)	In GVG outlier within Franciscan	Convergent/ atop serpentinite diapirs in forearc basin	Deposit was first mapped by Berkland (1973) and crops out in unnamed marine siliciclastics of the GVG forearc strata (R.J. McLaughlin, pers. comm.). The carbonates were described by Berkland (1973) as "coquinoid pale-gray limestone lenses" cropping out of greenish-gray shales interbedded with fine-grained sandstones. It was later documented by Campbell (1995), although Campbell found only minor outcrops.	unknown	-12.95 to -21.54	3.21 to 0.61	Campbell (1995), Kiel et al., (2008)
Cold Fork of Cottonwood Creek	CFCC	Early Cretaceous (Aptian to Albian)	10 526921E 4446205N	Lodoga Formation	GVG	Convergent/ syn-sedimentary faults in forearc basin	Lens of light gray carbonate cropping out along syn-sedimentary faults and surrounded by fine-grained sandstone and mudstone deposits of the GVG forearc strata	6,000 m^2: (~300 m long, ~20 to ~40 m wide, and ~1 to ~2 m tall)	-20.10 to -24.90	-2.60 to -11.20	Campbell (1993, 1995), Campell et al., (2002), Kiel et al., (2008)
Harrington Flat Road	HFR	Late Cretaceous (Campanian)	10 522413E 4301428N	Unnamed marine strata	GVG	Convergent/ forearc	Comprised of 20 roughly circular to elliptical mounds, varying in size from a maximum of 142.1 m^2 to a minimum of 5.57 m^2. The mounds crop in unnamed marine siliciclastics of the GVG forearc strata (R.J. McLaughlin, pers. comm.). At the northwest end of the locality, instead of mounds, the carbonate crops out as conduits and chimneys that are devoid of fossils.	10,075 m^2	0.17 to -28.62	-1.12 to -5.43	R. J. McLaughlin (pers. comm.)
Romero Creek	RmC	Late Cretaceous (Late Campanian)	10 672566E 4110291N	Moreno Formation	GVG	Convergent/ forearc	Is comprised of discontinuous light-gray carbonate float and two outcrops of *in situ* carbonate cobbles and boulders. The two *in situ* outcrops are situated at the northern and southern portions of the deposit and are likely a single horizon, with Cenozoic alluvium obscuring their relationship. The float sits above this alluvium horizon.	83,612 m^2	-16.48 to -20.34	-3.16 to -4.02	K. A. Campbell (pers. comm.), Kiel et al., (2008)
Guenoc Ranch	GR	Late Cretaceous (Campanian to Maastrichtian)	10 541228E 4286088N	Sediment gravity flow deposits representing various facies of a submarine fan complex	GVG	Convergent/ forearc	Light gray carbonate pods cropping out in slumped GVG sediment gravity flow deposits consisting of interbedded wackestone, shale, and clast-supported pebble-to-pebble conglomerates (Ojakangas, 1964; Dickinson and Seely, 1979)	2 km x 4 km	-3.41 to -24.50	0.48 to -10.42	Hepper et al., (2003), Hepper (2004)

Chapter 2

Diversity Patterns in Great Valley Group Hydrocarbon Seep Deposits, northern California, U.S.A.

Abstract

Ancient hydrocarbon seeps typically crop out as single, isolated, laterally discontinuous units that correspond to a discrete period of hydrocarbon expulsion. Research on these ancient deposits has largely focused on general locality characterization, with faunas being limited to diversity lists.

Approximately twenty regions of hydrocarbon seepage are now known to crop out of the GVG forearc strata and the Franciscan Complex in northern and central California. These deposits are spatially and stratigraphically constrained, cropping out over 700 km^2 and from the Late Jurassic to the Latest Cretaceous. This study examines the faunal distribution patterns within 10 morphologically variable and stratigraphically discrete hydrocarbon seep deposits from the GVG forearc strata, addressing species richness, diversity, and abundance patterns in greater detail at four of them. There is a surprising degree of heterogeneity between the 10 localities and this heterogeneity is clearly not driven by deposit size, age, or location. Additionally, the GVG and Franciscan faunas do not exhibit patterns of zonation or clusters characterized by higher diversity, however, there is a distinct order to the arrival of the faunal community, separated by a high flux of hydrogen sulfide expulsion and which is consistent at

all localities. In general, these seeps are less mature than typical modern seeps, with this immaturity closely related to variable rates and volumes of fluid advection.

1. Introduction

The deepest parts of the marine realm have drawn the interest of scientists for generations, however, it has only been in recent years that we have been able to access these extreme depths and study the organisms found there. With the aid of new technologies, we have discovered that life in the oceans is unevenly distributed; some parts are astonishingly productive and diverse while others appear to be nearly barren. One of the most surprising discoveries has been hydrocarbon seeps and their associated chemosymbiosis-based ecosystems, which flourish well below the photic zone and under extreme conditions of low oxygen levels, high pressures, and cold temperatures.

Seeps have been documented throughout modern oceans (Levin 2005) and are fundamentally different from most other marine ecosystems, except for hydrothermal vents, which both use a limited and localized source of energy that produces a highly ephemeral and variable environmental setting. The two differ in that hydrocarbon seeps mostly occur along continental margins, where methane and hydrogen sulfide seep out of oceanic sediments at ambient seawater temperatures, while hydrothermal vents are oceanic hot springs found

in volcanically active areas where hot (up to 400˚ C) mineral and hydrogen sulfide-laden water is violently emitted from fissures along mid-ocean ridges.

Hydrocarbon seeps are intimately coupled to the seepage of methane and hydrogen sulfide at the seafloor, commonly hosting complex chemoautotrophic communities nourished by the chemicals dissolved in the seeping fluids. Chemosynthetic archaea form the base of the food chain and transform the advecting fluids into useable organic nutrients for themselves, as well as for the macrofaunal communities above them in the food chain.

Modern hydrocarbon seep faunal communities are variably structured, ranging from zoned to patchy, with the biological zones and patches relating to changes in pore water chemistry, alkalinity, oxygen levels and oxygen penetration, as well as the rates and volumes of advecting fluids (Sibuet and Olu 1998, Levin 2005). Concentric (circular) zonation of faunas has been noted at many modern localities, such as at Hydrate Ridge off the coast of Oregon (Sahling et al. 2002), in Monterey Bay off the coast of California (Barry et al. 1997, Rathburn et al. 2003), and at mud volcanoes near the Barbados accretionary prism (Olu et al. 1997), among others. The central areas of these seeps are characterized by higher volumes of fluid advection and are surrounded by bacterial mats (Levin 2005). As distance from the central area increases, the faunas change according to their species specific fluid flux, oxygen level, and chemical preferences (Levin 2005). At the other end of the spectrum, fluid

advection can also be temporally and spatially inconsistent, resulting in patchy distributions of the associated communities (Sibuet and Olu 1998).

Variability in faunal distribution and species richness are coupled to the longevity, as well as the rate and volume of fluid advection, with diversity being a predictor of locality maturity (Sibuet and Olu 1998). The most mature localities are those that are the largest and which have the highest diversities. They are typically characterized by continuous fluid advection at high rates and volumes and commonly exhibit concentric zonation or large clusters of fauna with high diversity. The least mature localities are those that are the smallest and that have the lowest diversities, commonly exhibiting no faunal distribution patterns. These immature localities are often associated with spatially and temporally patchy or short lived fields of fluid expulsion (Sibuet and Olu 1998). Establishment of a mature ecosystem is thought to be possible only if the field is sustained by constant and protracted fluid flow (Sibuet and Olu 1998).

Characterizing modern seep community structure has been challenging due to the difficulty of accessing them on the seafloor and in sampling them without disturbing the communities of interest. Each study of these modern communities records only a geologic snapshot of that community and what came before or comes after in its life history is difficult, if not impossible, to ascertain. Ecological succession, although expected, is difficult to establish when only seeing temporal snapshots of the communities under study. Unlike the modern, however, seeps in the stratigraphic record are easier to access yet also preserve

fossils *in situ*. Due to their time-averaged nature, fossilized seeps preserve nearly complete records of their faunal histories, providing natural laboratories for evaluating ecological succession of biomineralized seep communities and for addressing seep maturity and its relationship to diversity and faunal distribution.

A particularly good record of ancient hydrocarbon seep deposits crop out in Mesozoic strata (Tithonian-Maastrichtian) along the western North American continental margin. These deposits are a by-product of the active tectonics of the region, which created the ideal setting for the production, accumulation, migration, and subsequent venting of hydrocarbon-rich fluids at the seafloor. In this study, the paleoecological signatures of 10 hydrocarbon seep deposits are documented, including Wilbur Springs (WS), Wide Awake Mine (WAM), Romero Creek (RmC), Rice Valley (RV), Guenoc Ranch (GR), Little Indian Valley (LIV), Bear Creek (BC), Rocky Creek (RC), Cold Fork of Cottonwood Creek (CFCC), and Harrington Flat Road (HFR, Figure 1). Four of these deposits, including CFCC, BC, HFR, and RC are also examined in greater detail to assess within seep macrofaunal distribution patterns. The purposes of this study are to deconstruct the paleoecological signatures preserved at these 10 localities and to determine, using the data collected at the four singled out deposits, if the systematic pattern of ecological succession and faunal distribution, exemplified in modern seep communities, also typifies ancient seep assemblages and to address if, as with modern seeps, diversity is proportional to seep maturity.

2. Geological Setting and Study Areas

The geologic evolution of the northern Californian region is interpreted as an Andean-style arc and trench system that resulted in the development of three broad tectonic provinces, including the Franciscan Accretionary Complex of the Coast Ranges to the west, the Sierra Nevada batholith to the east, and the GVG forearc strata in between (Godfrey et al. 1997, Dickinson 2008), with the relative timing of formation including the coeval deposition of 12,000 m of GVG and Franciscan sediments (Ingersoll 1978a, Blake and Jones 1981). The GVG succession is comprised of well-bedded mudstone and siltstone deposits derived from submarine slope turbidites, sandstone and conglomerate deposits derived from granitic basement of the Sierran and Klamath regions (Blake and Jones 1981, Bertucci 1983), as well as variable deposits of hydrocarbon seep carbonate.

The Franciscan Complex is the most westerly of the three tectonic provinces, forming as an accretionary prism when the Farallon plate subducted eastward beneath the western margin of the North American craton (Hamilton 1969, Dickinson 2008, Ernst et al. 2008). It is subdivided into three terranes, which are comprised of basaltic pillow flows, pillow breccias, and tuffs intruded by diabase sills, mudstone and sandstone, with thick lenses of polymict conglomerate and minor shale, greenstone, bedded chert, and limestone, commonly separated by zones of mélange (Swe and Dickinson 1970, Blake and Jones 1981, Blake and McLaughlin 1989). Today, the Franciscan trends NNW

and forms a complexly deformed region that structurally underlies a less-deformed upper plate of GVG forearc strata (Hamilton 1969, Swe and Dickinson 1970), bounded by the San Andreas Fault to the east and by the Coast Range Fault to the west.

Strata of the GVG began accumulating in the Late Jurassic. The sediments were deposited in the elongate forearc basin above the Coast Range Ophiolite and adjacent to the active Klamath-Sierran arc complex and Sierra Nevada batholith to the east and the Franciscan Accretionary Complex of the Coast Ranges to the west (Swe and Dickinson 1970, Blake and Jones 1981, Dickinson 1981, Blake and McLaughlin 1989). Sediment deposition continued until the end of the Cretaceous, by which time the forearc basin had filled nearly to sea level and the subduction complex had migrated westward and the magmatic arc had migrated eastward (Ingersoll 1978a, Dickinson and Seely 1979, Ingersoll 1982, Dickinson 2008).

Today, Upper Jurassic through Lower Cretaceous strata of the GVG are exposed along the west side of the Sacramento Valley and predominantly consist of basin plain and outer fan deposits (Ingersoll 1978b, Constenius et al. 2000) that form an asymmetric syncline with a steeply east-dipping west limb (Godfrey et al. 1997). Upper Cretaceous strata crop out nearly continuously along the length of the Sacramento and San Joaquin Valleys (Ingersoll 1978b), comprising sediments that were principally sub-sea fan turbidites that prograded into the forearc trough from eastern sources in the arc massif (Dickinson 1981).

Recent work has documented the presence of approximately seventeen regions of hydrocarbon seepage throughout the GVG forearc strata (Campbell et al. 2002, Kiel et al. 2008), with perhaps up to several hundred remaining to be found. These deposits crop out in a narrow band spanning northern and central California (~700 km x 100 km), from Red Bluff to Santa Barbara. Petrographically and isotopically all 10 deposits fall into known ranges for hydrocarbon seep derived carbonate, including previously sampled GVG hydrocarbon seep deposits (e.g., Campbell et al. 2002, Hepper 2004, Kiel et al. 2008; Table 1).

3. Materials and Methods

In order to characterize the morphology of the outcrops, as well as their faunal assemblages, each of the 10 deposits was mapped and replicate bulk samples, were collected throughout each locality, for later petrographic and faunal analyses, with each sample filling one sample bag (4,500 cm^3). Standard sedimentological (e.g., clastic texture, degree of sorting, rounding of grains, fabric, diagenetic features, etc), stratigraphic (e.g., beds and bedding, grading of turbidites, depositional bed forms and structures, etc), and paleontologic (e.g., species richness, abundance, etc) data were recorded in the field, with an emphasis on facies criteria (e.g., lithology, rock colors, grain size and shape, particle types, bedding and lamination, sedimentary structures and textures, fossil content, stratigraphic and structural relationships, geometry of carbonate

bodies, etc; Flügel 1982). Taphonomic data was recorded to assess mechanical or biological degradation, lithification, and/or chemical dissolution of skeletal aragonite (e.g., Titschack and Freiwald 2005), while the amount of fragmentation and abrasion was recorded for interpretation of amount of transport. Where available, bivalved shells were used to determine whether the assemblage was preserved in life position. Close packing of fossil concentrations, along with orientation and evidence of sorting were used to interpret the amount of energy in the original depositional environment. However, due to weathering of outcrop surfaces and the small size of a number of the GVG seep taxa, the point counts generally led to an underestimate of assemblage density and diversity, as determined once material was returned for study in the laboratory.

Due to the dissimilar outcrop morphologies of the four deposits addressed in greater detail, characterization, mapping, and sampling methods were modified to extract the most useful and directly comparable data from each. At the CFCC deposit, the goal was to collect replicate bulk samples and map the deposit at 10 m intervals, documenting the size, shape, and distribution of the carbonate and the fossil assemblages within each segment. Outcrop availability was highly variable and consequently, 10 m intervals were not always feasible; therefore, replicate bulk sampling and mapping, although averaged every 10 m, was adjusted based on outcrop availability (Figure 2). At BC, 14 small seeps were documented vertically over a 32 m interval, for which a stratigraphic column was compiled (Figure 3). Replicate bulk samples were collected from each seep,

documenting its overall size and shape, as well as the distribution of its fossil assemblage. The HFR deposit consists of twenty circular to elliptical mounds cropping out in a single stratigraphic interval. The location of each mound was mapped and their sizes, shapes, and fossil assemblages were documented (Figure 4). Replicate bulk samples were collected at each mound for later faunal analyses. Finally, the RC deposit, which consists of 800 m^2 of microcrystalline carbonate (micarb) cobbles, boulders and pods cropping out in a single stratigraphic interval, was gridded, with each square measuring 1 m to a side. In each square, each micarb outcrop >15.25 cm in diameter and demonstrating no evidence of transport, was numbered and mapped (Figure 5). Forty-three individual outcrops were mapped and the size, shape, and distribution of the micarb and the fossil assemblages within each outcrop were recorded. Replicate bulk samples were collected at each of the forty-three outcrops for later faunal analyses.

In the laboratory, hand-samples were cut and polished to reveal cross-sectional views. Twenty-five to 30 thin sections (30 to 70 microns thick), representative of sedimentary surfaces, cements, textures, microbial fabrics, matrix material, and shell material were made for each locality (300-350 thin sections in total). Thin sections were used for both petrographic and isotopic analyses and were analyzed on a Boreal Polarizing Microscope using plane-polarized and cross-polarized light. Standard petrographic analyses were performed and a paragenetic sequence, divided into early and late stage events,

was compiled for each locality. This sequence was used to determine relative timing and order of arrival of the faunal communities.

Bulk samples were used for taxonomic identification and to calculate faunal assemblage relative abundance through assemblage point-counts and for establishing assemblage diversity to obtain an estimate of taxonomic contribution to each locality. Abundance data (Table 2) was collected via crack-outs and a dissecting microscope. Material preserved as steinkerns or identifiable only to class or ordinal level was also counted. Identifications were made primarily on the basis of descriptions and figures in Stanton (1895), Anderson (1938), Kiel and Campbell (2005), Campbell et al. (2008), and Kiel et al. (2008).

3.1 *Paleoecological Measures*

All paleoecological measures were calculated using the statistical program PAST (PAlaeontological Statistics; Hammer et al. 2001, Hammer and Harper 2006) and all definitions are from Hammer et al. (2001) and Hammer and Harper (2006). Initially, diversity indices were calculated using abundance data, including species richness (S, generally equivalent to alpha diversity), a measurement of the number of species present in a sample at a given horizon or locality and relative abundance, a measurement of the number of organisms of a particular kind as a percentage of the total number of organisms of a given area or assemblage. When calculating biodiversity indices, it is important to remember that the count of species richness in a sample will usually be an underestimate for total taxonomic richness, as sample species richness generally

increases with sample size, thus, the Menhinick and Margalef indices, which are measures of taxon richness developed for extrapolation of rarefaction curves, were also taken into consideration because unlike species richness, they attempt to compensate for this effect. Additional indices used include the Shannon diversity index (H), which takes into account the number of individuals as well as the number of taxa (varying from 0 for assemblages with only a single taxon to values up to 5.0 for assemblages with many taxa, each with a few individuals), the Berger Parker diversity index, which measures degree of dominance and evenness within an assemblages, and the Fisher alpha diversity index, which although does not in itself contain relative abundances, assumes that they are distributed according to a logarithmic abundance model. These indices are valuable because they evaluate sample richness, as well as the combination of richness and evenness by incorporating relative abundances of taxa, which minimizes sample size bias.

Similarity and distance indices were used to measure the similarity of the taxon compositions of two samples, potentially suggesting shared environmental settings. To measure the similarity between different horizons within a locality, association, similarity, and distances indices were calculated on the basis of a presence-absence matrix. The indices used include the Bray-Curtis and the Jaccard, which established which localities or horizons grouped together based on their faunal makeup. These association similarity and distance indices also provided distances for cluster analysis, making it possible to create Q-mode

cluster diagrams, which were used to find groupings of localities that could then be interpreted in terms of biogeography or paleoenvironment.

4. Deposit Descriptions

Hydrocarbon seep deposits of northern and central California occur as heavily weathered, variably sized, discrete, fossiliferous units eroding out of the marine siliciclastics of the GVG and Franciscan Complex. The 10 study deposits reveal variable outcrop morphologies, some of which are illustrated in Figure 6 and which include the following three primary morphologies: (1) individual carbonate cobbles (≤ 15.25 cm across), boulders (≥ 15.26 cm), pods (clusters of cobbles and boulders), and/or lenses (10 to 40 cm thick and 20 to ≥ 300 cm long); (2) discrete, roughly circular to elliptical carbonate mounds (ranging from 142.1 m^2 to a minimum of 5.57 m^2); and (3) vertical or linear carbonate outcrops that extend continuously or discontinuously, from a few meters to hundreds of meters in length. Differential erosion between the more resistant carbonate and the surrounding host turbidites has left the outcrops as isolated topographic highs on the landscape, surrounded by Cenozoic alluvium, usually without any stratigraphic context.

These 10 deposits are stratigraphically discrete and temporally constrained and differ in faunal composition, size, and outcrop morphology. The four chosen for more in-depth analysis were selected specifically due to their considerable morphological differences, their large sizes, as well as due to their

abundant faunal assemblages. Descriptions of the 10 deposits are included in Table 1, while variability between the four addressed in greater detail are described here.

Cold Fork of Cottonwood Creek is a ~300 m long, ~4 to ~32 m wide, and ~1 to ~2 m high, large, gray, variably exposed, micarb outcrop that was deposited between the Albian and Aptian, in the Middle Cretaceous. The outcrop is comprised of large, nearly continuous micarb lenses, broken by short expanses with no visible exposure. The micarb strikes northwest to southeast and is exposed along a low ridge surrounded by fine-grained sandstone and mudstone deposits of the GVG forearc strata (Campbell and Bottjer 1993).

Bear Creek is a multiple seep system deposited in the Valanginian. The deposit is comprised of 14 discrete seepage events of micarb cobbles, boulders, and lenses varying from 10 to 40 cm in thickness and from 20 to 300 cm in length, cropping out over a 32 m interval. Each of the 14 seeps are interbedded with mudstone and fine-grained sandstone turbidites of the GVG forearc strata. These submarine slope turbidite deposits are characterized by a low sand-to-shale ratio, with each mudstone-sandstone couplet representing a single depositional event. The individual sandstone layers have distinct bases and tops with no obvious coarsening/fining or thickening/thinning of beds upwards. The turbidite beds are often cemented with calcium carbonate, resulting in erosion-resistant cliff-forming beds.

Harrington Flat Road is a variably fossiliferous Campanian aged hydrocarbon seep deposit that crops out over 12,000 m^2, in unnamed marine siliciclastics of the GVG forearc strata, in a single stratigraphic interval (R.J. McLaughlin, pers. comm.). The deposit consists of twenty roughly circular to elliptical, light to dark gray micarb mounds. The twenty mounds vary in size from a maximum of 142.1 m^2 to a minimum of 5.57 m^2, deposits of Cenozoic alluvium obscure the precise relationships between the mounds (one continuous deposit with topographic highs visible at the surface vs. discrete unconnected deposits).

Rocky Creek, also a Valanginian deposit, consists of forty-three closely associated, discrete, variably fossiliferous micarb cobbles, boulders, and pods cropping out over 800 m^2, in a single stratigraphic interval. The outcrops range from 5.94 m^2 and 0.01 m^2, with overlying Cenozoic alluvium obscuring the precise relationship between the outcrops (one continuous deposit with topographic highs visible at the surface vs. discrete unconnected deposits).

5. Petrography

The unique nature of the hydrocarbon seep depositional environment produces a distinct suite of petrographic features that occur in a predictable paragenetic sequence, reflecting the changing chemistry of the depositional to burial environments (cf. Harris et al. 1985). Relevant seep-related petrographic features are present throughout most samples in this study and demonstrate that despite stratigraphic and spatial segregation, as well as variable local conditions,

remarkably similar petrographic and paragenetic signatures developed (cf. Beauchamp and Savard 1992, Godfrey et al. 1997, Campbell et al. 2002, Barbieri and Cavalazzi 2005, Peckmann et al. 2007).

The typical sequence of paragenesis of the GVG and Franciscan hydrocarbon seep carbonates can be divided into early seafloor and late diagenetic phases, with the earliest phases (phases 1-4) precipitating in conjunction with macrofaunal activity (Figure 7). The early phases include deposition of (1) detrital-rich micarb, including (1a) peloids, (1b) calcispheres, and (1c) pyrite framboids; followed by (2) a corrosion event (CE1), (3) worm tube activity, and (4) deposition of yellow calcite, (5) fibrous calcite, including (5a) fibrous, (5b) botryoidal, and (5c) dentate habits, and (6) microbial fabrics. The late phases include (7) a second corrosion event (CE2), (8) ± deposition of siliciclastic silt-clay fill, (9) a fracturing event creating veins, (10) the deposition of equant calcite spar in the remaining open pore space, vugs, and veins, and (11) the *in situ* replacement of earlier phase cements by neomorphosed microspar. Although there is some variability within the later phases of the paragenetic sequence, after examining ~300 thin sections, this paragenetic sequence characterizes all 10 of the localities.

In the early diagenetic phases, micarb pervasively fills the pore spaces of the marine sediments and encases abundant seep fossils, including articulated and disarticulated bivalves and brachiopods, gastropods, ammonites, and shell hash. Micarb precipitation (phase 1) occurs because sulfate reduction, coupled

to the anaerobic oxidation of methane causes an increase in alkalinity (Ritger et al. 1987, Paull et al. 1992). All faunas, excepting worm tubes, arrived during this earliest phase (concurrent with phase 1) of seep formation, followed by the colonization by worm tubes (phase 3) at 6 of the 10 localities. The presence of pyrite framboids in the micarb indicate that the early phase events (phases 1-3) precipitated in anoxic sediments, likely at or below the sediment-water interface and were linked to the anaerobic oxidation of methane and sulfate reduction (Berner 1970, 1984, Beauchamp and Savard 1992). These phases culminated in CE1 (phase 2) and in the creation of pyrite coated corrosion surfaces and suggest an increased flux of hydrogen sulfide into the system. This flux occurred due to continued sulfate reduction in the sediments, which depleted pore water sulfate concentrations, and caused the build up of hydrogen sulfide in the pore water. The hydrogen sulfide subsequently diffused out of the sediment (Berner 1970), resulting in localized acidic conditions, causing CE1 (phase 2) to occur. Worm tubes were introduced into the community at this time, indicated by their encrustation by anhedral yellow calcite (phase 4), which indicates that worm tube colonization (phase 3) occurred successive to the other faunas, however, were still confined to the earliest stages of seep formation. Subsequent to these phases, the system transitioned to aerobic conditions, as indicated by the lack of organic matter and pyrite in the later paragenetic phases (phases 5 through 10).

6. Paleontology

Fossils were collected at all 10 localities. The faunal assemblages are populated by eighteen taxa (Tables 1, 2), including five clades: brachiopods (at WS, WAM), gastropods (at BC, HFR, WS, WAM, GR, LIV, RC, CFCC), bivalves (at BC, HFR, RV, RmC, LIV, GR), ammonites (at GR, BC, HFR), and siboglinid worm tubes (at BC, CFCC, HFR, LIV, GR), in addition to indeterminate bivalves, gastropods, and ammonites. These deposits are characterized by spatial and temporal heterogeneity in faunal composition and relative abundance, which is illustrated in Figure 8. Of the 10 seeps, three are dominated by steinkerns of bivalves and gastropods that are not identifiable below class level, including HFR (bivalves), LIV (bivalves), and RC (gastropods). Five of the deposits are dominated by different identifiable species, including BC, CFCC, RV, RmC, and GR. Each of these dominating taxa are also minor components of other faunal assemblages. For example, the gastropod *P. paskentaensis* comprises 62% of the BC assemblage, while it only comprises 1% of the WAM assemblage and the gastropod *Retiskenea*? *kieli* (Figure 9B) comprises 49% of the CFCC assemblage, but only 4% of the RC assemblage. The remaining two deposits, WS and WAM, are both dominated by *Peregrinella whitneyi,* which comprises 91% and 93% of the two assemblages, respectively. However, WS and WAM are the same age, and are in close proximity to each other, and it is possible that they represent a single coeval seep system, rather than discrete seepage events, but exposure precludes testing this relationship. The bivalve and gastropod

steinkerns at HFR and RC, respectively, are better preserved than the bivalve steinkerns at LIV, which are completely unidentifiable. Those at HFR are most likely thyasirids or *Astarte trapezoidalis* (Figure 9C) and at RC are most likely *Atresius liratus* (Figure 9E). There are no taxa common to *all* 10 localities and although worm tubes are found at 6 of the 10 localities; they are never dominant in an assemblage.

7. Paleoecology

7.1 *Ten Hydrocarbon Seep Deposits*

Modern seeps are characterized by variable species richness and by high dominance and low evenness (Levin 2005), as are the 10 GVG and Franciscan seep faunal assemblages (Table 3). Diversity is lowest at RV and RmC (one taxon found at each) and therefore, the two deposits have the highest dominance and lowest evenness values, however, these results are likely due to taphonomic biases, since previous studies report a wider range of core seep taxa present that were not found during the course of this study, such as *Peregrinella whitneyi* at RV (Berkland 1973) and large solemyid and thyasirid bivalves at RmC. Cold Fork of Cottonwood Creek, with only three identifiable taxa, has the next lowest diversity and highest dominance and lowest evenness values. In contrast, RC and BC have the highest evenness and lowest dominance values, which is consistent with their high diversities. WS and WAM are the only two deposits with nearly identical assemblages and other than these two, there is minimal

overlap between the 10 faunal assemblages. There are no temporal or spatial trends in similarity of sizes, ages, diversities, or relative abundances. This is confirmed by cluster analysis (Figure 10), which demonstrates that similarity and clusters are not related to deposit ages, which range from Late Jurassic to latest Cretaceous, or their overall size or the density of their faunal assemblages, which range from very patchy, cropping out over 8 km^2 (GR), to very dense, cropping out over 100 m^2 (WAM and LIV).

7.2 *Four Hydrocarbon Seep Deposits*

Modern hydrocarbon seeps indicate that there are two typical indicators of a long-lived, continuous seep, including (1) concentric or linear zonation patterns of faunal distribution and (2) high diversity. Locality maturity is closely tied to both of these indicators, with the most mature localities exhibiting the clearest faunal distribution patterns and the highest diversities. Each faunal deposit was tested for both of these indicators; however, they do not exhibit obvious traceable faunal distribution patterns, areas of higher diversity, or a record of systematic changes after the introduction of worm tubes.

The number of estimated species and the shape of the rarefaction curves of the different localities are variable, although do fall into two distinct groups. Further sampling at BC would likely have recovered more taxa, while CFCC, HFR, and RC reach an asymptote (Figure 11). Although all four localities have fossils, the assemblages vary considerably in abundance, distribution, diversity, and complexity. Some sections are extremely fossiliferous, some are poorly

fossiliferous, some have only a monospecific assemblage present, and some lack fossils entirely. For comparative size and fossil density distributions, see Figures 2, 3, 4, and 5.

The CFCC deposit was divided into 31 segments, averaging ~10 m in length. 26.65% of the segments are fossil-free, 26.65% of the segments are monospecific, while the remaining 46.7% of the segments have ≥ 2 taxa present. Diversity is low throughout all 30 segments and at each, diversity and abundance are not predictors of segment or faunal assemblage similarity (Figure 12).

The entire deposit is dominated by the gastropod *R.*? *kieli* (49%), followed by worm tubes (28%), *Bathypurpurinopsis stantoni* (22%) (Figure 9F), and bivalve steinkerns (1%), although dominant taxon varies without pattern from one segment to the next (Figure 2 and 12). The taxa are randomly distributed and there are no repeated patterns of faunal associations, abundances, or diversities. There are two 30 m segments completely devoid of fossils, surrounded by segments of high abundance, dominated by worm tubes, *B. stantoni*, or *R.*? *kieli*. Abundance rises rapidly adjacent to these two fossil-free segments, although the dominant taxon is unpredictable in the adjacent segments. These two 30 m segments could represent areas of higher fluid advection, which based on observations of modern seeps, would have precluded their colonization by anything other than microbial mats (Joye et al. 2004, Levin 2005).

The Menhinick and Margalef richness indices indicate that diversity is variable throughout the locality and stays within a narrow range, neither

increasing nor decreasing overall. (Table 4). This is confirmed by the Shannon-Weiner, Simpson, Equitability, and Fisher alpha indices (Table 4). In segments 2 through 14 diversity rose and fell less than it did in segments 19 through 31, indicating an environmental gradient that reflects stress on the community, due possibly to fluid flux, fluid volume, or other environmental factors.

Similarity and distance indices were used to determine which segments grouped together based on community composition. The Dice, Jaccard, Simpson, and Raup Crick similarity and distance indices (Table 5) indicate that the segments that are the most similar are 2 and 25; 13, 4, 9,12, and 31; 27 and 29; 22 and 24; 14, 3, and 5; as well as 30, 11, 18, 19, and 21 and thus, group together on the Q mode cluster diagram (Figure 13). The segments that group together are erratically distributed throughout the length of the locality, demonstrating that environmental conditions were not constant both throughout the area over which it formed and during its period of formation. Despite this distribution, segments 2 through 14 are notably similar (values ≥ 0.667), segments 15 through 17 were fossil-free; while segments 18 through 31 are characterized by less similarity (values ranging from 0 to ≤ 0.5).

Bear Creek is a multiple seep system that includes fourteen discrete seepage events cropping out over a 32 m vertical interval (Figure 3). Each of the fourteen seeps have the entire paragenetic sequence present, beginning with the earliest stages of diagenesis (deposition of detrital-rich micarb) and progressing

through to the latest stages (deposition of sparry calcite and neomorphosed micrite).

Nearly a quarter of the fourteen seeps are fossil-free, none are monospecific, and those remaining are fossil-rich. The faunal assemblage for the entire seep system includes four clades and ten taxa, although the maximum number of identifiable taxa found in any of the fourteen seeps is six. The entire faunal assemblage is dominated by *P. paskentaensis* (62%), although 48.6% of the *P. paskentaensis* samples come from the stratigraphically lowest seeps, including seeps S through UUU (Figure 14). The faunal assemblage transitions up section, in seeps V through WW, from *P. paskentaensis* to worm tubes, and transitions up section again from worm tubes to *P. paskentaensis*, in seeps X through ZZ. Species richness and diversity increase up section, although are periodically punctuated by sharp declines in horizons U, UUU, VV through W, Y, and ZZ. At each of the seeps, species richness, diversity, and abundance are not predictors of seep similarity or faunal assemblage similarity.

The Menhinick and Margalef richness indices indicate that diversity is variable throughout the locality (Table 6). The Shannon-Weiner, Simpson, Equitability, and Fisher alpha indices (Table 6) indicate that diversity increased and decreased episodically through time. The decrease of diversity is likely the result of episodic turbidite deposition periodically smothering the hydrocarbon seep community, followed by the reestablishment of the community as

hydrocarbon seep fluids once again erupted at the seafloor, resulting in the subsequent increase of diversity.

According to the Dice, Jaccard, Simpson, and Raup Crick similarity and distance indices (Table 7), four genera and six species are slowly introduced into the system, peaking at horizon Z, close to the top of the stratigraphic column and the top of the locality. According to these same indices, horizons U and UUU are the most alike and thus plot close together on the Q mode cluster diagram (Figure 15), while the remaining horizons are characterized by less similarity (values ≥ 0.667).

The HFR deposit encloses a diverse faunal assemblage that includes four clades and six taxa, in addition to unidentifiable ammonites and bivalve and gastropod steinkerns. 20% of the mounds are fossil-free, 20% have monospecific faunal assemblages, and 60% have ≥ 2 taxa present. The assemblage is dominated by the bivalve steinkerns (43%), which are most likely *A. trapezoidalis* or thyasirid bivalves, followed by the worm tubes (32%).

Diversity and abundance are lowest or zero at mounds 6, 8, 11, 14, 15, and 16, are intermediate at 3, 4, 9, 12, 18, and 19, and peak at mounds 5, 7, 10, 13, and 20. This is confirmed by the Menhinick and Margalef richness indices (Table 8), as well as by the Shannon-Weiner, Simpson, Equitability, and Fisher alpha indices (Table 8). The twenty mounds were randomly labeled and the diversity data mimics this random behavior, while staying within a narrow range

and neither increasing nor decreasing overall. Species, number of taxa present, and size of the mound were not a predictor of mound diversity.

Similarity and distance indices were used to determine which mounds grouped together based on community composition. According to the Dice, Jaccard, Simpson, and Raup Crick similarity and distance indices (Table 9), mounds 17 and 6, 17 and 8, 19 and 10, 12 and 3, and 8 and 6 are the most alike, and thus plot close together on the Q mode cluster diagram (Figure 16). Based on this data, the location of a mound was not an indicator of mound similarity, as similar mounds (values = 1) were irregularly distributed; however, in all cases, except for mounds 12 and 3 (240 m apart), the similar mounds were near each other (< 30 m apart). Mounds 1 and 2, located in the north-east corner of the locality, are the least like the other sixteen fossiliferous mounds and are closest to the conduits and chimneys, which likely represents the center of the seep, as seen in the modern, while the remaining fourteen mounds have variable similarity and distance indices values, ranging from very little similarity (values < 0.4) to considerable similarity (values > 0.5).

The RC deposit encloses a faunal assemblage comprised of three clades and seven taxa, in addition to a large number of poorly preserved gastropod and bivalve steinkerns. The gastropods are most likely either *Lithomphalus enderlini* or *A. liratus*, while, based on the size and morphological attributes that remain, the bivalve steinkerns are most certainly *A. trapezoidalis*.

The RC assemblage is dominated by gastropod steinkerns (50%), followed by bivalve steinkerns (17%), and the bivalve *Pecten complexicosta* (9%). 43.2% of the forty-three outcrops are fossil-free, 11.6% are monospecific, and 43.2% have ≥ 2 taxa present.

The Menhinick and Margalef richness indices indicate that diversity is variable throughout the locality (Table 10), which is confirmed by the Shannon-Weiner, Simpson, Equitability, and Fisher alpha indices (Table 10). The original forty-three individual outcrops measured in the field were randomly labeled, and the diversity data mimics this random sampling method, while staying within a narrow range and neither increasing nor decreasing, overall. Species, number of taxa present, and size of the carbonate unit were not a predictor of outcrop diversity.

Similarity and distance indices were used to determine which outcrops grouped together based on community composition. The Dice, Jaccard, Bray Curtis, and Raup Crick indices (Table 11) show strong similarities with regard to taxonomic composition between many of the outcrops. Unit location, however, was not an indicator of outcrop similarity, as similar outcrops (values = 1) were erratically distributed throughout the locality. This result is also confirmed by Q mode cluster analysis based on comparison of the taxonomic composition of the localities (Figure 17). Outcrops 5, 2, 20, 22, 24, and 33, as well as 12, 19, and 26 are randomly dispersed throughout the locality, however, are extremely similar (values = 1). The 43 outcrops have variable similarity values, ranging

from values indicating little similarity (values < 0.5) to values indicating considerable similarity (values ≥ 0.5). Proximity of the outcrops is not an indicator of diversity. Although some outcrops are dominated by the same taxon, have similar sizes, and/or similar abundances, these outcrops are erratically distributed.

8. Discussion

8.1 *Ten Hydrocarbon Seep Deposits*

The most striking aspect of these 10 hydrocarbon seep deposits and their associated faunal assemblages is the spatial and temporal heterogeneity of taxonomic composition and relative abundance from site to site. This heterogeneity is interesting in light of the continuity of the geochemically-based characteristics through time. Within this heterogeneity, there are three paleoecological patterns.

(1) *The relationship between species richness and deposit size*. It is reasonable to predict that as seep size increases, species richness will proportionately increase; however, in the GVG and Franciscan seeps, there is no relationship between deposit size and species richness. For example, CFCC, has 3 taxa present, WAM has 3 taxa present, and BC has 15 taxa present. These three deposits range in size, shape, and age, however, in all three cases, size is clearly not an indicator of species richness.

Due to the difficulty in accessing them, it is difficult to capture more than an ecological snapshot of an active seep. In contrast, an ancient seep preserves a time-averaged physical record of its faunal assemblages. Surprisingly, even when time-averaged, there is no significant increase of diversity in the GVG and Franciscan's larger seeps. This is unexpected because the larger seeps must have formed over a longer period of time compared to the smaller ones, and thus would have had more time for species recruitment. However, based on these data, additional time does not appear to have affected accumulated diversity.

(2) *The temporal heterogeneity*. During this time, there is expected evolution of the seep faunas, which is demonstrated by the shift in faunal assemblage compositions between the Early and Late Cretaceous deposits (Figure 18A). Although many seep families are long lived, such as the bivalve families Lucinidae, Solemyidae, Inoceramidae, and Siboglinidae (Little and Vrijenhoek 2003), seep genera and species commonly have short stratigraphic ranges and thus, change through time (Figure 18B). This is exhibited in these seeps by a number of different groups. While the family Solemyidae is known to have a temporal distribution extending from the Silurian through modern day, *Solemya occidentalis*, found at WS, is limited to the Early Cretaceous. A similar example is seen in the family Pectinidae, which has a temporal distribution extending from the Carboniferous through modern day. Despite *Pecten* having a long temporal history, *Pecten complexicosta*, which is found only at Rocky Creek, is also limited to the Early Cretaceous. Some families, such as the Lucinidae,

Inoceramidae, and Siboglinidae are found in both the Early and Late Cretaceous deposits. Since specimens could only be identified to the family level, genus or species transitions cannot be ascertained. However, it is likely, that these groups had different species representatives in the Early versus Late Cretaceous deposits. This is consistent with the gastropod genus *Hokkaidoconcha*, which is found in this region from the Tithonian through the Campanian. The group is represented by three species, *Hokkaidoconcha occidentalis,* which is limited to the Early Cretaceous and is known only from Paskenta, a hydrocarbon seep deposit not included in this study due to private property restrictions, but reported by Kiel et al. (2008), *Hokkaidoconcha bilirata* sp. nov., which is found in the Early to Middle Cretaceous, and *Hokkaidoconcha morenoensis* sp. nov., which is found in the Late Cretaceous.

(3) *The spatial heterogeneity*. The most important paleontological pattern is that even those seep deposits that have faunas with overlapping stratigraphic ranges, are unalike, with the exception of WS and WAM. The deposits include a variety of recurring seep taxa and endemic faunas, including five clades, but there are no patterns to taxon or clade distribution. For example, BC, RC, and LIV were all deposited in the Valanginian and the stratigraphic ranges of their faunas overlap. Despite this overlap though, the three deposits are dominated by two different clades and have different faunal assemblages, characterized by different relative abundances.

In island-like ecosystems such as hydrocarbon seeps, factors that influence faunal spatial patterns, include chance (MacArthur and Wilson 1967), location relative to ocean currents and distance to the next closest seep, advecting fluid rate, volume, and composition, as well as the unpredictable rates of faunal dispersal, invasion, extinction, and adaptation (MacArthur and Wilson 1967, Carney 1994). However, islands are generally populated by taxa from either the closest mainland or from other nearby islands. This limits the number of possible taxa that can immigrate onto an island and should result in adjacent islands having overlapping faunal assemblages (MacArthur and Wilson 1967). In light of these typical patterns of faunal distribution among isolated islands, the GVG and Franciscan hydrocarbon seep spatial heterogeneity is surprising, since there is very little overlap between their faunal assemblages, excluding WS and WAM.

The faunal assemblages do not exhibit lateral or vertical faunal distribution patterns or clusters of increased diversity, however, thin section analyses demonstrate that (1) there was a systematic change from bivalve, gastropod, or brachiopod dominated seeps (phase 1) to worm tube dominated seeps (phase 3), (2) that the arrival of phase 1 taxa was random, and (3) that there were only two arrival events and that they were restricted to the earliest phases of seep formation. This pattern is consistent throughout all 10 seeps and is also consistent with other documented ancient hydrocarbon seep deposits, such as

the seeps of the Canadian Arctic (Beauchamp and Savard 1992) and the seeps of the Dwyka Group in southern Namibia (Himmler et al. 2008), among others.

The observed difference in arrival times during the earliest phases of diagenesis suggest that the worm tubes had different environmental requirements compared to the earlier arriving taxa. This is especially interesting for two reasons. First, worm tubes at modern seeps are known to co-occur with other cold seep taxa (bivalves, gastropods, etc), such as those from the Gulf of Mexico (MacAvoy et al. 2002) and the South Barbados accretionary prism (Jollivet et al. 1990, Olu et al. 1996). Second, taxa with sulfur-oxidizing chemosymbionts are found from phase 1 (detrital-rich micarb) through phase 3 (worm tubes), however, the taxa are not the same. Thyasirid and lucinid bivalves, which are part of the HFR and BC assemblages, respectively, are found as part of the phase 1 assemblages, while worm tubes, which are part of six of the ten assemblages, are part of the phase 3 assemblage. According to the pyrite coated corrosion surfaces, these two phases are separated by an influx of hydrogen sulfide. Perhaps during and after this flux, hydrogen sulfide concentrations exceeded what the phase 1 macrofauna could handle and killed them. It is known that modern taxa exposed to high hydrogen sulfide concentrations have adapted to transport, metabolize, and detoxify hydrogen sulfide (Gaill 1993), however, there is a limit to how far these adaptations can be pushed.

8.2 *Four Hydrocarbon Seep Deposits*

The four deposits addressed in greater detail vary in age, size, outcrop morphology, and faunal assemblage composition, despite deposition occurring in similar tectonic settings and under the same overarching environmental parameters. Species richness, diversity, abundance, and species distribution vary unpredictably and exhibit no concentric or linear zonation or increased diversity of fossils, as would be predicted from modern seeps. Given that the seeps cover an 80 m.y. interval, it is expected that the genera and species are different between the four assemblages.

Since hydrocarbon seep taxa are stratigraphically short lived at the genus and species levels, evolution of the faunas is expected (Figure 18B). Early and Late Cretaceous seep taxa share a number of families but other than worm tubes are distinctly different. Based on this pattern, it is predictable that Valanginian aged BC and RC would have moderately overlapping faunal assemblages and/or faunal distributions, while being dissimilar to CFCC and HFR, which are also dissimilar to each other. BC and RC are, in fact, more similar to each other than to any other pair of localities. They share four identifiable species, while all other pairs (CFCC and BC, CFCC and HFR, RC and HFR, etc.) share between one and two species. This similarity is likely related to the Early Cretaceous specific faunal pool these seeps were drawing on to populate their communities. By the Late Cretaceous, this pool would have largely evolved to include new genera and

species, with only a rare genus or species ranging stratigraphically from the Early to the Late Cretaceous.

Modern seeps demonstrate that diversity and faunal distribution are closely tied to fluid advection rates, with the most “ecologically complex” localities associated with long lived and continuous fluid expulsion and the least complex localities associated with patchy and short lived fields of fluid expulsion (Sibuet and Olu 1998). Additionally, those seeps with distinct faunal distribution patterns and/or increased diversity are the most mature, while the reverse characterizes the least mature. This, however, does not characterize the four GVG deposits. For example, RC and HFR are medium-sized deposits that have the highest diversity, while CFCC is the largest deposit and has the lowest diversity. This is unexpected because based on CFCC’s size, it would be predicted that the deposit would have the highest diversity and evidence of faunal distribution patterns, neither of which it has. BC, which is the smallest deposit, has diversity levels nearly equal to, but just under, RC and HFR, but still higher than CFCC. Despite RC and HFR having the highest diversity, they do not appear to be any more mature than CFCC, which has the lowest diversity.

Additionally, each seep deposit has been time-averaged, thus each deposit preserves accumulated diversity, rather than the geologic snapshots of the modern. This is significant because each deposit had the opportunity to accumulate diversity, however, did not. This suggests that the GVG seeps are, in comparison to other ancient seeps, relatively immature. Since maturity is

closely tied to fluid advection and since all four deposits are equally immature, it could be that fluid advection throughout the forearc basin was patchy, discontinuous, or simply occurred over geologically short intervals that hindered the development of higher diversity or more complex faunal distribution patterns.

Although these four deposits do not exhibit lateral or vertical faunal patterns or patches with increased diversity, these results are still consistent with one aspect of modern hydrocarbon seep deposits. Modern seeps have been documented changing physically, chemically, and faunally over very short distances and timescales (Levin 2005). These changes have been linked to the variability of physical and chemical conditions beneath the area of seepage, as well as the rate or volume of fluid flow (Sibuet and Olu 1998, Levin 2005, Orcutt et al. 2005).

Each hydrocarbon seep is subjected to variable environmental conditions that result in physically variable deposits that are the product of a highly localized energy source that is unique to their location. The rate, volume, origin, etc. of fluid advection is not only different from one active seep to the next, but can vary within a single seep and over very short distances. Since biomass is directly proportional to the intensity of fluid flow, large spatial and temporal fluctuations in fluid expulsion would have resulted in patchy, erratic deposits, such as at BC, whereas continuous fluid flow would have formed proportionately continuous segments, mounds, or outcrops, such as at CFCC, HFR, and RC, respectively.

The lack of lateral and vertical faunal patterns at these four localities was likely driven by not only the longevity, volume, and rate of fluid expulsion, but also by the transient nature of the seep environment, which is in constant flux, including variations in origin and composition of venting fluids (Carney 1994, Sibuet and Olu 1998, Bergquist et al. 2003, Campbell 2006), and physiological attributes related to the environmental setting and/or biological conditions (Campbell 2006).

9. Conclusions

The deposits are nearly identical petrographically and paragenetically and in comparison to seawater, are consistently anomalous geochemically, although at outcrop scale, are morphologically variable, with the variability being unrelated to deposit size or location. The most significant results to arise from these data are (1) the degree of temporal and spatial heterogeneity between the taxonomic compositions of these 10 deposits and (2) that deposit size, age, and location were not significant drivers of this heterogeneity.

In-depth analyses of the morphological and paleontological signatures of the CFCC, BC, HFR, and RC localities has demonstrated that there are no obvious patterns to diversity and abundance at these four localities. This lack of faunal pattern is interpreted to be related to changes in environmental stability connected to variability in fluid flow volume, rate, and area, due to interactions with their immediate physical, chemical, and biological environments. These

assemblages record the combined effect of rich but oscillating fluid fluxes, which produced ephemeral environmental conditions. Seep maturation was closely tied to this transience on a local scale, but was also affected by overarching regional advection characteristics.

Today, hydrocarbon seeps are known from localities that span the globe and that vary in age, tectonic setting, size, outcrop morphology, and faunal composition. Studies of ancient hydrocarbon seeps have demonstrated that chemosynthetic paleoenvironments have varied geologically and taxonomically through time and consequently, have opened a window onto the evolution of organisms living in extreme environments (Campbell 2006). Today, most organisms are found in oxygen- and sunlight-rich environments, but life likely arose under more extreme conditions of low-oxygen and high-temperatures that predominated early in Earth's history. Extreme environments have been recognized since the Precambrian, however, tracking long-term paleoecological patterns has been difficult due to their rarity in the stratigraphic record and their tendency to crop out as localized deposits, generally without spatial or temporal replication.

This study is especially significant because not only are these 10 deposits a record of 80 m.y. of intermittent methane seepage on the floor of the forearc basin and in the accretionary prism, but they also present the opportunity to examine the evolution of seep communities through time. Understanding the patterns of evolutionary diversification, biogeography, and adaptation within

hydrocarbon seep paleocommunities through time and space provides one of the best-known analogues for the evolution of early life.

References Cited

Anderson, F. M. 1938. Lower Cretaceous Deposits in California and Oregon. Geological Society of America, Baltimore.

Barbieri, R., and B. Cavalazzi. 2005. Microbial fabrics from Neogene cold seep carbonates, Northern Apennine, Italy. Palaeogeography, Palaeoclimatology, Palaeoecology 227:143-155.

Barry, J. P., R. E. Kochevar, and C. H. Baxter. 1997. The Influence of Pore-Water Chemistry and Physiology on the Distribution of Vesicomyid Clams at Cold Seeps in Monterey Bay: Implications for Patterns of Chemosynthetic Community Organization. Limnology and Oceanography 42(2):318-328.

Beauchamp, B., and M. Savard. 1992. Cretaceous Chemosynthetic Carbonate Mounds in the Canadian Arctic. Palaios 7:434-450.

Bergquist, D. C., T. Ward, E. E. Cordes, T. McNelis, S. Howlett, R. Kosoff, S. Hourdez, R. Carney, and C. R. Fisher. 2003. Community structure of vestimentiferan-generated habitat islands from Gulf of Mexico cold seeps. Journal of Experimental Marine Biology and Ecology 289:197-222.

Berkland, J. O. 1973. Rice Valley Outlier-New Sequence of Cretaceous-Paleocene Strata in Northern Coast Ranges, California. Geological Society of America Bulletin 84:2389-2406.

Berner, R. A. 1970. Sedimentary Pyrite Formation. American Journal of Science 268:1-23.

Berner, R. A. 1984. Sedimentary pyrite formation: An update. Geochimica et Cosmochimica Acta 48:605-615.

Bertucci, P. F. 1983. Petrology and Provenance of the Stony Creek Formation Northwestern Sacramento Valley, California. Pp. 1-16. *In* P. F. Bertucci, and R. V. Ingersoll, eds. Guidebook to the Stony Creek Formation, Great Valley Group, Sacramento Valley, California. The Pacific Section Society of Economic Paleontologists and Mineralogists, Los Angeles.

Blake, M. C., Jr., and D. L. Jones. 1981. The Franciscan Assemblage and Related Rocks in Northern California: A Reinterpretation. Pp. 307-328. *In* W. R. Ernst, ed. The Geotectonic Development of California. Prentice Hall, New Jersey.

Blake, M. C., Jr., and R. J. McLaughlin. 1989. Terranes of the Northern Coast Ranges. P. 75. *In* M. C. Blake, and D. S. Harwood, eds. Tectonic Evolution of Northern California. American Geophysical Union, Washington D.C.

Campbell, K. A., and D. J. Bottjer. 1993. Fossil Cold Seeps. National Geographic Research and Exploration 9(3):326-343.

Campbell, K. A., J. D. Farmer, and D. Des Marais. 2002. Ancient hydrocarbon seeps from the Mesozoic convergent margin of California: carbonate geochemistry, fluids and palaeoenvironments. Geofluids 2:63-94.

Campbell, K. A. 2006. Hydrocarbon seep and hydrothermal vent paleoenvironments and paleontology: Past developments and future research directions. Palaeogeography, Palaeoclimatology, Palaeoecology 232:362-407.

Campbell, K. A., D. E. Peterson, and A. C. Alfaro. 2008. Two New Species of *Retiskenea*? (Gastropoda: Neomphalidae) from Lower Cretaceous Hydrocarbon-Seep Carbonates of Northern California. Journal of Paleontology 82(1):140-153.

Carney, R. S. 1994. Consideration of the oasis analogy for chemosynthetic communities at Gulf of Mexico hydrocarbon vents. Geo-Marine Letters 14:149-159.

Constenius, K. N., R. A. Johnson, W. R. Dickinson, and T. A. Williams. 2000. Tectonic Evolution of the Jurassic-Cretaceous Great Valley forearc; California: Implications for the Franciscan Thrust-Wedge Hypothesis. Geological Society of America Bulletin 112(11):1703-1723.

Dickinson, W. R., and D. R. Seely. 1979. Structure and Stratigraphy of Forearc Regions. American Association of Petroleum Geologists Bulletin 63(1):2-31.

Dickinson, W. R. 1981. Plate Tectonics and the Continental Margin of California. Pp. 1-28. *In* W. R. Ernst, ed. The Geotectonic Development of California. Prentice Hall, New Jersey.

Dickinson, W. R. 2008. Accretionary Mesozoic-Cenozoic Expansion of the Cordilleran Continental Margin in California and Adjacent Oregon. Geosphere 4(2):329-353.

Ernst, W. G., C. A. Snow, and H. H. Scherer. 2008. Mesozoic Transpression, Transtension, Subduction and Metallogenesis in Northern and Central California. Terra Nova 20(5):394-413.

Flügel, E. 1982. Microfacies Analysis of Limestones. Springer-Verlag, Berlin.

Gaill, F. 1993. Aspects of life development at deep sea hydrothermal vents. The Journal of the Federation of American Societies for Experimental Biology 7:558-565.

Godfrey, N. J., B. C. Beaudoin, and S. L. Klemperer. 1997. Ophiolitic basement to the Great Valley forearc basin, California, from seismic and gravity data: Implications for crustal growth at the North American continental margin. GSA Bulletin 109(12):1536-1562.

Hamilton, W. 1969. Mesozoic California and the Underflow of Pacific Mantle. Geological Society of America Bulletin 80:2409-2430.

Hammer, Ø., D. A. T. Harper, and P. D. Ryan. 2001. PAST: Paleontological Statistics Software Package for Education and Data Analysis. Palaeontologia Electronica 4(1):9.

Hammer, Ø., and D. Harper. 2006. Paleontological Data Analysis. Blackwell Publishing, Malden.

Harris, P. M., C. G. S. C. Kendall, and I. Lerche. 1985. Carbonate Cementation—A Brief Review. Pp. 79-95. *In* N. Schneidermann, and P. M. Harris, eds. Carbonate Cements. Society of Economic Paleontologists and Mineralogists Special Publication 36, Tulsa.

Hepper, K. 2004. A New Hydrocarbon Seep Locality in the Mesozoic Great Valley Group, Guenoc Ranch, northern California. MS. San Francisco State University, San Francisco.

Himmler, T., A. Freiwald, H. Stollhofen, and J. Peckmann. 2008. Late Carboniferous hydrocarbon-seep carbonates from the glaciomarine Dwyka Group, southern Namibia. Palaeogeography, Palaeoclimatology, Palaeoecology 257:185-197.

Ingersoll, R. V. 1978a. Paleogeography and Paleotectonics of the Late Mesozoic Forearc Basin of Northern and Central California. Pp. 471-482. *In* D. G. Howell, and K. A. McDougall, eds. Mesozoic Paleogeography of the Western United States. SEPM Pacific Section, Los Angeles.

Ingersoll, R. V. 1978b. Submarine Fan Facies of the Upper Cretaceous Great Valley Sequence, northern and central California. Sedimentary Geology 21:205-230.

Ingersoll, R. V. 1982. Initiation and evolution of the Great Valley forearc basin of northern and central California, U.S.A. Pp. 459-467. *In* J. K. Leggett, ed. Trench-Forearc Geology; Sedimentation and Tectonics on Modern and Ancient Active Plate Margins. Special Publication-Geological Society of London, London.

Jollivet, D., J.-C. Faugeres, R. Griboulard, D. Desbryuyeres, and G. Blanc. 1990. Composition and spatial organization of a cold seep community on the South Barbados accretionary prism: tectonic, geochemical and sedimentary context. Progress in Oceanography 24:25-45.

Joye, S. B., A. Boetius, B. N. Orcutt, J. P. Montoya, H. N. Schulz, M. J. Erickson, and S. K. Lugo. 2004. The anaerobic oxidation of methane and sulfate reduction in sediments from Gulf of Mexico cold seeps. Chemical Geology 205:219-238.

Kiel, S., and K. A. Campbell. 2005. *Lithomphalus enderlini* gen. et sp. nov. from cold-seep carbonates in California-Cretaceous neomphalid gastropod? Palaeogeography, Palaeoclimatology, Palaeoecology 227:232-241.

Kiel, S., K. A. Campbell, W. P. Elder, and C. T. S. Little. 2008. Jurassic and Cretaceous Gastropods from Hydrocarbon Seeps in Forearc Basin and Accretionary Prism Settings, California. Acta Palaeontologica Polonica 53(4):679-703.

Levin, L. A. 2005. Ecology of Cold Seep Sediments: Interactions of Fauna with Flow, Chemistry, and Microbes. Oceanography and Marine Biology: An Annual Review 43:1-46.

Little, C. T. S., and R. C. Vrijenhoek. 2003. Are hydrothermal vent animals living fossils? Trends in Ecology & Evolution 18(11):582-588.

MacArthur, R. H., and E. O. Wilson. 1967. The Theory of Island Biogeography. Princeton University Press, Princeton.

MacAvoy, S. E., S. A. Macko, and S. B. Joye. 2002. Fatty acid carbon isotope signatures in chemosynthetic mussels and tube worms from gulf of Mexico hydrocarbon seep communities. Chemical Geology 185:1-8.

Olu, K., M. Sibuet, F. Harmegnies, J.-P. Foucher, and A. Fiala-Médioni. 1996. Spatial distribution of diverse cold seep communities living on various

diapiric structures of the southern Barbados prism. Progress in Oceanography 38:347-376.

Olu, K., S. Lance, M. Sibuet, P. Henry, A. Fiala-MÈdioni, and A. Dinet. 1997. Cold seep communities as indicators of fluid expulsion patterns through mud volcanoes seaward of the Barbados accretionary prism. Deep Sea Research Part I: Oceanographic Research Papers 44(5):811-819.

Orcutt, B., A. Boetius, M. Elvert, V. Samarkin, and S. B. Joye. 2005. Molecular biogeochemistry of sulfate reduction, methanogenesis and the anaerobic oxidation of methane at Gulf of Mexico cold seeps. Geochimica et Cosmochimica Acta 69(17):4267-4281.

Paull, C. K., J. P. Chanton, A. C. Neumann, J. A. Coston, C. S. Martens, and W. Showers. 1992. Indicators of Methane-Derived Carbonates and Chemosynthetic Organic Carbon Deposits: Examples from the Florida Escarpment. Palaios 7:361-375.

Peckmann, J., K. A. Campbell, O. H. Walliser, and J. Reitner. 2007. A Late Devonian Hydrocarbon-Seep Deposit Dominated by Dimerelloid Brachiopods, Morocco. Palaios 22:114-122.

Rathburn, A. E., M. E. PereŸ, J. B. Martin, S. A. Day, C. Mahn, J. Gieskes, W. Siebis, D. Williams, and A. Bahls. 2003. Relationships between the distribution and stable isotopic composition of living benthic foraminifera and cold methane seep biogeochemistry in Monterey Bay, California. Geochemistry, Geophysics, Geosystems 4(12):1-28.

Ritger, S., B. Carson, and E. Suess. 1987. Methane-derived authigenic carbonates formed by subduction-induced pore-water expulsion along the Oregon/Washington margin. Geological Society of America Bulletin 98:147-156.

Sahling, H., D. Rickert, R. W. Lee, P. Linke, and E. Suess. 2002. Macrofaunal community structure and sulfide flux at gas hydrate deposits from the Cascadia convergent margin, NE Pacific. Marine Ecology Progress Series 231:121-138.

Sibuet, M., and K. Olu. 1998. Biogeography, biodiversity and fluid dependence of deep-sea cold-seep communities at active and passive margins. Deep-Sea Research II 45:517-567.

Stanton, T. W. 1895. Contributions to the Cretaceous Paleontology of the Pacific Coast: The Fauna of the Knoxville Beds. Bulletin of the United States Geological Survey 133:9-132.

Swe, W., and W. R. Dickinson. 1970. Sedimentation and Thrusting of Late Mesozoic Rocks in the Coast Ranges near Clear Lake, California. Geological Society of America Bulletin 81:165-188.

Titschack, J., and A. Freiwald. 2005. Growth, deposition, and facies of Pleistocene bathyal coral communities from Rhodes, Greece. Pp. 41-59. *In* J. Titschack, and J. M. Roberts, eds. Cold-Water Corals and Ecosystems. Springer, Berlin.

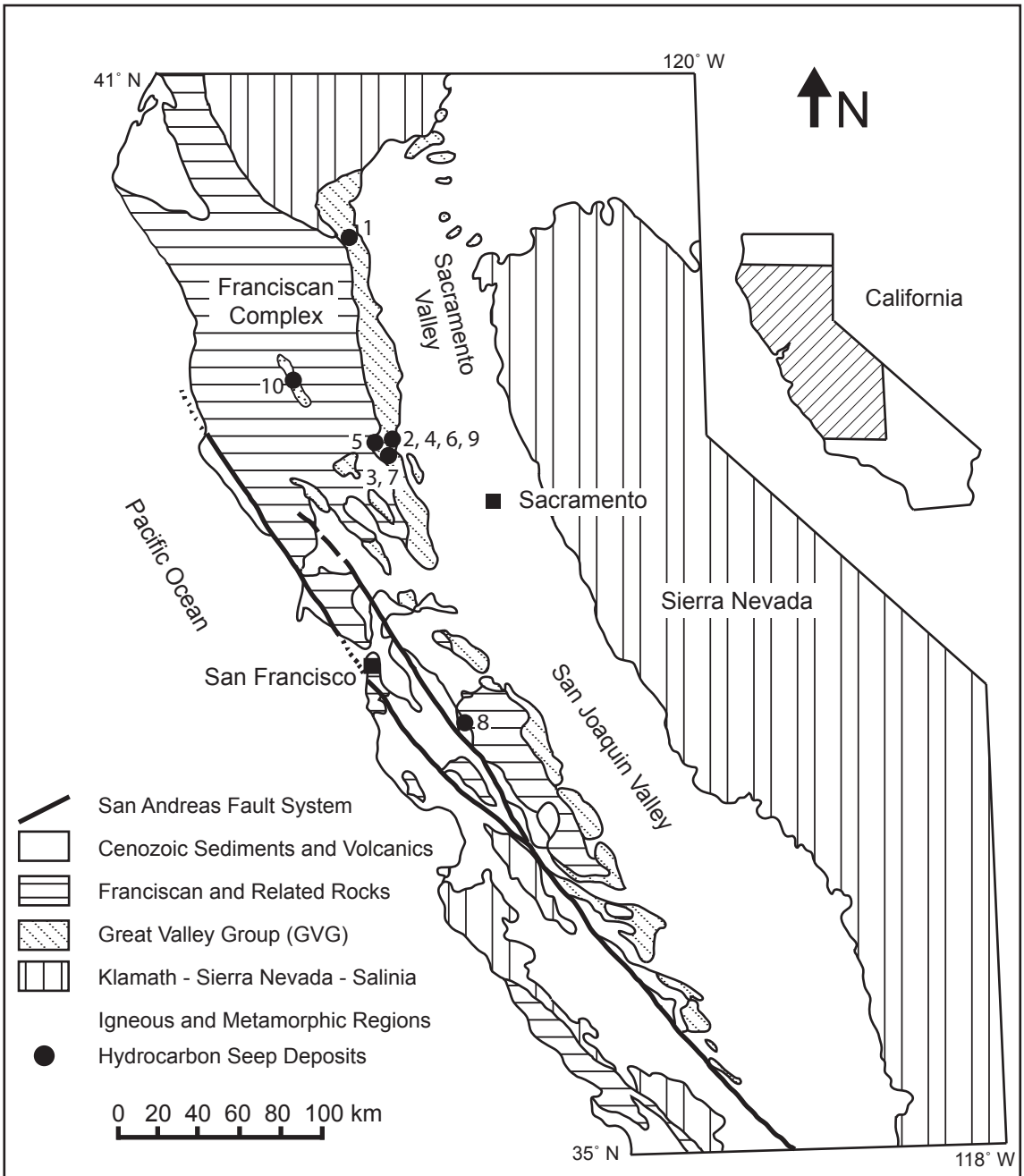

Figure 1. Locality map for the ten Mesozoic hydrocarbon seep localities included in this study. The localities include: (1) Cold Fork of Cottonwood Creek, (2) Wilbur Springs, (3) Guenoc Ranch, (4) Bear Creek, (5) Harrington Flat Road, (6) Little Indian Valley, (7) Rocky Creek, (8) Romero Creek, (9) Wide Awake Mine, and (10) Rice Valley. Simplified geology of the western North American Continental margin, including from west to east, the Franciscan complex, the GVG forearc strata, and the Sierra Nevada batholith. Map after Ingersoll (1978).

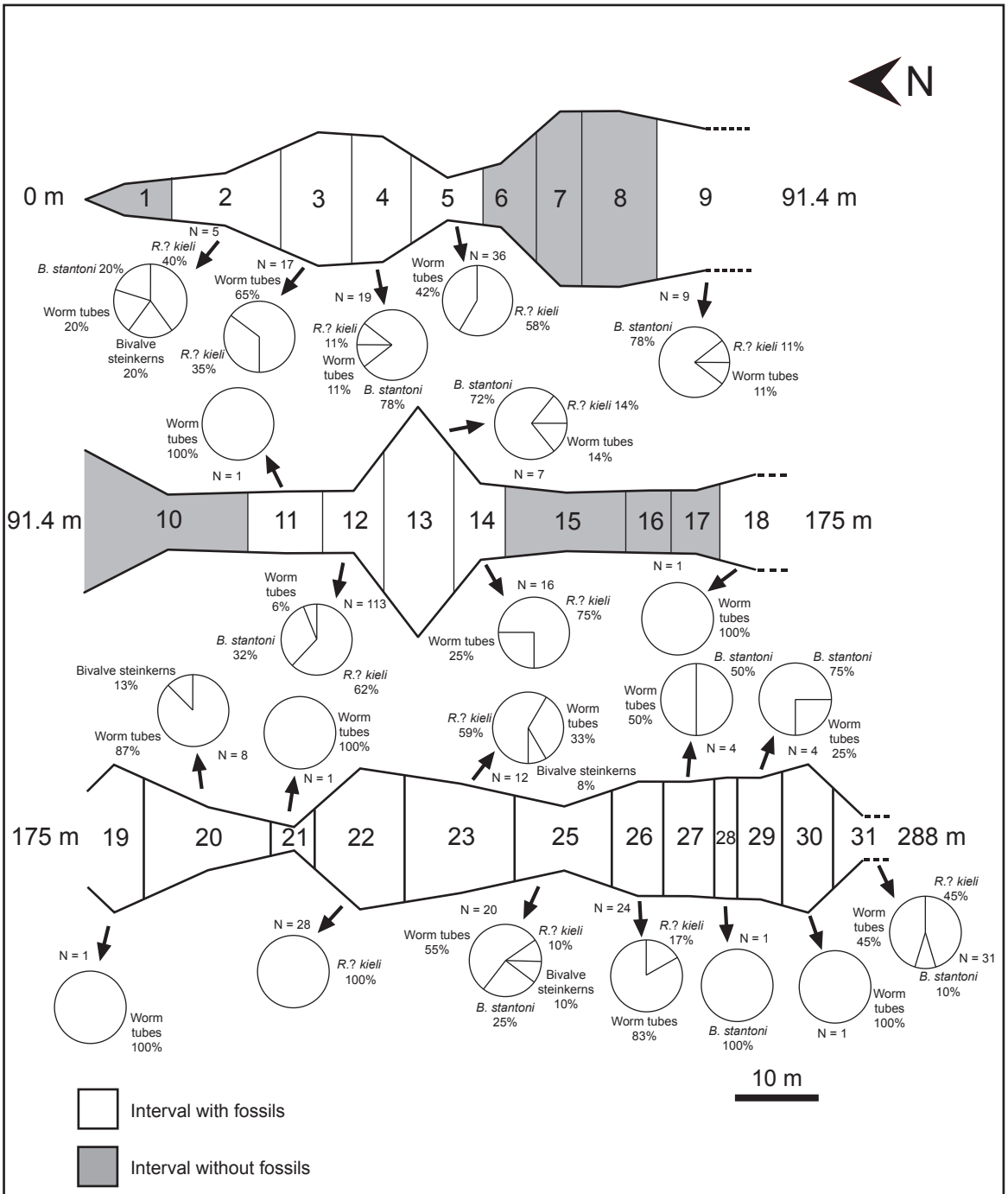

Figure 2. Map of Cold Fork of Cottonwood Creek. This is a to scale representation of the length and width of the locality, as well as the locations of all fossils collected and the segments without fossils. Includes relative abundances of the faunas at each of the 31 segments.

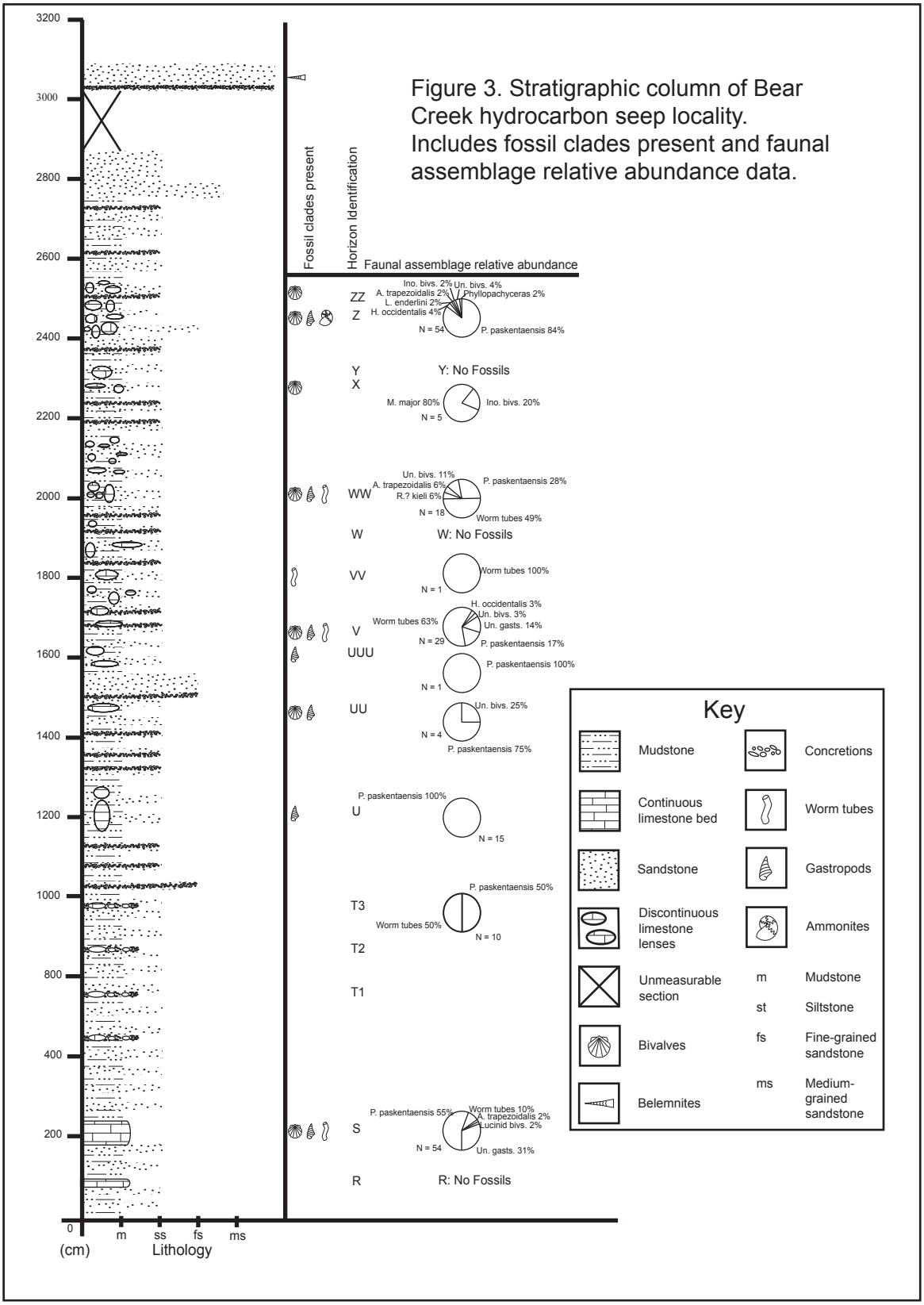

Figure 3. Stratigraphic column of Bear Creek hydrocarbon seep locality. Includes fossil clades present and faunal assemblage relative abundance data.

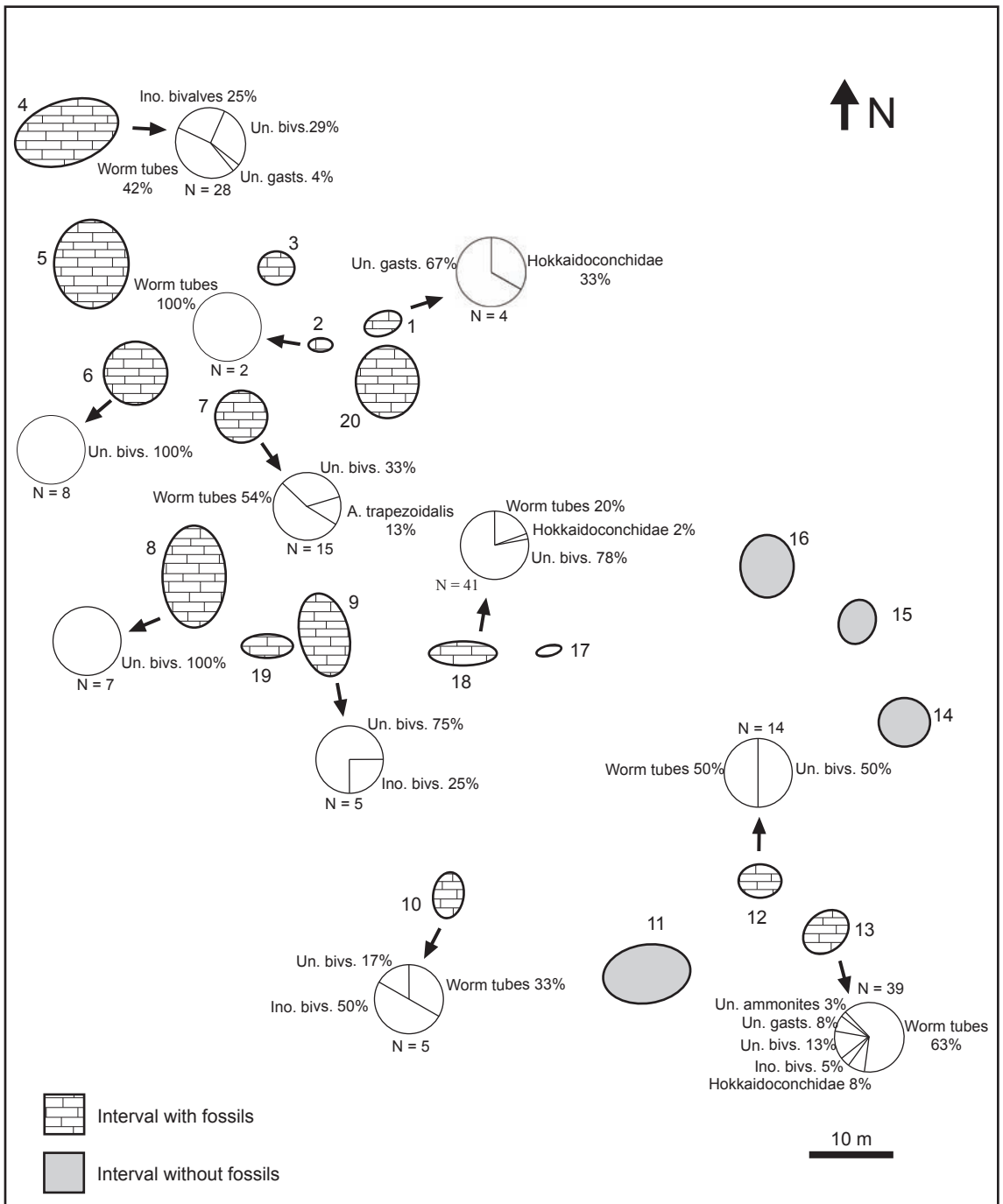

Figure 4. Map of the Harrington Flat Road hydrocarbon seep mounds. Mounds are to scale. Includes relative abundance of faunas at each mound and well as mounds without fossils.

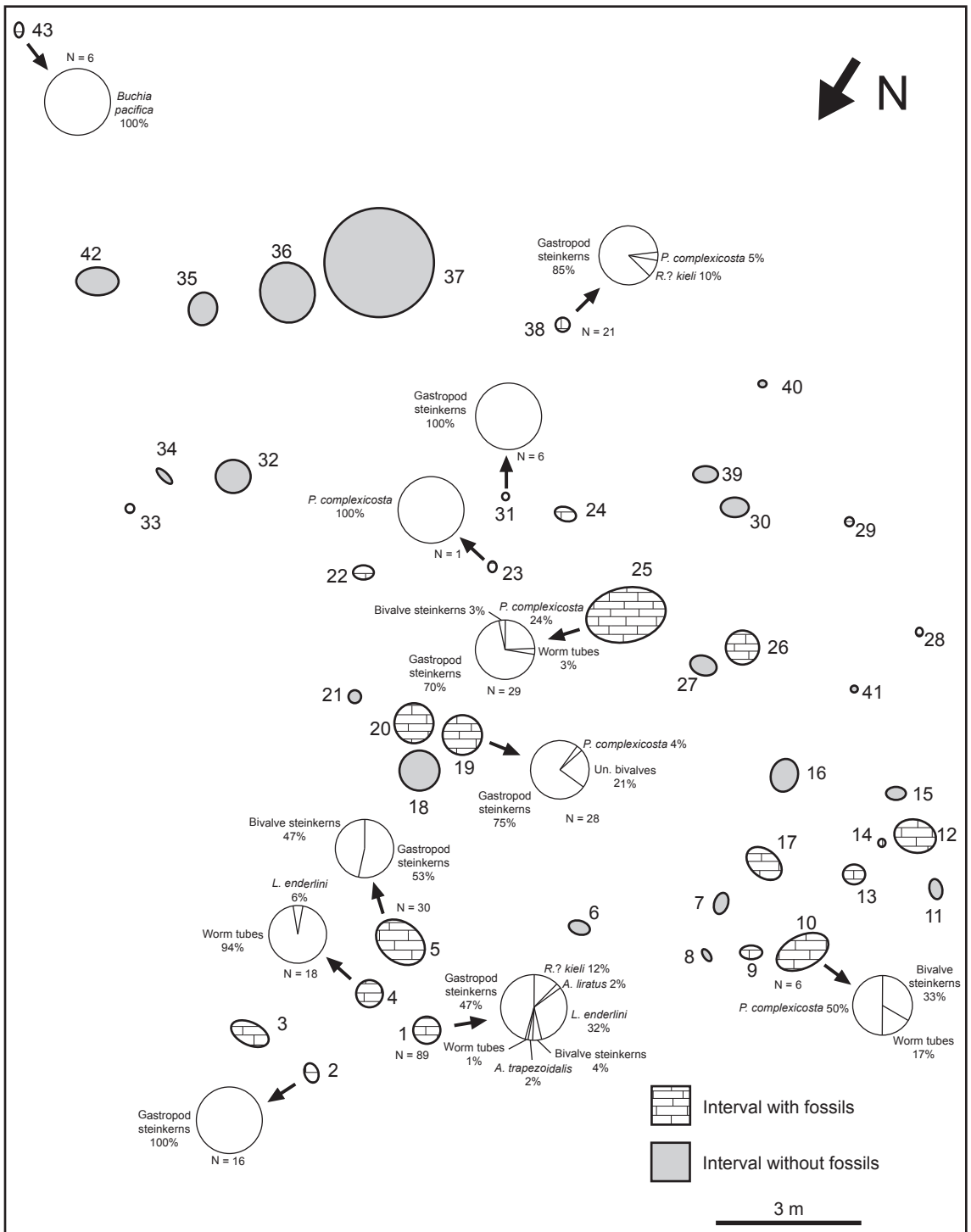

Figure 5. Map of the Rocky Creek locality. Outcrops are to scale. Deposit includes forty-three individual outcrops, each ≥ 15.25 cm. Includes realtive abundances of faunas at each outcrop and outcrops without fossils.

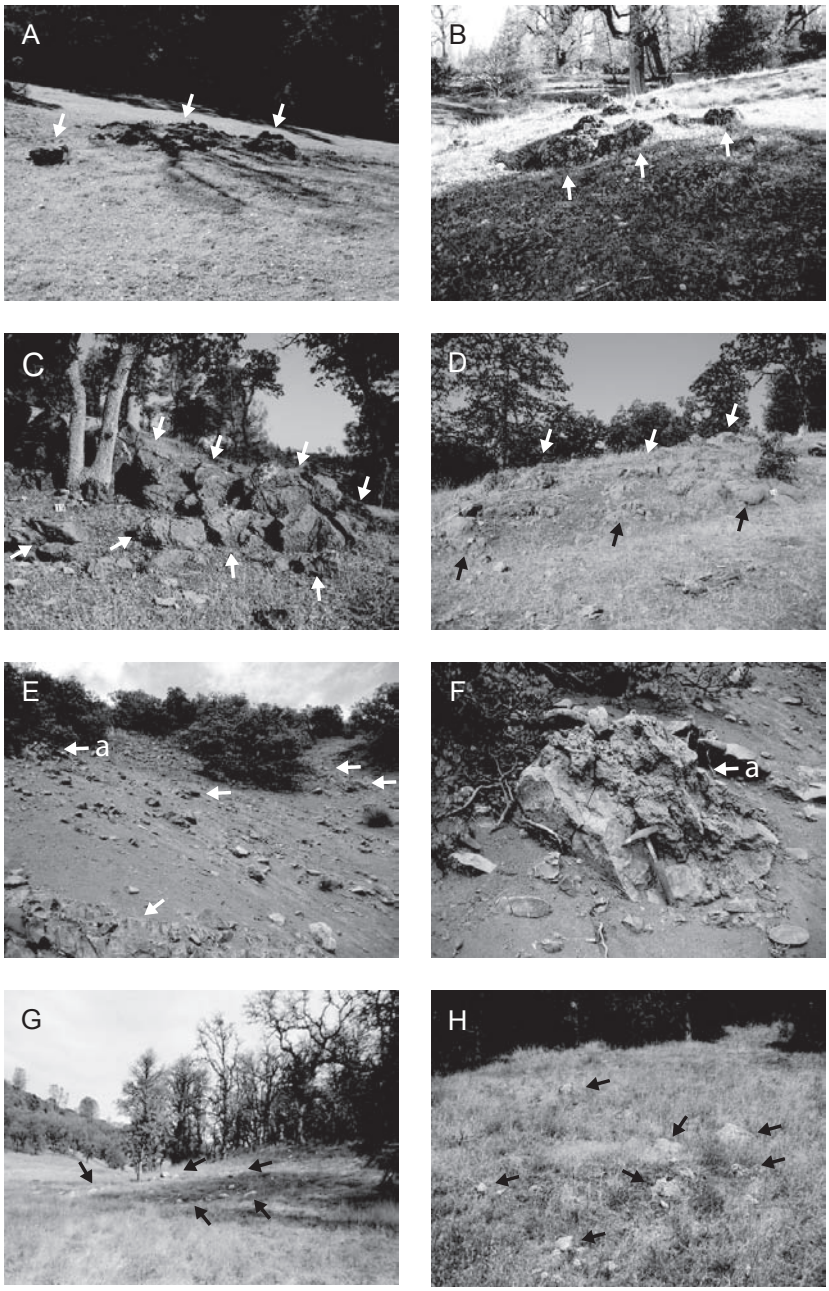

Figure 6. Outcrop variability of some of the hydrocarbon seep localities included in this study. (A-B) Harrington Flat Road, two of twenty roughly circular mounds. (C-D) Cold Fork of Cottonwood Creek, ~300 m linear outcrop. (E) Bear Creek, 32 m vertical succession of micarb lenses, pods, etc. (F) Bear Creek, *in situ* lens of micarb surrounded by GVG turbidites and concretions. (G-H) Rocky Creek, low lying micarb outcrops.

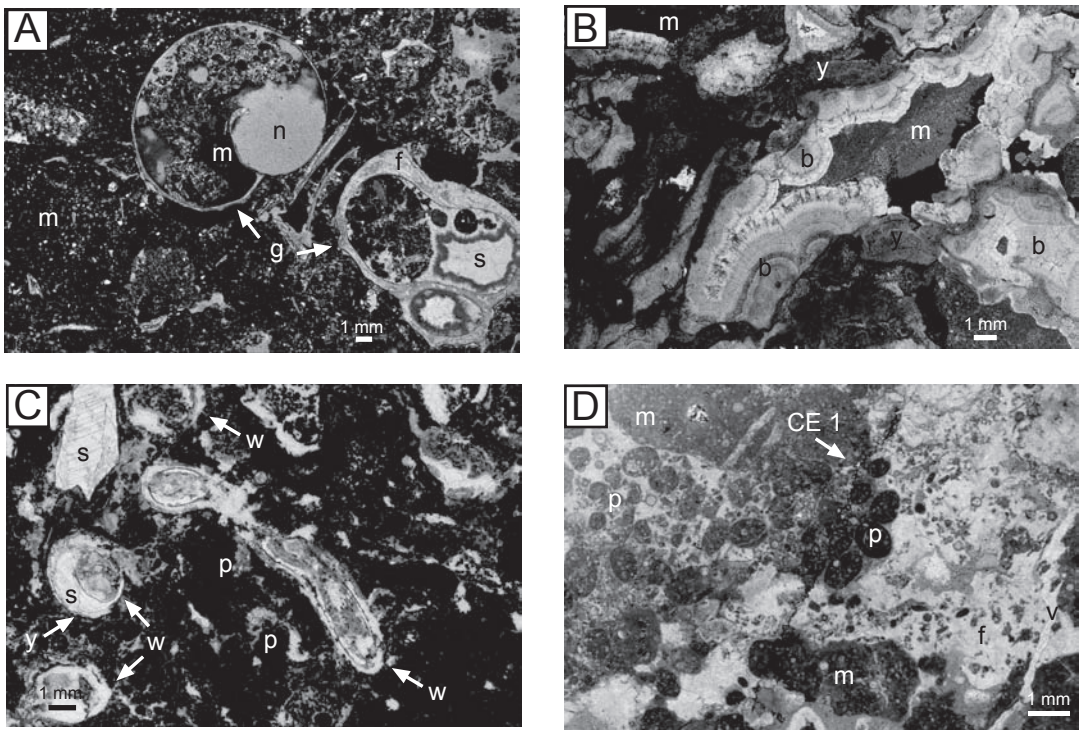

Figure 7. Illustrations of petrographic textures, fabrics, and cements present in some of the GVG and Franciscan thin sections. (A) Pyrite- and peloid-rich detrital-rich micarb (m), including pyrite framboids, calcispheres, peloids, and unidentifiable detritus, encasing gastropods (g, *Paskentana paskentaensis*) incompletely filled with fibrous (f) and sparry (s) calcite and replaced by neomorphosed micrite (n), BC 2A. (B) Horizons of botryoidal calcite (b) and anhedral yellow calcite (y) filling vugs and encrusting remnants of detrital-rich micarb, BC 3A. (C) Worm tube fossils (w) in longitudinal and cross section, encased in peloid-rich (p) detrital-rich micarb and filled with anhedral yellow (y) calcite and sparry calcite. Tube wall has been replaced by pyrite, HFR 13A. (D) Peloids filled with detrital-rich micarb, with detritus including calcispheres and pyrite framboids, as well as fibrous calcite, late stage veins, and evidence of pyrite coated CE1, HFR 13B.

Figure 8. Relative abundances of the faunas in each of the ten assemblages

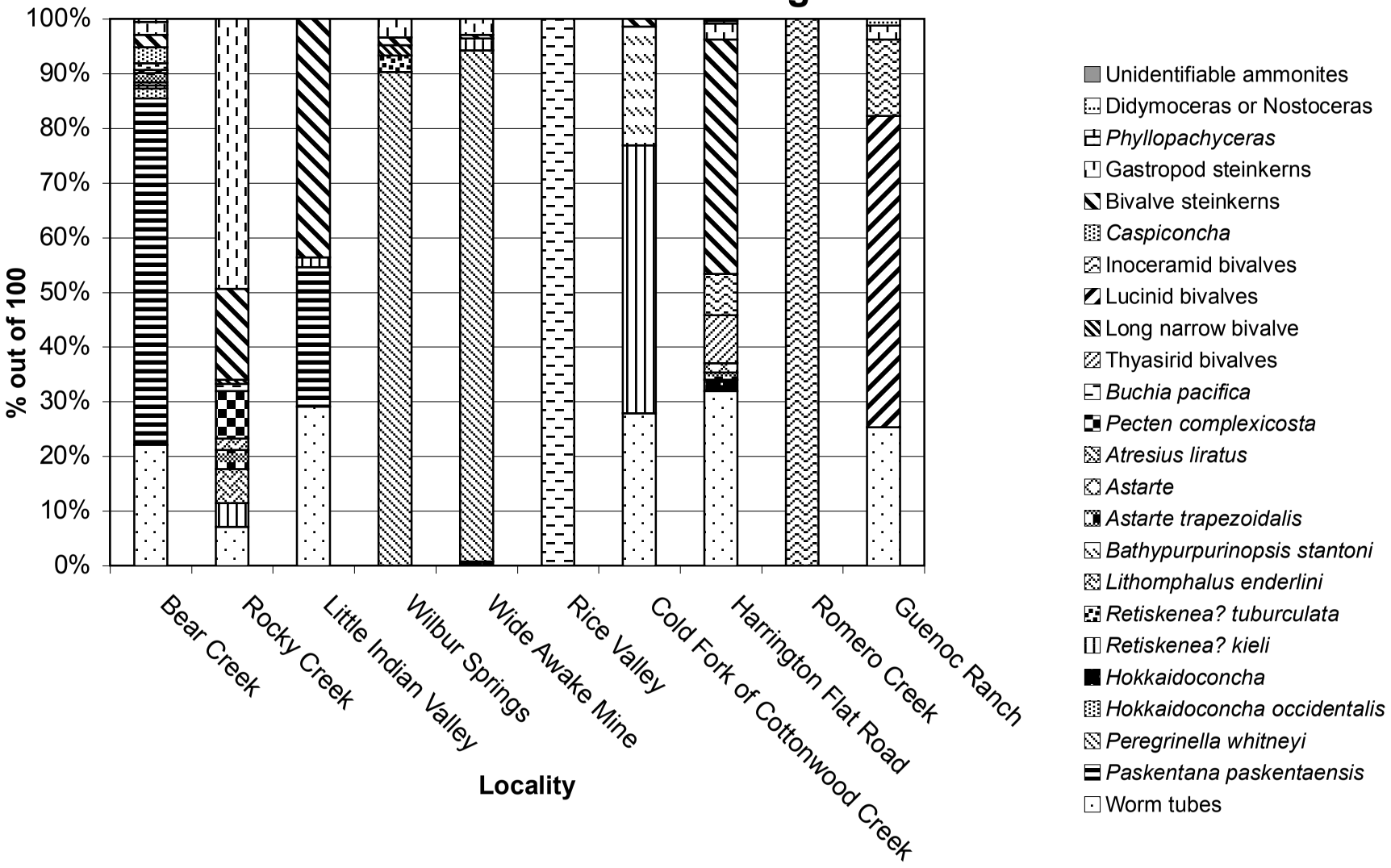

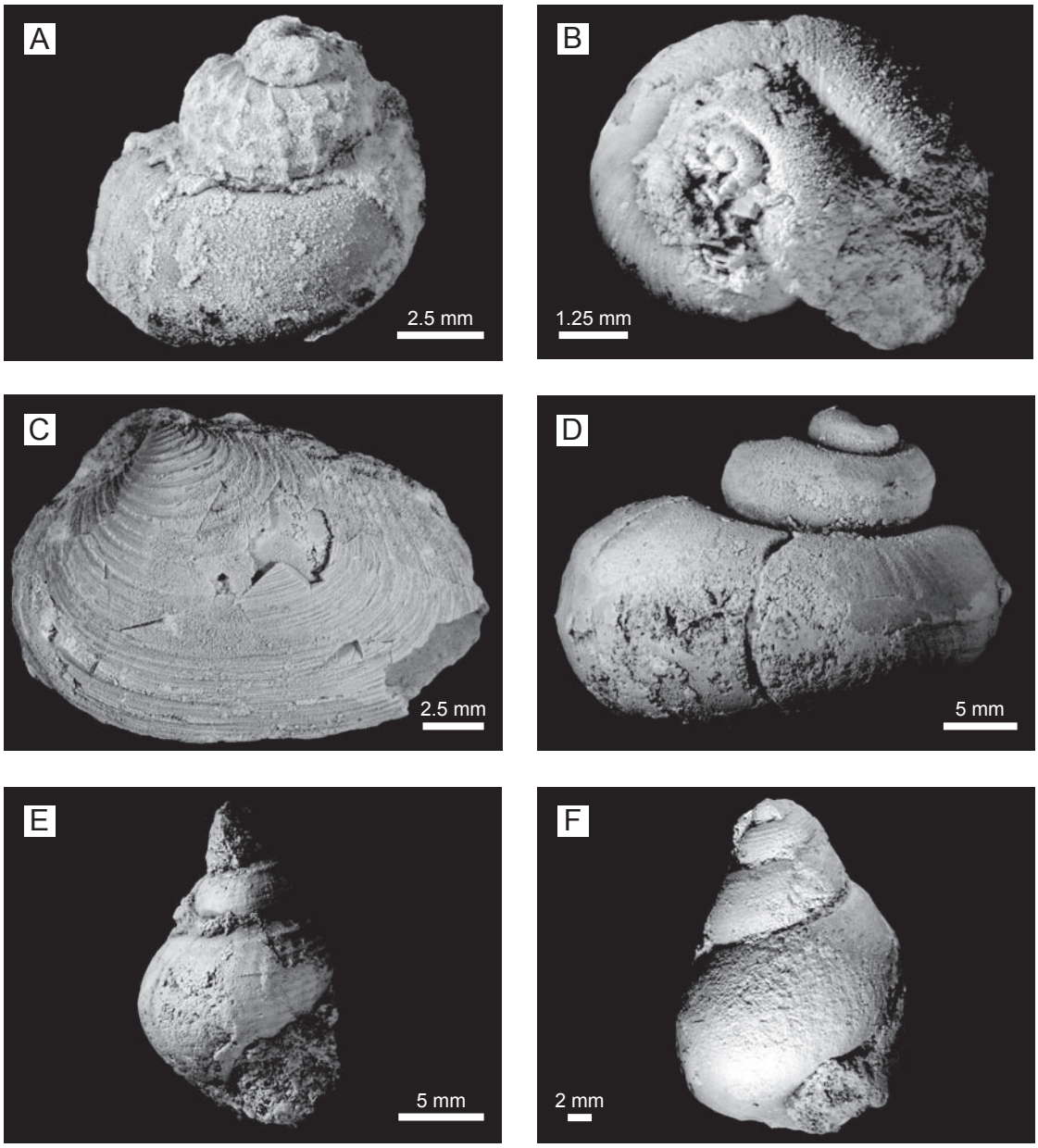

Figure 9. Illustrations of some of the fossils from the 10 localities included in this study. (A) *Paskentana paskentaensis*, Bear Creek; (B) *Retiskenea*? *kieli*, Cold Fork of Cottonwood Creek; (C) *Astarte trapezoidalis*, Harrington Flat Road; (D) *Lithomphalus enderlini*, Rocky Creek; (E) *Atresius liratus*, Rocky Creek; and (F) *Bathypurpurinopsis stantoni*, Cold Fork of Cottonwood Creek.

Figure 10. Cluster analysis of the ten localities, demonstrating that other than Wilbur Springs and Wide Awake Mine, which are heavily dominated by the brachiopod *Peregrinella whitneyi*, there are no patterns to the clusterings. Similarity Measure: Correlation. Correlation coefficient: 0.948.

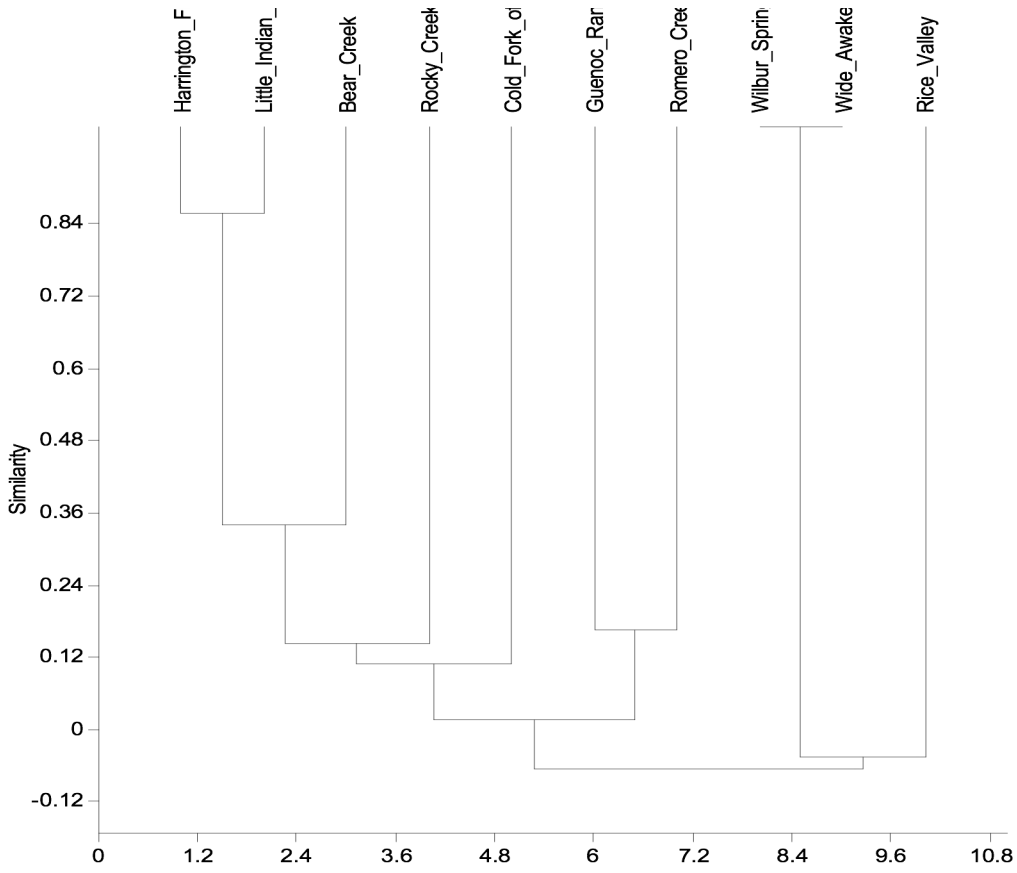

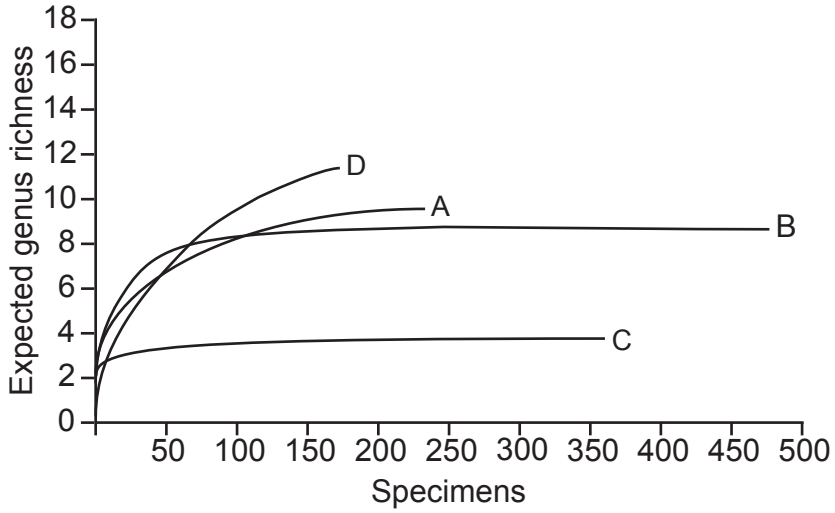

Figure 11. Rarefaction curves for the four hydrocarbon seeps with >1 taxon found during the course of this study. A. Harrington Flat Road, B. Rocky Creek, C. Cold Fork of Cottonwood Creek, D. Bear Creek. A, B, and C, reach an asymptote indicating further sampling would not have increased the number of taxa recovered, while D does not reach an asymptote and thus, further sampling would likely have recovered more taxa.

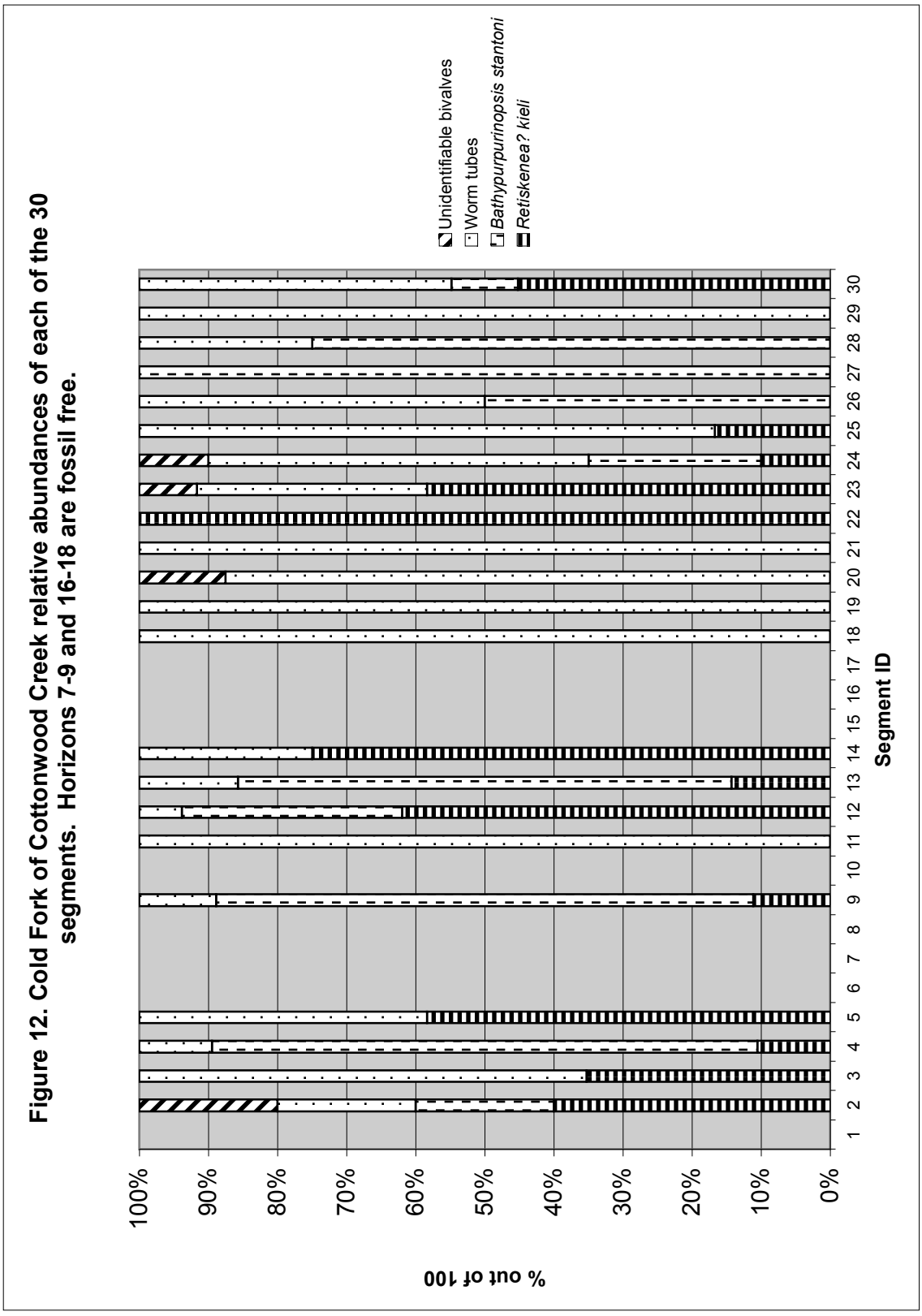

Figure 12. Cold Fork of Cottonwood Creek relative abundances of each of the 30 segments. Horizons 7-9 and 16-18 are fossil free.

Figure 13. Q mode cluster diagram for Cold Fork of Cottonwood Creek, using the Jaccard similarity and distance indice. Correlation coefficient = 0.85.

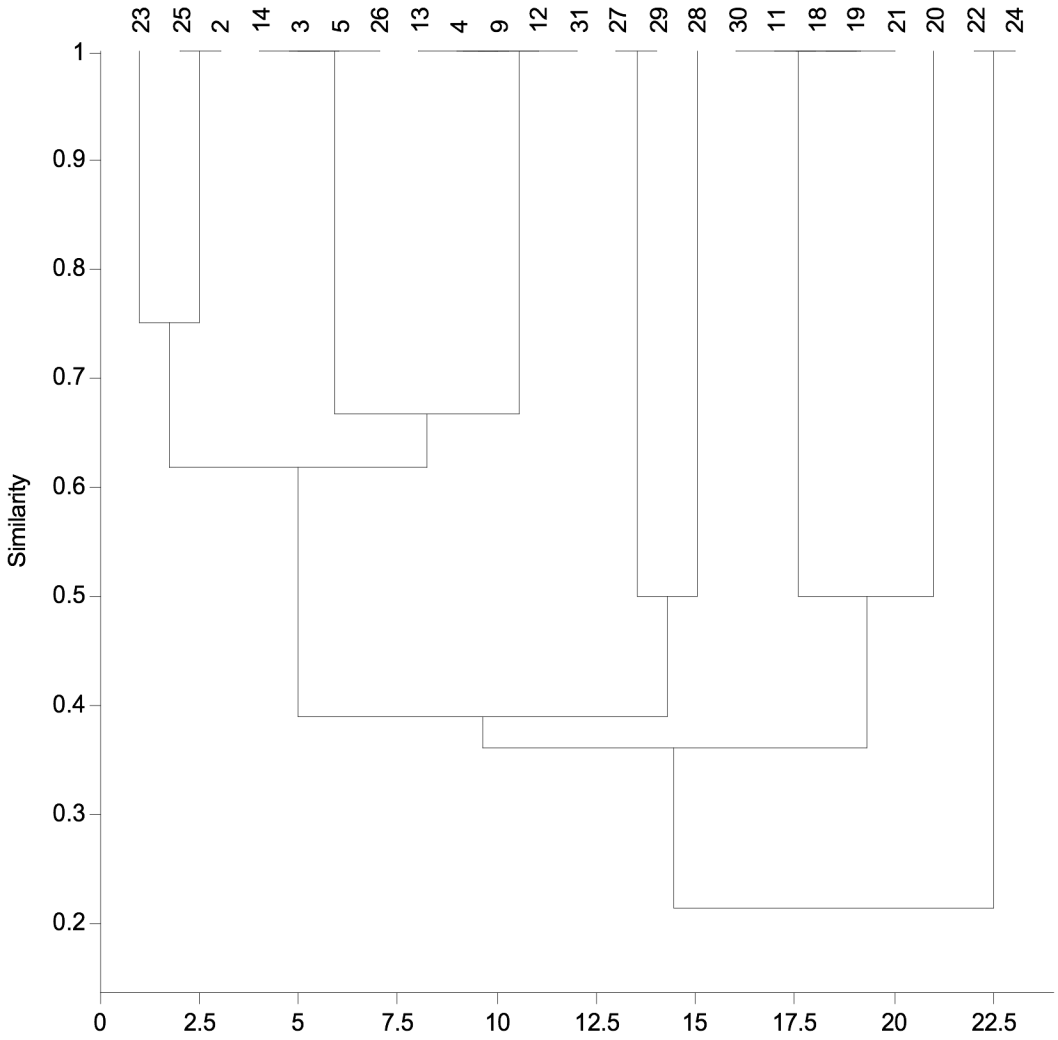

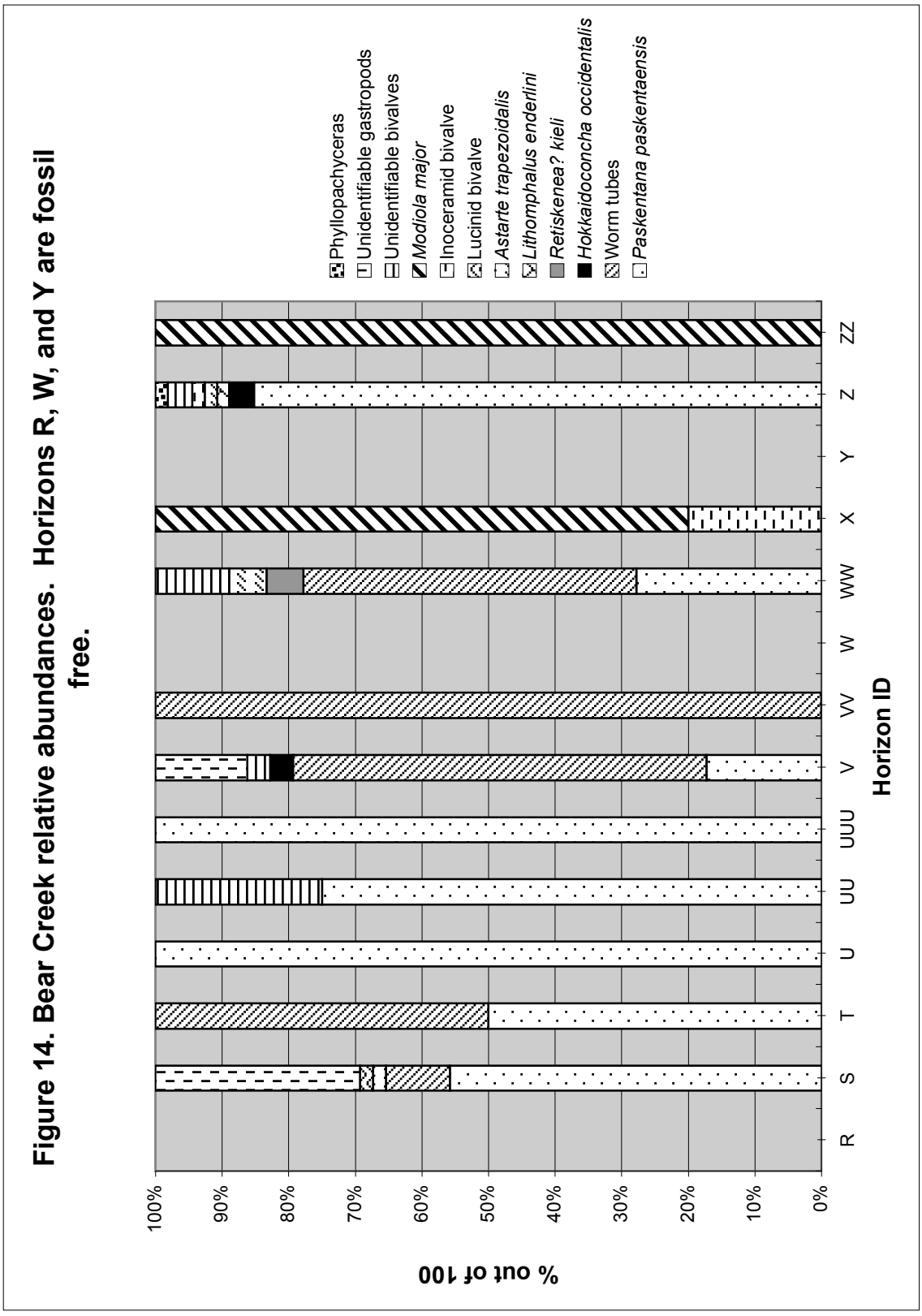

Figure 14. Bear Creek relative abundances. Horizons R, W, and Y are fossil free.

Figure 15. Q mode cluster diagram for Bear Creek, using the Jaccard similarity and distance indice. Correlation coefficient = 0.95.

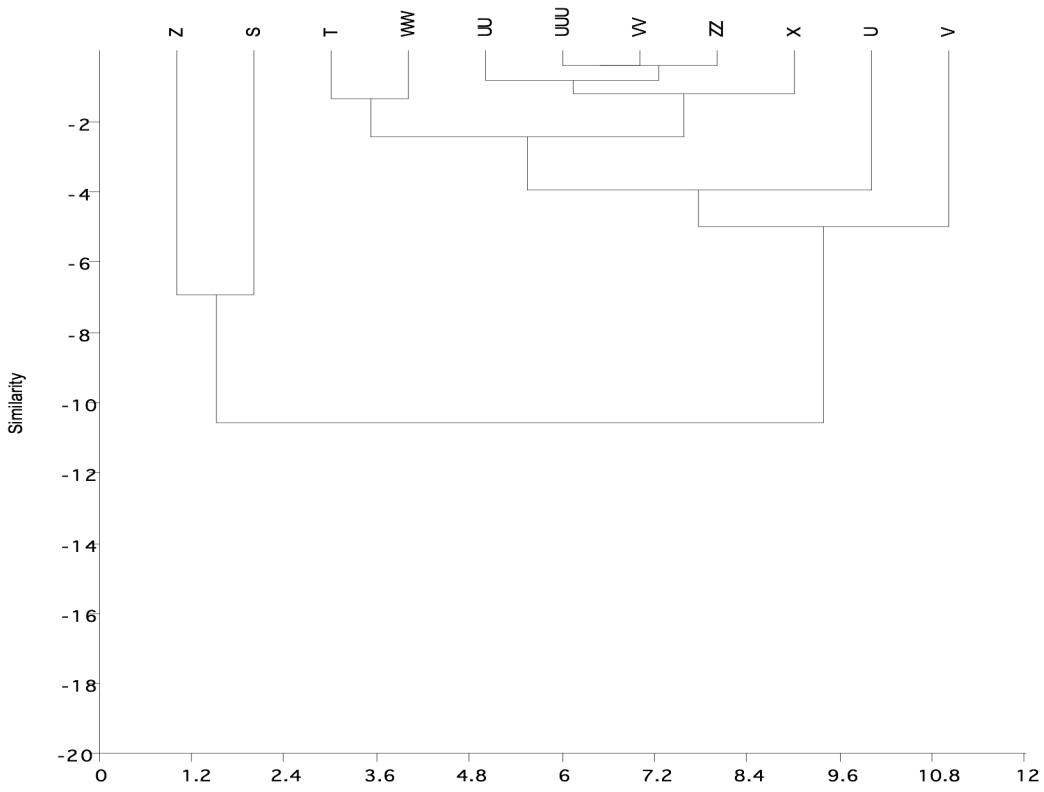

Figure 16. Q mode cluster diagram for Harrington Flat Road, using the Jaccard similarity and distance indice. Correlation coefficient = 0.86.

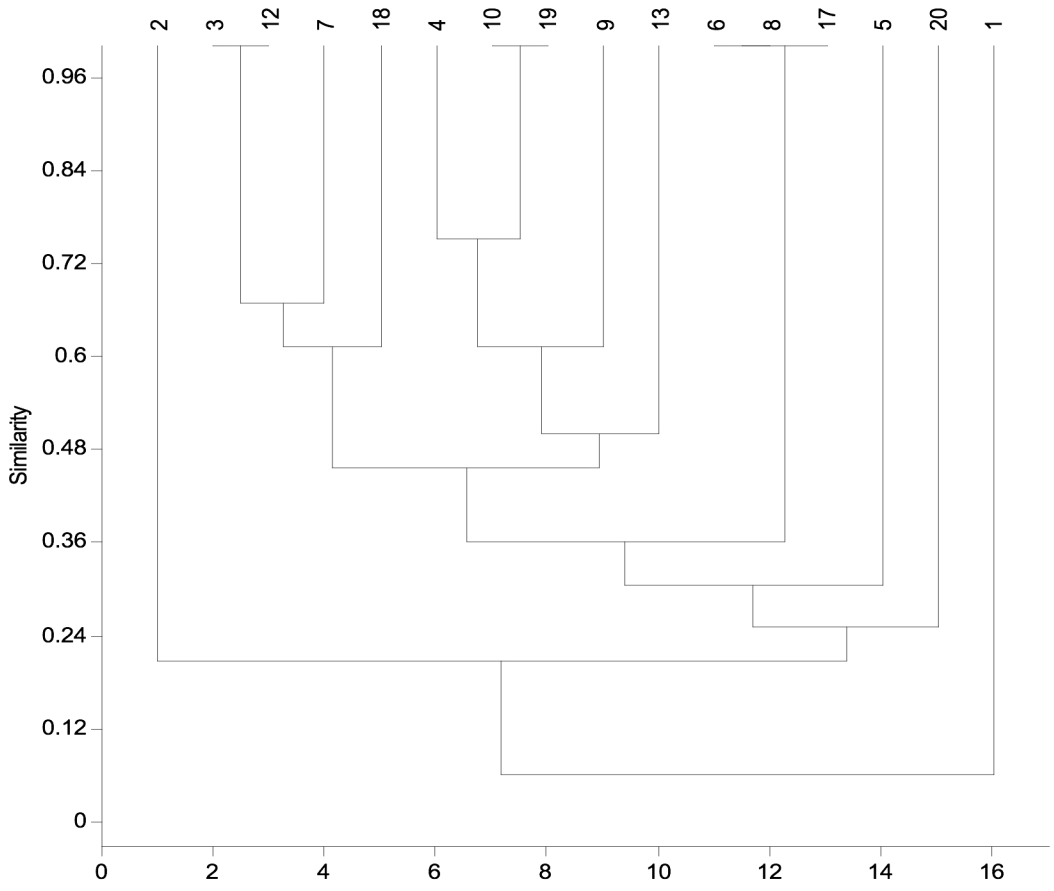

Figure 17. Q mode cluster diagram for Rocky Creek, using the Jaccard similarity and distance indice. Correlation coefficient = 0.84.

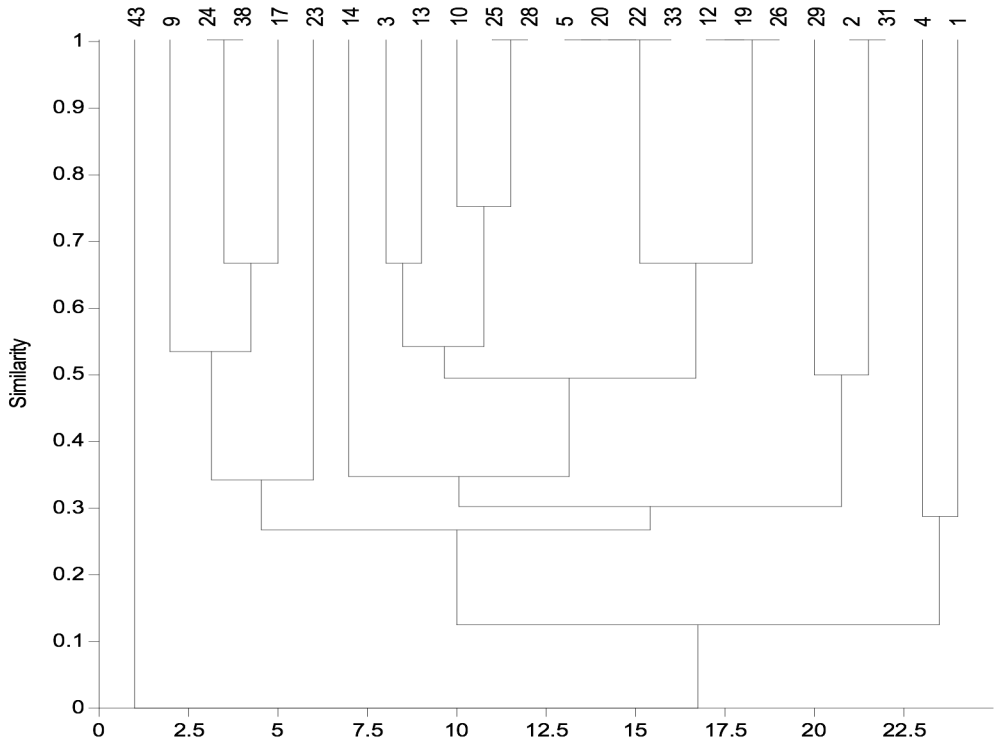

Figure 18.

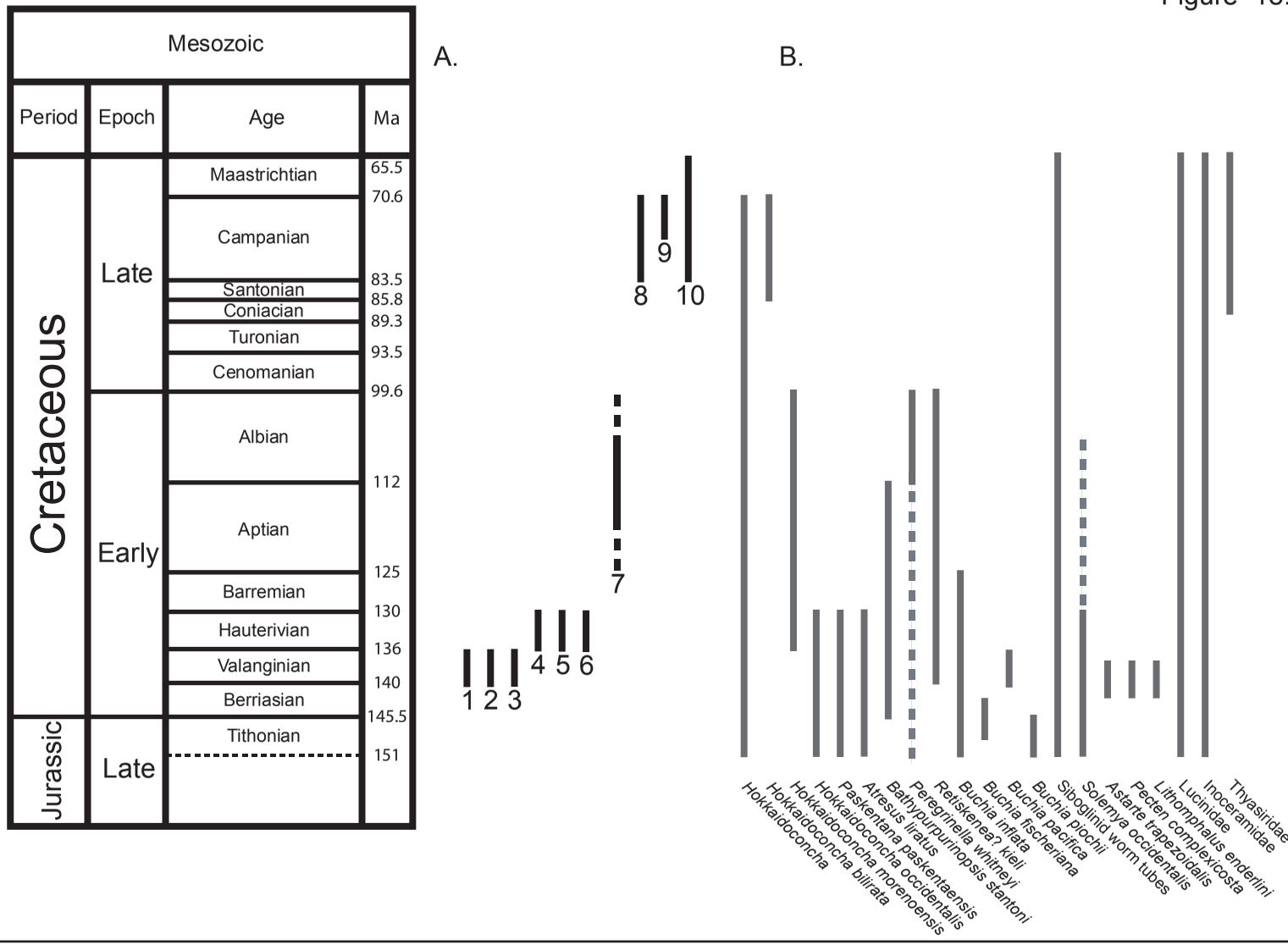
Mesozoic
Period
Epoch
Age
Ma
Cretaceous
Late
Early
Jurassic
Late
Maastrichtian
Campanian
Santonian
Coniacian
Turonian
Cenomanian
Albian
Aptian
Barremian
Hauterivian
Valanginian
Berriasian
Tithonian
65.5
70.6
83.5
85.8
89.3
93.5
99.6
112
125
130
136
140
145.5
151
A.
B.
1 2 3
4 5 6
7
8
9
10
Hokkaidoconcha
Hokkaidoconcha bilirata
Hokkaidoconcha morenoensis
Hokkaidoconcha occidentalis
Paskentana paskentaensis
Atresius liratus
Bathypurpurinopsis stanton
Peregrinella whitneyi
Retiskenea? kieli
Buchia inflata
Buchia fischeriana
Buchia pacifica
Buchia piochii
Sboglinid worm tubes
Solemya occidentalis
Astarte trapezoidalis
Pecten complexicosta
Lithomphalus enderlini
Lucinidae
Inoceramidae
Thyasiridae

Figure 18. Stratigraphic ranges of (A) the 10 deposits and (B) some of the primary faunas collected. (1) Bear Creek, (2) Rocky Creek, (3) Little Indian Valley, (4) Wilbur Springs, (5) Wide Awake Mine, (6) Rice Valley, (7) Cold Fork of Cottonwood Creek, (8) Harrington Flat Road, (9) Romero Creek, and (10) Guenoc Ranch. Faunal stratigraphic ranges from Kiel et al. (2008).

Table 1. Summarized characteristics for the 10 GVG and Franciscan hydrocarbon seep localities included in this study.

Locality Name	Locality Abbreviation	Age	GPS Coordinates (UTM, NAD 83/WGS84)	Formation/ Description	Litho-stratigraphy	Deposit Size	δ13C (‰)	δ18O (‰)	Selected Citations
Bear Creek	BC	Early Cretaceous (Valanginian)	10 551181E 4322704N	Crack Canyon Formation (informal name of Lawton 1956)	GVG	~ 32 m vertical succession	-14.63 to -26.82	-0.88 to -6.73	Kiel and Campbell (2005), Kiel et al., (2008)
Rocky Creek	RC	Early Cretaceous (Valanginian)	See Kiel and Campbell (2005)	Crack Canyon Formation (informal name of Lawton 1956)	GVG	800 m^2	-19.40 to -12.25	0.26 to -1.66	Kiel and Campbell (2005), Kiel et al., (2008)
Little Indian Valley	LIV	Early Cretaceous (Valanginian?)	10 537222E 4325965N	Occurs in Little Indian Valley terrane	Franciscan	100 m^2	-17.12 to -23.40	-2.73 to -9.07	McLaughlin (1989), Kiel et al., (2008)
Wilbur Springs	WS	Early Cretaceous (Hauterivian)	10 550449E 4320227N	Stony Creek Formation	GVG	2,500 m^2	-18.43 to -24.30	1.42 to -1.79	McLaughlin (1989), Campbell (1993, 1995), Campell et al., (2002), Kiel
Wide Awake Mine	WAM	Early Cretaceous (Hauterivian)	10 549491E 4320049N	Stony Creek Formation	GVG	100 m^2	-20.20 to -22.27	0.98 to -2.74	McLaughlin (1989)
Rice Valley	RV	Early Cretaceous (Hauterivian)	10 512567E 4354487N	Unnamed marine strata (R. J. McLaughlin, pers. comm.)	In GVG outlier within Franciscan	unknown	-12.95 to -21.54	3.21 to 0.61	Campbell (1995), Kiel et al., (2008)
Cold Fork of Cottonwood Creek	CFCC	Early Cretaceous (Aptian to Albian)	10 526921E 4446205N	Lodoga Formation	GVG	6,000 m^2: (~300 m long, ~20 to ~40 m wide, and ~1 to ~2 m tall)	-20.10 to -24.90	-2.60 to -11.20	Campbell (1993, 1995), Campell et al., (2002), Kiel et al., (2008)
Harrington Flat Road	HFR	Late Cretaceous (Campanian)	10 522413E 4301428N	Unnamed marine strata	GVG	10,075 m^2	0.17 to -28.62	-1.12 to -5.43	R. J. McLaughlin (pers. comm.)
Romero Creek	RmC	Late Cretaceous (Late Campanian)	10 672566E 4110291N	Moreno Formation	GVG	83,612 m^2	-16.48 to -20.34	-3.16 to -4.02	K. A. Campbell (pers. comm.), Kiel et al., (2008)
Guenoc Ranch	GR	Late Cretaceous (Campanian to Maastrichtian)	10 541228E 4286088N	Sediment gravity flow deposits representing various facies of a submarine fan complex	GVG	2 km x 4 km	-3.41 to -24.50	0.48 to -10.42	Hepper et al., (2003), Hepper (2004)

Table 2. Faunal abundance data collected in the laboratory via crack-outs for each of the 10 deposits. Replicate bulk samples were collected throughout each locality, with ~1.3 kg of material processed from each sample bag. The number of samples processed per locality reflects the overall size of the deposit and the number of samples collected. Values included in this table represent the total number of specimens found of a taxon, throughout an entire locality.

Locality Diversity List and Abundances	Bear Creek	Rocky Creek	Little Indian Valley	Wilbur Springs	Wide Awake Mine	Rice Valley	Cold Fork of Cottonwood Creek	Harrington Flat Road	Romero Creek	Guenoc Ranch	Total
Worm tubes	38	34	16	0	0	0	100	76	0	20	**284**
Paskentana paskentaensis	109	0	14	0	1	0	0	0	0	0	**124**
Peregrinella whitneyi	0	0	0	242	129	0	0	0	0	0	**371**
Hokkaidoconcha occidentalis	3	0	0	0	0	0	0	0	0	0	**3**
Hokkaidoconcha	0	0	0	0	0	0	0	5	0	0	**5**
Retiskenea? kieli	1	21	1	0	3	0	176	0	0	0	**202**
Retiskenea? tuburculata	0	0	0	8	0	0	0	0	0	0	**8**
Lithomphalus enderlini	1	30	0	0	0	0	0	0	0	0	**31**
Bathypurpurinopsis stantoni	0	0	0	0	0	0	78	0	0	0	**78**
Astarte trapezoidalis	3	17	0	0	0	0	0	3	0	0	**23**
Astarte	0	0	0	0	0	0	0	4	0	0	**4**
Atresius liratus	0	10	0	0	0	0	0	0	0	0	**10**
Pecten complexicosta	0	42	0	0	0	0	0	0	0	0	**42**
Buchia pacifica	0	6	0	0	0	2	0	0	0	0	**8**
Thyasirid bivalves	0	0	0	0	0	0	0	21	0	0	**21**
Long narrow bivalve	0	4	0	5	0	0	0	0	0	0	**9**
Lucinid bivalves	1	0	0	0	0	0	0	0	0	45	**46**
Inoceramid bivalves	2	0	0	0	0	0	0	18	5	11	**36**
Caspiconcha	5	0	0	0	0	0	0	0	0	0	**5**
Bivalve steinkerns	4	80	24	4	1	0	5	102	0	0	**220**
Gastropod steinkerns	4	238	0	9	4	0	0	7	0	2	**264**
Phyllopachyceras	1	0	0	0	0	0	0	1	0	0	**2**
Didymoceras* or *Nostoceras	0	0	0	0	0	0	0	0	0	1	**1**
Unidentifiable ammonites	0	0	0	0	0	0	0	1	0	0	**1**
N =	**172**	**482**	**55**	**268**	**138**	**2**	**359**	**238**	**5**	**79**	**1798**

Table 3. Diversity indices for the ten hydrocarbon seep localities; calculations are based on abundance data for each locality.

	Bear Creek	Rocky Creek	Little Indian Valley	Wilbur Springs	Wide Awake Mine	Rice Valley	Cold Fork of Cottonwood Creek	Harrington Flat Road	Romero Creek	Guenoc Ranch
Taxa (S)	12	10	4	5	5	1	4	10	1	5
Individuals (N)	172	482	55	268	138	2	359	238	5	79
Shannon (H)	1.213	1.648	1.142	0.448	0.3203	0	1.097	1.492	0	1.091
Menhinick	0.915	0.4555	0.5394	0.3054	0.4256	0.7071	0.2111	0.6482	0.4472	0.5625
Margalef	2.137	1.457	0.7486	0.7154	0.8118	0	0.5099	1.645	0	0.9154
Fisher alpha	2.936	1.785	0.9917	0.8725	1.017	0.7959	0.6302	2.113	0.3759	1.187
Berger-Parker	0.6337	0.4938	0.4364	0.903	0.9348	1	0.4903	0.4286	1	0.5696

Table 4. Diversity indices calculated for each of the 30 segments documented at Cold Fork of Cottonwood Creek.

Segment ID	1	2	3	4	5	6	7	8	9	10
Taxa	0	4	2	3	2	0	0	0	3	0
Individuals	0	5	17	19	36	0	0	0	9	0
Shannon	0	1.33	0.65	0.66	0.68	0	0	0	0.68	0
Simpson	0	0.72	0.46	0.35	0.49	0	0	0	0.37	0
Menhinick	0	1.79	0.49	0.69	0.33	0	0	0	1.00	0
Margalef	0	1.86	0.35	0.68	0.28	0	0	0	0.91	0
Equitability	0	0.96	0.94	0.60	0.98	0	0	0	0.62	0
Fisher alpha	0	9.28	0.59	1.00	0.46	0	0	0	1.58	0
Berger-Parker	0	0.40	0.65	0.79	0.58	0	0	0	0.78	0

Segment ID	11	12	13	14	15	16	17	18	19	20
Taxa	1	3	3	2	0	0	0	1	1	2
Individuals	1	113	7	16	0	0	0	1	1	8
Shannon	0	0.83	0.80	0.56	0	0	0	0	0	0.38
Simpson	0	0.51	0.45	0.38	0	0	0	0	0	0.22
Menhinick	0	0.28	1.13	0.50	0	0	0	0	0	0.71
Margalef	0	0.42	1.03	0.36	0	0	0	0	0	0.48
Equitability	0	0.76	0.72	0.81	0	0	0	0	0	0.54
Fisher alpha	0	0.57	1.99	0.60	0	0	0	0	0	0.86
Berger-Parker	1	0.62	0.71	0.75	0	0	0	1	1	0.88

Segment ID	21	22	23	24	25	26	27	28	29	30
Taxa	1	1	3	1	4	2	2	1	2	1
Individuals	1	28	12	6	20	24	4	1	4	1
Shannon	0	0	0.89	0	1.14	0.45	0.69	0	0.56	0
Simpson	0	0	0.54	0	0.62	0.28	0.5	0	0.38	0
Menhinick	0	0.19	0.87	0.41	0.89	0.41	1	0	1	0
Margalef	0	0	0.80	0	1.00	0.31	0.72	0	0.72	0
Equitability	0	0	0.81	0	0.82	0.65	1	0	0.81	0
Fisher alpha	0	0.20	1.28	0.34	1.50	0.52	1.59	0	1.59	0
Berger-Parker	1	1	0.58	1	0.55	0.83	0.5	1	0.75	1

Table 5. Cold Fork of Cottonwood Creek similarity and distance indices. The horizons that did not contain fossils were excluded.

Dice	2	3	4	5	9	11	12	13	14	18	19	20	21	22	23	24	25	26	27	28	29	30
2	1	0.667	0.857	0.667	0.857	0.4	0.857	0.857	0.667	0.4	0.4	0.667	0.4	0.4	0.857	0.4	1	0.667	0.667	0.4	0.667	0.4
3	0.667	1	0.8	1	0.8	0.667	0.8	0.8	1	0.667	0.667	0.5	0.667	0.667	0.8	0.667	0.667	1	0.5	0	0.5	0.667
4	0.857	0.8	1	0.8	1	0.5	1	1	0.8	0.5	0.5	0.4	0.5	0.5	0.667	0.5	0.857	0.8	0.8	0.5	0.8	0.5
5	0.667	1	0.8	1	0.8	0.667	0.8	0.8	1	0.667	0.667	0.5	0.667	0.667	0.8	0.667	0.667	1	0.5	0	0.5	0.667
9	0.857	0.8	1	0.8	1	0.5	1	1	0.8	0.5	0.5	0.4	0.5	0.5	0.667	0.5	0.857	0.8	0.8	0.5	0.8	0.5
11	0.4	0.667	0.5	0.667	0.5	1	0.5	0.5	0.667	1	1	0.667	1	0	0.5	0	0.4	0.667	0.667	0	0.667	1
12	0.857	0.8	1	0.8	1	0.5	1	1	0.8	0.5	0.5	0.4	0.5	0.5	0.667	0.5	0.857	0.8	0.8	0.5	0.8	0.5
13	0.857	0.8	1	0.8	1	0.5	1	1	0.8	0.5	0.5	0.4	0.5	0.5	0.667	0.5	0.857	0.8	0.8	0.5	0.8	0.5
14	0.667	1	0.8	1	0.8	0.667	0.8	0.8	1	0.667	0.667	0.5	0.667	0.667	0.8	0.667	0.667	1	0.5	0	0.5	0.667
18	0.4	0.667	0.5	0.667	0.5	1	0.5	0.5	0.667	1	1	0.667	1	0	0.5	0	0.4	0.667	0.667	0	0.667	1
19	0.4	0.667	0.5	0.667	0.5	1	0.5	0.5	0.667	1	1	0.667	1	0	0.5	0	0.4	0.667	0.667	0	0.667	1
20	0.667	0.5	0.4	0.5	0.4	0.667	0.4	0.4	0.5	0.667	0.667	1	0.667	0	0.8	0	0.667	0.5	0.5	0	0.5	0.667
21	0.4	0.667	0.5	0.667	0.5	1	0.5	0.5	0.667	1	1	0.667	1	0	0.5	0	0.4	0.667	0.667	0	0.667	1
22	0.4	0.667	0.5	0.667	0.5	0	0.5	0.5	0.667	0	0	0	0	1	0.5	1	0.4	0.667	0	0	0	0
23	0.857	0.8	0.667	0.8	0.667	0.5	0.667	0.667	0.8	0.5	0.5	0.8	0.5	0.5	1	0.5	0.857	0.8	0.4	0	0.4	0.5
24	0.4	0.667	0.5	0.667	0.5	0	0.5	0.5	0.667	0	0	0	0	1	0.5	1	0.4	0.667	0	0	0	0
25	1	0.667	0.857	0.667	0.857	0.4	0.857	0.857	0.667	0.4	0.4	0.667	0.4	0.4	0.857	0.4	1	0.667	0.667	0.4	0.667	0.4
26	0.667	1	0.8	1	0.8	0.667	0.8	0.8	1	0.667	0.667	0.5	0.667	0.667	0.8	0.667	0.667	1	0.5	0	0.5	0.667
27	0.667	0.5	0.8	0.5	0.8	0.667	0.8	0.8	0.5	0.667	0.667	0.5	0.667	0	0.4	0	0.667	0.5	1	0.667	1	0.667
28	0.4	0	0.5	0	0.5	0	0.5	0.5	0	0	0	0	0	0	0	0	0.4	0	0.667	1	0.667	0
29	0.667	0.5	0.8	0.5	0.8	0.667	0.8	0.8	0.5	0.667	0.667	0.5	0.667	0	0.4	0	0.667	0.5	1	0.667	1	0.667
30	0.4	0.667	0.5	0.667	0.5	1	0.5	0.5	0.667	1	1	0.667	1	0	0.5	0	0.4	0.667	0.667	0	0.667	1
31	0.857	0.8	1	0.8	1	0.5	1	1	0.8	0.5	0.5	0.4	0.5	0.5	0.667	0.5	0.857	0.8	0.8	0.5	0.8	0.5

Jaccard	**2**	**3**	**4**	**5**	**9**	**11**	**12**	**13**	**14**	**18**	**19**	**20**	**21**	**22**	**23**	**24**	**25**	**26**	**27**	**28**	**29**	**30**
2	1	0.5	0.75	0.5	0.75	0.25	0.75	0.75	0.5	0.25	0.25	0.5	0.25	0.25	0.75	0.25	1	0.5	0.5	0.25	0.5	0.25
3	0.5	1	0.667	1	0.667	0.5	0.667	0.667	1	0.5	0.5	0.333	0.5	0.5	0.667	0.5	0.5	1	0.333	0	0.333	0.5
4	0.75	0.667	1	0.667	1	0.333	1	1	0.667	0.333	0.333	0.25	0.333	0.333	0.5	0.333	0.75	0.667	0.667	0.333	0.667	0.333
5	0.5	1	0.667	1	0.667	0.5	0.667	0.667	1	0.5	0.5	0.333	0.5	0.5	0.667	0.5	0.5	1	0.333	0	0.333	0.5
9	0.75	0.667	1	0.667	1	0.333	1	1	0.667	0.333	0.333	0.25	0.333	0.333	0.5	0.333	0.75	0.667	0.667	0.333	0.667	0.333
11	0.25	0.5	0.333	0.5	0.333	1	0.333	0.333	0.5	1	1	0.5	1	0	0.333	0	0.25	0.5	0.5	0	0.5	1
12	0.75	0.667	1	0.667	1	0.333	1	1	0.667	0.333	0.333	0.25	0.333	0.333	0.5	0.333	0.75	0.667	0.667	0.333	0.667	0.333
13	0.75	0.667	1	0.667	1	0.333	1	1	0.667	0.333	0.333	0.25	0.333	0.333	0.5	0.333	0.75	0.667	0.667	0.333	0.667	0.333
14	0.5	1	0.667	1	0.667	0.5	0.667	0.667	1	0.5	0.5	0.333	0.5	0.5	0.667	0.5	0.5	1	0.333	0	0.333	0.5
18	0.25	0.5	0.333	0.5	0.333	1	0.333	0.333	0.5	1	1	0.5	1	0	0.333	0	0.25	0.5	0.5	0	0.5	1
19	0.25	0.5	0.333	0.5	0.333	1	0.333	0.333	0.5	1	1	0.5	1	0	0.333	0	0.25	0.5	0.5	0	0.5	1
20	0.5	0.333	0.25	0.333	0.25	0.5	0.25	0.25	0.333	0.5	0.5	1	0.5	0	0.667	0	0.5	0.333	0.333	0	0.333	0.5
21	0.25	0.5	0.333	0.5	0.333	1	0.333	0.333	0.5	1	1	0.5	1	0	0.333	0	0.25	0.5	0.5	0	0.5	1
22	0.25	0.5	0.333	0.5	0.333	0	0.333	0.333	0.5	0	0	0	0	1	0.333	1	0.25	0.5	0	0	0	0
23	0.75	0.667	0.5	0.667	0.5	0.333	0.5	0.5	0.667	0.333	0.333	0.667	0.333	0.333	1	0.333	0.75	0.667	0.25	0	0.25	0.333
24	0.25	0.5	0.333	0.5	0.333	0	0.333	0.333	0.5	0	0	0	0	1	0.333	1	0.25	0.5	0	0	0	0
25	1	0.5	0.75	0.5	0.75	0.25	0.75	0.75	0.5	0.25	0.25	0.5	0.25	0.25	0.75	0.25	1	0.5	0.5	0.25	0.5	0.25
26	0.5	1	0.667	1	0.667	0.5	0.667	0.667	1	0.5	0.5	0.333	0.5	0.5	0.667	0.5	0.5	1	0.333	0	0.333	0.5
27	0.5	0.333	0.667	0.333	0.667	0.5	0.667	0.667	0.333	0.5	0.5	0.333	0.5	0	0.25	0	0.5	0.333	1	0.5	1	0.5
28	0.25	0	0.333	0	0.333	0	0.333	0.333	0	0	0	0	0	0	0	0	0.25	0	0.5	1	0.5	0
29	0.5	0.333	0.667	0.333	0.667	0.5	0.667	0.667	0.333	0.5	0.5	0.333	0.5	0	0.25	0	0.5	0.333	1	0.5	1	0.5
30	0.25	0.5	0.333	0.5	0.333	1	0.333	0.333	0.5	1	1	0.5	1	0	0.333	0	0.25	0.5	0.5	0	0.5	1
31	0.75	0.667	1	0.667	1	0.333	1	1	0.667	0.333	0.333	0.25	0.333	0.333	0.5	0.333	0.75	0.667	0.667	0.333	0.667	0.333

Simpson	2	3	4	5	9	11	12	13	14	18	19	20	21	22	23	24	25	26	27	28	29	30
2	1	1	1	1	1	1	1	1	1	1	1	1	1	1	1	1	1	1	1	1	1	1
3	1	1	1	1	1	1	1	1	1	1	1	0.5	1	1	1	1	1	1	0.5	0	0.5	1
4	1	1	1	1	1	1	1	1	1	1	1	0.5	1	1	0.667	1	1	1	1	1	1	1
5	1	1	1	1	1	1	1	1	1	1	1	0.5	1	1	1	1	1	1	0.5	0	0.5	1
9	1	1	1	1	1	1	1	1	1	1	1	0.5	1	1	0.667	1	1	1	1	1	1	1
11	1	1	1	1	1	1	1	1	1	1	1	1	1	0	1	0	1	1	1	0	1	1
12	1	1	1	1	1	1	1	1	1	1	1	0.5	1	1	0.667	1	1	1	1	1	1	1
13	1	1	1	1	1	1	1	1	1	1	1	0.5	1	1	0.667	1	1	1	1	1	1	1
14	1	1	1	1	1	1	1	1	1	1	1	0.5	1	1	1	1	1	1	0.5	0	0.5	1
18	1	1	1	1	1	1	1	1	1	1	1	1	1	0	1	0	1	1	1	0	1	1
19	1	1	1	1	1	1	1	1	1	1	1	1	1	0	1	0	1	1	1	0	1	1
20	1	0.5	0.5	0.5	0.5	1	0.5	0.5	0.5	1	1	1	1	0	1	0	1	0.5	0.5	0	0.5	1
21	1	1	1	1	1	1	1	1	1	1	1	1	1	0	1	0	1	1	1	0	1	1
22	1	1	1	1	1	0	1	1	1	0	0	0	0	1	1	1	1	1	0	0	0	0
23	1	1	0.667	1	0.667	1	0.667	0.667	1	1	1	1	1	1	1	1	1	1	0.5	0	0.5	1
24	1	1	1	1	1	0	1	1	1	0	0	0	0	1	1	1	1	1	0	0	0	0
25	1	1	1	1	1	1	1	1	1	1	1	1	1	1	1	1	1	1	1	1	1	1
26	1	1	1	1	1	1	1	1	1	1	1	0.5	1	1	1	1	1	1	0.5	0	0.5	1
27	1	0.5	1	0.5	1	1	1	1	0.5	1	1	0.5	1	0	0.5	0	1	0.5	1	1	1	1
28	1	0	1	0	1	0	1	1	0	0	0	0	0	0	0	0	1	0	1	1	1	0
29	1	0.5	1	0.5	1	1	1	1	0.5	1	1	0.5	1	0	0.5	0	1	0.5	1	1	1	1
30	1	1	1	1	1	1	1	1	1	1	1	1	1	0	1	0	1	1	1	0	1	1
31	1	1	1	1	1	1	1	1	1	1	1	0.5	1	1	0.667	1	1	1	1	1	1	1

Raup-Crick	2	3	4	5	9	11	12	13	14	18	19	20	21	22	23	24	25	26	27	28	29	30
2	1	0.5	0.5	0.5	0.5	0.5	0.5	0.5	0.5	0.5	0.5	0.5	0.5	0.5	0.5	0.5	0.5	0.5	0.5	0.5	0.5	0.5
3	0.5	1	0.653	0.848	0.668	0.693	0.675	0.653	0.888	0.685	0.7	0.46	0.683	0.69	0.663	0.735	0.5	0.898	0.433	0.2	0.42	0.705
4	0.5	0.653	1	0.675	0.79	0.578	0.79	0.778	0.66	0.59	0.573	0.145	0.613	0.55	0.278	0.575	0.5	0.688	0.665	0.588	0.708	0.558
5	0.5	0.848	0.675	1	0.663	0.713	0.655	0.655	0.853	0.693	0.665	0.428	0.69	0.673	0.675	0.72	0.5	0.888	0.428	0.2	0.448	0.678
9	0.5	0.668	0.79	0.663	1	0.568	0.775	0.773	0.638	0.598	0.57	0.168	0.59	0.568	0.298	0.585	0.5	0.668	0.675	0.578	0.673	0.565
11	0.5	0.693	0.578	0.713	0.568	1	0.585	0.575	0.7	0.84	0.843	0.693	0.838	0.345	0.58	0.338	0.5	0.72	0.703	0.335	0.72	0.838
12	0.5	0.675	0.79	0.655	0.775	0.585	1	0.763	0.69	0.575	0.563	0.143	0.588	0.58	0.295	0.57	0.5	0.685	0.653	0.593	0.645	0.57
13	0.5	0.653	0.778	0.655	0.773	0.575	0.763	1	0.683	0.598	0.565	0.145	0.578	0.573	0.283	0.578	0.5	0.67	0.648	0.573	0.678	0.558
14	0.5	0.888	0.66	0.853	0.638	0.7	0.69	0.683	1	0.725	0.698	0.453	0.693	0.693	0.65	0.7	0.5	0.873	0.423	0.213	0.425	0.735
18	0.5	0.685	0.59	0.693	0.598	0.84	0.575	0.598	0.725	1	0.85	0.725	0.863	0.33	0.585	0.295	0.5	0.698	0.703	0.323	0.69	0.853
19	0.5	0.7	0.573	0.665	0.57	0.843	0.563	0.565	0.698	0.85	1	0.715	0.828	0.36	0.56	0.36	0.5	0.7	0.713	0.34	0.723	0.85
20	0.5	0.46	0.145	0.428	0.168	0.693	0.143	0.145	0.453	0.725	0.715	1	0.683	0.215	0.685	0.22	0.5	0.453	0.428	0.195	0.41	0.7
21	0.5	0.683	0.613	0.69	0.59	0.838	0.588	0.578	0.693	0.863	0.828	0.683	1	0.32	0.59	0.35	0.5	0.688	0.7	0.348	0.73	0.863
22	0.5	0.69	0.55	0.673	0.568	0.345	0.58	0.573	0.693	0.33	0.36	0.215	0.32	1	0.59	0.838	0.5	0.685	0.215	0.355	0.178	0.36
23	0.5	0.663	0.278	0.675	0.298	0.58	0.295	0.283	0.65	0.585	0.56	0.685	0.59	0.59	1	0.573	0.5	0.65	0.153	0.068	0.16	0.573
24	0.5	0.735	0.575	0.72	0.585	0.338	0.57	0.578	0.7	0.295	0.36	0.22	0.35	0.838	0.573	1	0.5	0.7	0.23	0.343	0.163	0.363
25	0.5	0.5	0.5	0.5	0.5	0.5	0.5	0.5	0.5	0.5	0.5	0.5	0.5	0.5	0.5	0.5	1	0.5	0.5	0.5	0.5	0.5
26	0.5	0.898	0.688	0.888	0.668	0.72	0.685	0.67	0.873	0.698	0.7	0.453	0.688	0.685	0.65	0.7	0.5	1	0.445	0.218	0.46	0.693
27	0.5	0.433	0.665	0.428	0.675	0.703	0.653	0.648	0.423	0.703	0.713	0.428	0.7	0.215	0.153	0.23	0.5	0.445	1	0.7	0.868	0.725
28	0.5	0.2	0.588	0.2	0.578	0.335	0.593	0.573	0.213	0.323	0.34	0.195	0.348	0.355	0.068	0.343	0.5	0.218	0.7	1	0.688	0.363
29	0.5	0.42	0.708	0.448	0.673	0.72	0.645	0.678	0.425	0.69	0.723	0.41	0.73	0.178	0.16	0.163	0.5	0.46	0.868	0.688	1	0.71
30	0.5	0.705	0.558	0.678	0.565	0.838	0.57	0.558	0.735	0.853	0.85	0.7	0.863	0.36	0.573	0.363	0.5	0.693	0.725	0.363	0.71	1
31	0.5	0.658	0.768	0.683	0.78	0.558	0.778	0.79	0.685	0.58	0.588	0.173	0.578	0.568	0.298	0.573	0.5	0.663	0.7	0.595	0.663	0.583

Table 6. Bear Creek diversity indices. Excludes fossil free horizons.

Horizon ID	S	T	U	UU	UUU	V	VV	WW	X	Z	ZZ
Taxa	5	2	1	2	1	5	1	5	2	7	1
Individuals	52	10	15	4	1	29	1	18	5	54	1
Dominance	0.4157	0.5	1	0.625	1	0.4364	1	0.3457	0.68	0.7298	1
Shannon	1.065	0.6931	0	0.5623	0	1.105	0	1.268	0.5004	0.6762	0
Simpson	0.5843	0.5	0	0.375	0	0.5636	0	0.6543	0.32	0.2702	0
Menhinick	0.6934	0.6325	0.2582	1	0	0.9285	0	1.179	0.8944	0.9526	0
Margalef	1.012	0.4343	0	0.7213	0	1.188	0	1.384	0.6213	1.504	0
Equitability	0.662	1	0	0.8113	0	0.6863	0	0.7877	0.7219	0.3475	0
Fisher alpha	1.363	0.7517	0.2412	1.592	0	1.742	0	2.293	1.235	2.144	0

Table 7. Similarity and distances indices for Bear Creek. Fossil free horizons have been excluded.

Bray Curtis											
Horizon ID	**S**	**T**	**U**	**UU**	**UUU**	**V**	**VV**	**WW**	**X**	**Z**	**ZZ**
S	1	0.32258	0.44776	0.10714	0.037736	0.34568	0.037736	0.31429	0	0.56604	0
T	0.32258	1	0.4	0.42857	0.18182	0.51282	0.18182	0.71429	0	0.15625	0
U	0.44776	0.4	1	0.31579	0.125	0.22727	0	0.30303	0	0.43478	0
UU	0.10714	0.42857	0.31579	1	0.4	0.24242	0	0.36364	0	0.13793	0
UUU	0.037736	0.18182	0.125	0.4	1	0.066667	0	0.10526	0	0.036364	0
V	0.34568	0.51282	0.22727	0.24242	0.066667	1	0.066667	0.6383	0	0.16867	0
VV	0.037736	0.18182	0	0	0	0.066667	1	0.10526	0	0	0
WW	0.31429	0.71429	0.30303	0.36364	0.10526	0.6383	0.10526	1	0	0.22222	0
X	0	0	0	0	0	0	0	0	1	0.033898	0.33333
Z	0.56604	0.15625	0.43478	0.13793	0.036364	0.16867	0	0.22222	0.033898	1	0
ZZ	0	0	0	0	0	0	0	0	0.33333	0	1

Dice											
Horizon ID	**S**	**T**	**U**	**UU**	**UUU**	**V**	**VV**	**WW**	**X**	**Z**	**ZZ**
S	1	0.57143	0.33333	0.28571	0.33333	0.6	0.33333	0.6	0	0.33333	0
T	0.57143	1	0.66667	0.5	0.66667	0.57143	0.66667	0.57143	0	0.22222	0
U	0.33333	0.66667	1	0.66667	1	0.33333	0	0.33333	0	0.25	0
UU	0.28571	0.5	0.66667	1	0.66667	0.57143	0	0.57143	0	0.44444	0
UUU	0.33333	0.66667	1	0.66667	1	0.33333	0	0.33333	0	0.25	0
V	0.6	0.57143	0.33333	0.57143	0.33333	1	0.33333	0.6	0	0.5	0
VV	0.33333	0.66667	0	0	0	0.33333	1	0.33333	0	0	0
WW	0.6	0.57143	0.33333	0.57143	0.33333	0.6	0.33333	1	0	0.5	0
X	0	0	0	0	0	0	0	0	1	0.22222	0.66667
Z	0.33333	0.22222	0.25	0.44444	0.25	0.5	0	0.5	0.22222	1	0
ZZ	0	0	0	0	0	0	0	0	0.66667	0	1

Jaccard											
Horizon ID	**S**	**T**	**U**	**UU**	**UUU**	**V**	**VV**	**WW**	**X**	**Z**	**ZZ**
S	1	0.4	0.2	0.16667	0.2	0.42857	0.2	0.42857	0	0.2	0
T	0.4	1	0.5	0.33333	0.5	0.4	0.5	0.4	0	0.125	0
U	0.2	0.5	1	0.5	1	0.2	0	0.2	0	0.14286	0
UU	0.16667	0.33333	0.5	1	0.5	0.4	0	0.4	0	0.28571	0
UUU	0.2	0.5	1	0.5	1	0.2	0	0.2	0	0.14286	0
V	0.42857	0.4	0.2	0.4	0.2	1	0.2	0.42857	0	0.33333	0
VV	0.2	0.5	0	0	0	0.2	1	0.2	0	0	0
WW	0.42857	0.4	0.2	0.4	0.2	0.42857	0.2	1	0	0.33333	0
X	0	0	0	0	0	0	0	0	1	0.125	0.5
Z	0.2	0.125	0.14286	0.28571	0.14286	0.33333	0	0.33333	0.125	1	0
ZZ	0	0	0	0	0	0	0	0	0.5	0	1

Raup Crick											
Horizon ID	**S**	**T**	**U**	**UU**	**UUU**	**V**	**VV**	**WW**	**X**	**Z**	**ZZ**
S	1	0.8575	0.7175	0.42	0.695	0.6675	0.7375	0.685	0.0875	0.065	0.1925
T	0.8575	1	0.8925	0.7275	0.8625	0.88	0.91	0.8625	0.3	0.255	0.3825
U	0.7175	0.8925	1	0.875	0.91	0.7425	0.4525	0.73	0.3725	0.615	0.435
UU	0.42	0.7275	0.875	1	0.8825	0.865	0.3625	0.825	0.29	0.7575	0.355
UUU	0.695	0.8625	0.91	0.8825	1	0.7475	0.4475	0.7275	0.3525	0.6125	0.45
V	0.6675	0.88	0.7425	0.865	0.7475	1	0.715	0.695	0.0925	0.335	0.23
VV	0.7375	0.91	0.4525	0.3625	0.4475	0.715	1	0.72	0.3825	0.1225	0.4325
WW	0.685	0.8625	0.73	0.825	0.7275	0.695	0.72	1	0.0775	0.355	0.225
X	0.0875	0.3	0.3725	0.29	0.3525	0.0925	0.3825	0.0775	1	0.28	0.89
Z	0.065	0.255	0.615	0.7575	0.6125	0.335	0.1225	0.355	0.28	1	0.1275
ZZ	0.1925	0.3825	0.435	0.355	0.45	0.23	0.4325	0.225	0.89	0.1275	1

Table 8. Diversity indices for Harrington Flat Road. Exludes fossil free mounds.

Horizon ID	1	2	3	4	5	6	7	8
Taxa	2	1	2	4	7	1	3	1
Individuals	3	2	12	28	44	8	15	7
Shannon	0.6365	0	0.2868	1.187	1.481	0	0.9701	0
Simpson	0.4444	0	0.1528	0.6709	0.6983	0	0.5867	0
Menhinick	1.155	0.7071	0.5774	0.7559	1.055	0.3536	0.7746	0.378
Margalef	0.9102	0	0.4024	0.9003	1.586	0	0.7385	0
Equitability	0.9183	0	0.4138	0.856	0.761	0	0.883	0
Fisher alpha	2.622	0.7959	0.6853	1.277	2.346	0.3017	1.128	0.3193

Horizon ID	9	10	12	13	17	18	19	20
Taxa	2	3	2	6	1	3	3	3
Individuals	5	6	14	39	1	41	10	4
Shannon	0.5004	1.011	0.6931	1.189	0	0.6029	0.8018	1.04
Simpson	0.32	0.6111	0.5	0.5575	0	0.3522	0.46	0.625
Menhinick	0.8944	1.225	0.5345	0.9608	0	0.4685	0.9487	1.5
Margalef	0.6213	1.116	0.3789	1.365	0	0.5386	0.8686	1.443
Equitability	0.7219	0.9206	1	0.6637	0	0.5487	0.7298	0.9464
Fisher alpha	1.235	2.388	0.6385	1.98	0	0.7452	1.453	5.453

Table 9. Similarity and distance indices for Harrington Flat Road. Excludes fossil free mounds.

Dice																
Horizon ID	**1**	**2**	**3**	**4**	**5**	**6**	**7**	**8**	**9**	**10**	**12**	**13**	**17**	**18**	**19**	**20**
1	1	0	0	0.3333	0.2222	0	0	0	0	0	0	0.5	0	0.4	0	0
2	0	1	0.6667	0.4	0.25	0	0.5	0	0	0.5	0.6667	0.2857	0	0.5	0.5	0
3	0	0.6667	1	0.6667	0.4444	0.6667	0.8	0.6667	0.5	0.8	1	0.5	0.6667	0.8	0.8	0.4
4	0.3333	0.4	0.6667	1	0.7273	0.4	0.5714	0.4	0.6667	0.8571	0.6667	0.8	0.4	0.5714	0.8571	0.2857
5	0.2222	0.25	0.4444	0.7273	1	0.25	0.4	0.25	0.4444	0.6	0.4444	0.6154	0.25	0.4	0.6	0.2
6	0	0	0.6667	0.4	0.25	1	0.5	1	0.6667	0.5	0.6667	0.2857	1	0.5	0.5	0.5
7	0	0.5	0.8	0.5714	0.4	0.5	1	0.5	0.4	0.6667	0.8	0.4444	0.5	0.6667	0.6667	0.6667
8	0	0	0.6667	0.4	0.25	1	0.5	1	0.6667	0.5	0.6667	0.2857	1	0.5	0.5	0.5
9	0	0	0.5	0.6667	0.4444	0.6667	0.4	0.6667	1	0.8	0.5	0.5	0.6667	0.4	0.8	0.4
10	0	0.5	0.8	0.8571	0.6	0.5	0.6667	0.5	0.8	1	0.8	0.6667	0.5	0.6667	1	0.3333
12	0	0.6667	1	0.6667	0.4444	0.6667	0.8	0.6667	0.5	0.8	1	0.5	0.6667	0.8	0.8	0.4
13	0.5	0.2857	0.5	0.8	0.6154	0.2857	0.4444	0.2857	0.5	0.6667	0.5	1	0.2857	0.6667	0.6667	0.2222
17	0	0	0.6667	0.4	0.25	1	0.5	1	0.6667	0.5	0.6667	0.2857	1	0.5	0.5	0.5
18	0.4	0.5	0.8	0.5714	0.4	0.5	0.6667	0.5	0.4	0.6667	0.8	0.6667	0.5	1	0.6667	0.3333
19	0	0.5	0.8	0.8571	0.6	0.5	0.6667	0.5	0.8	1	0.8	0.6667	0.5	0.6667	1	0.3333
20	0	0	0.4	0.2857	0.2	0.5	0.6667	0.5	0.4	0.3333	0.4	0.2222	0.5	0.3333	0.3333	1

Jaccard																
Horizon ID	**1**	**2**	**3**	**4**	**5**	**6**	**7**	**8**	**9**	**10**	**12**	**13**	**17**	**18**	**19**	**20**
1	1	0	0	0.2	0.125	0	0	0	0	0	0	0.3333	0	0.25	0	0
2	0	1	0.5	0.25	0.1429	0	0.3333	0	0	0.3333	0.5	0.1667	0	0.3333	0.3333	0
3	0	0.5	1	0.5	0.2857	0.5	0.6667	0.5	0.3333	0.6667	1	0.3333	0.5	0.6667	0.6667	0.25
4	0.2	0.25	0.5	1	0.5714	0.25	0.4	0.25	0.5	0.75	0.5	0.6667	0.25	0.4	0.75	0.1667
5	0.125	0.1429	0.2857	0.5714	1	0.1429	0.25	0.1429	0.2857	0.4286	0.2857	0.4444	0.1429	0.25	0.4286	0.1111
6	0	0	0.5	0.25	0.1429	1	0.3333	1	0.5	0.3333	0.5	0.1667	1	0.3333	0.3333	0.3333
7	0	0.3333	0.6667	0.4	0.25	0.3333	1	0.3333	0.25	0.5	0.6667	0.2857	0.3333	0.5	0.5	0.5
8	0	0	0.5	0.25	0.1429	1	0.3333	1	0.5	0.3333	0.5	0.1667	1	0.3333	0.3333	0.3333
9	0	0	0.3333	0.5	0.2857	0.5	0.25	0.5	1	0.6667	0.3333	0.3333	0.5	0.25	0.6667	0.25
10	0	0.3333	0.6667	0.75	0.4286	0.3333	0.5	0.3333	0.6667	1	0.6667	0.5	0.3333	0.5	1	0.2
12	0	0.5	1	0.5	0.2857	0.5	0.6667	0.5	0.3333	0.6667	1	0.3333	0.5	0.6667	0.6667	0.25
13	0.3333	0.1667	0.3333	0.6667	0.4444	0.1667	0.2857	0.1667	0.3333	0.5	0.3333	1	0.1667	0.5	0.5	0.125
17	0	0	0.5	0.25	0.1429	1	0.3333	1	0.5	0.3333	0.5	0.1667	1	0.3333	0.3333	0.3333
18	0.25	0.3333	0.6667	0.4	0.25	0.3333	0.5	0.3333	0.25	0.5	0.6667	0.5	0.3333	1	0.5	0.2
19	0	0.3333	0.6667	0.75	0.4286	0.3333	0.5	0.3333	0.6667	1	0.6667	0.5	0.3333	0.5	1	0.2
20	0	0	0.25	0.1667	0.1111	0.3333	0.5	0.3333	0.25	0.2	0.25	0.125	0.3333	0.2	0.2	1

Simpson																
Horizon ID	**1**	**2**	**3**	**4**	**5**	**6**	**7**	**8**	**9**	**10**	**12**	**13**	**17**	**18**	**19**	**20**
1	1	0	0	0.5	0.5	0	0	0	0	0	0	1	0	0.5	0	0
2	0	1	1	1	1	0	1	0	0	1	1	1	0	1	1	0
3	0	1	1	1	1	1	1	1	0.5	1	1	1	1	1	1	0.5
4	0.5	1	1	1	1	1	0.6667	1	1	1	1	1	1	0.6667	1	0.3333
5	0.5	1	1	1	1	1	0.6667	1	1	1	1	0.6667	1	0.6667	1	0.3333
6	0	0	1	1	1	1	1	1	1	1	1	1	1	1	1	1
7	0	1	1	0.6667	0.6667	1	1	1	0.5	0.6667	1	0.6667	1	0.6667	0.6667	0.6667
8	0	0	1	1	1	1	1	1	1	1	1	1	1	1	1	1
9	0	0	0.5	1	1	1	0.5	1	1	1	0.5	1	1	0.5	1	0.5
10	0	1	1	1	1	1	0.6667	1	1	1	1	1	1	0.6667	1	0.3333
12	0	1	1	1	1	1	1	1	0.5	1	1	1	1	1	1	0.5
13	1	1	1	1	0.6667	1	0.6667	1	1	1	1	1	1	1	1	0.3333
17	0	0	1	1	1	1	1	1	1	1	1	1	1	1	1	1
18	0.5	1	1	0.6667	0.6667	1	0.6667	1	0.5	0.6667	1	1	1	1	0.6667	0.3333
19	0	1	1	1	1	1	0.6667	1	1	1	1	1	1	0.6667	1	0.3333
20	0	0	0.5	0.3333	0.3333	1	0.6667	1	0.5	0.3333	0.5	0.3333	1	0.3333	0.3333	1

Raup Crick																
Horizon ID	**1**	**2**	**3**	**4**	**5**	**6**	**7**	**8**	**9**	**10**	**12**	**13**	**17**	**18**	**19**	**20**
1	1	0.335	0.19	0.3875	0.135	0.31	0.1125	0.2975	0.21	0.1125	0.1725	0.695	0.315	0.5	0.115	0.1175
2	0.335	1	0.7975	0.6975	0.5525	0.4025	0.7425	0.4125	0.3425	0.745	0.82	0.5925	0.3975	0.75	0.7225	0.2875
3	0.19	0.7975	1	0.8375	0.65	0.825	0.8975	0.805	0.65	0.89	0.9675	0.6675	0.805	0.89	0.88	0.5125
4	0.3875	0.6975	0.8375	1	0.78	0.6675	0.6325	0.6825	0.8175	0.91	0.8325	0.8575	0.6675	0.5925	0.955	0.2125
5	0.135	0.5525	0.65	0.78	1	0.555	0.2375	0.5675	0.6225	0.7275	0.6275	0.275	0.59	0.245	0.72	0.0275
6	0.31	0.4025	0.825	0.6675	0.555	1	0.755	0.925	0.83	0.755	0.82	0.615	0.8825	0.76	0.7325	0.745
7	0.1125	0.7425	0.8975	0.6325	0.2375	0.755	1	0.755	0.48	0.7525	0.9125	0.3125	0.745	0.7775	0.74	0.755
8	0.2975	0.4125	0.805	0.6825	0.5675	0.925	0.755	1	0.81	0.77	0.815	0.6025	0.93	0.745	0.72	0.75
9	0.21	0.3425	0.65	0.8175	0.6225	0.83	0.48	0.81	1	0.8775	0.6375	0.6825	0.8325	0.5	0.885	0.5175
10	0.1125	0.745	0.89	0.91	0.7275	0.755	0.7525	0.77	0.8775	1	0.92	0.795	0.725	0.74	0.9875	0.3175
12	0.1725	0.82	0.9675	0.8325	0.6275	0.82	0.9125	0.815	0.6375	0.92	1	0.7	0.8125	0.875	0.895	0.4625
13	0.695	0.5925	0.6675	0.8575	0.275	0.615	0.3125	0.6025	0.6825	0.795	0.7	1	0.5875	0.77	0.7575	0.05
17	0.315	0.3975	0.805	0.6675	0.59	0.8825	0.745	0.93	0.8325	0.725	0.8125	0.5875	1	0.7575	0.765	0.755
18	0.5	0.75	0.89	0.5925	0.245	0.76	0.7775	0.745	0.5	0.74	0.875	0.77	0.7575	1	0.795	0.3375
19	0.115	0.7225	0.88	0.955	0.72	0.7325	0.74	0.72	0.885	0.9875	0.895	0.7575	0.765	0.795	1	0.325
20	0.1175	0.2875	0.5125	0.2125	0.0275	0.745	0.755	0.75	0.5175	0.3175	0.4625	0.05	0.755	0.3375	0.325	1

Table 10. Rocky Creek diversity indices. Excludes fossil free horizons.

Horizon ID	1	2	3	4	5	9	10	12
Taxa	7	1	2	2	2	5	3	3
Individuals	89	16	12	18	30	89	6	52
Shannon	1.34	0	0.2868	0.2146	0.6909	1.377	1.011	0.4503
Simpson	0.6704	0	0.1528	0.1049	0.4978	0.6916	0.6111	0.2374
Menhinick	0.742	0.25	0.5774	0.4714	0.3651	0.53	1.225	0.416
Margalef	1.337	0	0.4024	0.346	0.294	0.8911	1.116	0.5062
Equitability	0.6885	0	0.4138	0.3095	0.9968	0.8553	0.9206	0.4099
Fisher alpha	1.78	0.2364	0.6853	0.5757	0.4824	1.145	2.388	0.6925

Horizon ID	13	14	17	19	20	22	23	24
Taxa	3	1	2	3	2	2	1	3
Individuals	5	1	5	28	31	3	1	14
Shannon	1.055	0	0.673	0.6649	0.1425	0.6365	0	0.8982
Simpson	0.64	0	0.48	0.3903	0.06243	0.4444	0	0.5612
Menhinick	1.342	0	0.8944	0.5669	0.3592	1.155	0	0.8018
Margalef	1.243	0	0.6213	0.6002	0.2912	0.9102	0	0.7578
Equitability	0.9602	0	0.971	0.6052	0.2056	0.9183	0	0.8176
Fisher alpha	3.167	0	1.235	0.8516	0.4775	2.622	0	1.171

Horizon ID	25	26	28	29	31	33	38	43
Taxa	4	3	4	2	1	2	3	1
Individuals	29	6	10	2	6	2	21	6
Shannon	0.8316	1.099	1.194	0.6931	0	0.6931	0.501	0
Simpson	0.4637	0.6667	0.66	0.5	0	0.5	0.254	0
Menhinick	0.7428	1.225	1.265	1.414	0.4082	1.414	0.6547	0.4082
Margalef	0.8909	1.116	1.303	1.443	0	1.443	0.6569	0
Equitability	0.5999	1	0.861	1	0	1	0.4561	0
Fisher alpha	1.258	2.388	2.471	0	0.3426	0	0.9578	0.3426

Table 11. Rocky Creek similarity and distance indices. Excludes fossil free horizons.

Dice

Horizon ID	1	2	3	4	5	9	10	12	13	14	17	19	20	22	23	24	25	26	28	29	31	33	38	43
1	1	0.25	0.444	0.444	0.222	0.667	0.2	0.2	0.4	0	0.222	0.2	0.222	0.222	0	0.4	0.364	0.2	0.364	0.444	0.25	0.222	0.4	0
2	0.25	1	0.667	0	0.667	0.333	0	0.5	0.5	0	0.667	0.5	0.667	0.667	0	0.5	0.4	0.5	0.4	0.667	1	0.667	0.5	0
3	0.444	0.667	1	0.5	0.5	0.286	0.4	0.4	0.8	0	0.5	0.4	0.5	0.5	0	0.4	0.667	0.4	0.667	0.5	0.667	0.5	0.4	0
4	0.444	0	0.5	1	0	0	0.4	0	0.4	0	0	0	0	0	0	0	0.333	0	0.333	0.5	0	0	0	0
5	0.222	0.667	0.5	0	1	0.286	0.4	0.8	0.8	0.667	0.5	0.8	1	1	0	0.4	0.667	0.8	0.667	0.5	0.667	1	0.4	0
9	0.667	0.333	0.286	0	0.286	1	0.25	0.5	0.25	0	0.571	0.5	0.286	0.286	0.333	0.75	0.444	0.5	0.444	0.286	0.333	0.286	0.75	0
10	0.2	0	0.4	0.4	0.4	0.25	1	0.667	0.667	0.5	0.4	0.667	0.4	0.4	0.5	0.333	0.857	0.667	0.857	0	0	0.4	0.333	0
12	0.2	0.5	0.4	0	0.8	0.5	0.667	1	0.667	0.5	0.8	1	0.8	0.8	0.5	0.667	0.857	1	0.857	0.4	0.5	0.8	0.667	0
13	0.4	0.5	0.8	0.4	0.8	0.25	0.667	0.667	1	0.5	0.4	0.667	0.8	0.8	0	0.333	0.857	0.667	0.857	0.4	0.5	0.8	0.333	0
14	0	0	0	0	0.667	0	0.5	0.5	0.5	1	0	0.5	0.667	0.667	0	0	0.4	0.5	0.4	0	0	0.667	0	0
17	0.222	0.667	0.5	0	0.5	0.571	0.4	0.8	0.4	0	1	0.8	0.5	0.5	0.667	0.8	0.667	0.8	0.667	0.5	0.667	0.5	0.8	0
19	0.2	0.5	0.4	0	0.8	0.5	0.667	1	0.667	0.5	0.8	1	0.8	0.8	0.5	0.667	0.857	1	0.857	0.4	0.5	0.8	0.667	0
20	0.222	0.667	0.5	0	1	0.286	0.4	0.8	0.8	0.667	0.5	0.8	1	1	0	0.4	0.667	0.8	0.667	0.5	0.667	1	0.4	0
22	0.222	0.667	0.5	0	1	0.286	0.4	0.8	0.8	0.667	0.5	0.8	1	1	0	0.4	0.667	0.8	0.667	0.5	0.667	1	0.4	0
23	0	0	0	0	0	0.333	0.5	0.5	0	0	0.667	0.5	0	0	1	0.5	0.4	0.5	0.4	0	0	0	0.5	0
24	0.4	0.5	0.4	0	0.4	0.75	0.333	0.667	0.333	0	0.8	0.667	0.4	0.4	0.5	1	0.571	0.667	0.571	0.4	0.5	0.4	1	0
25	0.364	0.4	0.667	0.333	0.667	0.444	0.857	0.857	0.857	0.4	0.667	0.857	0.667	0.667	0.4	0.571	1	0.857	1	0.333	0.4	0.667	0.571	0
26	0.2	0.5	0.4	0	0.8	0.5	0.667	1	0.667	0.5	0.8	1	0.8	0.8	0.5	0.667	0.857	1	0.857	0.4	0.5	0.8	0.667	0
28	0.364	0.4	0.667	0.333	0.667	0.444	0.857	0.857	0.857	0.4	0.667	0.857	0.667	0.667	0.4	0.571	1	0.857	1	0.333	0.4	0.667	0.571	0
29	0.444	0.667	0.5	0.5	0.5	0.286	0	0.4	0.4	0	0.5	0.4	0.5	0.5	0	0.4	0.333	0.4	0.333	1	0.667	0.5	0.4	0
31	0.25	1	0.667	0	0.667	0.333	0	0.5	0.5	0	0.667	0.5	0.667	0.667	0	0.5	0.4	0.5	0.4	0.667	1	0.667	0.5	0
33	0.222	0.667	0.5	0	1	0.286	0.4	0.8	0.8	0.667	0.5	0.8	1	1	0	0.4	0.667	0.8	0.667	0.5	0.667	1	0.4	0
38	0.4	0.5	0.4	0	0.4	0.75	0.333	0.667	0.333	0	0.8	0.667	0.4	0.4	0.5	1	0.571	0.667	0.571	0.4	0.5	0.4	1	0
43	0	0	0	0	0	0	0	0	0	0	0	0	0	0	0	0	0	0	0	0	0	0	0	1

Jaccard

Horizon ID	1	2	3	4	5	9	10	12	13	14	17	19	20	22	23	24	25	26	28	29	31	33	38	43
1	1	0.143	0.286	0.286	0.125	0.5	0.111	0.111	0.25	0	0.125	0.111	0.125	0.125	0	0.25	0.222	0.111	0.222	0.286	0.143	0.125	0.25	0
2	0.143	1	0.5	0	0.5	0.2	0	0.333	0.333	0	0.5	0.333	0.5	0.5	0	0.333	0.25	0.333	0.25	0.5	1	0.5	0.333	0
3	0.286	0.5	1	0.333	0.333	0.167	0.25	0.25	0.667	0	0.333	0.25	0.333	0.333	0	0.25	0.5	0.25	0.5	0.333	0.5	0.333	0.25	0
4	0.286	0	0.333	1	0	0	0.25	0	0.25	0	0	0	0	0	0	0	0.2	0	0.2	0.333	0	0	0	0
5	0.125	0.5	0.333	0	1	0.167	0.25	0.667	0.667	0.5	0.333	0.667	1	1	0	0.25	0.5	0.667	0.5	0.333	0.5	1	0.25	0
9	0.5	0.2	0.167	0	0.167	1	0.143	0.333	0.143	0	0.4	0.333	0.167	0.167	0.2	0.6	0.286	0.333	0.286	0.167	0.2	0.167	0.6	0
10	0.111	0	0.25	0.25	0.25	0.143	1	0.5	0.5	0.333	0.25	0.5	0.25	0.25	0.333	0.2	0.75	0.5	0.75	0	0	0.25	0.2	0
12	0.111	0.333	0.25	0	0.667	0.333	0.5	1	0.5	0.333	0.667	1	0.667	0.667	0.333	0.5	0.75	1	0.75	0.25	0.333	0.667	0.5	0
13	0.25	0.333	0.667	0.25	0.667	0.143	0.5	0.5	1	0.333	0.25	0.5	0.667	0.667	0	0.2	0.75	0.5	0.75	0.25	0.333	0.667	0.2	0
14	0	0	0	0	0.5	0	0.333	0.333	0.333	1	0	0.333	0.5	0.5	0	0	0.25	0.333	0.25	0	0	0.5	0	0
17	0.125	0.5	0.333	0	0.333	0.4	0.25	0.667	0.25	0	1	0.667	0.333	0.333	0.5	0.667	0.5	0.667	0.5	0.333	0.5	0.333	0.667	0
19	0.111	0.333	0.25	0	0.667	0.333	0.5	1	0.5	0.333	0.667	1	0.667	0.667	0.333	0.5	0.75	1	0.75	0.25	0.333	0.667	0.5	0
20	0.125	0.5	0.333	0	1	0.167	0.25	0.667	0.667	0.5	0.333	0.667	1	1	0	0.25	0.5	0.667	0.5	0.333	0.5	1	0.25	0
22	0.125	0.5	0.333	0	1	0.167	0.25	0.667	0.667	0.5	0.333	0.667	1	1	0	0.25	0.5	0.667	0.5	0.333	0.5	1	0.25	0
23	0	0	0	0	0	0.2	0.333	0.333	0	0	0.5	0.333	0	0	1	0.333	0.25	0.333	0.25	0	0	0	0.333	0
24	0.25	0.333	0.25	0	0.25	0.6	0.2	0.5	0.2	0	0.667	0.5	0.25	0.25	0.333	1	0.4	0.5	0.4	0.25	0.333	0.25	1	0
25	0.222	0.25	0.5	0.2	0.5	0.286	0.75	0.75	0.75	0.25	0.5	0.75	0.5	0.5	0.25	0.4	1	0.75	1	0.2	0.25	0.5	0.4	0
26	0.111	0.333	0.25	0	0.667	0.333	0.5	1	0.5	0.333	0.667	1	0.667	0.667	0.333	0.5	0.75	1	0.75	0.25	0.333	0.667	0.5	0
28	0.222	0.25	0.5	0.2	0.5	0.286	0.75	0.75	0.75	0.25	0.5	0.75	0.5	0.5	0.25	0.4	1	0.75	1	0.2	0.25	0.5	0.4	0
29	0.286	0.5	0.333	0.333	0.333	0.167	0	0.25	0.25	0	0.333	0.25	0.333	0.333	0	0.25	0.2	0.25	0.2	1	0.5	0.333	0.25	0
31	0.143	1	0.5	0	0.5	0.2	0	0.333	0.333	0	0.5	0.333	0.5	0.5	0	0.333	0.25	0.333	0.25	0.5	1	0.5	0.333	0
33	0.125	0.5	0.333	0	1	0.167	0.25	0.667	0.667	0.5	0.333	0.667	1	1	0	0.25	0.5	0.667	0.5	0.333	0.5	1	0.25	0
38	0.25	0.333	0.25	0	0.25	0.6	0.2	0.5	0.2	0	0.667	0.5	0.25	0.25	0.333	1	0.4	0.5	0.4	0.25	0.333	0.25	1	0
43	0	0	0	0	0	0	0	0	0	0	0	0	0	0	0	0	0	0	0	0	0	0	0	1

Simpson

Horizon ID	1	2	3	4	5	9	10	12	13	14	17	19	20	22	23	24	25	26	28	29	31	33	38	43
1	1	1	1	1	0.5	0.8	0.333	0.333	0.667	0	0.5	0.333	0.5	0.5	0	0.667	0.5	0.333	0.5	1	1	0.5	0.667	0
2	1	1	1	0	1	1	0	1	1	0	1	1	1	1	0	1	1	1	1	1	1	1	1	0
3	1	1	1	0.5	0.5	0.5	0.5	0.5	1	0	0.5	0.5	0.5	0.5	0	0.5	1	0.5	1	0.5	1	0.5	0.5	0
4	1	0	0.5	1	0	0	0.5	0	0.5	0	0	0	0	0	0	0	0.5	0	0.5	0.5	0	0	0	0
5	0.5	1	0.5	0	1	0.5	0.5	1	1	1	0.5	1	1	1	0	0.5	1	1	1	0.5	1	1	0.5	0
9	0.8	1	0.5	0	0.5	1	0.333	0.667	0.333	0	1	0.667	0.5	0.5	1	1	0.5	0.667	0.5	0.5	1	0.5	1	0
10	0.333	0	0.5	0.5	0.5	0.333	1	0.667	0.667	1	0.5	0.667	0.5	0.5	1	0.333	1	0.667	1	0	0	0.5	0.333	0
12	0.333	1	0.5	0	1	0.667	0.667	1	0.667	1	1	1	1	1	1	0.667	1	1	1	0.5	1	1	0.667	0
13	0.667	1	1	0.5	1	0.333	0.667	0.667	1	1	0.5	0.667	1	1	0	0.333	1	0.667	1	0.5	1	1	0.333	0
14	0	0	0	0	1	0	1	1	1	1	0	1	1	1	0	0	1	1	1	0	0	1	0	0
17	0.5	1	0.5	0	0.5	1	0.5	1	0.5	0	1	1	0.5	0.5	1	1	1	1	1	0.5	1	0.5	1	0
19	0.333	1	0.5	0	1	0.667	0.667	1	0.667	1	1	1	1	1	1	0.667	1	1	1	0.5	1	1	0.667	0
20	0.5	1	0.5	0	1	0.5	0.5	1	1	1	0.5	1	1	1	0	0.5	1	1	1	0.5	1	1	0.5	0
22	0.5	1	0.5	0	1	0.5	0.5	1	1	1	0.5	1	1	1	0	0.5	1	1	1	0.5	1	1	0.5	0
23	0	0	0	0	0	1	1	1	0	0	1	1	0	0	1	1	1	1	1	0	0	0	1	0
24	0.667	1	0.5	0	0.5	1	0.333	0.667	0.333	0	1	0.667	0.5	0.5	1	1	0.667	0.667	0.667	0.5	1	0.5	1	0
25	0.5	1	1	0.5	1	0.5	1	1	1	1	1	1	1	1	1	0.667	1	1	1	0.5	1	1	0.667	0
26	0.333	1	0.5	0	1	0.667	0.667	1	0.667	1	1	1	1	1	1	0.667	1	1	1	0.5	1	1	0.667	0
28	0.5	1	1	0.5	1	0.5	1	1	1	1	1	1	1	1	1	0.667	1	1	1	0.5	1	1	0.667	0
29	1	1	0.5	0.5	0.5	0.5	0	0.5	0.5	0	0.5	0.5	0.5	0.5	0	0.5	0.5	0.5	0.5	1	1	0.5	0.5	0
31	1	1	1	0	1	1	0	1	1	0	1	1	1	1	0	1	1	1	1	1	1	1	1	0
33	0.5	1	0.5	0	1	0.5	0.5	1	1	1	0.5	1	1	1	0	0.5	1	1	1	0.5	1	1	0.5	0
38	0.667	1	0.5	0	0.5	1	0.333	0.667	0.333	0	1	0.667	0.5	0.5	1	1	0.667	0.667	0.667	0.5	1	0.5	1	0
43	0	0	0	0	0	0	0	0	0	0	0	0	0	0	0	0	0	0	0	0	0	0	0	1

Raup Crick

Horizon ID	1	2	3	4	5	9	10	12	13	14	17	19	20	22	23	24	25	26	28	29	31	33	38	43
1	1	0.565	0.593	0.628	0.11	0.41	0.003	0.02	0.22	0.058	0.128	0.01	0.105	0.098	0.043	0.195	0.02	0.025	0.038	0.618	0.548	0.103	0.198	0.043
2	0.565	1	0.823	0.3	0.833	0.618	0.223	0.773	0.735	0.408	0.828	0.733	0.813	0.803	0.415	0.77	0.67	0.738	0.67	0.825	0.918	0.823	0.74	0.428
3	0.593	0.823	1	0.643	0.64	0.25	0.515	0.513	0.9	0.345	0.643	0.528	0.64	0.69	0.305	0.515	0.803	0.488	0.823	0.635	0.793	0.655	0.535	0.333
4	0.628	0.3	0.643	1	0.218	0.028	0.525	0.115	0.508	0.35	0.223	0.108	0.203	0.188	0.31	0.108	0.37	0.108	0.385	0.698	0.338	0.208	0.128	0.303
5	0.11	0.833	0.64	0.218	1	0.275	0.508	0.89	0.895	0.84	0.675	0.89	0.955	0.978	0.328	0.478	0.815	0.903	0.815	0.668	0.825	0.958	0.5	0.338
9	0.41	0.618	0.25	0.028	0.275	1	0.068	0.418	0.065	0.098	0.755	0.403	0.24	0.26	0.608	0.85	0.203	0.41	0.175	0.258	0.608	0.275	0.813	0.128
10	0.003	0.223	0.515	0.525	0.508	0.068	1	0.74	0.74	0.735	0.498	0.743	0.495	0.483	0.745	0.31	0.928	0.76	0.933	0.103	0.26	0.518	0.318	0.24
12	0.02	0.773	0.513	0.115	0.89	0.418	0.74	1	0.738	0.733	0.913	0.978	0.9	0.87	0.76	0.71	0.913	0.973	0.913	0.518	0.708	0.888	0.715	0.248
13	0.22	0.735	0.9	0.508	0.895	0.065	0.74	0.738	1	0.733	0.503	0.77	0.888	0.905	0.225	0.298	0.898	0.755	0.913	0.508	0.778	0.895	0.335	0.255
14	0.058	0.408	0.345	0.35	0.84	0.098	0.735	0.733	0.733	1	0.305	0.755	0.83	0.85	0.415	0.26	0.66	0.74	0.693	0.288	0.408	0.808	0.23	0.41
17	0.128	0.828	0.643	0.223	0.675	0.755	0.498	0.913	0.503	0.305	1	0.91	0.645	0.683	0.815	0.905	0.8	0.905	0.818	0.623	0.81	0.675	0.915	0.373
19	0.01	0.733	0.528	0.108	0.89	0.403	0.743	0.978	0.77	0.755	0.91	1	0.89	0.905	0.778	0.738	0.918	0.97	0.923	0.505	0.735	0.9	0.698	0.258
20	0.105	0.813	0.64	0.203	0.955	0.24	0.495	0.9	0.888	0.83	0.645	0.89	1	0.958	0.33	0.538	0.813	0.915	0.833	0.638	0.81	0.95	0.523	0.308
22	0.098	0.803	0.69	0.188	0.978	0.26	0.483	0.87	0.905	0.85	0.683	0.905	0.958	1	0.308	0.565	0.82	0.923	0.8	0.665	0.84	0.958	0.505	0.363
23	0.043	0.415	0.305	0.31	0.328	0.608	0.745	0.76	0.225	0.415	0.815	0.778	0.33	0.308	1	0.748	0.67	0.728	0.688	0.318	0.415	0.343	0.768	0.418
24	0.195	0.77	0.515	0.108	0.478	0.85	0.31	0.71	0.298	0.26	0.905	0.738	0.538	0.565	0.748	1	0.533	0.728	0.548	0.553	0.723	0.515	0.97	0.24
25	0.02	0.67	0.803	0.37	0.815	0.203	0.928	0.913	0.898	0.66	0.8	0.918	0.813	0.82	0.67	0.533	1	0.913	0.975	0.37	0.705	0.82	0.583	0.2
26	0.025	0.738	0.488	0.108	0.903	0.41	0.76	0.973	0.755	0.74	0.905	0.97	0.915	0.923	0.728	0.728	0.913	1	0.925	0.508	0.713	0.908	0.733	0.265
28	0.038	0.67	0.823	0.385	0.815	0.175	0.933	0.913	0.913	0.693	0.818	0.923	0.833	0.8	0.688	0.548	0.975	0.925	1	0.378	0.705	0.828	0.603	0.16
29	0.618	0.825	0.635	0.698	0.668	0.258	0.103	0.518	0.508	0.288	0.623	0.505	0.638	0.665	0.318	0.553	0.37	0.508	0.378	1	0.833	0.623	0.48	0.323
31	0.548	0.918	0.793	0.338	0.825	0.608	0.26	0.708	0.778	0.408	0.81	0.735	0.81	0.84	0.415	0.723	0.705	0.713	0.705	0.833	1	0.813	0.74	0.413
33	0.103	0.823	0.655	0.208	0.958	0.275	0.518	0.888	0.895	0.808	0.675	0.9	0.95	0.958	0.343	0.515	0.82	0.908	0.828	0.623	0.813	1	0.545	0.335
38	0.198	0.74	0.535	0.128	0.5	0.813	0.318	0.715	0.335	0.23	0.915	0.698	0.523	0.505	0.768	0.97	0.583	0.733	0.603	0.48	0.74	0.545	1	0.283
43	0.043	0.428	0.333	0.303	0.338	0.128	0.24	0.248	0.255	0.41	0.373	0.258	0.308	0.363	0.418	0.24	0.2	0.265	0.16	0.323	0.413	0.335	0.283	1

Chapter 3

An Initial Paleoecological Investigation of the Bivalve Genus *Buchia* Present at the Bear Creek Hydrocarbon Seep Locality, Great Valley Group Forearc Strata, Northern California

Abstract

The bivalve genus *Buchia* is a extremely important for Mesozoic biostratigraphy and has been employed throughout northern California's Great Valley Group (GVG) forearc strata for stratigraphic classification and correlation. From the Late Jurassic to the latest Cretaceous, these strata were deposited in a forearc basin between an eastward migrating volcanic arc and a westward migrating subduction zone. *Buchia* occur commonly in the GVG marine siliciclastic rocks, as well as in a number of the hydrocarbon seep carbonate deposits that are distributed throughout the region. Despite the common presence of *Buchia* in these strata and their use in biostratigraphy, little is known about the paleoecology of the group. This study addresses their paleoecological signature at one Valanginian aged hydrocarbon seep deposit, within which they are found in fine-grained sandstone, mudstone, and hydrocarbon seep carbonate. The deposit includes two discrete, monospecific *Buchia* shell-pavements, as well as an 80 m stratigraphic interval that has a monospecific faunal assemblage of *Buchia* throughout the stratigraphically oldest 50 m of

section and a diverse and seep-typical faunal assemblage throughout the stratigraphically youngest 30 m of section.

Based on data collected during the course of this study, including both stable isotopic and petrographic signatures, *Buchia* was likely present in the hydrocarbon seep due to the harboring of chemosymbionts in their tissues. Sedimentologic and petrographic data indicate that the *Buchia* preserved in sandstone did not form in a hydrocarbon seep environment, which is confirmed by the morphometric analyses and which indicate that the *Buchia* in the sandstone and micarb are morphometrically distinct, suggesting that the assemblages were drawn from different populations or represent an example of ecophenotypic variation.

1. Introduction

The bivalve genus *Buchia* is among the most biostratigraphically important genera of the Mesozoic (Late Triassic—Early Cretaceous) due to its global distribution (Zakharov 1987, Zhiqiang and Zunyi 2006) and the wide variety of facies and depositional environments in which it is found. These include beach conglomerates, shallow marine sandstones, offshore and deep-water mudstones, and submarine fans (Smelror and Dypvik 2006), as well as bathyal to abyssally deposited sedimentary rocks (Århus et al. 1990, Smelror and Dypvik 2006). Due to the relative ease of identification and their regular stratigraphic distribution, *Buchia* has become an important index fossil (Xiaochi and Grant-

Mackie 1988) and is frequently employed in stratigraphic classification and correlation in most contemporaneous strata (Zhiqiang and Zunyi 2006). Although generally considered a cosmopolitan genus, *Buchia*-rich strata are found in greatest abundance in moderate to high latitudes, including in both polar regions (Sha and Fursich 1993).

Buchia are common throughout the Great Valley Group (GVG) forearc strata, a 12 to 15 km thick sequence, exposed throughout northern and central California, along the west side of the Sacramento Valley. The GVG sediments were deposited in the GVG forearc basin, which is one of the most thoroughly studied and best understood ancient basins of its kind in the world (Ingersoll 1978b). Active deposition occurred throughout the Mesozoic, with the basin bounded by an active magmatic arc (Sierra Nevada batholith) to the east and a trench-subduction complex (Franciscan Accretionary Complex of the Coast Ranges) to the west (Ingersoll 1978b, 1979). These *Buchia*-hosting sediments were deposited in a distal submarine fan environment in an outer arc basin (Ingersoll 1979, Suchecki 1984), which today consist of a series of mudstone, siltstone, sandstone and/or conglomerate turbidites (Ingersoll 1979, Suchecki 1984), with rare occurrences of concurrently deposited fossiliferous hydrocarbon seep carbonate.

Studies of this region have largely focused on its tectonic and sedimentologic history (Upper Jurassic–Upper Cretaceous) and *Buchia*, along with scattered ammonites, radiolarians, and calcareous nannofossils, have been

used for biostratigraphic control (Jones et al. 1969, Bralower 1990). The *Buchia* are used as aids in understanding and interpreting major structural and stratigraphic features in northwestern California and have successfully been used to divide Tithonian through Valanginian stages throughout the region (Jones et al. 1969). Despite their common usage in biostratigraphic studies, little is known about their paleoecology. Although they have been described from a variety of environments and have been previously mentioned as constituents of hydrocarbon seep deposits in northern California (see Kiel et al. 2008), their paleoecology has never been addressed.

Buchia has been reported as common constituents of fine-grained sandstone turbidites and small dark gray carbonate deposits in the GVG forearc strata and although was commonly used for biostratigraphic control, their ecology was only minimally described (see Imlay 1959). The purpose of this study is to explore the paleoecological environment of Buchiid bivalves occurring in (1) fine-grained sandstones and in (2) hydrocarbon seep carbonate, in adjacent deposits at Bear Creek; a Valanginian aged hydrocarbon seep deposit, cropping out in the GVG forearc strata (Figure 1). This study uses sedimentological, geochemical, paleoecological, and morphometric analyses to ascertain if the two *Buchia* assemblages originated in the same environment, as well as if the *Buchia* themselves came from the same population.

2. Buchiid Bivalves

The family Buchiidae was distributed widely in marine environments from the Late Triassic to the Early Cretaceous, while the genus *Buchia*, the last known representative of the family Monotoidea, is known only from the Late Oxfordian (Late Jurassic) to Hauterivian (Early Cretaceous) (Zakharov 1987, Grey 2009). Imlay (1959) describes *Buchia* as having an obliquely elongate inequivalve shell, with its beaks inclined forward, often with a variably strong left or right twist (Figure 2B, F). The beak of the left valve is more prominent than that of the right, rising above and generally overhanging the right valve. It has a long and narrow byssal notch and a shell surface covered with concentric ribs, radial striae, or both. The cardinal plate is short, straight, or nearly straight and mostly posterior to the beak. The posterior is occupied by a long, triangular ligamental groove and its anterior by a notch. Teeth are absent. These characters are thought to suggest that members of this genus were sessile, byssally attached, epifaunal organisms that preferred a moderately cohesive substrate and low energy conditions, although they were tolerant of a wide spectrum of environmental factors, including variable energy level, depth, and oxygen concentration (Stanley 1972, De la Mora et al. 2000, Marinov et al. 2006). They are generally found in strata indicative of relatively deep, moderately cold environmental settings, where they likely could inhabit both oxic and suboxic environments, although it has been suggested that they could have survived oxygen deficiency for a limited period of time (Marinov et al. 2006).

In a single population, buchiids often have a wide range of shapes, sizes, degree of beak curvature, and ornamentation, which is attributed to different degrees of crowding, changes in environmental conditions during growth, and/or due to deformation after burial (Imlay 1959, Jeletzky 1965). Identification of particular species of *Buchia* is hampered by their variable morphologies and by their variability in distribution, ranging from some species being facies limited and regionally restricted, with others spanning multiple facies-types and having circumboreal distributions (Jeletzky 1965). Disagreements in the designation of *Buchia* species are common and it has only been recently that multivariate morphometrics have been applied to assess the reliability of these designations (Grey et al. 2008, Grey 2009).

3. Bear Creek

The Bear Creek deposit is principally comprised of the Valanginian species *Buchia pacifica* (Figure 2A, B, C, E, F, G), although a limited number of *Buchia inflata* specimens were also collected (Figure 2D). *B. pacifica* is distinct from other buchiid species in that it typically has a large, short, thick and commonly heavily sculptured shell with prominent concentric ribs on the surface of the shell and on the internal cast (Jeletzky 1965). The shell is variably inequivalve, despite both valves being thick and swollen (Jeletzky 1965). The right valve is mostly thick to very thick and swollen in the middle, however, relatively thin right valves are not uncommon (Jeletzky 1965). The left valve is

always larger, thicker, and longer than the right and the beak has both a strong swelling, as well as a truncation of both valves. This is thought to have been an adaptation to the extreme crowding of its shells, which mostly occurred in thick banks similar to those of present day oysters or mytillids (Jeletzky 1965) and which likely delayed its becoming covered by the sediment or being overgrown by younger shells of the same species (Jeletzky 1965). The beaks of both valves have pronounced left-handed incurvature and instead of tapering gradually toward the lower margins from the place of their maximum thickness, the valves bend abruptly toward each other within the lower most part of the shell (Jeletzky 1965). This abrupt bend becomes “mushroom-shaped” in extreme cases and is the most diagnostic feature of the species. Their remains are often the dominant to exclusive macrofossil in the faunal assemblages that they are a part of.

The second species found at Bear Creek is *Buchia inflata* (Figure 2D), which is morphologically similar to *B. pacifica* (Jeletzky 1965). *B. inflata* is characterized by medium to moderately large-sized, sub-triangular, almost equilateral specimens, with both valves displaying marked inflation. The shells are thick and short, often globulous, with short, blunt beaks (Jeletzky 1965) and shell surfaces commonly covered by regularly spaced concentric ribs (Jeletzky 1965).

4. Geochemistry

Most organisms rely on phototrophic primary production, however, in the hydrocarbon seep ecosystem, a consortium of methane-oxidizing and sulfate-reducing microbes form the base of the food chain and provide most, if not all, of the nutritional needs of the macrofaunal communities (Somero 1984). During chemosynthesis, the energy required for basal metabolism and growth is derived from the enzyme-catalyzed oxidation of reduced chemical species (e.g., sulfide, elemental sulfur, thiosulfate, methane, hydrogen, and ammonium, Kennicutt II et al. 1992). Methane and hydrogen sulfide are the two most common sources of energy utilized by the microbes (Gaillard et al. 1992), forming via diagenesis of organic matter shed from neighboring continents or mountain chains or through primary productivity in the sediment column (Cavagna et al. 1999). They can migrate from their zones of genesis along permeable fault zones, stratigraphic layers, or via mud and serpentinite diapirs (Orange and Campbell 1997, Conti and Fontana 1999, Van Dover et al. 2002) and can be captured in rising pore water being driven out of the sedimentary unit by compression, compaction, or cementation, and/or by the deformation that is common in tectonically active areas (Ritger et al. 1987, Campbell and Bottjer 1993). In chemoautotrophic symbioses, the bivalves provide the bacteria with access to the substrates necessary for the generation of energy and bacterial biomass (Cavanaugh et al. 2006), in exchange, a portion of the methane or sulfur fixed by the symbiont is used, either directly or indirectly for host energy or biosynthesis.

Seep carbonates tend to yield carbon isotope values ranging from -25‰ to -80‰ PDB, depending on the origin of the methane (Ritger et al. 1987, Paull et al. 1992, Cavagna et al. 1999). These values are the product of the anaerobic oxidation of methane, which is usually mediated in a marine environment by a consortium of methanotrophic archaea and sulfate-reducing bacteria (Elvert and Suess 1999, Thiel et al. 1999, Pancost and Damsté 2000, Hinrichs and Boetius 2003), which consume methane and sulfate and produce isotopically depleted dissolved inorganic carbon (DIC) and hydrogen sulfide, according to the generalized net reaction: $SO_4^{2-} + CH_4 \rightarrow HS^- + HCO_3^- + H_2O$, as proposed by Reeburgh (1976). From their point of origin, both diffuse upward along a concentration gradient. The ^{13}C-depleted bicarbonate is consumed by carbonate precipitation, resulting in $\delta^{13}C$-depleted carbonate (Werne et al. 2004) and the H_2S is oxidized from sulfide to sulfate or elemental sulfur by the sulfide oxidizing bacteria living symbiotically within the bivalves.

5. Geologic Setting

The geologic evolution of the Mesozoic western North American continental margin classically was interpreted as an Andean-style arc and trench system, which resulted in the development of three broad tectonic provinces, including the Franciscan Accretionary Complex of the Coast Ranges, the Great Valley Group (GVG) forearc strata, and the Sierra Nevada batholith (Godfrey et al. 1997), with the relative timing of formation including the coeval deposition of

GVG forearc strata and the Franciscan Complex (Ingersoll 1978b, Blake and Jones 1981).

Formation of the GVG forearc strata extended from the late Jurassic to the latest Cretaceous, without an appreciable hiatus (Swe and Dickinson 1970, Blake and Jones 1981, Blake and McLaughlin 1989). These strata were deposited along the outer arc of the forearc basin in deep water by longitudinal flow parallel to the structural grain defined by the basin margins, which were located at the flank of the arc massif on the east and at the position of the accretionary subduction complex on the west. By the end of the Jurassic, the subduction complex had enlarged, the basin had subsided, and sediments were filling the basin, including ophiolite clasts from the Coast Range Ophiolite and from the uplifted and eroding accretionary complex (Ingersoll 1978b, 1982). Throughout this time, the forearc basin evolved by the westward and upward growth of the subduction complex, by sedimentary loading, and by the eastward migration of the magmatic arc (Dickinson and Seely 1979). During the Early Cretaceous, the forearc basin evolved systematically as the arc-gap widened and sedimentation continued (Ingersoll 1982). During the Late Cretaceous, shorelines and submarine fans migrated eastward and the arc and trench gap continued to widen. By the end of the Late Cretaceous parts of the forearc basin had been filled nearly to sea level, with arc-derived detritus deposited on the basin floor via deepwater turbidity flow (Ingersoll 1978b).

Today, Upper Jurassic through Lower Cretaceous strata of the GVG are exposed along the west side of the Sacramento Valley and predominantly consist of a series of mudstone, siltstone, sandstone and/or conglomerate turbidites, deposited in a distal submarine fan environment in an outer-arc basin (Ingersoll 1978a, 1979, Suchecki 1984). These strata were deposited on a deep basin floor that was confined by margins located at the flank of the Sierra Nevada arc massif to the east and the Franciscan Complex to the west (Ingersoll 1978b, Dickinson 1981). Upper Cretaceous strata crop out nearly continuously along the length of the Sacramento and San Joaquin Valleys (Ingersoll 1978a), comprising sediments that were principally sub-sea fan turbidites that prograded into the forearc trough from eastern sources in the arc massif (Dickinson 1981). The 12 km succession of GVG sediments generally consist of well-bedded mudstone, siltstone, sandstone, and conglomerate derived from granitic basement of the Sierran and Klamath regions (Blake and Jones 1981) and form an asymmetric syncline with a steeply east-dipping west limb (Godfrey et al. 1997).

6. Methods

Initially, Bear Creek was surveyed to ascertain deposit morphology and faunal composition. Bedding plane and/or cross-sectional distribution patterns were addressed and standard geologic data including sedimentological (e.g., clastic texture, degree of sorting, rounding of grains, fabric, diagenetic features,

etc.), stratigraphic (e.g., beds and bedding, grading of turbidites, depositional bed forms and structures, etc), paleontologic (e.g., species diversity, degree of bioturbation, trace fossils, etc.), and paleoecologic (e.g., relative abundance, species richness, dominance, etc.) data was recorded for each interval for environmental interpretation, with an emphasis on facies criteria (e.g., lithology, rock colors, grain size and shape, particle types, bedding and lamination, sedimentary structures and textures, fossil content, stratigraphic and structural relationships, geometry of carbonate bodies, etc.; Flügel 1982). Samples of all major lithologies were collected for petrographic, paleontologic, and geochemical analyses.

Detailed, bed-by-bed sedimentary logging was undertaken at the centimeter scale for one 80 m *Buchia*-bearing stratigraphic interval (Figure 3). An additional two, discrete, intervals consisting of monospecific *Buchia* shell pavements were also documented (Figure 4). Samples were systematically collected throughout each measured section and the shell beds, with sample volumes filling between one and two sample bags (~4,500 to 9,000 cm^3), depending on the availability of material.

The *in situ* paleontologic data included the cataloguing of faunal distribution patterns, including taxonomic identification, determination of relative abundance through assemblage point-counts, and establishing assemblage diversity to obtain an estimate of taxonomic contribution to each assemblage. Faunal assemblage taphonomic data was recorded to assess mechanical or

biological degradation, lithification, and/or chemical dissolution of skeletal aragonite (e.g., Titschack and Freiwald 2005), while the amount of fragmentation and abrasion was recorded for interpretation of amount of transport. Where available, bivalved shells were used to determine whether the community was preserved in life position. Close packing of fossil concentrations, along with orientation and evidence of sorting were used to interpret the amount of energy in the depositional environment. The principal goal of the fieldwork was to quantitatively characterize variation in the physical attributes of each of the two shell beds and one measured section, as well as faunal composition and distribution patterns.

In the laboratory, twenty to thirty sample bags were processed for each measured section. Hand-samples were cut and polished to reveal cross-sectional views and used to study the lithology and facies of each locality. About fifty-five, 30 to 70 μm thick thin sections were made, with attention paid to representing all sedimentary surfaces, matrix material, and shell material. The thin sections were created from the unweathered interior of the cobbles and boulders to avoid contamination and were used for both petrographic and isotopic analyses. They were analyzed on a Boreal Polarizing Microscope using plane-polarized and cross-polarized light.

Hand samples were broken apart with a rock hammer or sledge hammer and all visible fossil material >1 mm in long dimension was identified to the finest possible taxonomic level. Identifications were made primarily on the basis of

descriptions and figures in Stanton (1895), Anderson (1938), Jeletzky (1965), and Grey (2009).

The carbonate was collected from multiple horizons within the 80 m stratigraphic section and was subjected to carbon and oxygen stable isotope analysis. Fifty-seven samples were collected for analysis, using a hand-held microdrill, from the surfaces of cut and polished thin section chips. The analyses were performed at the University of California, Riverside, on the Thermo Electron Corporation Delta V Plus Isotope Ratio Mass Spectrometer using the ISODAT 2.5 software. Sample material was collected from the turbidites above and below each carbonate horizon, as well as from the *Buchia*-rich carbonate horizons. Between ~0.150 and ~0.200 micrograms of material was collected into sample vials and placed into the mass spectrometer. The $\delta^{13}C$ and the $\delta^{18}O$ results are given in standard delta (δ) notation relative to the PeeDee belemnite (PDB) standard and appropriate correction factors were applied (Craig 1957). The average precision for $\delta^{13}C$ and $\delta^{18}O$ are ± 0.06‰ and ± 0.1‰, respectively.

The phenetic approach (as opposed to the phylogenetic) was used for morphometric analyses to define and evaluate the buchiid morphospecies. Ten morphometric variables that have been used successfully in a previous study for taxonomic discrimination in buchiids (see Grey et al. 2008) were measured on a total of 173 specimens, collected from three stratigraphic sections, encompassing eight stratigraphic horizons, that include two distinct lithologies. The morphometric analyses included both angular and linear measurements and

were made by measurement of the three shell axes, namely length (maximum distance on the anterior-posterior axis), height (maximum distance on the dorsal-ventral axis, across the shell middle axis), and width (maximum distance on the lateral axis, between both valves of the closed shell). All variables were measured to the nearest 0.01 mm with digital calipers.

The shell dimensions were analyzed using traditional multivariate morphometric techniques (e.g., Kowalewski et al. 1997, Hammer and Harper 2006, Grey 2009), ultimately testing the *Buchia* horizons for their morphological distinctiveness. Statistical methods included principal component analysis (PCA), canonical variate analysis (CVA), and discriminant analysis (DA). For all multivariate analyses, the data were log-transformed to create a scale-invariant matrix that preserves all allometries (Kowalewski et al. 1997, Hammer and Harper 2006). The multivariate methods used in this study follow those used in Kowalewski et al. (1997), Hammer and Harper (2006), and Grey (2009).

PCA is a technique that condenses information from many correlated variables into a few quantities that account for as much variance in the multidimensional data as possible, according to a particular model of axis reduction. PCA was used to explore the buchiids shell morphospace, searching for the presence of natural morphogroups. Thus, we performed principal component analyses with lithology as the grouping variable (2 horizons of *Buchia* in sandstone and 6 horizons of *Buchia* in carbonate) to assess the correlation between changes in shell morphology and lithology (a proxy for

paleoenvironment). If the data group by lithology, then morphological variation is dependent on environmental conditions, suggesting that ecophenotypic variation is an important factor controlling morphology. This study, however, does not rule out biological factors such as predation or population density or other environmental, physical, or human error factors, such as length of exposure at the seafloor, nutrient availability, quality of preservation, or incorrect species identification.

CVA was used for predictive classification. CVA produces a scatter plot of specimens along the two first canonical axes, producing maximal and second to maximal separation between all groups (multigroup discriminant analysis). The axes are linear combinations of the original variables as in PCA, and eigenvalues indicate the amount of variation explained by these axes. A priori grouping for the canonical analysis was based on collection horizon.

DA was used to assess the statistical robustness of the groups delineated in the CVA, by visually confirming or rejecting the hypothesis that two horizons are morphologically distinct. Using a cutoff point at zero (the midpoint between the means of the discriminant scores of the two groups), a classification into two groups is shown as a histogram and the percentage of correctly classified is calculated. Horizons were recognized statistically if the PCA showed distinctive morphospaces and/or the CVA and DA's indicated a reasonably high discriminatory power (i.e., a high percentage of individuals were classified to the correct horizon; ≥ 90 %). The statistical program PAST (PAlaeontological

STatistics) was used to calculate these multivariate statistical measures. PAST is a comprehensive program that makes comparisons of community structure and includes measures such as relative abundance, species richness, dominance, diversity, PCA, DA, CVA, and many others (Hammer et al. 2001, Hammer and Harper 2006).

7. Results

Bear Creek is a Valanginian aged hydrocarbon seep deposit that crops out in the Crack Canyon Formation (informal name of Lawton, 1956), within the GVG forearc strata. The absence of large-scale cross stratification and indigenous shallow water organisms indicate that the locality was deposited below-wave base.

Buchia occur in three substrates at Bear Creek, including (1) sandstone, (2) mudstone, and (3) microcrystalline carbonate (micarb) horizons (Figure 5). This study addressed Buchiid populations within two monospecific sandstone shell beds from two discrete regions of the locality, as well as from multiple discrete horizons within the lower 58 m (Figure 6A) of an 80 m (Figure 6) stratigraphic interval. In all three cases the horizons of interest are enclosed in submarine slope turbidite deposits characterized by a low sand-to-shale ratio, with each mudstone-sandstone couplet representing a single depositional event. These couplets have distinct bases and tops with no obvious coarsening/fining or

thickening/thinning of beds upwards and are often cemented with calcium carbonate, resulting in erosion-resistant cliff-forming beds.

In both of the monospecific sandstone shell beds included in this study, the *Buchia* are articulated, disarticulated, and occasionally fragmentary and are closely packed, often with imbrication of disarticulated shells. The *Buchia* are not oriented and likely were transported a short distance from their point of origin. The third Buchiid population included in this study was collected from discrete micarb horizons, which occur in the stratigraphically lowest 58 m (Figure 6A) of the 80 m stratigraphic interval (Figure 6). These *Buchia* are articulated, disarticulated, and very rarely fragmentary, occasionally occurring as horizons of shell hash interbedded with the fine-grained mudstone turbidites. When present, the concentration of *Buchia* often increases or decreases unpredictably, although lithologic characteristics have not changed. Horizon BC 0 has both *Buchia inflata* and *B. pacifica* present, while the remaining five contain only *B. pacifica*.

The 32 m interval (Figure 6B) occurring stratigraphically above the *Buchia* micarb horizons, encase a diverse macrofaunal assemblage that includes both endemic and typical seep taxa, such as worm tubes and lucinid bivalves (Table 1). Throughout this 32 m interval are 14 stratigraphically discrete seepage events of micarb cobbles, boulders, and lenses varying from 10 to 40 cm in thickness and from 20 to 300 cm in length (Figure 3, Figure 6). Each of the 14 seeps are interbedded with mudstone and fine-grained sandstone turbidites of

the GVG forearc strata. Nearly a quarter of the fourteen seeps are fossil-free, none are monospecific, and those remaining are fossil-rich (Table 1).

The faunal assemblage for the two shell beds and one stratigraphic section involved in this study includes four clades and twelve taxa, with between one and six taxa found in each horizon. The clades include gastropods, bivalves, worm tubes and ammonites. Regardless of substrate (sandstone, mudstone, micarb), the horizons in which *Buchia* occurs are always monospecific. In contrast, the 14 stratigraphically younger seeps are dominated by *Paskentana paskentaensis* (62%). In respect to all horizons, many of these faunas are common constituents of hydrocarbon seeps, with considerable overlap between Bear Creek and other Great Valley hydrocarbon seep localities (e.g., Harrington Flat Road and Little Indian Valley, see chapters 1 and 2).

Petrographic analyses were performed on all of the micarb horizons. The thin sections are dominated by standard hydrocarbon seep fabrics, cements, and textures, such as detrital-rich micarb, fibrous, yellow, botryoidal, dentate, and sparry calcites, microbial fabrics, calcispheres, pyrite framboids, peloids, vugs, and neomorphosed micrite, all of which are consistent with other regional and globally distributed hydrocarbon seep deposits (Figure 7). Thin sections were created from material collected throughout all micarb horizons, all of which demonstrates remarkable consistency, with considerable overlap of the cements, microbial fabrics, and textures from one thin section to the next.

7.1 *Isotopic Analyses*

Carbon and oxygen analyses were performed on all of the micarb horizons, including both those with *Buchia* present, as well as those without *Buchia* present; however, were not performed on the sandstone *Buchia* horizons. The $\delta^{13}C$ values range from -26.82‰ to +19.26‰, while the δ^{18} O values range from -12.06‰ to -0.88‰ (Figure 8, Table 2). Samples of shell material were also processed for carbon and oxygen isotope analyses and the $\delta^{13}C$ values of the shells are significantly heavier than those generally measured on bivalve shells living in normal marine environments (e.g., Lloyd 1964, Rio et al. 1992). The $\delta^{13}C$ values of shell material are consistent with extant bivalves containing symbiotic sulfide oxidizers, and have signatures similar to the bivalves *Bathymodiolus thermophilus* and *Codakia orbicularis* (Rio et al. 1992). MacLeod and Hoppe (1992) and Kauffman and Sageman (1990) found similar results for inoceramid bivalves, which they used to suggest that some in the family might have harbored chemosymbionts.

In the *Buchia* horizons, the depleted $\delta^{13}C$ values suggest that the *Buchia* lived in a hydrocarbon seep, with the wide range in carbon values (both enriched and depleted) implies that both methane formation and methane or hydrocarbon oxidation occurred in the same deposit and influenced carbonate formation. In contrast, the upper 32 m of the 80 m stratigraphic section, which are non-*Buchia* bearing horizons, have only variably depleted $\delta^{13}C$ values, indicating methane

oxidation, without methanogenesis. This strongly suggests that different processes were occurring in the two parts of the deposit.

Although, the $\delta^{13}C$ values for both the *Buchia* intervals and the non-*Buchia* intervals in the lower 58 m of section, are not low enough to exclude organic carbon sources other than hydrocarbons (Peckmann and Thiel 2004), the negative values are likely the product of hydrocarbon-rich fluids generated from organic detritus in the sediment column that, along with organic-rich pore water, were driven to the seafloor by tectonic or stratigraphic compression, compaction, or by buoyancy (Ritger et al. 1987, Campbell and Bottjer 1993, Orange and Campbell 1997).

The positive $\delta^{13}C$ values, recorded only for the *Buchia* horizons, are likely the result of *in situ* methanogenesis by the archaeal methanogens, a process that enriches the CO_2 pool in ^{13}C, the heavier isotope (Irwin et al. 1977, Boehme et al. 1996). During the anaerobic oxidation of methane (AOM), advecting methane was trapped in the zone of sulfate reduction (SR), where it was used for energy synthesis, along with seawater sulfate that diffused down into the sediment column by a syntrophic consortium of methane oxidizers and sulfate reducers (Joye et al. 2004, Orcutt et al. 2005). This consortium preferentially used ^{12}C over ^{13}C, enriching the pore water in heavy carbon and depleting the newly produced bicarbonate in light carbon (Joye et al. 2004). This process continued until pore water sulfate concentrations were depleted, which caused the zone of AOM and SR to shallow. Fluid advection rates could also have

increased at this time and as a result, the zone of AOM was less capable of trapping the higher rates of advecting methane, which resulted in more fluid venting at the seafloor and mixing with seawater. If the isotopically depleted bicarbonate vented and mixed with seawater, the available carbon pool shifted to that produced by methanogenesis, a process that results in the production of isotopically heavy carbon dioxide (Irwin et al. 1977). This carbon dioxide readily dissolved in pore water and increased bicarbonate concentrations, and caused the precipitation of calcium carbonate with a heavy isotopic signature (Figure 9).

7.2 *Morphometrics*

Initially, PCA was conducted with the linear measurement data pooled for all eight horizons. The scores generated for the PC's accounting for >1% of the variance, excluding PC1, were added to the angular measurements, which typically reflects size, and PCA (in addition to DA and CVA) was run again. The first three principal components account for most of the variation in the data (93.8%) and therefore, higher PCs are not considered here (Table 3). The principal component axes, including PC1, PC2, and PC3 represent 47.62%, 40.19%, and 5.99% of the character variation, respectively. PC1 is a function of the dorsal angle of the crest-line and inflation, PC2 is a function of the dorsal angle of the crest-line, and PC3 is a function of the ventral angle of the crest-line, as well as both inflation and the anterior width.

All eight horizons show a considerable amount of variability in morphospace; however, the two sandstone horizons, BC 2F and BC 3C, have

the greatest size variation and cluster in the upper right corner, falling into morphospace unoccupied by the carbonate horizons (Figure 10). This suggests that these specimens had greater inflation and larger dorsal angles of the crest-line than the carbonate horizons. In general, however, there is considerable overlap in morphospace for all eight horizons, which suggests that (1) the eight horizons are populated by only a single *Buchia* species, likely *Buchia pacifica* and (2) that shell morphology is largely unrelated to lithofacies.

PCA and DA were also conducted on data pairs, specifically comparing horizons BC 2F, BC 3C, or BC 6A to each of the other horizons (BC 6A was chosen randomly because it is representative of all of the seep horizons). On average, when comparing BC 6A to the other five carbonate horizons, the primary principal component axis (PC1) and PC2 accounted for 87.24% of the character variation within the data, while when comparing a sandstone horizon, BC 2F or BC 3C, to the carbonate horizons, on average, PC1 and PC2 accounted for between 91.73% and 87.82% of the character variation within the data, respectively. As with the pooled horizon data, PC1 is a function of the dorsal angle of the crest-line and inflation and PC2 is a function of the dorsal angle of the crest-line.

DA can be used to visually confirm or reject the hypothesis that two groups are morphologically distinct (Figure 11). On average, it correctly distinguishes between sandstone horizon 3C and the five carbonate horizons 89.38% of the time, between sandstone horizon 2F and the five carbonate

horizons 91.49% of the time, while only 77.42% of the time between the carbonate horizon 6A and the other five carbonate horizons. Values of correctly classified individuals >90%, allow the two groups being compared to be split into different morphospecies. The DA correctly classified values (89.38% to 91.49%) straddle 90%, which suggests that there are considerable differences between the two lithologic populations and that they are potentially different morphospecies. This, however, is not consistent with PCA run with the pooled data from the eight horizons.

The highest percentage yields (those closest to correctly distinguishing the different horizons 100% of the time) and thus, the horizons with *Buchia* that are the least morphologically alike, are always the product of a comparison between two different lithologic horizons (sandstone vs. carbonate), while the lowest percentage yields (those correctly distinguishing between the different horizons < 90% of the time) and thus, the horizons with the most morphologically alike *Buchia* are the product of a comparison between like lithologies (carbonate vs. carbonate or sandstone vs. sandstone); however, DA has more difficulty discriminating between any two of the carbonate horizons, than the two sandstone horizons. This suggests that the carbonate horizons shared enough environmental similarities to result in *Buchia* with similar morphologies through time, while environmental variations resulted in the sandstone and carbonate horizons having populations with fewer morphological similarities.

The Wilk's lambda, p (same): $3.61E^{-22}$ and Pillai trace, p (same): $4.72E^{-18}$ values, products of MANOVA analysis, indicate a highly significant difference in the multivariate means of the eight horizons, establishing overall inequality. Once this inequality was established, the equality of the means of horizon pairs was tested by a multivariate analogue to the *t* test, called Hotelling's T-squared (T^2), and a *p* value for this test is given. If the *p* value is ≤ 0.05 (white boxes), then horizon pairs are drawn from populations with statistically different multivariate means, while if the *p* value is > 0.05 (gray boxes), then horizon pairs are drawn from populations with statistically equal multivariate means. The eight horizons result in twenty-eight pair wise comparisons (Table 4). The Hotelling's pair wise analysis reports a highly significant difference in the multivariate means of twenty-four of these pairs, and no significant difference between four of them (BC 1A and BC 6A, BC 0 and BC 8, BC 1A and BC 8, and BC 2F and BC 3C). Horizons 2F and 3C have a *p* value = 0.272, indicating that the *Buchia* are drawn from populations with equal multivariate means, however, they do not share equality of multivariate means with any of the six carbonate horizons. Thus, MANOVA analysis successfully separates lithologically different horizons, suggesting that it is sensitive to environmental differences (turbidite vs. seep).

The CVA scatterplot (Figure 12) is the visual representation of Table 4. The six carbonate horizons largely group together in the coordinate system of the first two canonical axes (CV1 and CV2 account together for 85.90% of the variation), although there is scatter within the morphospace. The four horizon

pairs that do not have statistically equal multivariate means have greater separation in morphospace, while the four with equal multivariate means plot closer together. There is no overlap between BC 9 and BC 2F or BC 3C, which could suggest that distinct morphogroups do exist. This separation from the seep horizons and plotting together in morphospace is in keeping with their Hotelling's *p* value, which indicates that they are statistically different than the seep horizons.

8. Discussion

The Bear Creek locality is unusual because it preserves hydrocarbon seep carbonate with two distinct faunal and isotopic signatures (*Buchia* vs. non *Buchia*), as well as sandstone intervals that preserve intervals of monospecific *Buchia* shell pavements. *Buchia* has been documented in micarb at a number of GVG hydrocarbon seep deposits, including at the Bear Creek (*Buchia pacifica, B. inflata*), Sandy's Creek (*B. piochii*), Rocky Creek (*B. pacifica*), Rice Valley (*B. pacifica*), and Paskenta (*B. piochii, B. fischeriana*) faunal assemblages. Although documented at each of these deposits, Bear Creek is unique because it preserves *Buchia* in both micarb and sandstone, as well as its disappearance up section, in a stratigraphically younger hydrocarbon seep deposit.

Although *Buchia* are not restricted to hydrocarbon seep settings, their presence at so many in the GVG forearc strata suggests that they might have been utilizing non-conventional life strategies or strategies that have never been

attributed to them. Surviving in the hydrocarbon seep environment requires the ability to live well below the photic zone, under extreme conditions of low oxygen levels, high pressures, cold temperatures, and in the presence of toxic advecting fluids (methane and hydrogen sulfide). Although it has been suggested that *Buchia*, in addition to inoceramid bivalves and the species *Pecten complexicosta* inhabited the seep environment to escape predation pressures (MacLeod and Hoppe 1992), their ubiquitous presence in hydrocarbon seep micarb cobbles, boulders, and lenses at Bear Creek and other Great Valley hydrocarbon seep deposits, a well as the depleted $\delta^{13}C$ and enriched $\delta^{13}C$ signatures at Bear Creek, suggests that *Buchia* could have been an inhabitant of the seep setting due to a previously undocumented symbiotic relationship with chemoautotrophic microbes that transformed the advecting fluids into usable organic compounds. They likely proliferated in a cold, high-pressure environment by exploiting the abundance of energy-rich reduced substrates, such as methane and hydrogen sulfide.

The validity of *Buchia* harboring chemosymbionts can be tested using sulfur isotopes incorporated into the shell during shell formation. Sulfate, a naturally occurring compound in seawater, diffuses into the sediment at the sediment/water interface where it is consumed in anaerobic sediments by sulfate reduction (Canfield et al. 2005). This produces isotopically light H_2S and enriches the seawater/porewater sulfate pool in the heavier isotope (Canfield et al. 2005). H_2S diffuses upward along a concentration gradient and is oxidized

from sulfide to sulfate by the sulfide oxidizing bacteria living symbiotically within the bivalves (Canfield et al. 2005). Sulfate formation is accompanied by little fractionation, causing the sulfate to inherit the sulfur isotopic composition of the H_2S, so oxidation of light sulfide yields light sulfate (Harrison and Thode 1957), unlike sulfate reduction, which drives the sulfate pool heavy. During precipitation, since sulfate is incorporated into the carbonate lattice of the macrofaunal shells as structurally substituted sulfate (SSS) ion (Kampschulte and Strauss 2004, Hoek and Canfield 2008) and the bivalves precipitate their shells from the local internal light sulfate isotope pool, the shells record this bacterially mediated isotopic depletion. Sulfur isotopes will be run on *Buchia* shell material during the summer of 2010.

The positive carbon values reported in this study are unusual, however, $\delta^{13}C$ values higher than +5‰ have been reported from a limited number of ancient seep deposits (Gaillard et al. 1992, Peckmann et al. 2002, Peckmann et al. 2003, Peckmann and Thiel 2004). These studies have generally reported the enriched values, however, have made few suggestions as to how the signal could have been captured. At Bear Creek, the positive carbon values can be explained by a shallowing of the zone of sulfate reduction and an increase in the rate of fluid advection, which brought the zone of methanogenesis closer to the seafloor and made it a less effective advecting fluids trap.

Modern hydrocarbon seep faunal communities are variably structured, ranging from zoned to patchy, with the biological zones and patches relating to

changes in pore water chemistry, alkalinity, oxygen levels and oxygen penetration, as well as the rates and volumes of advecting fluids (Sibuet and Olu 1998, Levin 2005). The central areas of seeps have distinct zones that are characterized by higher volumes of fluid advection and are surrounded by bacterial mats (Levin 2005). As distance from the central area increases, the faunas change according to their species specific fluid flux, oxygen level, and chemical preferences (Levin 2005). This modern pattern is significant because, perhaps like modern bacterial mats, *Buchia* preferred to live under higher methane flux conditions; however, the small size of the deposit suggests that methane flux tapered off too quickly with increasing distance from the seep center to host other taxa, resulting in the monospecific associations preserved in the micarb.

A change from conditions characterized by a high methane flux to lower methane flux could provide an explanation for the transition from *Buchia* dominated horizons to typical hydrocarbon seep taxa dominated horizons, in the 80 m measured stratigraphic interval. This flux change is consistent with modern seeps, which have been documented changing physically, chemically, and faunally over very short distances and timescales (Levin 2005). These changes have been linked to the variability of physical and chemical conditions beneath the area of seepage, as well as the rate or volume of fluid flow (Sibuet and Olu 1998, Levin 2005, Orcutt et al. 2005).

The close proximity of the sandstone and micarb *Buchia* intervals suggest that the *Buchia* both came from the same environment and from the same population, while the sedimentologic and petrographic analyses indicate that the *Buchia* preserved in sandstone did not come from a hydrocarbon seep, while those in the micarb did. The sandstone *Buchia* are not encased in micarb, nor is micarb in the sediments surrounding them except for the occasional concretion. Additionally, there are no petrographic textures, cements, or microbial fabrics present that are consistent with the hydrocarbon seep depositional environment, all of which indicates that the sandstone *Buchia* did not form in a hydrocarbon seep.

To test the distinctiveness of the *Buchia* populations in the 8 horizons and spanning two lithologies, a series of multivariate statistical procedures were employed. At this time, morphometric analyses are inconclusive since some analyses indicate that the sandstone and micarb *Buchia* populations fall into different morphospace, although with some overlap, suggesting that they come from two distinct populations, while other analyses suggest that they cannot be delineated into different morphospecies. This could suggest that the two lithologies actually host two different species or that the two lithologies produced ecophenotypic variation in a single species. Without further knowledge of the environment the sandstone *Buchia's* originated in, however, a concrete conclusion cannot be drawn at this time.

9. Conclusions

The hydrocarbon seeps of the Great Valley Group (GVG) are distributed over 700 km of distance and 80 m.y. of subduction history (Campbell et al. 1993) and provide an evolutionary and paleogeographic window to study organisms, fluids, and tectonics interacting in the eastern Pacific Ocean. Although *Buchia* have been documented throughout this region, their paleoecologic context has never before been addressed in detail. Based on this study, *Buchia* should be considered a typical hydrocarbon seep fauna for the GVG forearc strata and that likely, at least some species harbored chemosymbionts.

There are thousands of outcrops throughout the Great Valley that include *Buchia* preserved in micarb, mudstone, and sandstone, thus this region provides a perfect natural laboratory to address the strength of the assertion that they had chemosymbionts. Since, the Great Valley also hosts a significant number of macrofossil-rich hydrocarbon seep deposits, this region has the potential to provide insights into the role that *Buchiid* bivalves played in the hydrocarbon seep setting as well. Further identification of *Buchia* paleoecologic signatures from this region will ultimately place them into the global, spatial, temporal, and stratigraphic system and will allow larger questions concerning their phylogenetic, biogeographic, and paleoecologic origins to be addressed.

References Cited

Anderson, F. M. 1938. Lower Cretaceous Deposits in California and Oregon. Geological Society of America, Baltimore.

Århus, N., S. R. A. Kelly, J. S. H. Collins, and M. R. Sandy. 1990. Systematic palaeontology and biostratigraphy of two Early Cretaceous condensed sections from the Barents Sea. Polar Research 8(2):165-194.

Blake, M. C., Jr., and D. L. Jones. 1981. The Franciscan Assemblage and Related Rocks in Northern California: A Reinterpretation. Pp. 307-328. *In* W. R. Ernst, ed. The Geotectonic Development of California. Prentice Hall, New Jersey.

Blake, M. C., Jr., and R. J. McLaughlin. 1989. Terranes of the Northern Coast Ranges. P. 75. *In* M. C. Blake, and D. S. Harwood, eds. Tectonic Evolution of Northern California. American Geophysical Union, Washington D.C.

Boehme, S. E., N. E. Blair, J. P. Chanton, and C. S. Martens. 1996. A Mass Balance of ^{13}C and ^{12}C in an Organic-rich Methane-producing Marine Sediment. Geochimica et Cosmochimica Acta 60(20):3835-3848.

Bralower, T. J. 1990. Lower cretaceous calcareous nannofossil stratigraphy of the Great Valley Sequence, Sacramento Valley, California. Cretaceous Research 11(2):101-123.

Campbell, K. A., and D. J. Bottjer. 1993. Fossil Cold Seeps. National Geographic Research and Exploration 9(3):326-343.

Campbell, K. A., C. Carlson, and D. J. Bottjer. 1993. Fossil Cold Seep Limestones and Associated Chemosymbiotic Macroinvertebrate Faunas, Jurassic-Cretaceous Great Valley Group, California. Pp. 37-50. *In* S. A. Graham, and D. R. Lowe, eds. Advances in the Sedimentary Geology of the Great Valley Group, Sacramento Valley, California. Pacific Section, SEPM, Los Angeles.

Canfield, D. E., B. Thamdrup, and E. Kristensen. 2005. Aquatic Geomicrobiology. Elsevier Academic Press, Amsterdam.

Cavagna, S., P. Clari, and L. Martire. 1999. The role of bacteria in the formation of cold seep carbonates: geological evidence from Monferrato (Tertiary, NW Italy). Sedimentary Geology 126:253-270.

Cavanaugh, C. M., Z. P. McKiness, I. L. G. Newton, and F. J. Stewart. 2006. Marine Chemosynthetic Symbiosis. Pp. 475-507. The Prokaryotes. Springer, New York.

Conti, S., and D. Fontana. 1999. Miocene chemoherms of the northern Apennines, Italy. Geology 27(10):927-930.

Craig, H. 1957. Isotopic standards for carbon and oxygen and correction factors for mass-spectrometric analysis of carbon dioxide. Geochimica et Cosmochimica Acta 12:133-149.

De la Mora, A., F. Olóriz, and C. González-Arreola. 2000. 'Autochthonous' bivalve assemblages and palaeoecologic interpretation in the Upper Jurassic-Lowermost Cretaceous La Caja Formation from the Cañón de San Matías (Zacatecas, México). Comptes Rendus de l'AcadÈmie des Sciences - Series IIA - Earth and Planetary Science 331(11):741-747.

Dickinson, W. R., and D. R. Seely. 1979. Structure and Stratigraphy of Forearc Regions. American Association of Petroleum Geologists Bulletin 63(1):2-31.

Dickinson, W. R. 1981. Plate Tectonics and the Continental Margin of California. Pp. 1-28. *In* W. R. Ernst, ed. The Geotectonic Development of California. Prentice Hall, New Jersey.

Elvert, M., and E. Suess. 1999. Anaerobic methane oxidation associated with marine gas hydrates: superlight C-isotopes from saturated and unsaturated C_{20} and C_{25} irregular isoprenoids. Naturwissenschaften 86:295-300.

Flügel, E. 1982. Microfacies Analysis of Limestones. Springer-Verlag, Berlin.

Gaillard, C., M. Rio, and Y. Rolin. 1992. Fossil Chemosynthetic Communities Related to Vents or Seeps in Sedimentary Basins: The Pseudobioherms of Southeastern France Compared to Other World Examples. Palaios 7:451-465.

Godfrey, N. J., B. C. Beaudoin, and S. L. Klemperer. 1997. Ophiolitic basement to the Great Valley forearc basin, California, from seismic and gravity data: Implications for crustal growth at the North American continental margin. GSA Bulletin 109(12):1536-1562.

Grey, M., J. W. Haggart, and P. L. Smith. 2008. A New Species of *Buchia* (Bivalvia: Buchiidae) From British Columbia, Canada, With An Analysis of Buchiid Bipolarity. Journal of Paleontology 82(2):391-397.

Grey, M. 2009. Exploring Evolutionary Patterns and Processes. The University of British Columbia, Vancouver.

Hammer, Ø., D. A. T. Harper, and P. D. Ryan. 2001. PAST: Paleontological Statistics Software Package for Education and Data Analysis. Palaeontologia Electronica 4(1):9.

Hammer, Ø., and D. Harper. 2006. Paleontological Data Analysis. Blackwell Publishing, Malden.

Harrison, A. G., and H. G. Thode. 1957. The kinetic isotope effect in the chemical reduction of sulphate. Transactions of the Faraday Society 53:1648-1651.

Hinrichs, K. U., and A. Boetius. 2003. The Anaerobic Oxidation of Methane: New Insights in Microbial Ecology and Biogeochemistry. P. 495. *In* G. Wefer, D. Billet, D. Hebbeln, B. B. Jørgensen, M. Schlüter, and T. v. Weering, eds. Ocean Margin Systems. Springer, Berlin.

Hoek, J., and D. E. Canfield. 2008. Controls on Isotope Fractionation During Dissimilatory Sulfate Reduction. Pp. 273-284. *In* C. Dahl, and C. G. Friedrich, eds. Microbial Sulfur Metabolism. Springer.

Imlay, R. W. 1959. Succession and Speciation of the Pelecypod *Aucella*. Washington, U.S. Govt. Print. Off., 1959., Washington D.C.

Ingersoll, R. V. 1978a. Submarine Fan Facies of the Upper Cretaceous Great Valley Sequence, northern and central California. Sedimentary Geology 21:205-230.

Ingersoll, R. V. 1978b. Paleogeography and Paleotectonics of the Late Mesozoic Forearc Basin of Northern and Central California. Pp. 471-482. *In* D. G. Howell, and K. A. McDougall, eds. Mesozoic Paleogeography of the Western United States. SEPM Pacific Section, Los Angeles.

Ingersoll, R. V. 1979. Evolution of the Late Cretaceous forearc basin, northern and central California. Geological Society of America Bulletin 90(9):813-826.

Ingersoll, R. V. 1982. Initiation and evolution of the Great Valley forearc basin of northern and central California, U.S.A. Pp. 459-467. *In* J. K. Leggett, ed. Trench-Forearc Geology; Sedimentation and Tectonics on Modern and Ancient Active Plate Margins. Special Publication-Geological Society of London, London.

Irwin, H., C. Curtis, and M. Coleman. 1977. Isotopic evidence for source of diagenetic carbonates formed during burial of organic-rich sediments. Nature 269(5625):209-213.

Jeletzky, J. A. 1965. Late Upper Jurassic and early Lower Cretaceous fossil zones of the Canadian western Cordillera, British Columbia. Geological Survey of Canada Bulletin 103:1-67.

Jones, D. L., E. H. Bailey, and R. W. Imlay. 1969. Structural and Stratigraphic Significance of the *Buchia* Zones in the Colyear Springs-Paskenta Area, California. United States Geological Survey Professional Paper 647-A:21.

Joye, S. B., A. Boetius, B. N. Orcutt, J. P. Montoya, H. N. Schulz, M. J. Erickson, and S. K. Lugo. 2004. The anaerobic oxidation of methane and sulfate reduction in sediments from Gulf of Mexico cold seeps. Chemical Geology 205:219-238.

Kampschulte, A., and H. Strauss. 2004. The sulfur isotopic evolution of Phanerozoic seawater based on the analysis of structurally substituted sulfate in carbonates. Chemical Geology 204:255-286.

Kauffman, E. G., and B. G. Sageman. 1990. Biological Sensing of Benthic Environments in Dark Shales and Related Oxygen-Restricted Facies. Pp. 121-138. *In* R. N. Ginsberg, and B. Beaudoin, eds. Cretaceous resources, events and rhythms. Kluwer Academic Publishers, Dordrecht, Netherlands.

Kennicutt II, M. C., R. A. Burke Jr., I. R. MacDonald, J. M. Brooks, G. J. Denoux, and S. A. Macko. 1992. Stable isotope partitioning in seep and vent organisms: chemical and ecological significance. Chemical Geology (Isotope Geoscience Section) 101:293-310.

Kiel, S., K. A. Campbell, W. P. Elder, and C. T. S. Little. 2008. Jurassic and Cretaceous Gastropods from Hydrocarbon Seeps in Forearc Basin and Accretionary Prism Settings, California. Acta Palaeontologica Polonica 53(4):679-703.

Kowalewski, M., E. Dyreson, J. D. Marcot, J. A. Vargas, K. W. Flessa, and D. P. Hallman. 1997. Phenetic Discrimination of Biometric Simpletons: Paleobiological Implications of Morphospecies in the Lingulide Brachiopod *Glottidia*. Paleobiology 23(4):444-469.

Lawton, J. E. 1956. Geology of the North Half of the Morgan Valley Quadrangle and the South Half of the Wilbur Springs Quadrangle. Dissertation. Stanford University, Palo Alto.

Levin, L. A. 2005. Ecology of Cold Seep Sediments: Interactions of Fauna with Flow, Chemistry, and Microbes. Oceanography and Marine Biology: An Annual Review 43:1-46.

Lloyd, R. M. 1964. Variations in the Oxygen and Carbon Isotope Ratios of Florida Bay Mollusks and Their Environmental Significance. The Journal of Geology 72(1):84-111.

MacLeod, K. G., and K. A. Hoppe. 1992. Evidence that inoceramid bivalves were benthic and harbored chemosynthetic symbionts. Geology 20(2):117-120.

Marinov, V. A., S. V. Meledina, O. S. Dzyuba1, O. S. Urman, O. V. Yazikova, V. A. Luchinina, A. G. Zamirailova, and A. N. Fomin. 2006. Biofacies of Upper Jurassic and Lower Cretaceous sediments of central West Siberia Stratigraphy and geological correlation 14(4):418.

Orange, D. L., and K. A. Campbell. 1997. Modern and Ancient Cold Seeps on the Pacific Coast-Monterey Bay, California, and Offshore Oregon as Modern-Day Analogs to the Hoh Accrectionary Complex and Quinault Formation, Washington. Washington Geology 25(4):3-13.

Orcutt, B., A. Boetius, M. Elvert, V. Samarkin, and S. B. Joye. 2005. Molecular biogeochemistry of sulfate reduction, methanogenesis and the anaerobic oxidation of methane at Gulf of Mexico cold seeps. Geochimica et Cosmochimica Acta 69(17):4267-4281.

Pancost, R. D., and J. S. S. Damsté. 2000. Biomarker Evidence for Widespread Anaerobic Methane Oxidation in Mediterranean Sediments by a Consortium of Methanogenic Archaea and Bacteria. Applied and Environmental Microbiology 66(3):1126-1132.

Paull, C. K., J. P. Chanton, A. C. Neumann, J. A. Coston, C. S. Martens, and W. Showers. 1992. Indicators of Methane-Derived Carbonates and Chemosynthetic Organic Carbon Deposits: Examples from the Florida Escarpment. Palaios 7:361-375.

Peckmann, J., J. L. Goedert, V. Thiel, W. Michaelis, and J. Reitner. 2002. A comprehensive approach to the study of methane-seep deposits from the Lincoln Creek Formation, western Washington State, USA. Sedimentology 49:855-873.

Peckmann, J., J. L. Goedert, T. Heinrichs, J. Hoefs, and J. Reitner. 2003. The Late Eocene 'Whiskey Creek' Methane-Seep Deposit (Western Washington State) Part II: Petrology, Stable Isotopes, and Biogeochemistry. Facies 48:241-254.

Peckmann, J., and V. Thiel. 2004. Carbon cycling in ancient methane-seeps. Chemical Geology 205:443-467.

Reeburgh, W. S. 1976. Methane Consumption in Cariaco Trench Waters and Sediments. Earth and Planetary Science Letters 28:337-344.

Rio, M., M. Roux, M. Renard, and E. Schein. 1992. Chemical and Isotopic Features of Present Day Bivalve Shells from Hydrothermal Vents or Cold Seeps. Palaios 7:351-360.

Ritger, S., B. Carson, and E. Suess. 1987. Methane-derived authigenic carbonates formed by subduction-induced pore-water expulsion along the Oregon/Washington margin. Geological Society of America Bulletin 98:147-156.

Sha, J., and F. T. Fursich. 1993. Biostratigraphy of the Upper Jurassic-Lower Cretaceous bivalves *Buchia* and Aucellina of eastern Heilongjiang, Northeast China. Geological Magazine 130(4):533-542.

Sibuet, M., and K. Olu. 1998. Biogeography, biodiversity and fluid dependence of deep-sea cold-seep communities at active and passive margins. Deep-Sea Research II 45:517-567.

Smelror, M., and H. Dypvik. 2006. The Sweet Aftermath: Environmental Changes and Biotic Restoration Following the Marine Mjølnir Impact (Volgian-Ryazanian Boundary, Barents Shelf). Pp. 143-178. Biological Processes Associated with Impact Events. Springer Berlin Heidelberg.

Somero, G. N. 1984. Physiology and Biochemistry of the Hydrothermal Vent Animals. Oceanus 27(3):67-72.

Stanley, S. M. 1972. Functional Morphology and Evolution of Byssally Attached Bivalve Mollusks. Journal of Paleontology 46(2):165-212.

Stanton, T. W. 1895. Contributions to the Cretaceous Paleontology of the Pacific Coast: The Fauna of the Knoxville Beds. Bulletin of the United States Geological Survey 133:9-132.

Suchecki, R. K. 1984. Facies history of the Upper Jurassic-Lower Cretaceous Great Valley Sequence; response to structural development of an outer-arc basin. Journal of sedimentary research 54(1):170-191.

Swe, W., and W. R. Dickinson. 1970. Sedimentation and Thrusting of Late Mesozoic Rocks in the Coast Ranges near Clear Lake, California. Geological Society of America Bulletin 81:165-188.

Thiel, V., J. Peckmann, R. Seifert, P. Wehrung, J. Reitner, and W. Michaelis. 1999. Highly isotopically depleted isoprenoids: Molecular markers for ancient methane venting. Geochimica et Cosmochimica Acta 63(23/24):3959-3966.

Titschack, J., and A. Freiwald. 2005. Growth, deposition, and facies of Pleistocene bathyal coral communities from Rhodes, Greece. Pp. 41-59. *In* J. Titschack, and J. M. Roberts, eds. Cold-Water Corals and Ecosystems. Springer, Berlin.

Van Dover, C. L., C. R. German, K. G. Speer, L. M. Parson, and R. C. Vrijenhoek. 2002. Evolution and Biogeography of Deep-Sea Vent and Seep Invertebrates. Science 295:1253-1257.

Werne, J. P., R. R. Haese, T. Zitter, G. Aloisi, I. Bouloubassi, S. Heijs, A. Fiala-Médioni, R. D. Pancost, J. S. S. Damsté, G. d. Lange, L. J. Forney, J. C. Gottschal, J.-P. Foucher, J. Mascle, and J. Woodside. 2004. Life at cold seeps: a synthesis of biogeochemical and ecological data from Kazan mud volcano, eastern Mediterranean Sea. Chemical Geology 205:367-390.

Xiaochi, L., and J. A. Grant-Mackie. 1988. Upper Jurassic and Lower Cretaceous *Buchia* (Bivalvia) from southern Tibet, and some wider considerations. Alcheringa: An Australasian Journal of Palaeontology 12(4):249 - 268.

Zakharov, V. A. 1987. The bivalve *Buchia* and the Jurassic-Cretaceous boundary in the boreal province. Cretaceous Research 8(2):141-153.

Zhiqiang, B., and X. Zunyi. 2006. Recent approach to *Buchia* biostratigraphy from the Tethyan Himalaya area, China. Front. Biol. China 2:213-218.

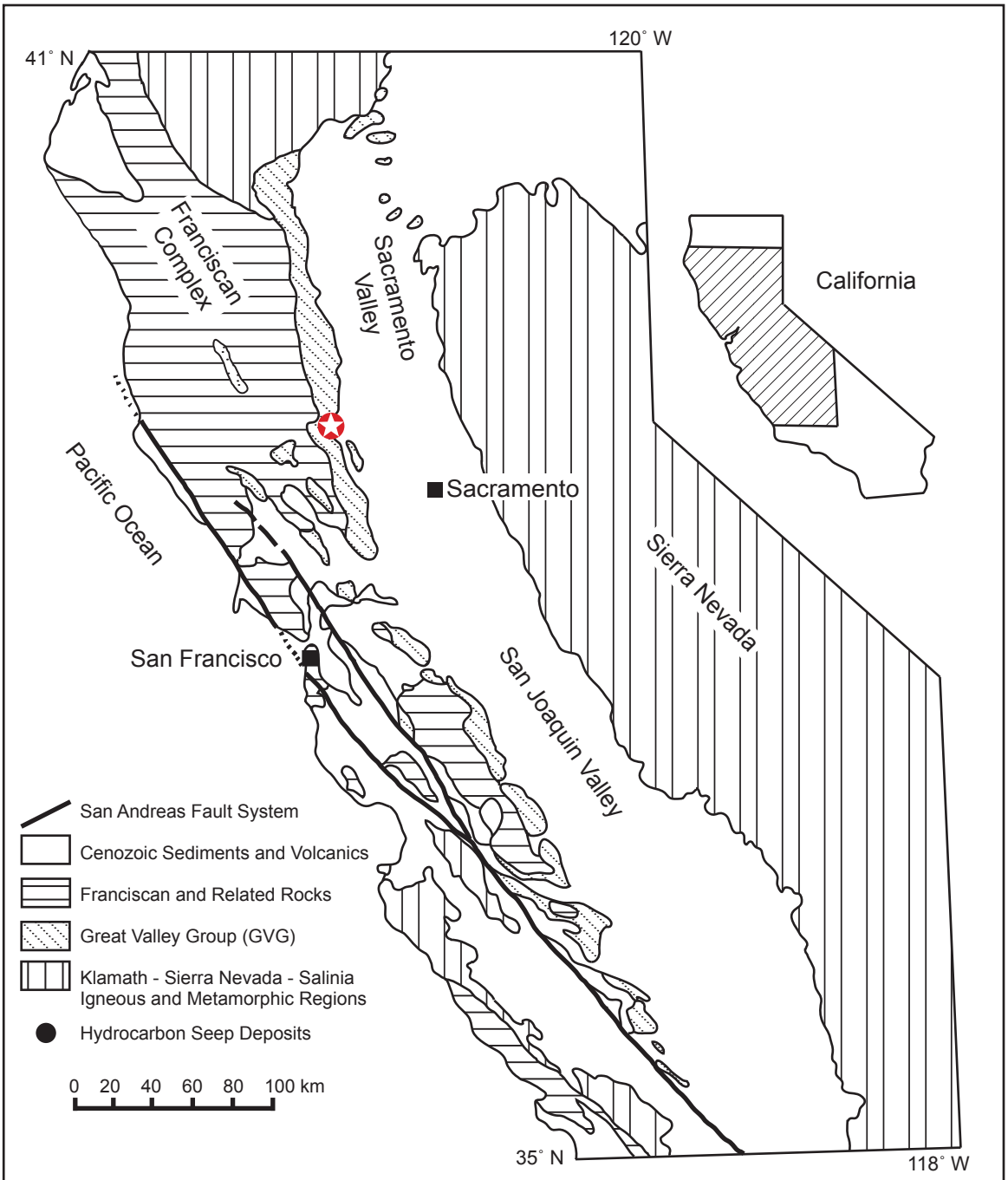

Figure 1. Locality map for Bear Creek (star), a Mesozoic hydrocarbon seep locality. Simplified geology of the western North American Continental margin, including from west to east, the Franciscan Complex, the GVG forearc strata, and the Sierra Nevada batholith. Map after Ingersoll (1978).

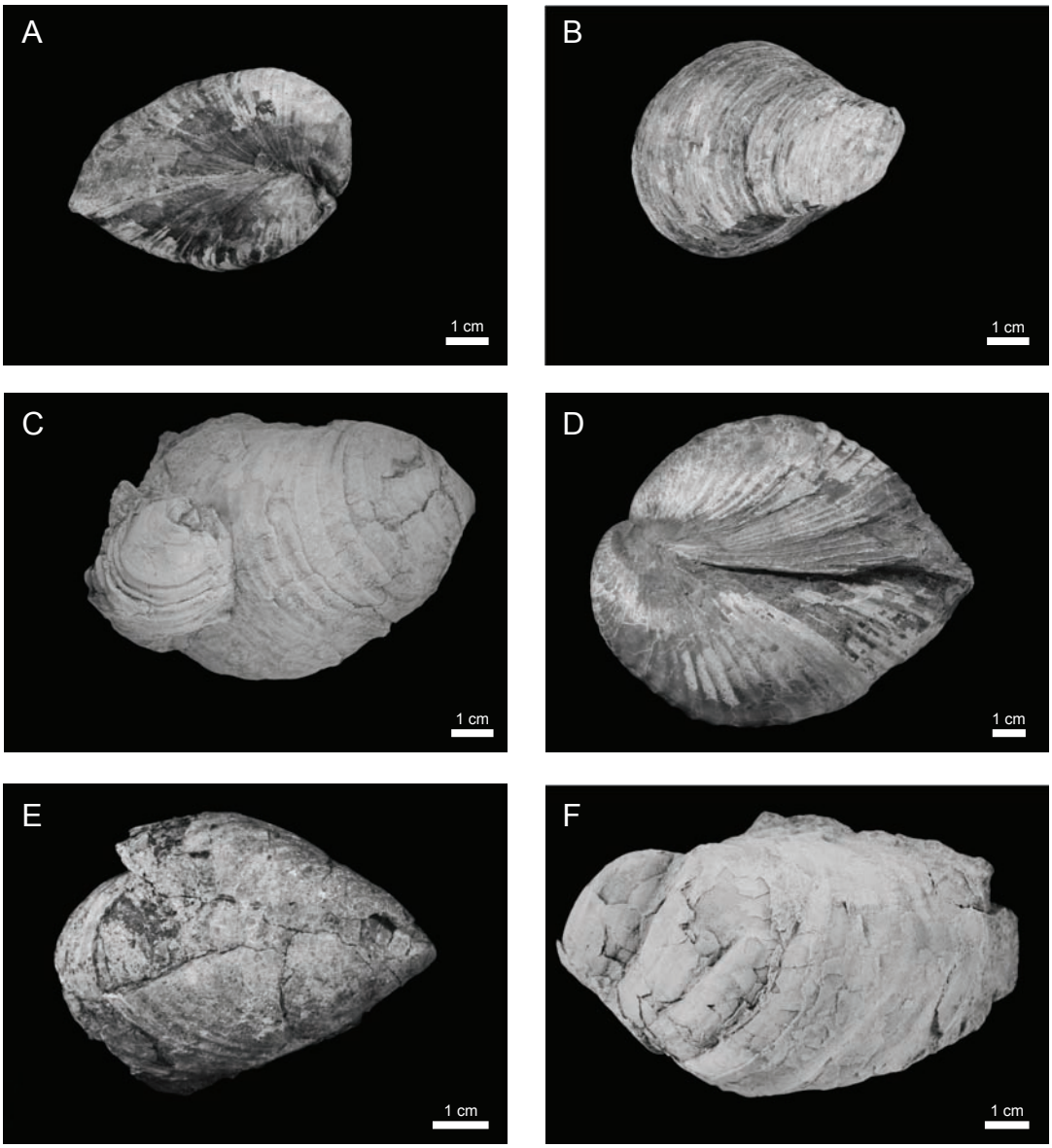

Figure 2. *Buchia* specimens from Bear Creek. (A) Side view of *Buchia pacifica* specimen, from horizon BC 9. (B) Top view of *B. pacifica* specimen from (A), from horizon BC 9. (C) Large and small specimen of *B. pacifica* preserved together, from horizon BC 2F. (D) Side view of *B. inflata* specimen, from horizon BC O. (E) *B. pacifica* specimen, from horizon BC 1A. (F) *B. pacifica* specimen from horizon BC 1E.

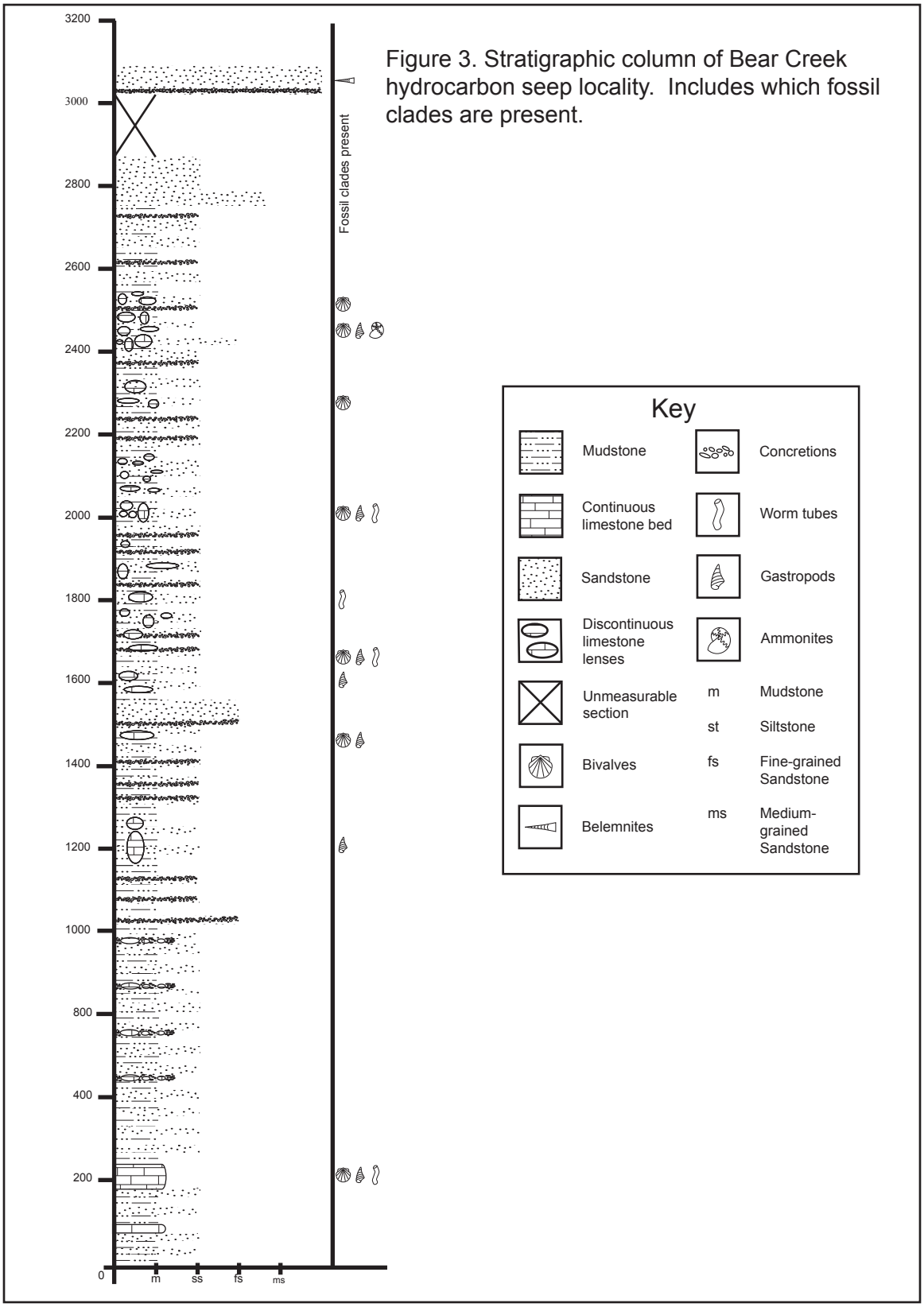

Figure 3. Stratigraphic column of Bear Creek hydrocarbon seep locality. Includes which fossil clades are present.

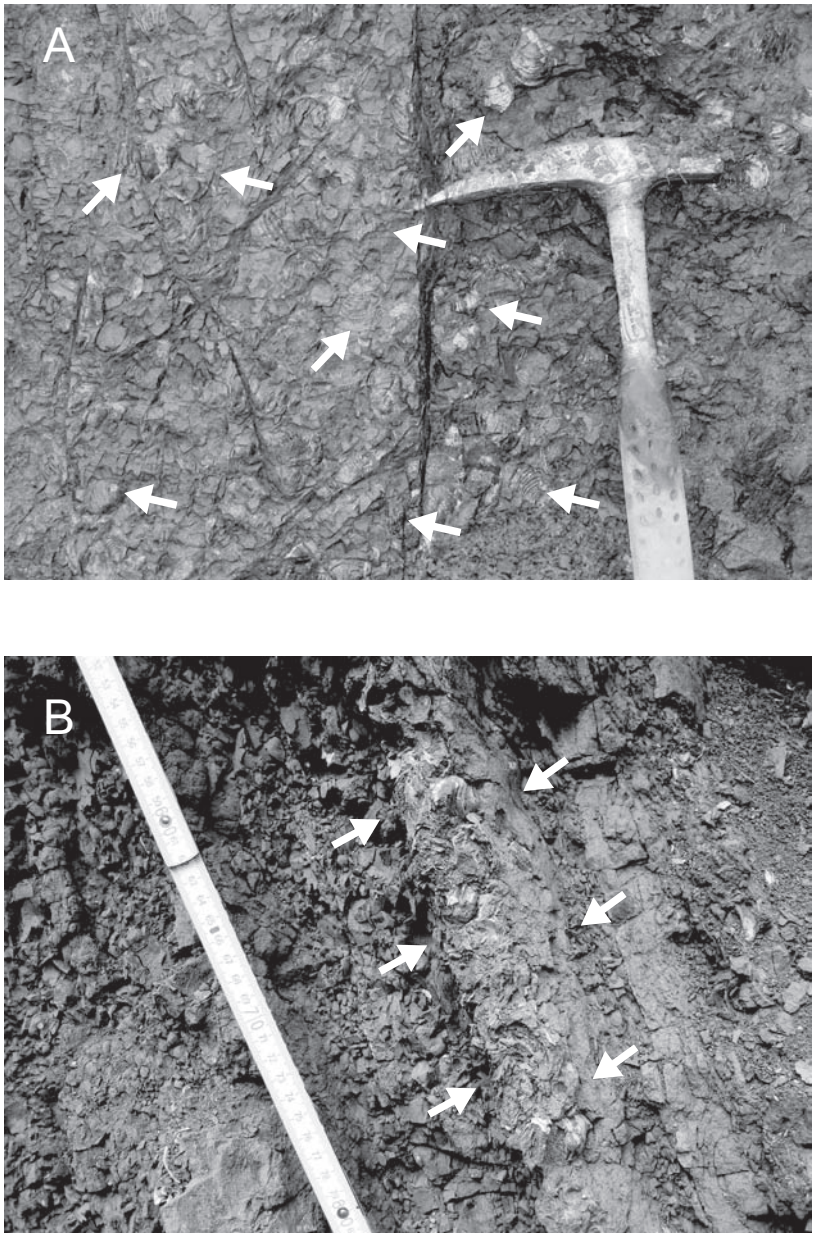

Figure 4. The two monospecific Buchia shell pavements intervals used in this study. (A) BC 3C and (B) BC 2F.

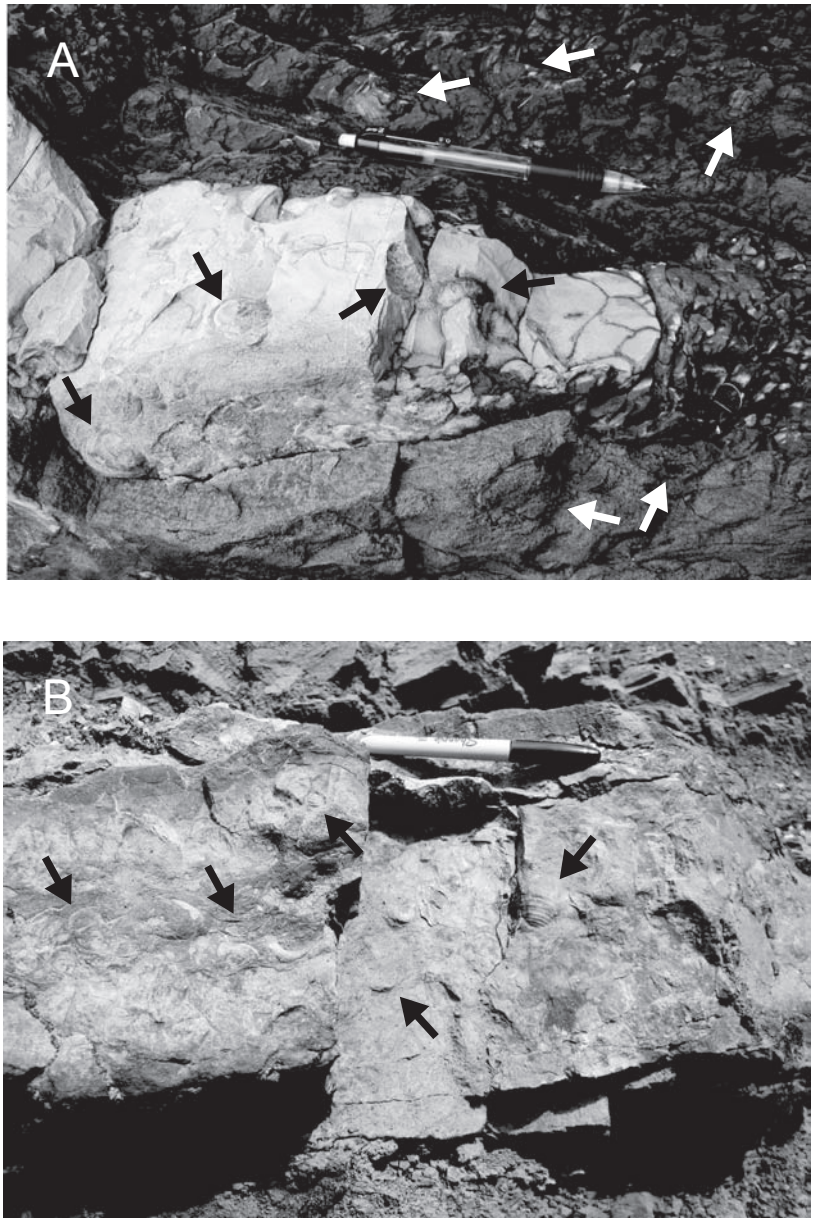

Figure 5. *Buchia* cropping out in micarb (black arrows) and mudstone (white arrows).

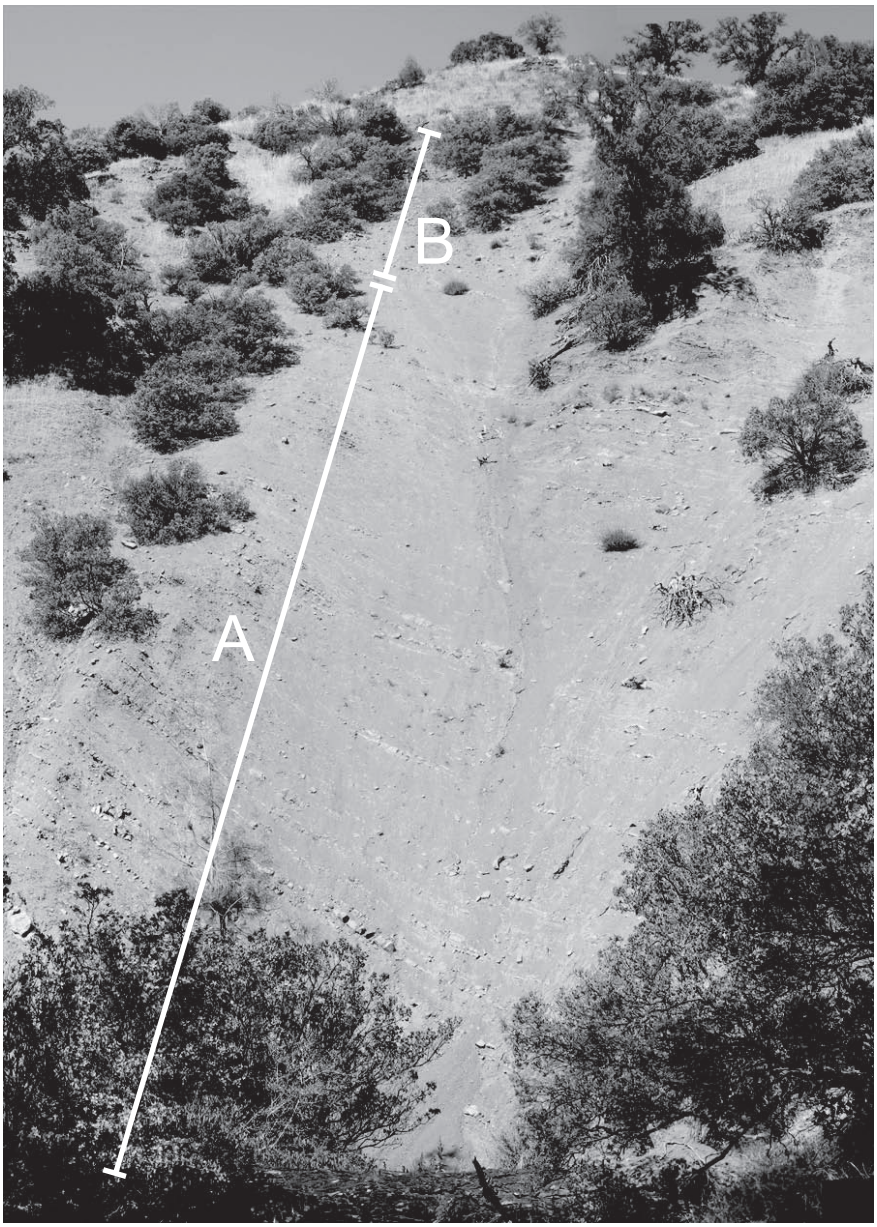

Figure 6. Composite picture of the Bear Creek locality. The entire stratigraphic section totals 80 m. (A) Consists of 58 m of stratigraphic section and includes the 6 horizons of monospecific *Buchia*-rich micarb included in this study. (B) Consists of 32 m of stratigraphic section and includes the 14 micarb horizons that encase a diverse macrofaunal assemblage that includes both endemic and typical seep taxa, such as worm tubes and lucinid bivalves.

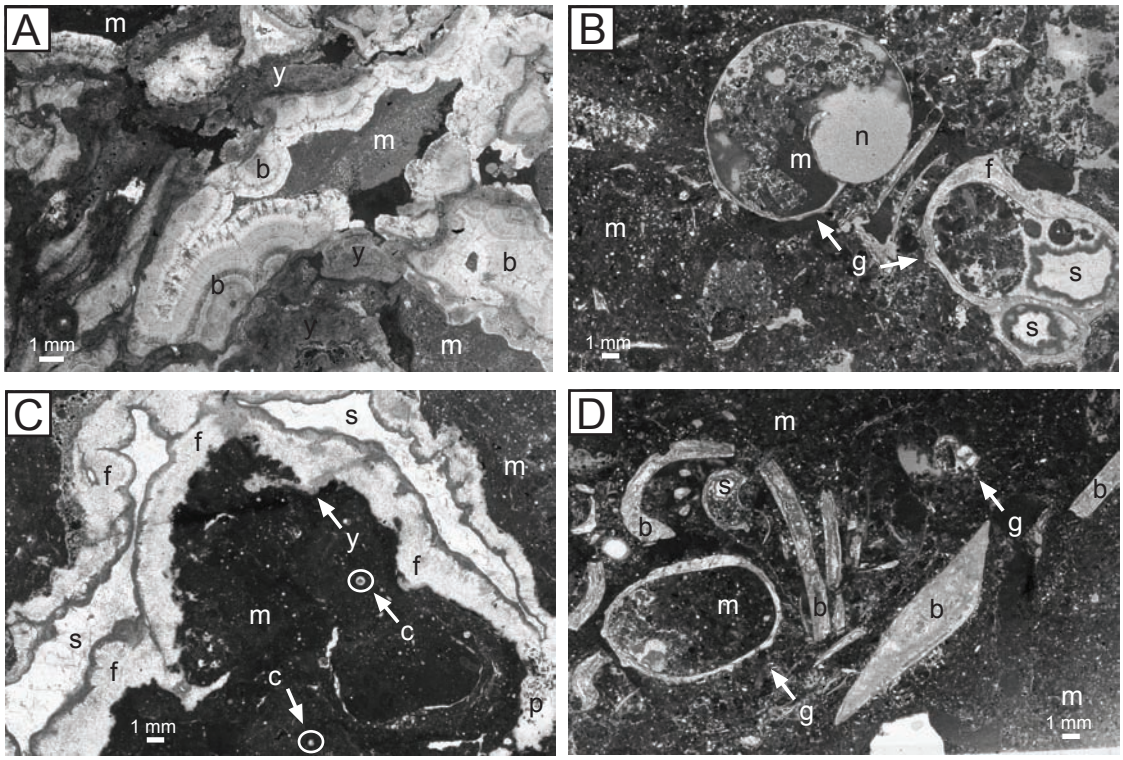

Figure 7. Illustrations of petrographic textures, fabrics, and cements present at Bear Creek. (A) Horizons of botryoidal calcite (b) and anhedral yellow calcite (y) filling vugs and encrusting remnants of detrital-rich micarb (m), BC 3A. (B) Pyrite- and peloid-rich detrital-rich micarb, including pyrite framboids, calcispheres (c), peloids (p), and unidentifiable detritus, encasing gastropods (g, *Paskentana paskentaensis*) incompletely filled with fibrous (f) and sparry (s) calcite and replaced by neomorphosed micrite (n), BC 2A. (C) Large vug filled with yellow calcite, fibrous calcite, and sparry calcite. Peloids rare, but present in sparry calcite. Exceptionatlly large calcispheres circled. BC 1E. (D) Both gastropods (P. paskentaensis) and unidentifiable bivalves surrounded by detrital-rich micrite. Detritus includes peloids, pyrite framboids, and calcispheres, BC 2F.

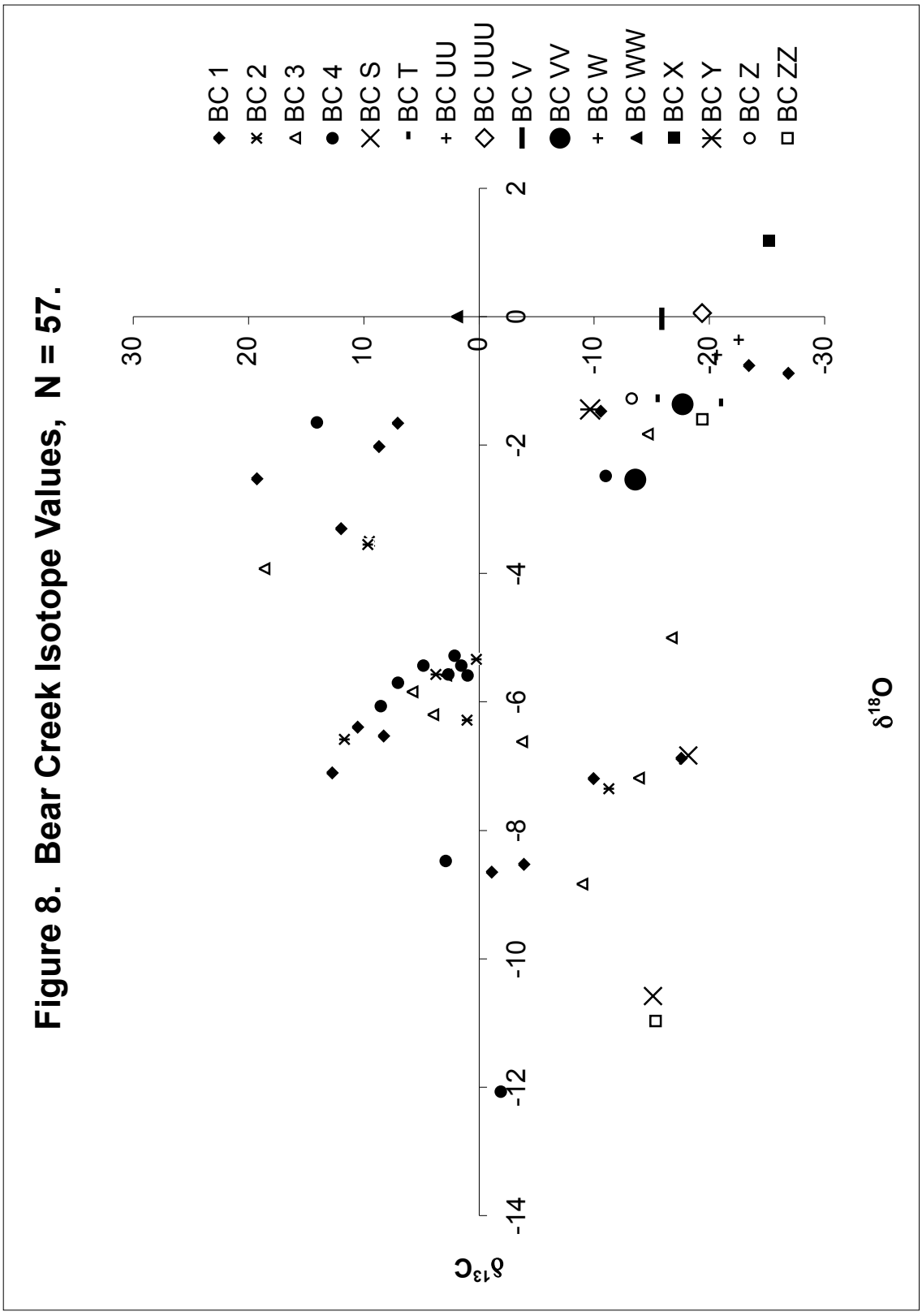
Figure 8. Bear Creek Isotope Values, N = 57.
BC 1
BC 2
BC 3
BC 4
BC S
BC T
BC UU
BC UUU
BC V
BC VV
BC W
BC WW
BC X
BC Y
BC Z
BC ZZ
30
20
10
0
-10
-20
-30
2
0
-2
-4
-6
-8
-10
-12
-14
δ13C
δ18O

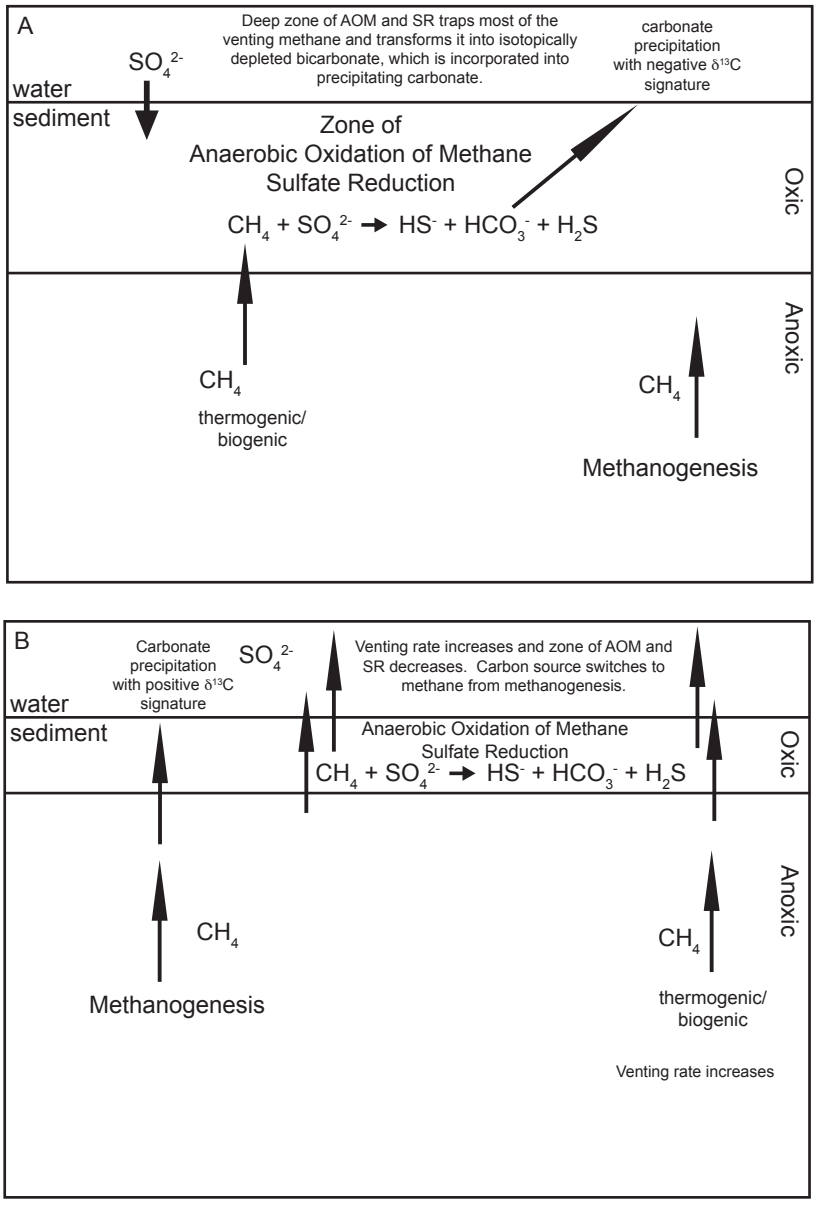

Figure 9. (A) During the anaerobic oxidation of methane (AOM), advecting methane, along with seawater sulfate that diffused down into the sediment column, was trapped in the zone of sulfate reduction (SR), where it was used for energy synthesis by a syntrophic consortium of methane oxidizers and sulfate reducers. This consortium preferentially used ^{12}C over ^{13}C, enriching the pore water in heavy carbon and depleting the newly produced bicarbonate in light carbon. This light signature is incorporated into the carbonate. (B) Depletion of pore water sulfate caused zone of AOM and SR to shallow. If fluid advection rates also increased, the zone of AOM becomes less capable of trapping the higher rates of advecting methane, which resulted in more fluid venting at the seafloor and mixing with seawater. If the isotopically depleted bicarbonate vented and mixed with seawater, the available carbon pool shifted to that produced by methanogenesis, a process that results in the production of isotopically heavy carbon dioxide, which is subsequently incorporated into precipitating carbonate.

Figure 10. Principal Component Analysis of all 8 horizons including convex hulls to illustrate groupings of points. PC1 is a function of the dorsal angle of the crest-line and inflation, while PC2 is a function of just the dorsal angle of the crest-line. The two sandstone horizons have the greatest size varation and due to their location in morphospace, likely had greater inflation and larger dorsal angles of the crest-line.

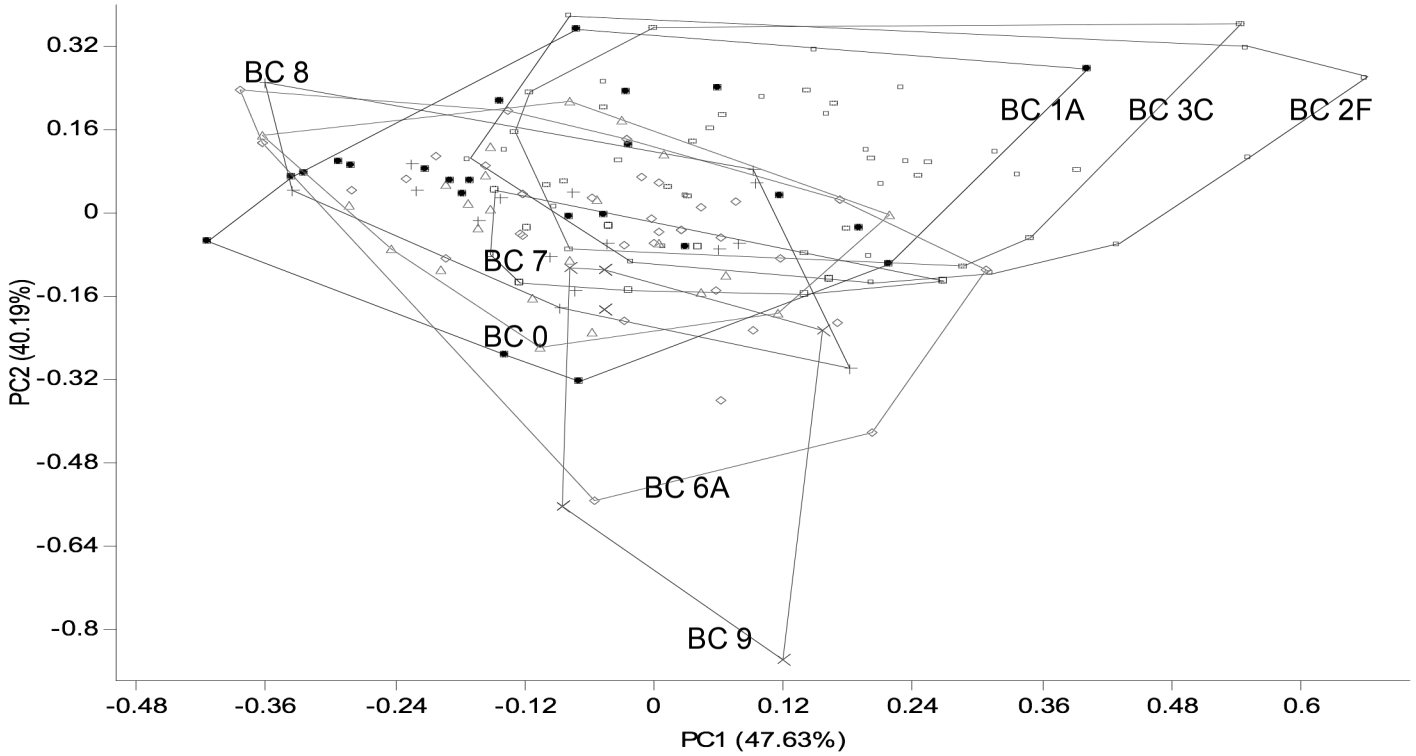

Figure 11. Discriminant analysis generated figures. (A) Horizon pairs BC 2F vs. BC 8. Percent correctly classified = 97.5%. These two horizons can be classified as different morphospecies. (B) Horizon pairs BC 6A vs. BC 8. Percent correctly classified = 77.78%. These two horizons cannot be classified as different morphospecies.

A.

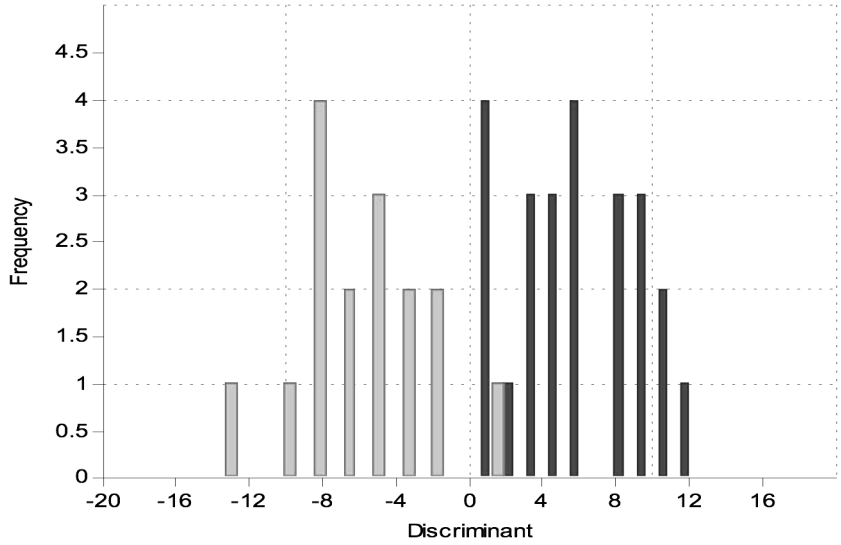

B.

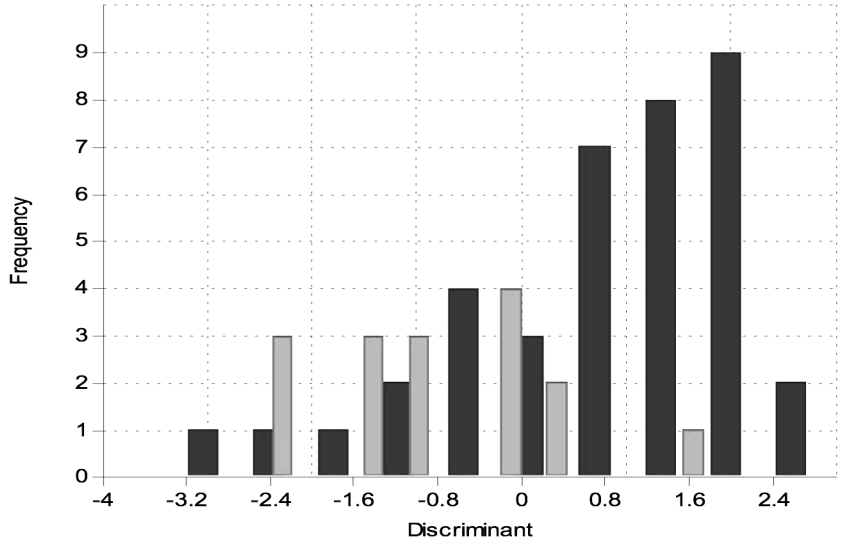

Figure 12. Scatterplot with convex hulls from CVA where location is the *a priori* grouping variable.

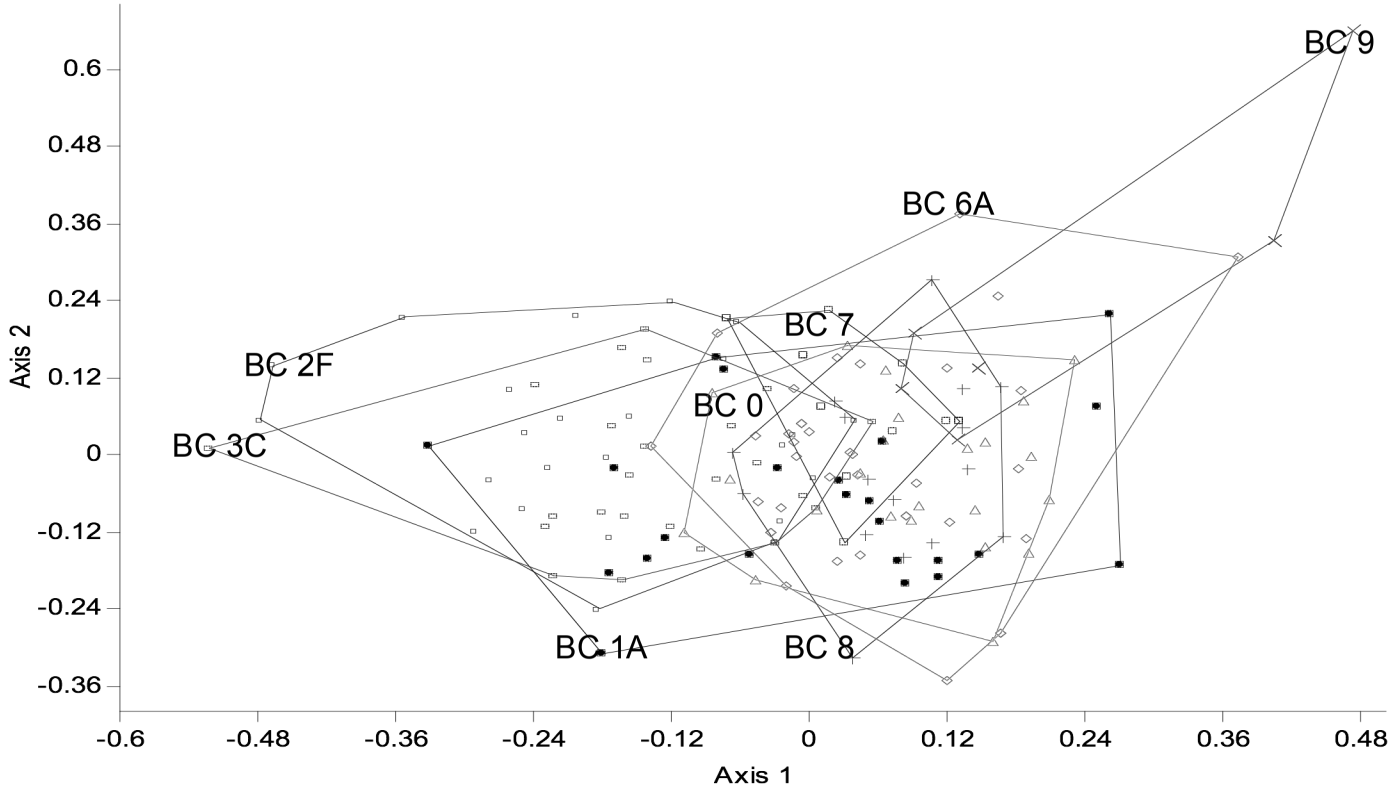

Table 1. Diversity and abundance data for the Bear Creek deposit. Includes all horizons containing *Buchia* as well as the seep horizons. The stratigraphically lowest horizon is BC 2F and the stratigraphically highest horison is ZZ.

	BC 2F	BC 3C	BC 0	BC 1A	BC 2A	BC 6A	BC 7	BC 8	BC 9	R	S	T
Paskentana paskentaensis	0	0	0	0	0	0	0	0	0	0	29	5
Worm tubes	0	0	0	0	0	0	0	0	0	0	5	5
Hokkaidoconcha occidentalis	0	0	0	0	0	0	0	0	0	0	0	0
Retiskenea? kieli	0	0	0	0	0	0	0	0	0	0	0	0
Lithomphalus enderlini	0	0	0	0	0	0	0	0	0	0	0	0
Astarte trapezoidalis	0	0	0	0	0	0	0	0	0	0	1	0
Buchia pacifica	27	24	31	26	10	42	21	19	11	0	0	0
Buchia inflata	0	0	10	0	0	0	0	0	0	0	0	0
Lucinid bivalve	0	0	0	0	0	0	0	0	0	0	1	0
Inoceramid bivalve	0	0	0	0	0	0	0	0	0	0	0	0
Modiola major	0	0	0	0	0	0	0	0	0	0	0	0
Unidentifiable bivalves	0	0	0	0	0	0	0	0	0	0	0	0
Unidentifiable gastropods	0	0	0	0	0	0	0	0	0	0	16	0
Phyllopachyceras	0	0	0	0	0	0	0	0	0	0	0	0

	U	UU	UUU	V	VV	W	WW	X	Y	Z	ZZ	Total
Paskentana paskentaensis	15	3	1	5	0	0	5	0	0	46	0	**109**
Worm tubes	0	0	0	18	1	0	9	0	0	0	0	**38**
Hokkaidoconcha occidentalis	0	0	0	1	0	0	0	0	0	2	0	**3**
Retiskenea? kieli	0	0	0	0	0	0	1	0	0	0	0	**1**
Lithomphalus enderlini	0	0	0	0	0	0	0	0	0	1	0	**1**
Astarte trapezoidalis	0	0	0	0	0	0	1	0	0	1	0	**3**
Buchia pacifica	0	0	0	0	0	0	0	0	0	0	0	**211**
Buchia inflata	0	0	0	0	0	0	0	0	0	0	0	**10**
Lucinid bivalve	0	0	0	0	0	0	0	0	0	0		**1**
Inoceramid bivalve	0	0	0	0	0	0	0	1	0	1	0	**2**
Modiola major	0	0	0	0	0	0	0	4	0	0	1	**5**
Unidentifiable bivalves	0	1	0	1	0	0	2	0	0	2	0	**6**
Unidentifiable gastropods	0	0	0	4	0	0	0	0	0	0	0	**20**
Phyllopachyceras	0	0	0	0	0	0	0	0	0	1	0	**1**
											N =	**411**

Table 2. Carbon and oxgyen data generated for the Bear Creek deposit. Ordered stratigraphically. BC 1 samples are stratigraphically the oldest, while BC 4 samples are stratigraphically the youngest. The BC followed by a letter represent the seep horizons.

Locality / Sample Name	**$\delta^{18}O$**	**$\delta^{13}C$**
BC1EA	-6.8791	-17.58045
BC1EB	-0.882899	-26.82249
BCR1A	-1.470706	-10.58956
BCR1B	-0.758035	-23.41523
BC1D	-3.303774	11.96692
BC1E	-7.191928	-9.934087
BC1F1	-6.532549	8.268595
BC1F2	-6.390294	10.53719
BC1G1	-7.107537	12.72579
BC1G2	-2.523992	19.26914
BC1B	-8.654448	-1.103239
BC1CA	-8.530296	-3.911978
BC1CB	-2.024298	8.67683
BC1CC	-1.660894	7.042707
BC2AA	-5.333099	0.192008
BC2AB	-5.567082	3.697472
BC2AC	-7.345143	-11.27496
BC2DA	-6.282188	1.020627
BC2DB	-3.494579	9.476443
BC2A2	-6.580482	11.65853
BC2A3	-3.540969	9.602332
BC3AA	-6.200929	3.967578
BC3AC	-7.186899	-13.87654
BC3DA	-3.920934	18.6539
BC3DB	-5.57954	2.868702
BC3CA	-1.826237	-14.63246
BC3CB	-5.00178	-16.68807
BC3F	-5.843319	5.777616
BC3B	-6.62214	-3.716767
BC3C	-8.838053	-8.958608
BC4AA	-5.432336	4.780398
BC4AB	-5.429136	1.531006
BC4D	-5.271691	2.110433
BC4EA	-5.693829	7.029908
BC4EB	-12.06333	-1.909815
BC4GA	-6.064696	8.494922

BC4GB	-1.644951	14.06251
BC4HA	-5.581403	0.959503
BC4HB	-5.570808	2.654703
BC4B	-8.471637	2.877139
BC4C	-2.475751	-11.00286
BCS3A	-6.83293	-18.18962
BCS3B	-10.58032	-15.11252
BCTA	-1.311993	-15.52833
BCTB	-1.377676	-21.01967
BCUU1	-0.59133	-20.67328
BCUUU2	0.060674	-19.35867
BCV1	-0.034619	-15.88678
BCVV2A	-1.359651	-17.69657
BCVVSB	-2.532353	-13.58383
BCWA	-0.353485	-22.55901
BCWW	-0.001328	1.921744
BCX2	1.185859	-25.15797
BCY2	-1.439025	-9.679329
BCZ1	-1.26982	-13.29402
BCZZ1A	-1.591543	-19.40417
BCZZ1C	-10.9638	-15.34995

Total number of samples	**$\delta^{13}C$ max**	**$\delta^{13}C$ min**	**$\delta^{13}C$ median**	**$\delta^{18}O$ max**	**min**
57	19.26914	-26.82249	-1.909815	1.185859	-12.06333

Table 3. Principal Component Analysis eigen values and the percent of the variance explained by each principal component axis (PC1-PC6). Only the first three axes are significant.

PC	eigenvalue	% variance
1	0.0374	47.63
2	0.0316	40.19
3	0.0047	5.99
4	0.0037	4.73
5	0.0009	1.09
6	0.0003	0.37

Table 4. If the MANOVA shows significant overall difference between horizons, then the analysis can proceed by pairwise Hotelling's comparisons. This is a post-hoc analysis that indicates which horizon pairs have equality of means. White boxes indicate pairs with different multivariate means, while gray boxes indicate pairs with statistically equal multivariate means.

Horizon	BC 0	BC 1A	BC 6A	BC 7	BC 8	BC 9	BC 2F	BC 3C
BC 0	0	0.0095	0.0048	0.0049	0.9515	0.0006	8.87E-09	1.60E-07
BC 1A		0	0.1185	0.0269	0.0674	0.0026	0.0005	0.0143
BC 6A			0	0.0017	0.0134	1.95E-05	7.14E-09	1.36E-06
BC 7				0	0.001	7.18E-06	1.47E-05	3.09E-05
BC 8					0	0.0193	9.66E-09	1.19E-07
BC 9						0	4.99E-07	3.38E-07
BC 2F							0	0.2729
BC 3C							1	0

Appendix A. Compilation of the basic information for each locality. This includes directions to each locality, the county each is located in, and the USGS quadrangle on which each can be found. The localities are presented in chronological order, from the oldest to the youngest.

Name	Paskenta
GVG or Franciscan	Great Valley Group, Stony Creek Formation
GPS Coordinates	Southeast ¼ of section 25, T. 24N., R. 7W.
Directions	-35 km west of Corning and 5 km northwest of the town of Paskenta
Age	The ubiquitous presence of *Buchia piochii* and *Buchia fischeriana* in both the limestone and the surrounding shale, indicate a Late Jurassic (Tithonian) age for the locality .
County	Tehama County
Quadrangle	USGS Paskenta 7.5 minute quadrangle

Name	Bear Creek
GVG or Franciscan	Great Valley Group, Crack Canyon Formation
GPS Coordinates	UTM 10 551181E 4322704N (NAD83/WGS84)
Directions	-Turn off of HW 20 onto Bear Creek Rd (just before or after, depending on direction you are coming from, HW 16) -Drive past the L turn for Wilbur Springs which is at the Silver Bridge -Drive up to Benchmark 1243 which is just before a small bridge and before the transmission line (visible on the Wilbur Springs topo map) -This bridge and benchmark are right at the opening to Hamilton Canyon -Walk E in creek bed (Oil Seep Creek?) bed towards Hamilton Canyon -Carbonate concretions/nodules in creek bed -After first bend in creek, cliff of shale (turbidites) had carbonate in it, including fossils -We continued into the canyon, up the creek and on the N wall found evidence of carbonate in shale (turbidites) and clams, and maybe gastropods -Apparently tube worms are present, but we didn't see any on this trip -The main deposit is an incredibly steep cliff that takes rock-climbing equipment to scale -All that we collected came from the base of this cliff or in the creek/riverbed towards the road
Age	Early Cretaceous, Valanginian, based on position of highest buchiid
County	Colusa County
Quadrangle	USGS Wilbur Springs 7.5 minute quadrangle

Name	Rocky Creek
GVG or Franciscan	Great Valley Group
GPS Coordinates	UTM 10 545211E 4305768N (WGS84/NAD83)
Directions	-HWY 29 North. -R onto Morgan Valley Rd. -L onto Rocky Creek Rd.
Age	Early Cretaceous, Valanginian
County	Lake County
Quadrangle	USGS Wilson Valley 7.5 minute quadrangle

Name	Little Indian Valley
GVG or Franciscan	Franciscan
GPS Coordinates	My locality and what I have officially named Little Indian Valley
Directions	-Get to HW 20. -Turn off onto Walker Ridge Road. -Follow this road (do not take any of the private roads, just continue to follow the main road) until you reach the dam. -It is ~20-30 minutes down to the dam. -Cross the dam, and continue up the dirt road on the other side and drive in as far as you can get. -The dirt road is in poor-moderate condition, so beware. -Definitely need 4WD in there. -There is a gate along this road that has to be opened by someone at the dam with the code.
Age	Late Jurassic-Early Cretaceous
County	Lake County
Quadrangle	USGS Benmore Canyon 7.5 minute quadrangle

Name	Wilbur Springs
GVG or Franciscan	Great Valley Group, Stony Creek Formation
GPS Coordinates	1. Not specific enough: East of southwest corner of section 28, T. 14N., R. 5W (KAC) 2. Correct Coordinates: UTM 10S 0550449E 4320227N (WGS84/NAD83)
Directions	-29N to -53 N -R onto HW 20 -turn off is ~625 ft before the R turn off for HW 16 -take a L onto Bear Valley Road and follow it for ~4 miles -turn L to cross Silver Bridge and drive down to the Wilbur Springs Resort -once there go in and talk to them and let them know you are there, they will give you a parking pass and have you fill out a release from injury form
Age	Lower Cretaceous (Hauterivian)
County	Colusa
Quadrangle	USGS Wilbur Springs 7.5 minute quadrangle

Name	Wide Awake Mine
GVG or Franciscan	Great Valley Group
GPS Coordinates	UTM 10 549491E 4320049N (WGS84/NAD83)
Directions	-29N to -53 N -R onto HW 20 -turn off is ~625 ft before the R turn off for HW 16 -take a L onto Bear Valley Road and follow it for ~4 miles -turn L to cross Silver Bridge and drive down to the Wilbur Springs Resort -once there go in and talk to them and let them know you are there, they will give you a parking pass and have you fill out a release from injury form -Note: Call in advance and let them know that you are coming
Age	Lower Cretaceous (Hauterivian)
County	Colusa County
Quadrangle	USGS Wilbur Springs 7.5 minute quadrangle

Name	Rice Valley
GVG or Franciscan	In Great Valley Group outlier within Franciscan Complex
GPS Coordinates	1. UTM, 10 0511326 4355713 → these will get you to the valley, but not to the limestone, the limestone still needs to be found 2. 39° 20' 23"N, 122° 51' 15"W (WGS84/NAD83) / UTM 10 512567E 4354487N (WGS84/NAD83) → these coordinates are taken from KAC notes where she mentions "other USGS locality data describe white limestones ("John Suppe's Fossil Rock") in northwestern part of Potato Hill Quad," and gives these coordinates.
Directions	-HW 29 to -HW 20, turn R on HW 20 -Turn L on Main St. -Turn L on Elk Mtn. Rd. (M1 according to Mendocino National Forest Roads) -Turn R onto Bear Creek Rd (M10), this is a dirt road that is in pretty good condition -Turn L onto Rice Creek Rd (M3), not marked as Rice Creek Rd. but instead as "NYE Campground" and M3 sign (must cross at least one moderately sized stream, ok for an SUV to cross, we stopped before the second stream and waded across it).
Age	Early Cretaceous (Hauterivian)→ based on *Peregrinella whitneyi*
County	Lake County
Quadrangle	USGS Potato Hill 7.5 minute quadrangle

Name	Cold Fork of Cottonwood Creek
GVG or Franciscan	Great Valley Group, Lodoga Formation
GPS Coordinates	1. UTM 10 526921E 4446205N (WGS84/NAD83)
Directions	1. 20 km west of Red Bluff, 1 mile up Cold Fork of Cottonwood Creek from Pettyjohn ranch house, northeast of Stevenson Peak and due west of Wilcox Flat 2. Take Hwy 5 north Take 36 west until it ends on Main St in Red Bluff Turn right onto Main St. Turn left onto Walnut St. Go all the way down Walnut St. until it curves around to the left and becomes Wilder Rd. Take a right onto Reeds Creek Rd. Follow Reeds Creek Rd (quite a ways) until you come to the intersection with Pope Dr. on your left, Vestal Rd. directly in front of you, and Cannon Rd on your right. Take a left onto Pope Dr. Pope Dr. twists and turns for a while eventually crossing Cold Fork River/Creek?? You come to an intersection with Pope Dr. turning into Pettyjohn Rd. and to your right you have Weemasoul Rd. If you want to get to Pettyjohn Place, turn right onto Weemasoul Rd. If you want to get to the Cold Fork of Cottonwood Creek outcrop, continue on Pettyjohn Rd for a short ways until you come to the following coordinates: UTM 10 526921E 4446205N (WGS84/NAD83)
Age	Early Cretaceous (Albian-Aptian), based on ammonites
County	Tehama County
Quadrangle	USGS Colyear Springs 7.5 minute quadrangle

Name	Harrington Flat Road
GVG or Franciscan	Great Valley Group
GPS Coordinates	UTM 10 522413E 4301428N (WGS84/NAD83)
Directions	-N on HW 29 to -N on HW 175 -Left on Harrington Flat Road (if you have passed the town of Loch Lomand, you have gone too far) -Continue past Sulphur Creek Road which will be on your left -The locality will be just a bit past Sulphur Creek Road on the right
Age	Upper Cretaceous (Campanian), pers. comm. Robert McLaughlin
County	Lake County
Quadrangle	Whispering Pines 7.5 minute quadrangle

Name	Romero Creek
GVG or Franciscan	Great Valley Group
GPS Coordinates	1. Locality 1: UTM 0672566E 4110291N WGS 84/NAD 83 └►no fossils found at this locality (2) 2. Locality 2: 37° 07’ 24”N, 121° 03’ 20”W (UTM 10 0672738E 4110324N (WGS84/NAD83))
Directions	-HW 101 S -HW 152 E -HW 33 N -L onto McCabe Rd. -Follow McCabe Rd. until you reach the aqueduct (which is right at the first big bend in the road), but follow the GPS coordinates to find it precisely.
Age	Late Campanian
County	Merced County
Quadrangle	USGS San Luis Dam Quadrangle 7.5 minute quadrangle

Name	Guenoc Ranch
GVG or Franciscan	Great Valley Group
GPS Coordinates	UTM 10 542263E 4284737N (NAD83/WGS84)
Directions	From San Francisco Bay Area: -Take I-80 E -Merge onto Marine World Pkwy/ CA-37 W toward Napa - 2.5 miles -Turn slight right onto Sonoma Blvd/ CA-29 N -Continue to follow CA-29 N. - 25.9 miles -Turn right onto Rutherford Rd / CA-128 -Continue to follow CA-128 - 2.9 miles -Turn left onto Sage Canyon Rd / CA-128 - 3.8 miles -Turn left onto Chiles Pope Valley Rd - 12.3 miles -Chiles Pope Valley Rd becomes Pope Valley Rd - 3.6 miles -Pope Valley Rd becomes Butts Canyon Rd - 8.9 miles -Arrive at 21000 Butts Canyon Rd
Age	Campanian-Maastrichtian
County	Lake County
Quadrangle	USGS Jericho Valley 7.5 minute quadrangle

Appendix B. Cuumulative isotope values generated for the 10 hydrocarbon seep localities found during the course of this study. N = 146.

Locality and Sample Name	$\delta^{13}C$ (‰)	$\delta^{18}O$ (‰)
Bear Creek (N = 57)		
BC1EA	-17.580	-6.879
BC1EB	-26.822	-0.883
BC3CA	-14.632	-1.826
BC3CB	-16.688	-5.002
BCR1A	-10.590	-1.471
BCR1B	-23.415	-0.758
BCS3A	-18.190	-6.833
BCS3B	-15.113	-10.580
BCTA	-15.528	-1.312
BCTB	-21.020	-1.378
BCUU1	-20.673	-0.591
BCUUU2	-19.359	0.061
BCV1	-15.887	-0.035
BCVV2A	-17.697	-1.360
BCVVSB	-13.584	-2.532
BCWA	-22.559	-0.353
BCWW	1.922	-0.001
BCX2	-25.158	1.186
BCY2	-9.679	-1.439
BCZ1	-13.294	-1.270
BCZZ1A	-19.404	-1.592
BCZZ1C	-15.350	-10.964
BC2A2	11.659	-6.580
BC2A3	9.602	-3.541
BC1D	11.967	-3.304
BC1E	-9.934	-7.192
BC1F1	8.269	-6.533
BC1F2	10.537	-6.390
BC1G1	12.726	-7.108
BC1G2	19.269	-2.524

BC2AA	0.192	-5.333
BC2AB	3.697	-5.567
BC2AC	-11.275	-7.345
BC2DA	1.021	-6.282
BC2DB	9.476	-3.495
BC3AA	3.968	-6.201
BC3AC	-13.877	-7.187
BC3DA	18.654	-3.921
BC3DB	2.869	-5.580
BC3F	5.778	-5.843
BC4AA	4.780	-5.432
BC4AB	1.531	-5.429
BC4D	2.110	-5.272
BC4EA	7.030	-5.694
BC4EB	-1.910	-12.063
BC4GA	8.495	-6.065
BC4GB	14.063	-1.645
BC4HA	0.960	-5.581
BC4HB	2.655	-5.571
BC1B	-1.103	-8.654
BC1CA	-3.912	-8.530
BC1CB	8.677	-2.024
BC1CC	7.043	-1.661
BC3B	-3.717	-6.622
BC3C	-8.959	-8.838
BC4B	2.877	-8.472
BC4C	-11.003	-2.476

Rocky Creek (N = 11)		
RC4AA	-9.204	-1.668
RC4AB	-9.209	-0.994
RC4AC	-10.924	-0.162
RC3AA	-13.549	-1.637
RC3AB	-12.475	0.259
RC2BA	-13.255	-0.126
RC2BB	-9.314	-0.288
RC4B	-12.253	-2.156
RC17A	-14.996	-0.040
RC30D	-18.045	-2.031
RC43B	-19.403	-0.259

Little Indian Valley (N = 3)		
LIV3BA	-17.115	-7.159
LIV3BB	-23.397	-9.074
LIV2AA	-18.417	-2.730

Wilbur Springs (N = 9)		
WS10CA	-20.675	1.543
WS10CB	-20.769	0.595
WS10CC	-22.893	1.427
WS3BA	-22.380	1.118
WS3BB	-22.317	1.353
WS2AA	-19.241	0.352
WS2AB	-18.423	-1.719
WS3CA	-21.214	0.327
WS3CB	-19.205	0.353

Wide Awake Mine (N = 6)		
WAM2AA	-20.201	0.545
WAM2AC	-21.811	-1.974
WAM3CA	-21.313	-0.719
WAM3CB	-21.349	1.678
WAM2CB	-22.274	-2.747
WAM2CB	-20.838	0.981

Rice Valley (N = 4)		
RV2BA	-21.541	0.610
RV2BB	-12.945	3.214
RV2CA	-20.707	1.120
RV2CB	-17.607	1.395

Cold Fork of Cottonwood Creek (N = 8)		
CFCC3CC	-21.688	-4.208
CFCC3CD	-23.753	-7.937
CFCC3CE	-20.515	-7.052
CFCC3CA	-21.927	-7.435
CFCC3CB	-22.298	-7.335
CFCC6AA	-25.439	-11.241
CFCC8BA	-25.386	-2.699
CFCC8EA	-24.623	-3.907

Harrington Flat Road (N = 13)		
HFR10BB	-11.790	-2.687
HFR12CA	-5.669	-3.534
HFR12CB	-7.107	-4.229
HFR12CC	-24.402	-2.167
HFR4AA	-24.508	-1.680
HFR2AB	-28.627	-5.435
HFR4	-19.845	-1.064
HFR7	-23.700	-1.799
HFR10	-15.871	-2.709
HFR11	-20.086	-4.143
HFR12	-23.272	-1.499
HFR13	-20.748	-3.792
HFR18	-11.332	-2.620

Romero Creek (N = 3)		
ROMCR1BA	-19.829	-3.159
ROMCR1BB	-20.341	-4.023
ROMCR2DA	-16.683	-3.970

Guenoc Ranch (N = 32)		
a	-17.730	-1.940
b	-19.470	-2.410
c	-24.480	-4.180
d	-18.720	-2.530
d*	-19.400	-2.500
e	-15.160	-5.390
f	-20.360	-2.220
g	-16.960	-2.960
h	-16.160	-4.450
i	-3.410	0.040
j	-21.990	-5.030
k	-21.030	-5.050
l	-22.140	-5.570
m	-17.750	0.480
m*	-17.590	0.950
n	-19.340	-3.620
o	-10.800	-2.290
p	-19.510	-3.840
q	-6.260	-1.720
r	-15.780	-3.520

s	-14.320	-5.760
t	-9.390	-3.360
u	-17.340	-10.420
v	-16.790	-9.450
w	-17.910	-4.950
x	-19.730	-5.380
y	-21.720	-2.590
z	-12.090	-7.420
aa	-15.130	-3.350
bb	-17.480	-2.640
cc	-16.790	-0.040
dd	-14.560	-0.530

Appendix C. Illustrations of petrographic textures, fabrics, and cements of the Franciscan and GVG hydrocarbon seeps, including both early and late diagenetic stages. Each figure was taken in plane polarized light.

Key

Early Phase Events

- detrital-rich micrite (m)
- peloids (p)
- pyrite framboids (pf)
- pyrite (p)
- calcispheres (c)
- *Peregrinella whitneyi* (pw)
- Inoceramid bivalve (i)
- gastropods (g)
- bivalve shell (bi)
- microfossils (mf)
- plant fragments (pl)
- pyrite encrusted corrosion horizons (CE1)
- worm tube fossils (w)
- anhedral yellow calcite (y)
- fibrous calcite (f, fibrous habit)
- botryoidal calcite (b)
- dentate calcite (d)
- clotted microbial fabrics (mf)
- silt-clay fill (sc)

Late Stage Events

- fracturing event, late stage veins (v)
- sparry calcite (s)

- neomorphosed micrite (n)
- dolomite (d)

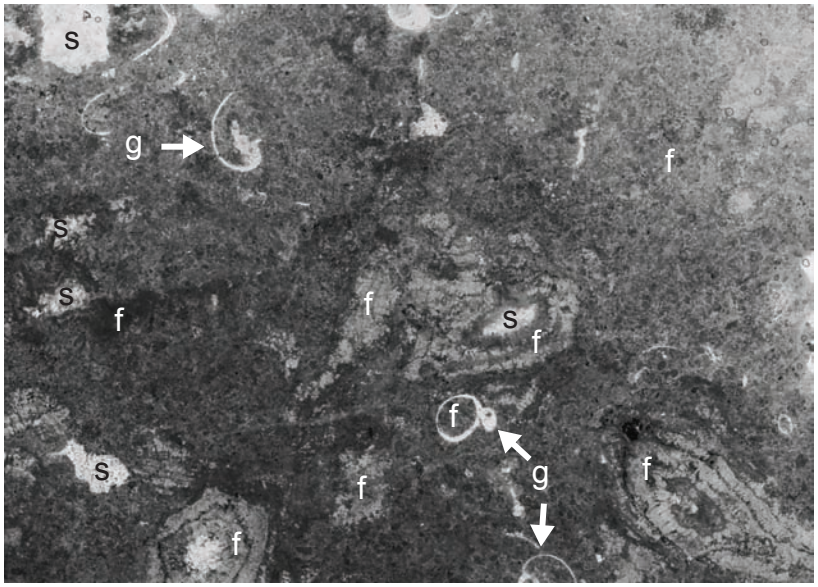

Figure 1. CFCC 12A 2. Cold Fork of Cottonwood Creek gastropods (g) surrounded by fibrous (f) calcite and exhibiting undulating extinction. Small vugs villed with fibrous and sparry (s) calcite present as well.

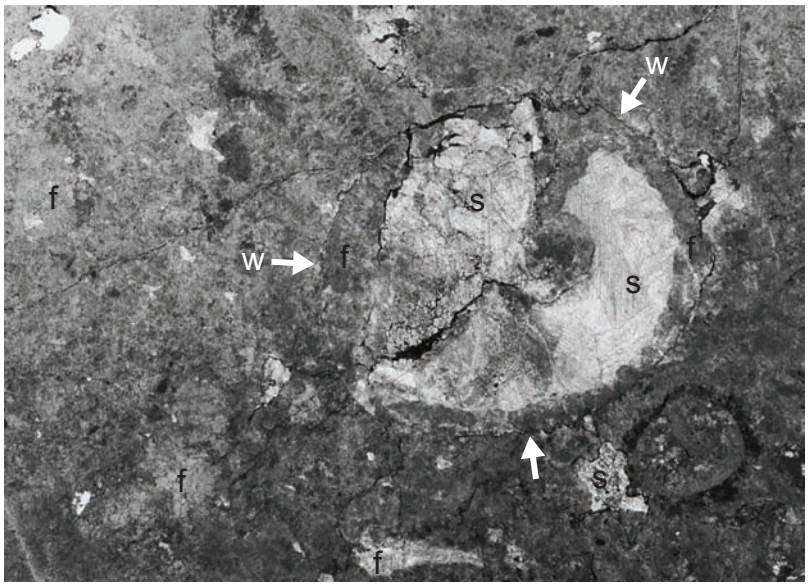

Figure 2. CFCC 27 A1. Cold Fork of Cottonwood Creek. Petrography and paragenetic associations of fossil worm tube (w) structures. Tubes delineated by thin dark outline of pyrite and lined by fibrous (f) cement, followed by sparry (s) calcite fill.

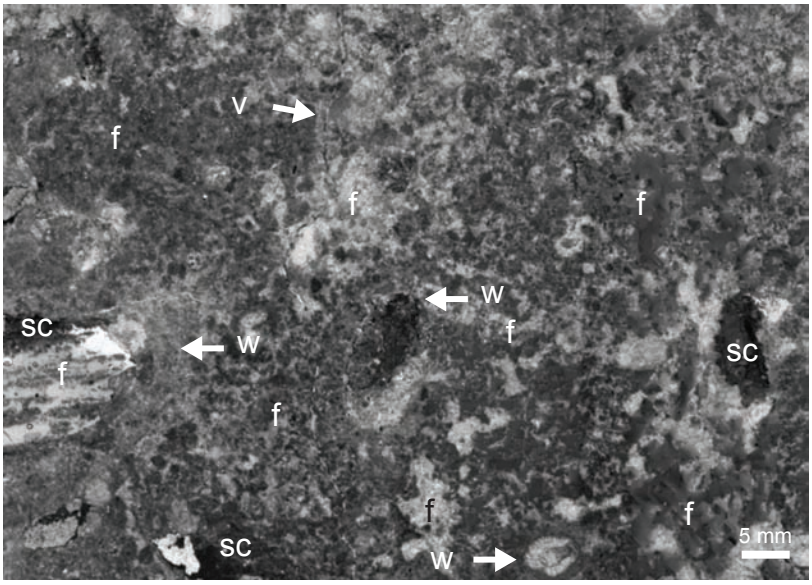

Figure 3. CFCC 3E. Cold Fork of Cottonwood Creek. Petrography and paragenetic associations of fossil worm tube structures surrounded and filled by fibrous (f) calcite with some silt-clay fill (sc). Cross cut by late stage veins (v).

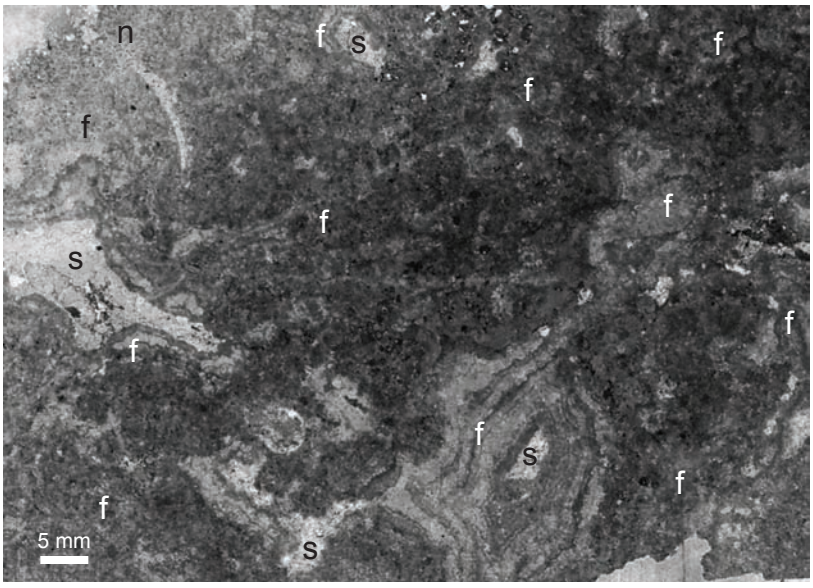

Figure 4. CFCC 8B. Cold Fork of Cottonwood Creek fibrous (f) calcite lining small vugs that were subsequently filled with sparry (s) calcite. Some neomorphosed micrite (m) present as well.

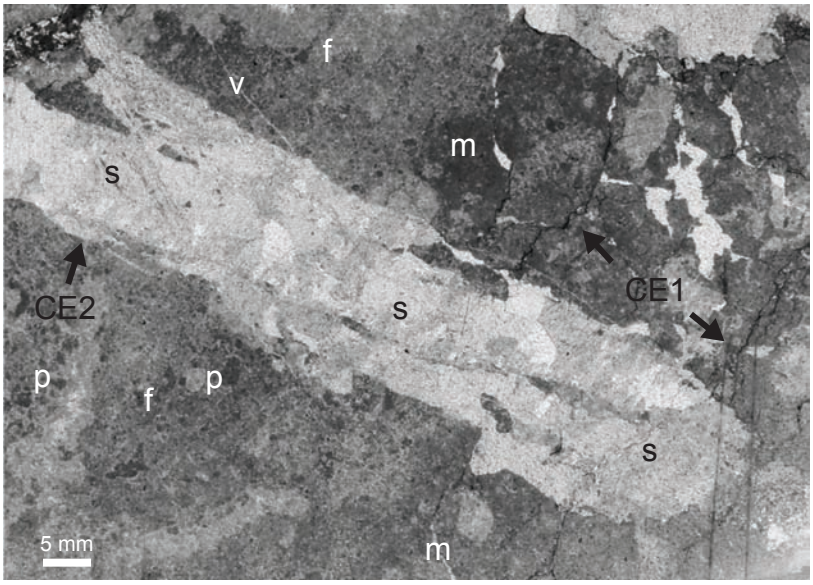

Figure 5. CFCC 6A. Cold Fork of Cottonwood Creek. Late stage calcite spar (s) filling vug created by a nonferroan corrosion event (CE2). Evidence of earlier corrosion event (CE1) present and coated in pyrite. Peloids (p) present and surrounded by fibrous (f) calcite and detrital-rich micarb (m).

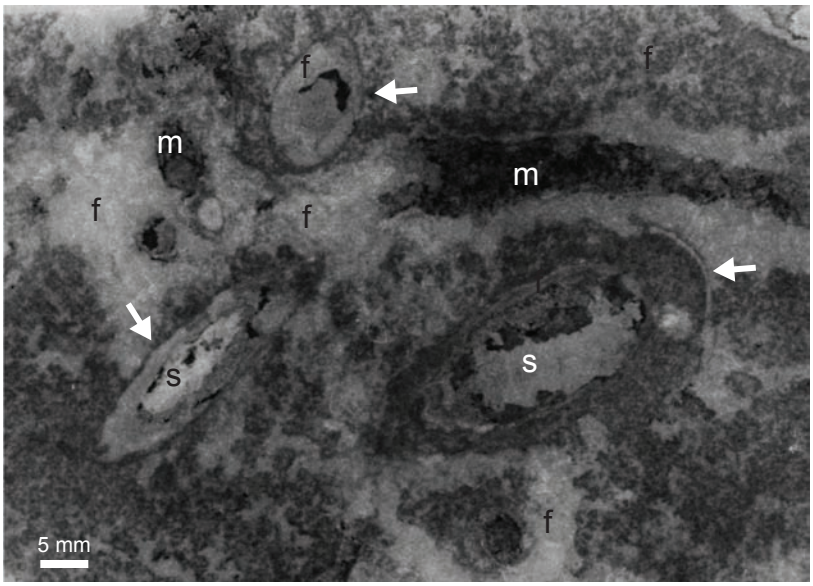

Figure 6. CFCC 7A. Cold Fork of Cottonwood Creek. Petrography and paragenetic associations of fossil worm tube structures. Tubes delineated by thin dark outlines of pyrite (white arrows) and lined by fibrous (f) calcite cement, followed by sparry (s) calcite fill.

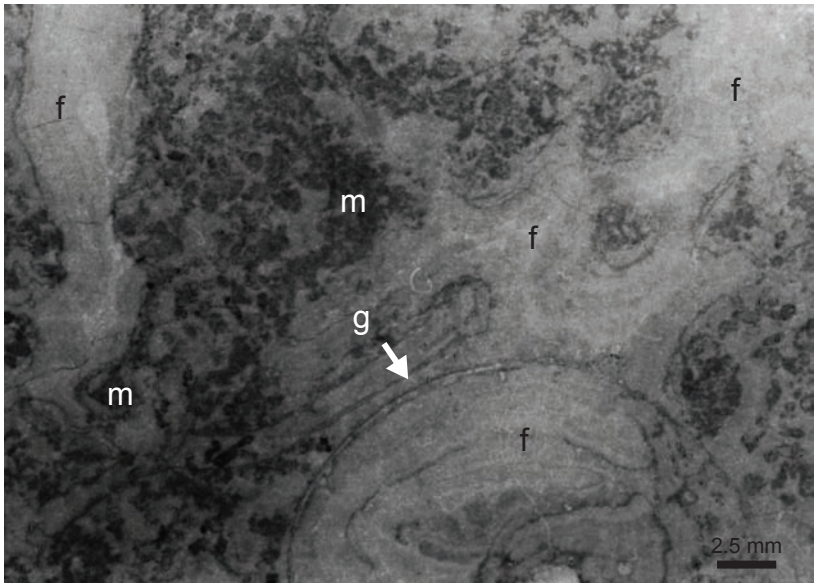

Figure 7. CFCC 3A. Cold Fork of Cottonwood Creek. Gastropod (g) with shell replaced by sparry calcite (s) and both filled and surrounded by fibrous calcite (f). Small amounts of detrital-rich micarb (m) present, surrounded by fibrous calcite.

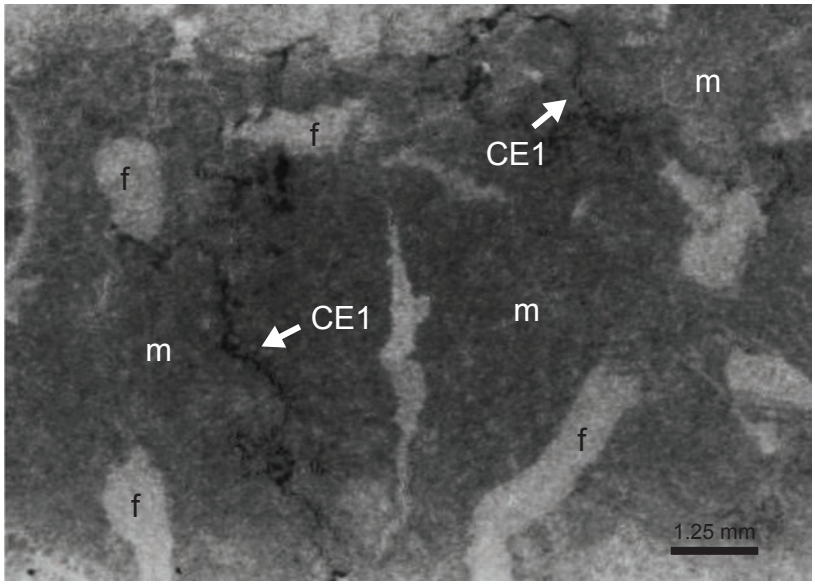

Figure 8. CFCC 6B. Cold Fork of Cottonwood Creek. Detrital-rich micarb (m) dominates, with small vugs filled with fibrous calcite (f) present. Evidence of pyrite coated corrosion surfaces (CE1) are present as well.

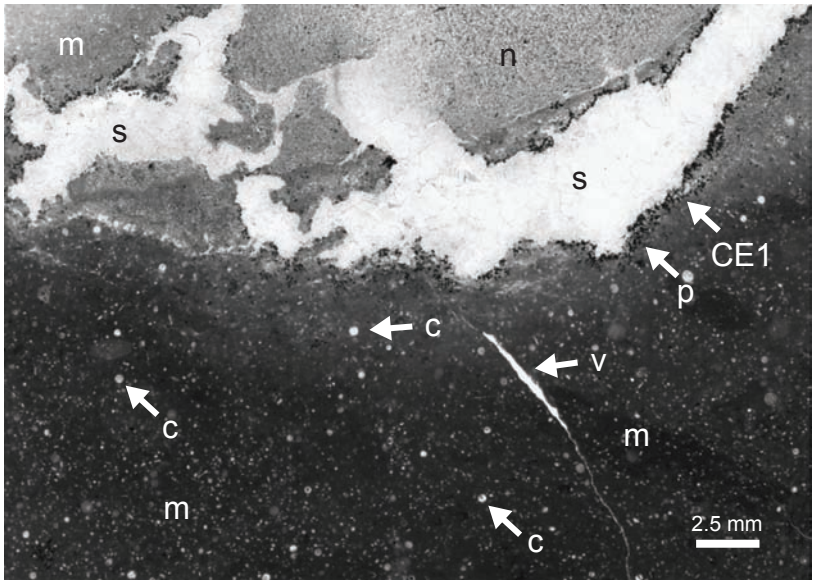

Figure 9. HFR 2B. Harrington Flat Road. Detrital-rich micarb (m) dominates and is cross cut by a corrosion event (CE1) lined incompletely with pyrite (p), creating vugs that were later filled in with sparry calcite (s). Neomorphosed micarb (n) is in the uppr right and calcispheres (c) are prevalent throughout.

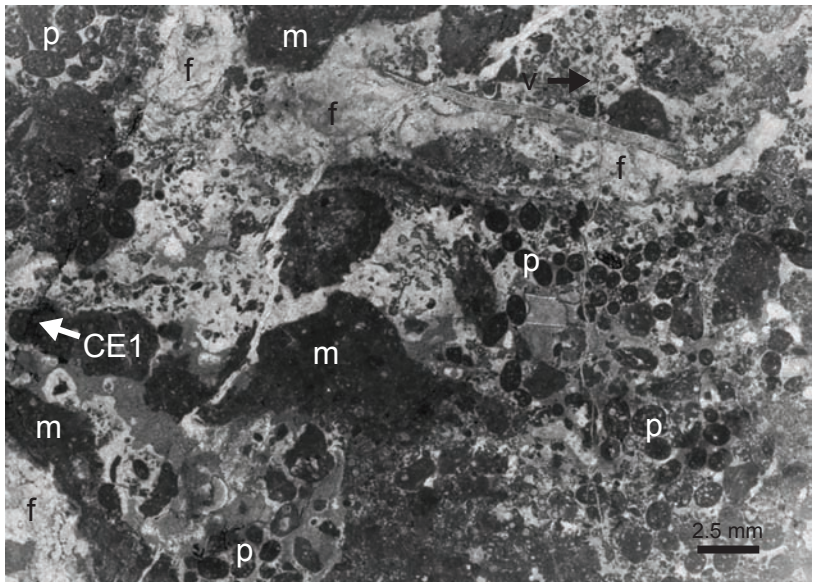

Figure 10. HFR 13B. Harrington Flat Road. Peloids (p) dominate and are surrounded by fibrous calcite (f) and detrital-rich micarb (m). Evidence of a corrosion event (CE1) and cross-cutting late stage veins (v) are also present.

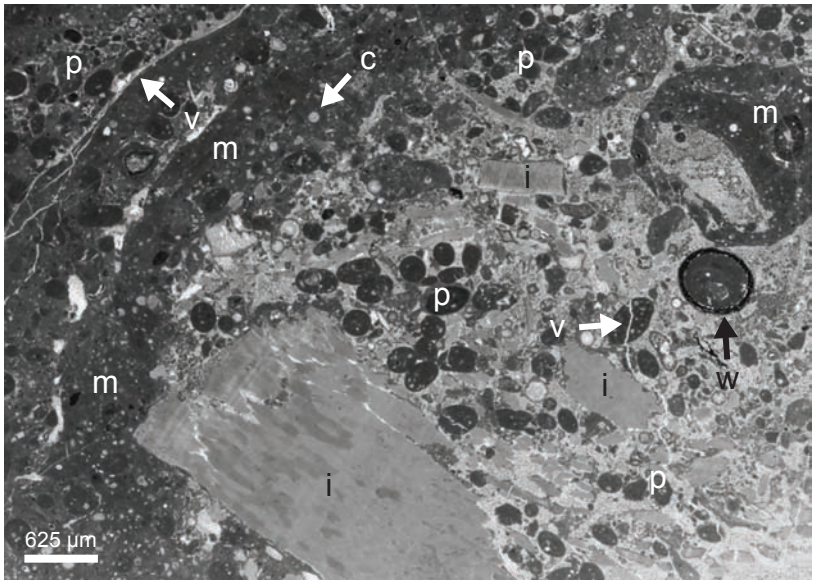

Figure 11. HFR 13C WT. Harrington Flat Road. Large fragments of inoceramid shell (i) surrounded by detrital-rich micarb (m), fibrous calcite (f), peloids (p), and calcispheres (c). Late stage veins (v) present, some of which cross-cut peloids.

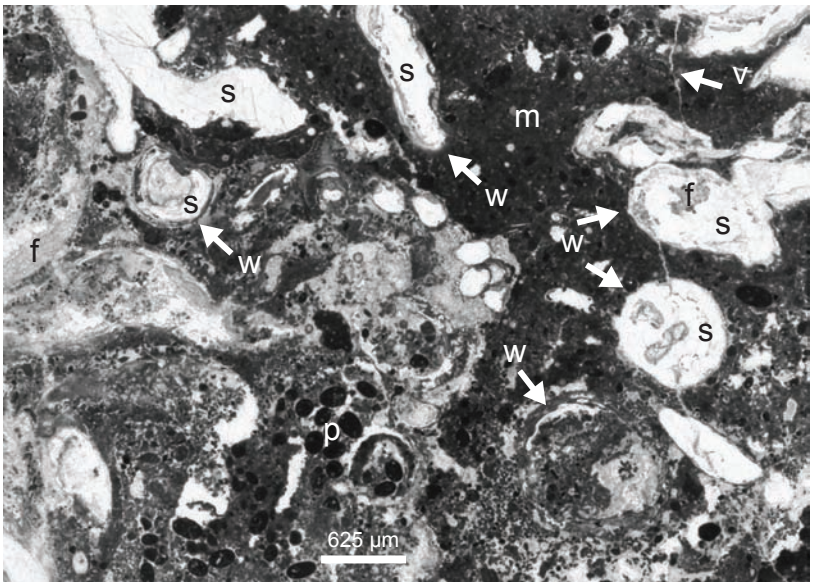

Figure 12. HFR 18A WT. Harrington Flat Road. Cross-sectional and longitudinal views of worm tubes (w), some of which are filled by fibrous calcite (f) and sparry calcite. Peloids (p) are also present, and detrital-rich micarb (m) surrounds it all.

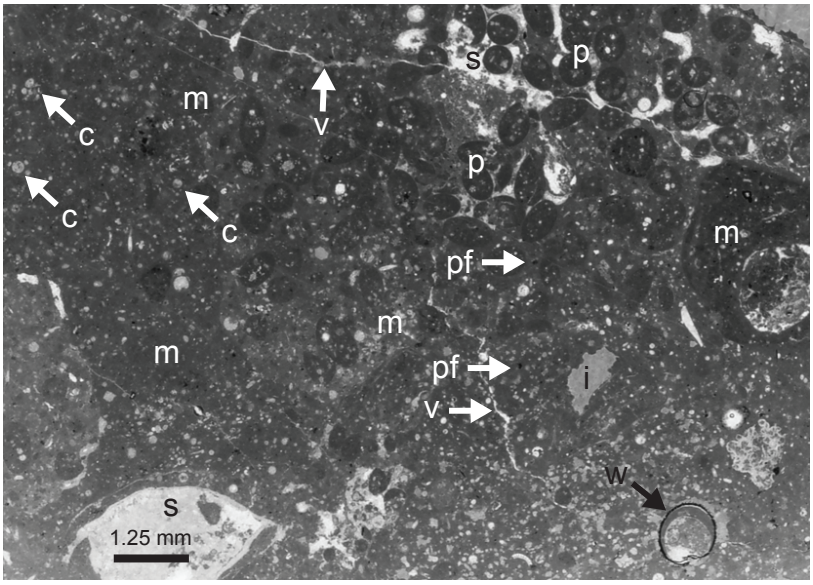

Figure 13. HFR 13 D WT. Harrington Flat Road. Detrital-rich micarb (m) with round to elliptical peloids and numerous calcispheres (c) and pyrite framboids (pf). Fragments of inoceramid (i) bivalve shell also present. Late-stage veins (v) also present and filled with sparry calcite (s), cutting through some peloids in upper right of field of view. Worm tube cross-section in lower right corner of field of view, with tube wall lined with pyrite.

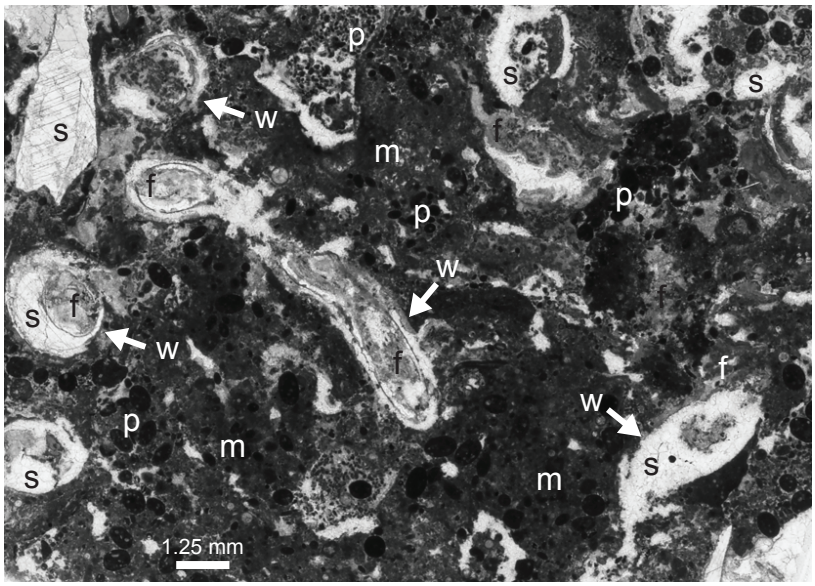

Figure 14. HFR 13 A WT. Harrington Flat Road. Cross-sectional and longitudinal views of worm tubes (w), some of which are filled by fibrous calcite (f) and sparry calcite. Peloids (p) are also present, and detrital-rich micarb (m) surrounds it all.

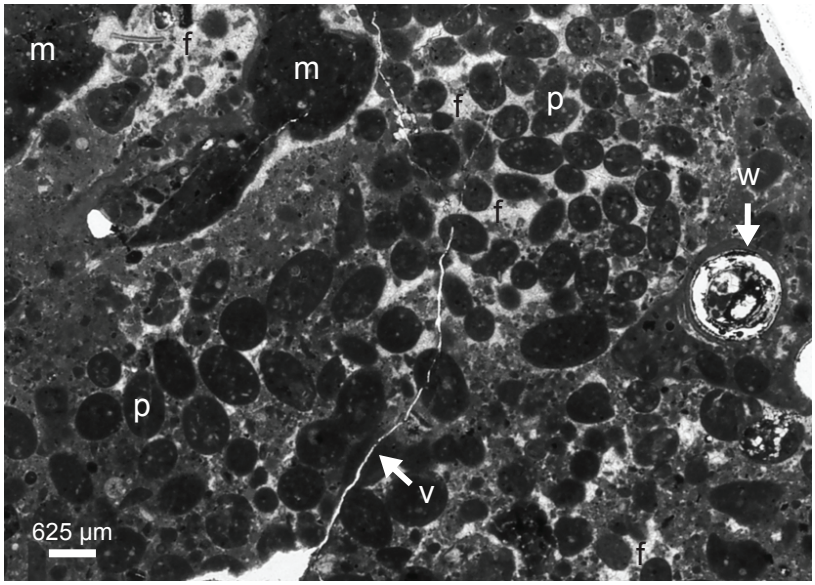

Figure 15. HFR 4 WT. Harrington Flat Road. Round to elliptical peloids surrounded by detrital-rich micarb (m) and fibrous (f) calcite. Calcispheres (c) and a single cross-sectional view of a worm tube (w) with the tube wall replaced incompletely by pyrite. Late stage vein (v) cuts through center of thin section.

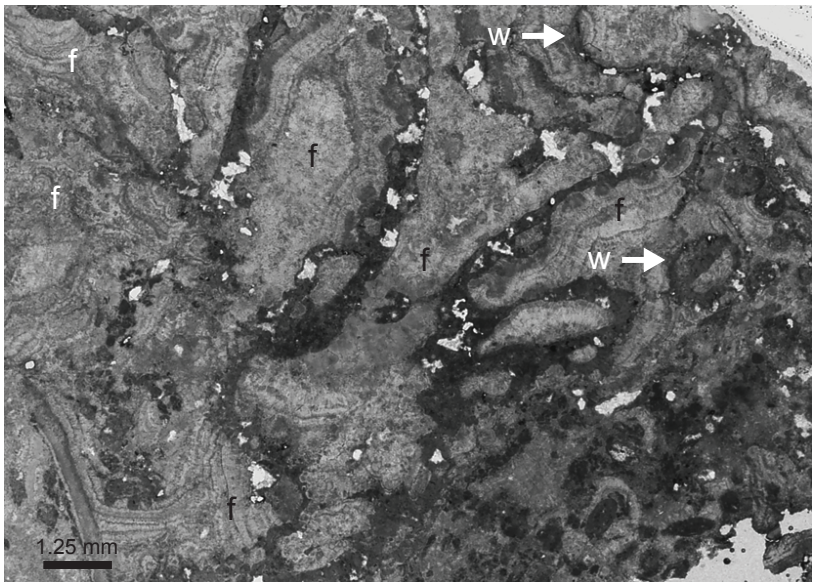

Figure 16. HFR A WT. Harrington Flat Road. Repeating horizons of fibrous (f) calcite that undulates under cross-polars. Fragments of worm tube (w) walls incompletely lined with pyrite.

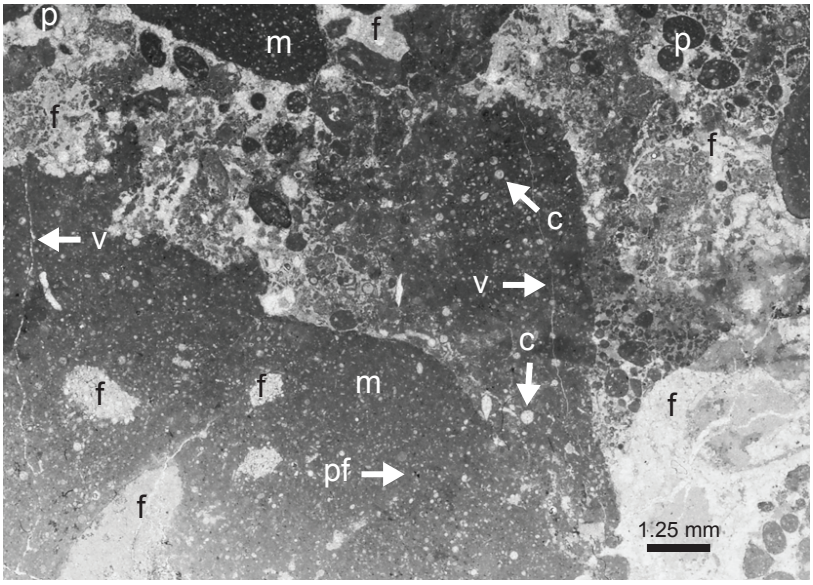

Figure 17. HFR 13A. Harrington Flat Road. Detrital-rich micarb (m) dominates, with peloids (p), calcispheres (c), and pyrite framboids (pf) present. Fibrous (f) calcite fills in open space around peloids and in vugs. Late stage veins (v) are also present and are filled with sparry calcite.

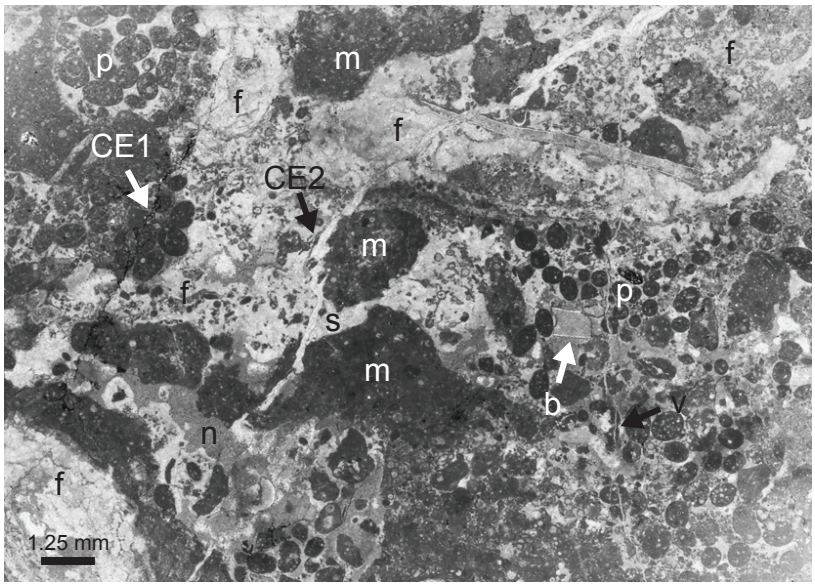

Figure 18. HFR 13B. Harrington Flat Road. Peloids (p), fibrous (f) calcite and detrital-rich micarb present. Evidence of both CE1, with pyrite coated surfaces and CE2, without pyrite coated surfaces present. Late stage veins (v) present and a single fragment of bivalve shell surrounded by fibrous calcite present.

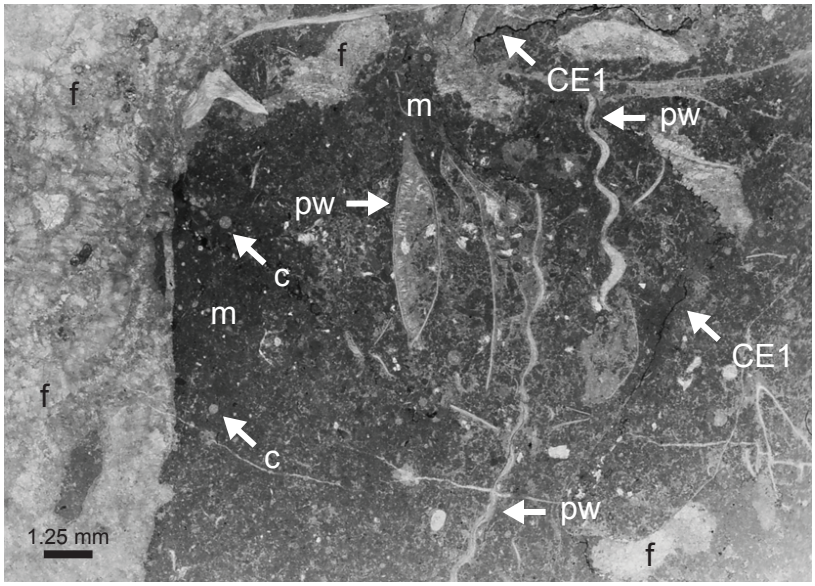

Figure 19. WS 1A. Wilbur Springs. The brachiopod *Peregrinella whitneyi* (pw) is present, surrounded by detrital-rich micarb (m) with calcispheres and pyrite framboids present throughout. The entire left side of the field of view is filled with fibrous (f) calcite. Evidence of corrosion is also present (CE1), as evidenced by pyrite coated corrosion surfaces.

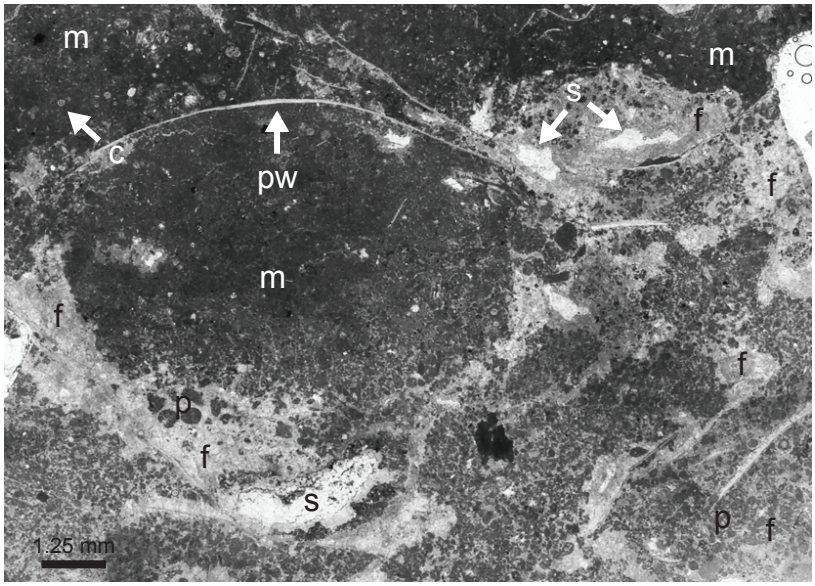

Figure 20. WS 1B x 2. Wilbur Springs. The brachiopod Peregrinella whitneyi is present, as well as a large number of small and irregular peloids (p) surrounded by fibrous calcite. Detrital-rich micarb (m) is also present with calcispheres and pyrite framboids throughout.

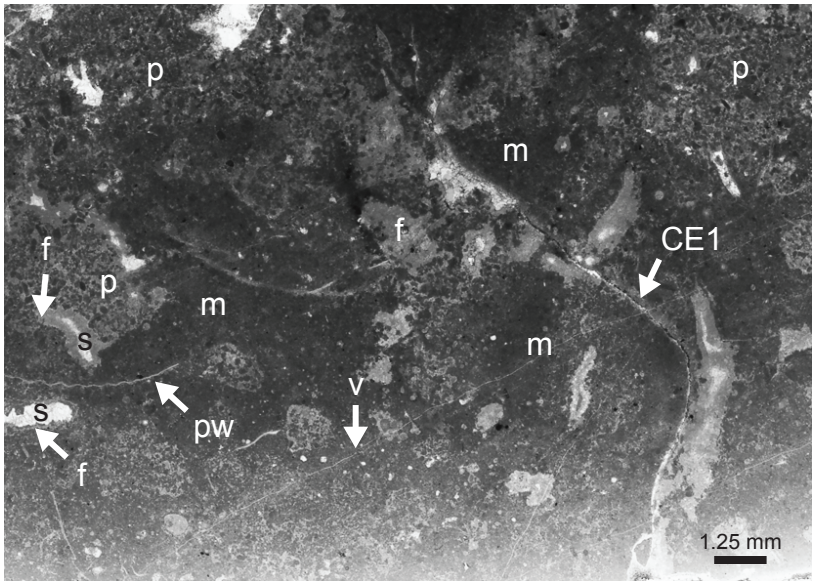

Figure 21. WS 1C. Wilbur Springs. Detrital-rich micarb (m) with peloids (p), surrounded by fibrous (f) calcite, calcispheres (c), and fragments of the brachiopod *Peregrinella whitneyi* (pw) present. Fibrous calcite and sparry (s) calcite present in small vugs. Evidence of a corrosion event (CE1) and late stage veins (v) filled with sparry calcite.

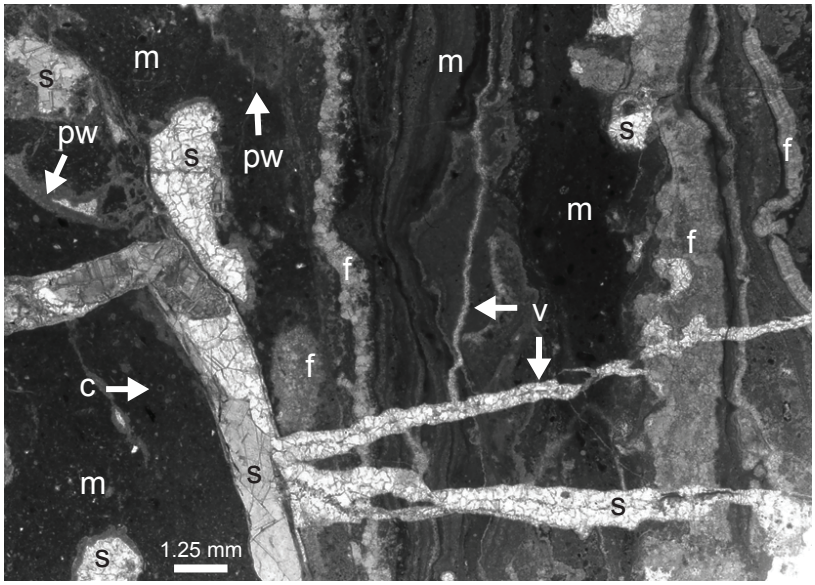

Figure 22. WS 10B. Wilbur Springs. Multiple depositional events of detrital-rich micarb (m), followed by deposition of fibrous (f) and sparry (s) calcites along corrosion surfaces and late stage veins (v). Calcispheres (c) and fragments of the brachiopod *Peregrinella whitneyi* (pw) present in the detrital-rich micarb.

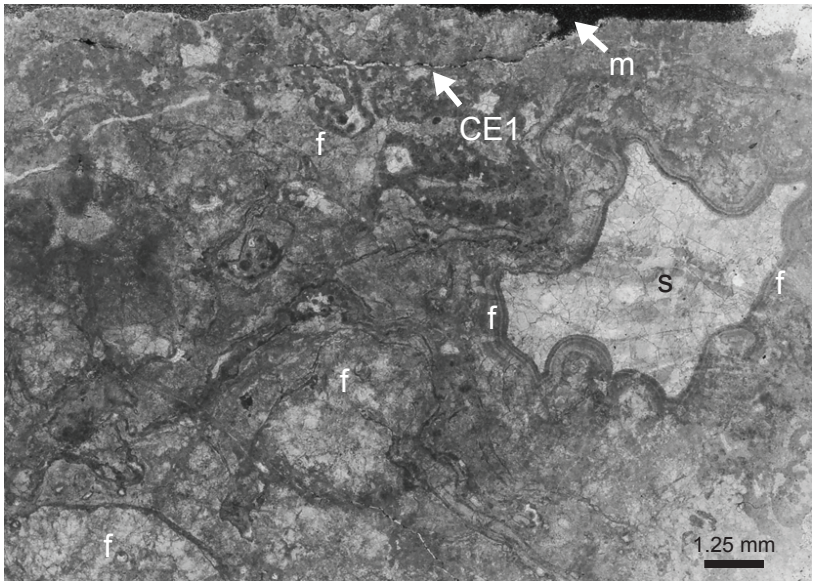

Figure 23. WS 3B. Wilbur Springs. This thin section is almost entirely comprised of multiple generations of fibrous (c), with one primary vug filled with sparry (c) calcite. Both a corrosion event (CE1) and late stage veins (v) are present as well.

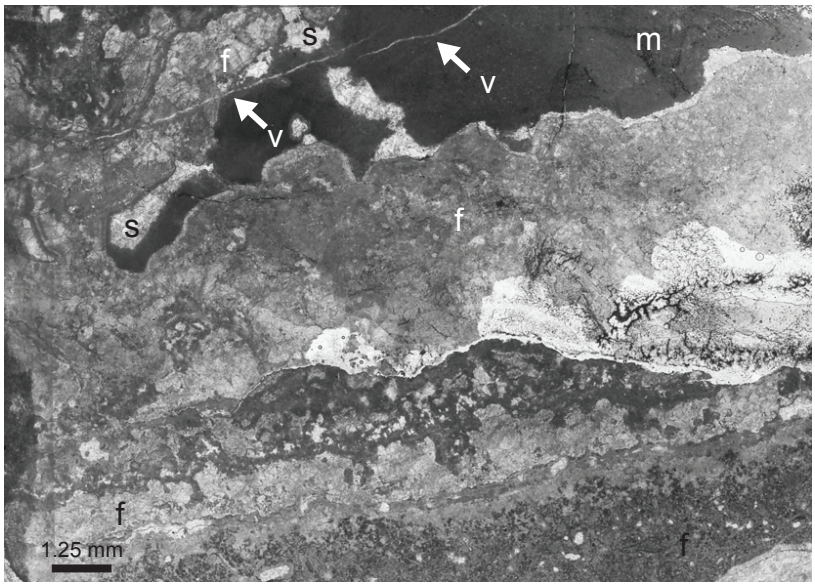

Figure 24. WS 3C. Wilbur Springs. A small amount of detrital-rich micarb (m) present. Fibrous (c) calcite comprises the bulk of the thin section, with a small amount of sparry (c) present as well. Late stage veins (v) filled with sparry calcite also present.

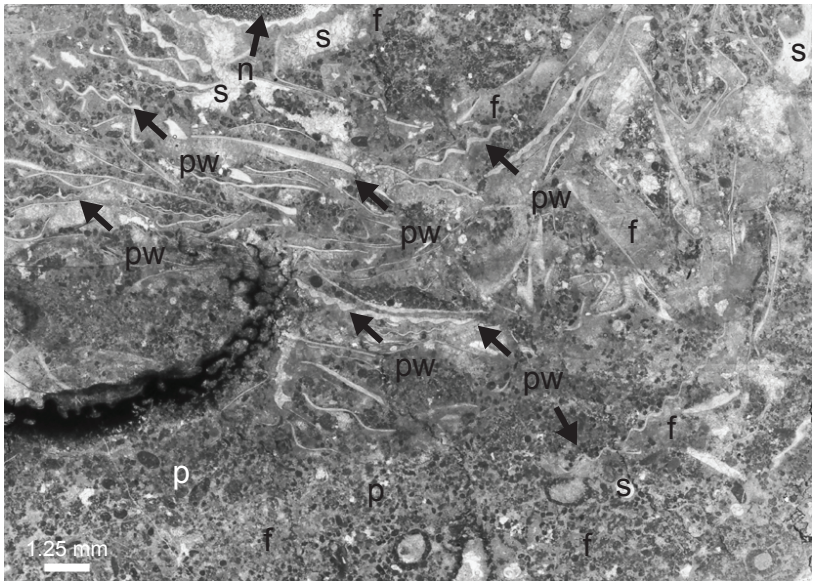

Figure 25. WS 2AA. Wilbur Springs. Fragments of the brachiopod Peregrinella whitneyi (pw) are surrounded by peloids (p) filled with detrital-rich micarb and fibrous (f) calcite. There are small vugs filled first with fibrous calcite and then by sparry (s) calcite.

Figure 26. WS 1A serpentine. The Wilbur Springs hydrocarbon seep deposit is surrounded by heavily weathered deposits of serpentine. This is a thin section made from some of the surrounding serpentine.

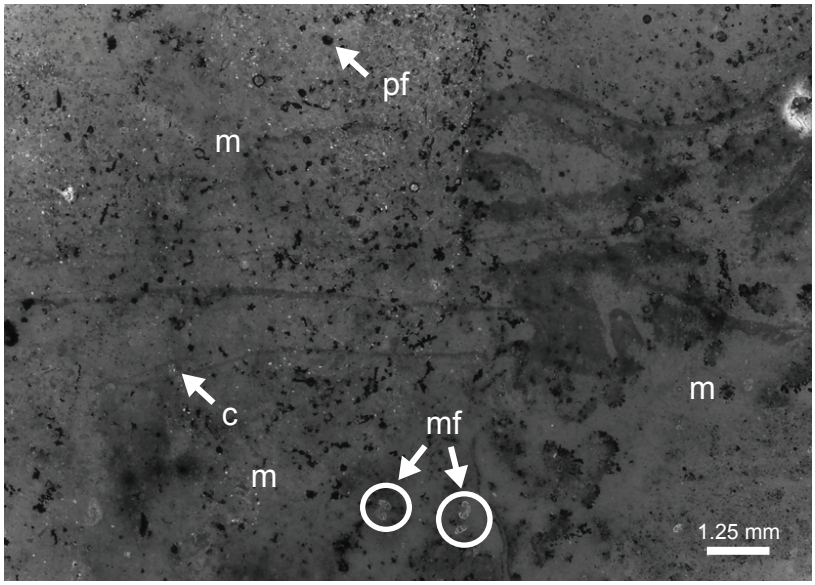

Figure 27. ROM CRK 2A. This Romero Creek thin section is heavily weathered, however, is dominated by detrital-rich micarb (m) with the detritus including pyrite framboids (pf) and calcispheres (c). Some microfossils (mf) are present as well.

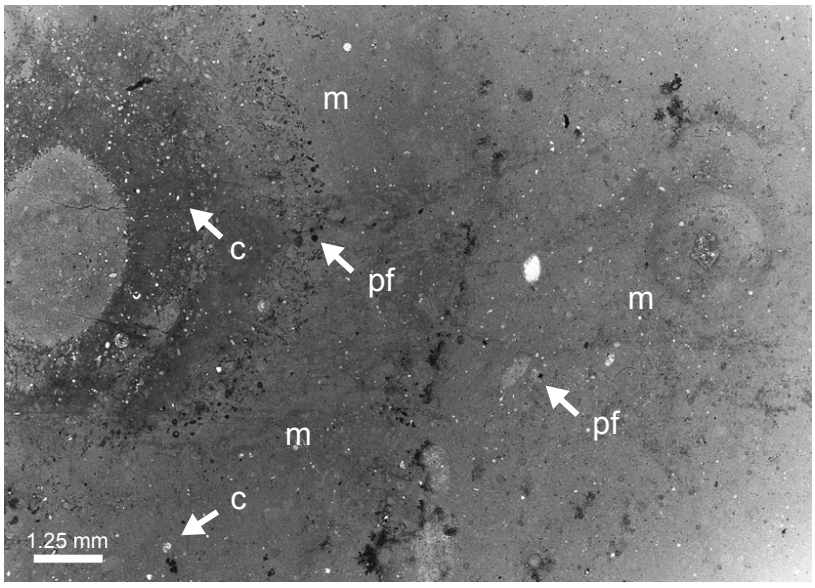

Figure 28. RC 3B-2. Romero Creek. Thin section is dominated by detrital-rich micarb (m) with the detritus including pyrite framboids (pf) and calcispheres (c).

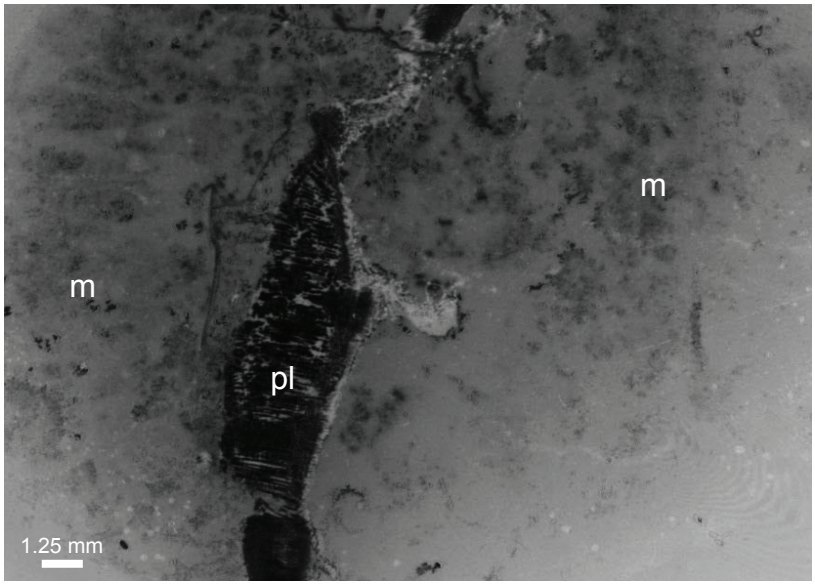

Figure 29. RC 2D. This Romero Creek thin section is heavily weathered, however, is dominated by detrital-rich micarb (m). Plant fragments (pl) are also present.

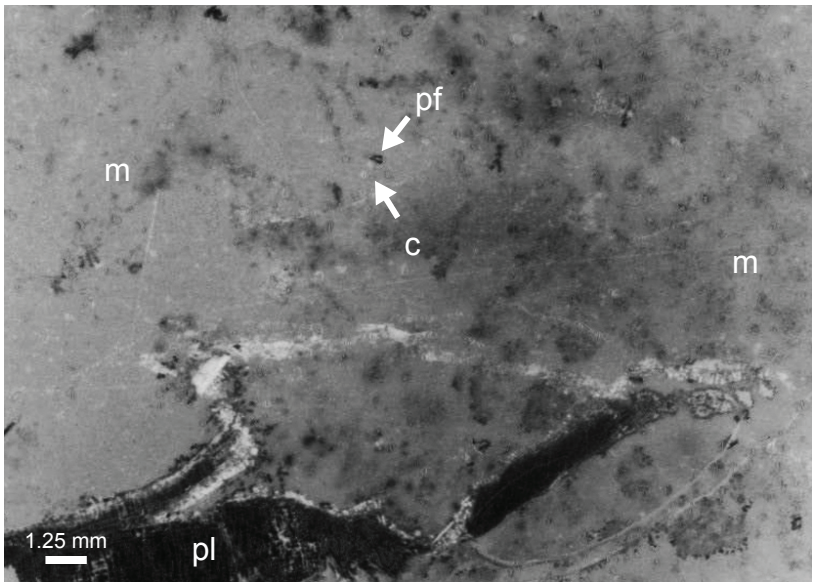

Figure 30. RC 2C. This Romero Creek thin section is heavily weathered, however, is dominated by detrital-rich micarb (m) with the detritus including pyrite framboids (pf) and calcispheres (c). Some plant fragments (pl) are present as well.

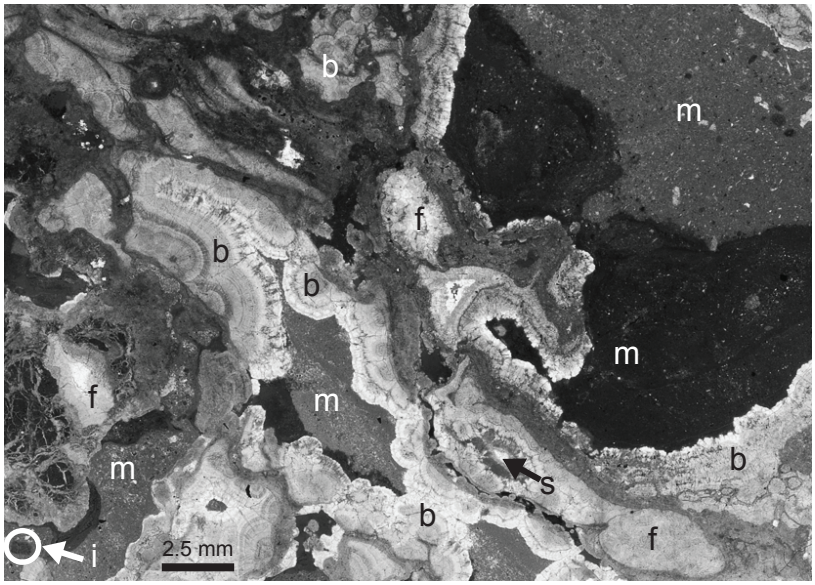

Figure 31. BC 3A-3. Bear Creek. Detrital-rich micarb (m) and fibrous calcite, including both the fibrous (f) and botryoidal (b) habits dominate this thin section. The detritus includes inoceramid bivalve (i) fragments, calcispheres (c), and pyrite framboids (pf).

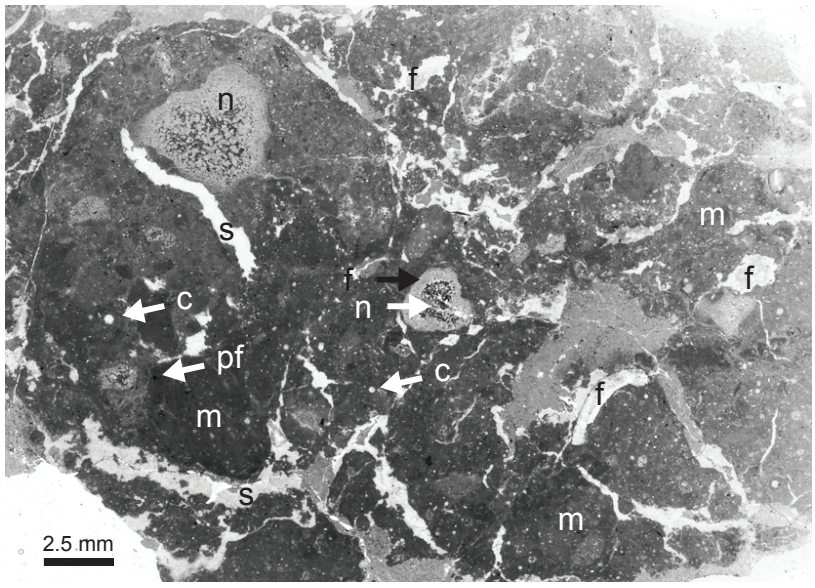

Figure 32. BC V1 x2-2. Bear Creek. Detrital-rich micarb (m) dominates this thin section, with the detritus including unusually large calcispheres (c) and a small number of pyrite framboids (pf). Neomorphosed micrite (n) is irregularly replacing regions of the detrital-rich micarb. A small amount of fibrous (f) calcite is also present.

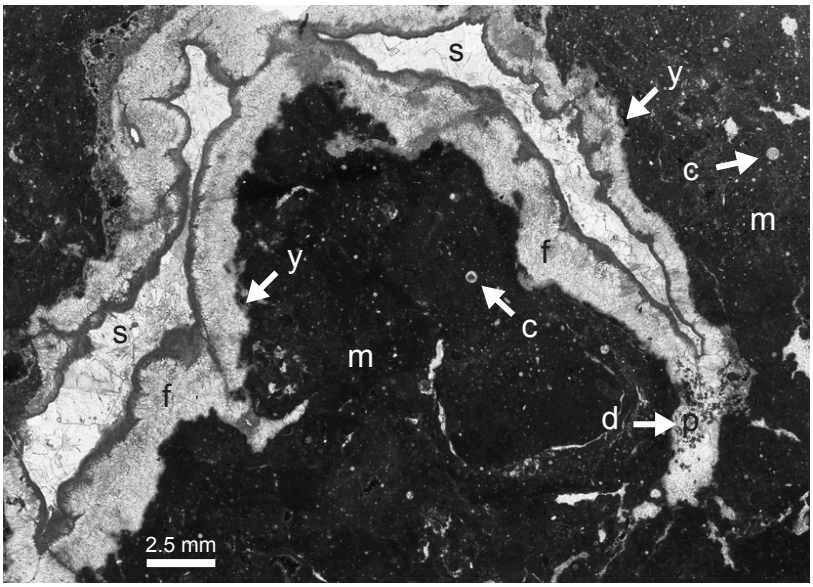

Figure 33. BC 1E x 2. Bear Creek. Detrital-rich micarb (m) dominates this thin section, with the detritus including variably sized calcispheres (c) and peloids (p). Yellow calcite (y) was deposited after the detrital-rich micarb, followed by fibrous calcite (both fibrous and dentate habits) and finally by sparry (s) calcite. Peloids (p) are surrounded by dentate calcite (d) and then by fibrous (f) calcite.

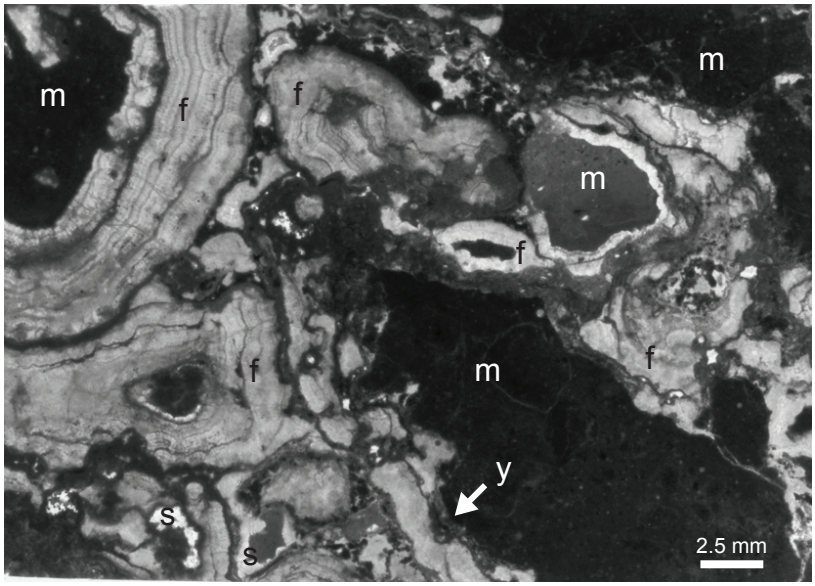

Figure 34. BC 3C. Bear Creek. Detrital-rich micarb (m) dominates this thin section, along with multiple generations of fibrous (f) calcite. There are also very small amounts of sparry (s) and yellow (y) calcite.

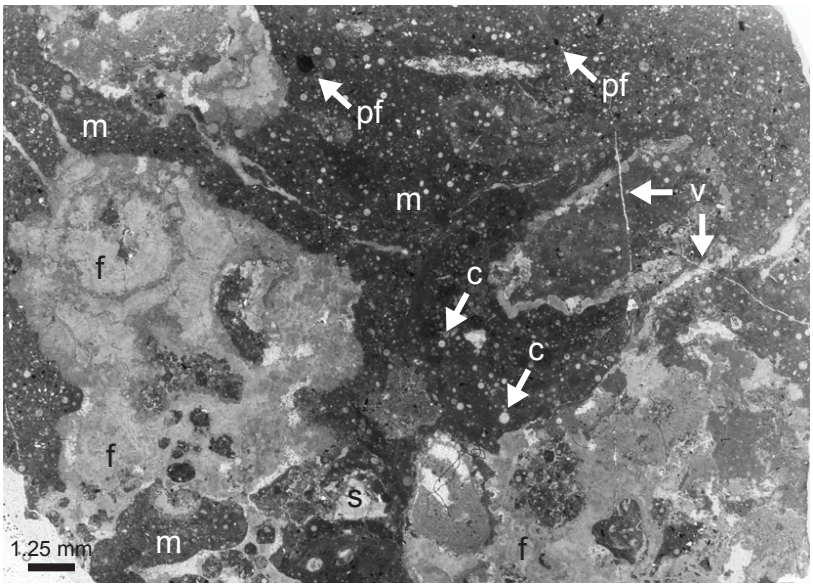

Figure 35. BC UUU2. Bear Creek. Detrital-rich micarb (m) dominates this thin section, with the detritus including variably sized calcispheres (c) and pyrite framboids (pf). There is a considerable amount of fibrous (f) and a limited amount of sparry (s) calcite, as well as some late stage veins (v) filled with sparry calcite.

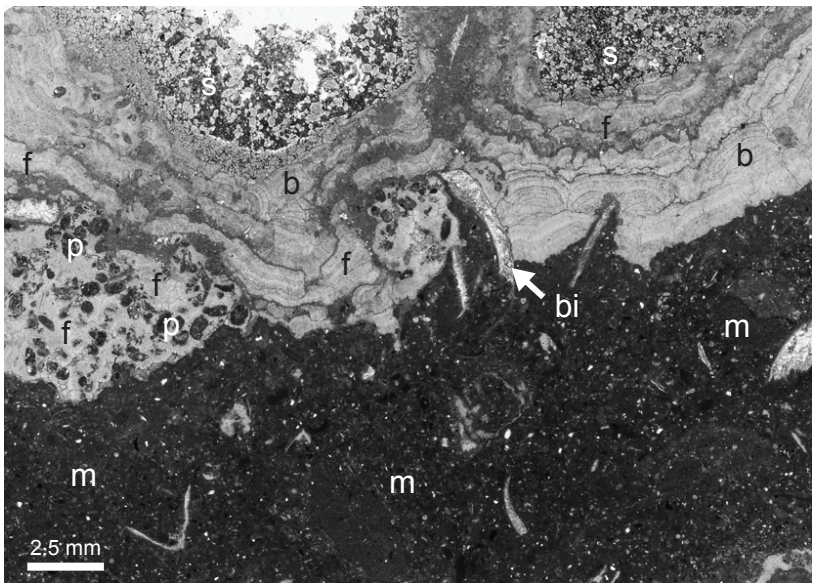

Figure 36. BC 2D-2. Bear Creek. Detrital-rich micarb (m) dominates this thin section, along with multiple generations of fibrous (f) and botryoidal (b) calcite. There are also peloids (p) surrounded by fibrous calcite and fragments of bivalve (bi) shell.

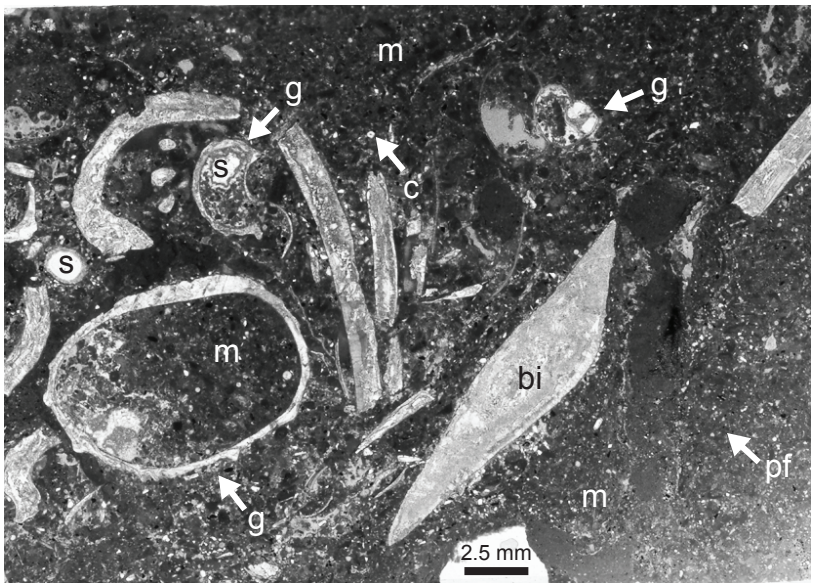

Figure 37. BC 2F. Bear Creek. Fragments of both bivalves (bi) and gastropods (g) are present. The shells in both cases are replaced by sparry (s) calcite. The gastropods are most likely *Paskentana paskentaensis*. All fragments are encased in detrital-rich micarb (m), with the detritus consisting of calcispheres (c) and pyrite framboids (pf).

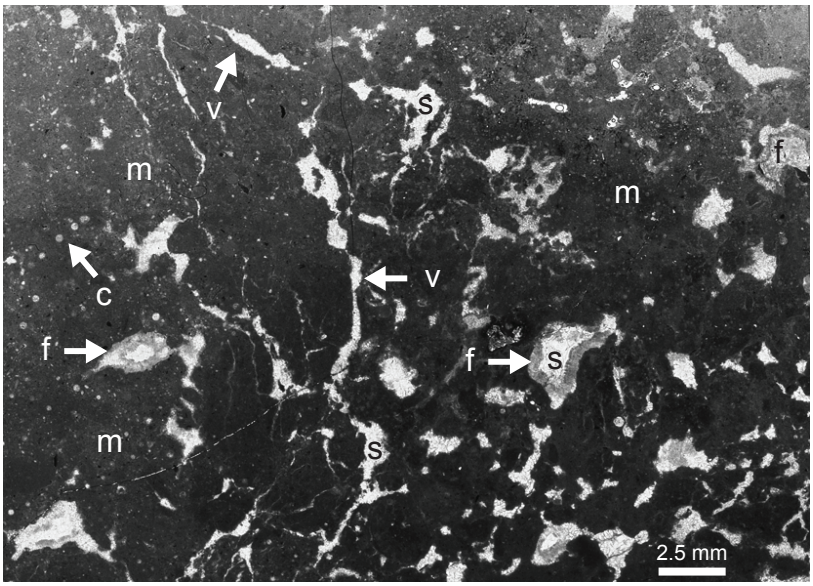

Figure 38. BC 1A-3. Bear Creek. Detrital-rich micarb (m) dominates this thin section, with the detritus including variably sized calcispheres. There is some fibrous (f) calcite lining vugs, which were subsequently filled with sparry (s) calcite. There are also some late stage veins (v) present filled with sparry calcite.

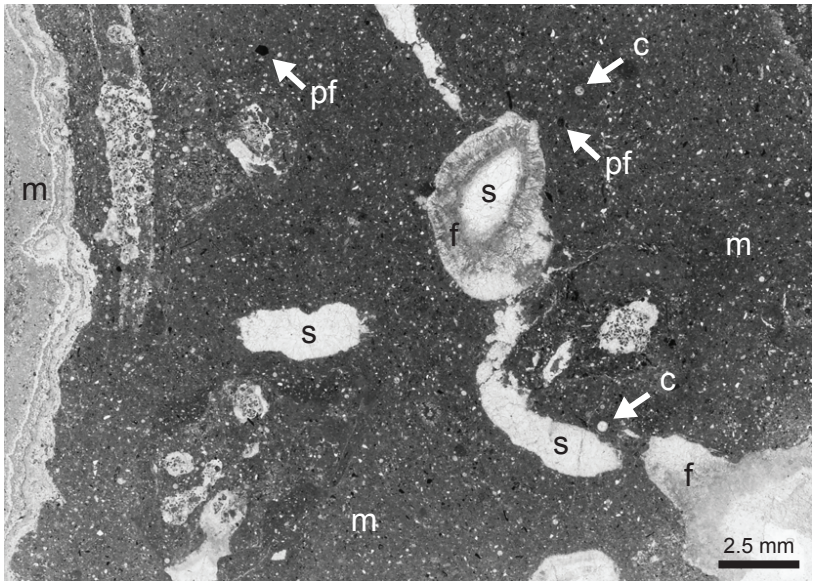

Figure 39. BC VV2. Bear Creek. Detrital-rich micarb (m) dominates this thin section, including some that is laminated, with the detritus including variably sized calcispheres (c) and pyrite framboids (pf). There are small regions of sparry (s) and fibrous (f) calcites as well.

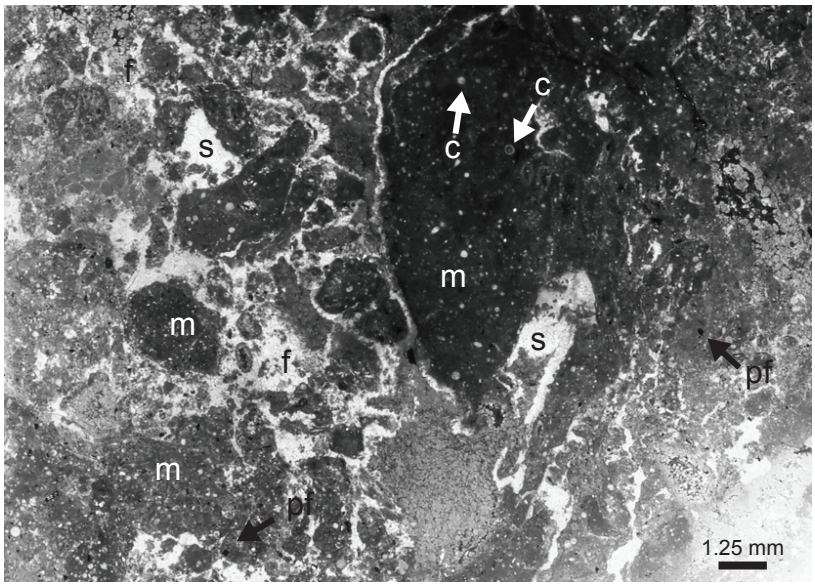

Figure 40. BC UU1-2. Bear Creek. Detrital-rich micarb (m) dominates this thin section, including some that is laminated, with the detritus including variably sized calcispheres (c) and pyrite framboids (pf). There are small regions of sparry (s) and fibrous (f) calcites as well.

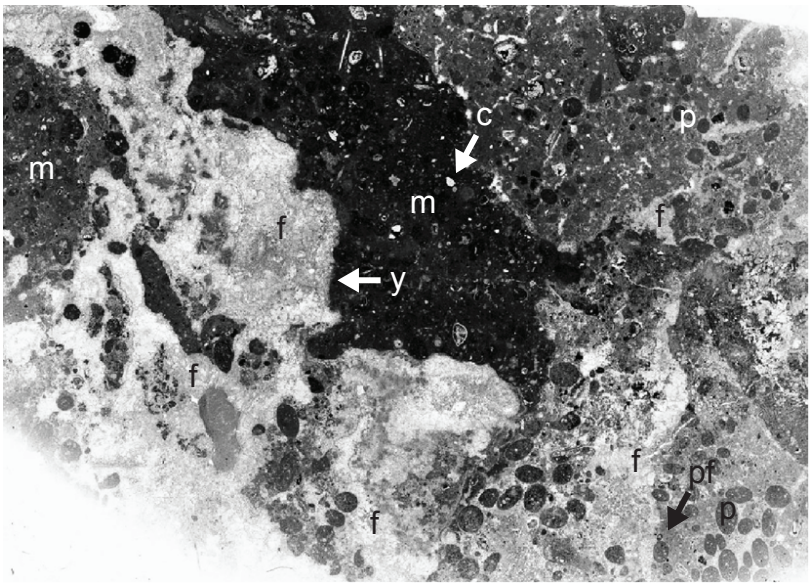

Figure 41. 9-SP6-11. Guenoc Ranch. 3.5 cm wide. Thin section is dominated by detrital-rich micarb (m) and by pervasive fibrous (f) calcite. Yellow (y) calcite is also present, as are peloids (p), pyrite framboids (pf) and calcispheres (c).

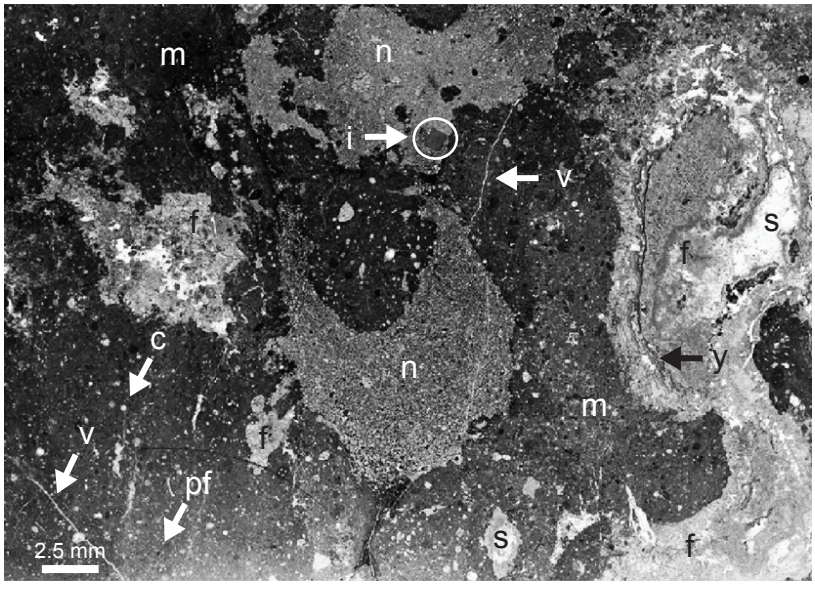

Figure 42. 10-Fence-3. Guenoc Ranch. Thin section is dominated by detrital-rich micarb (m), although there are also large regions of fibrous (f) calcite with centers of sparry (s) calcite, two large areas of neomorphosed micrite (n) and a cavity filled with microbial fabrics (mf), sparry calcite, fibrous calcite, and a narrow horizon of yellow calcite. The detritus includes pyrite framboids (pf) and calcispheres (c) and there are late stage cross-cutting veins (v) present as well.

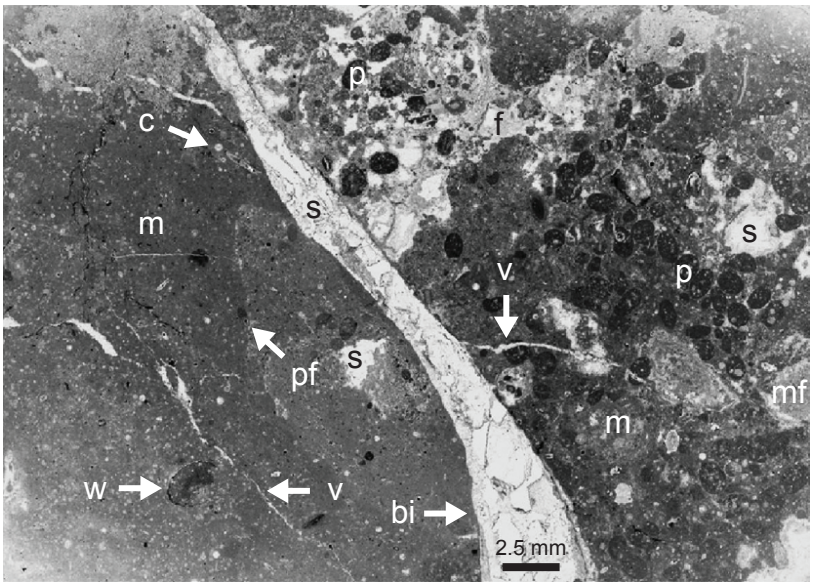

Figure 43. 12-Fence 2 2. Guenoc Ranch. Detrital-rich micarb (m) dominates this thin section, with the detritus including variably sized calcispheres (c) and pyrite framboids (pf). A bivalve (bi) shell replaced by sparry (s) calcite cuts through the middle of the thin section. Worm tube (w) with walled replaced by pyrite. There is some fibrous (f) calcite and a limited amount of sparry calcite, as well as some late stage veins (v) filled with sparry calcite. The peloids (p) are surrounded by fibrous calcite.

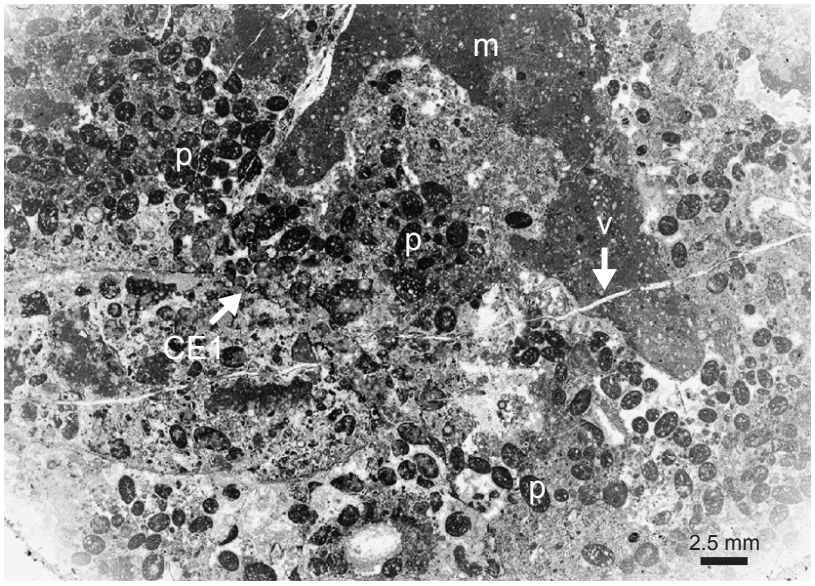

Figure 44. 11-Fence 2 5. Guenoc Ranch. The bulk of this thin section is comprised of peloids (p) surrounded by fibrous (f) calcite. There is also a small amount of sparry (s) calcite and detrital-rich micarb (m) present, as well as evidence of a corrosion event (CE1) and the formation of late stage veins (v) filled with sparry calcite.

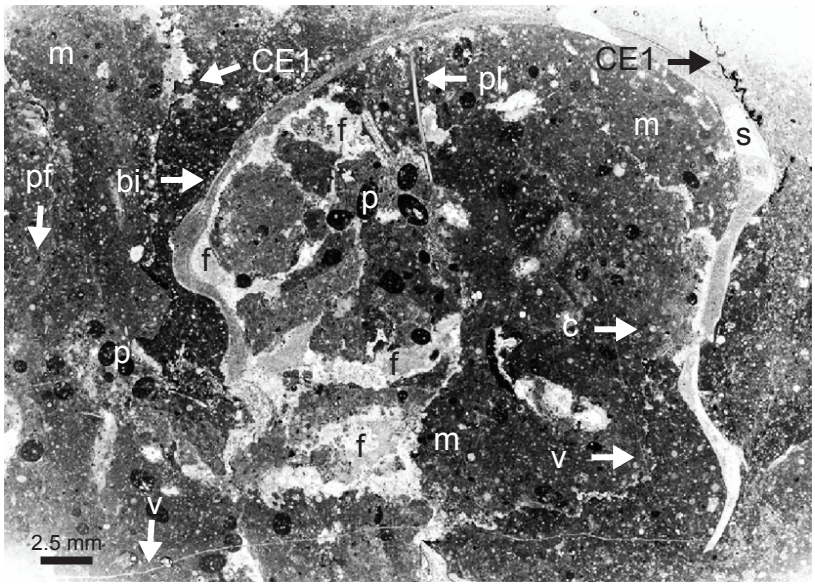

Figure 45. 15-DL 1C 1. Guenoc Ranch. A bivalve (bi) shell partially replaced with sparry (s) calcite is surrounded by detrital-rich micarb (m), with the detritus including peloids (p), pyrite framboids (pf), and calcispheres (c) and cross cut by a pyrite coated corrosion event (CE1). Fibrous (f) calcite, plant fragments (pl), and late stage veins (v) filled with sparry calcite are also present.

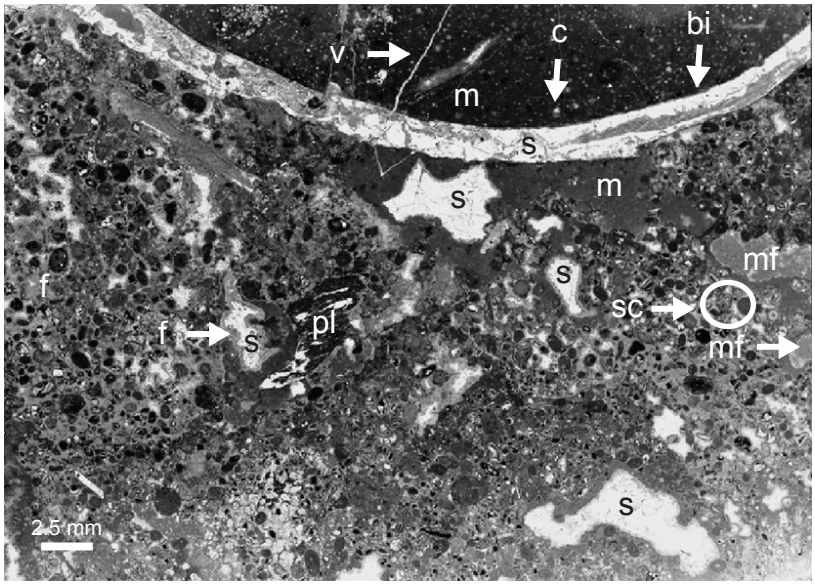

Figure 46. 3-Spring. Guenoc Ranch. Detrital-rich micarb (m) is found only in the top portion of this thin section, with detritus including calcispheres (c). A bivalve shell (bi) replaced with sparry (s) calcite is also present, as are vugs filled with first fibrous (f) calcite and then sparry calcite. There are small regions of microbial fabrics (mf) and of silt-clay fill (sc), as well as fibrous calcite enclosing much of the irregularly shaped peloids, plant fragments (pl) and other detritus. A late stage vein (v) cuts through the top portion of the thin section.

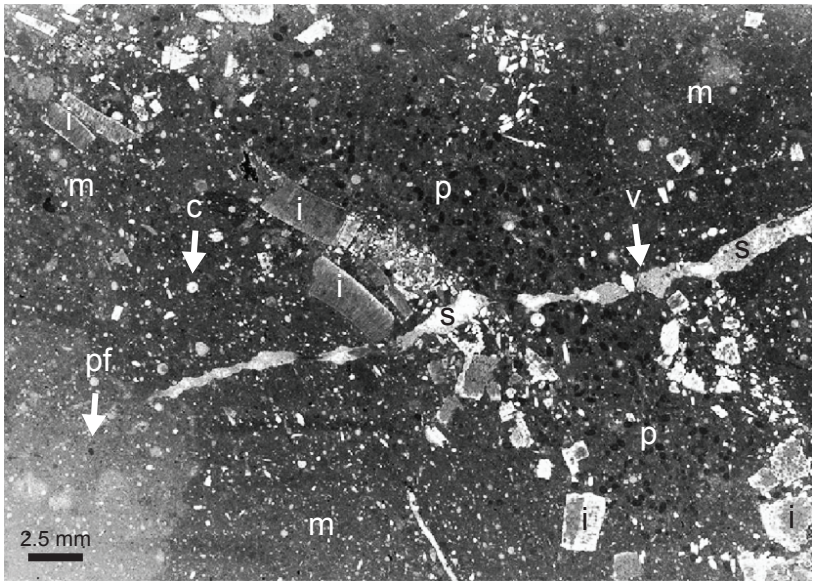

Figure 47. 6-SP6 4. Guenoc Ranch. Detrital-rich micarb (m) fills the bulk of this thin section, with the detritus including pyrite framboids (pf) and calcispheres (c). There are a considerable number of inoceramid bivalve (i) fragments and then late stage veins (v) filled with sparry (s) calcite.

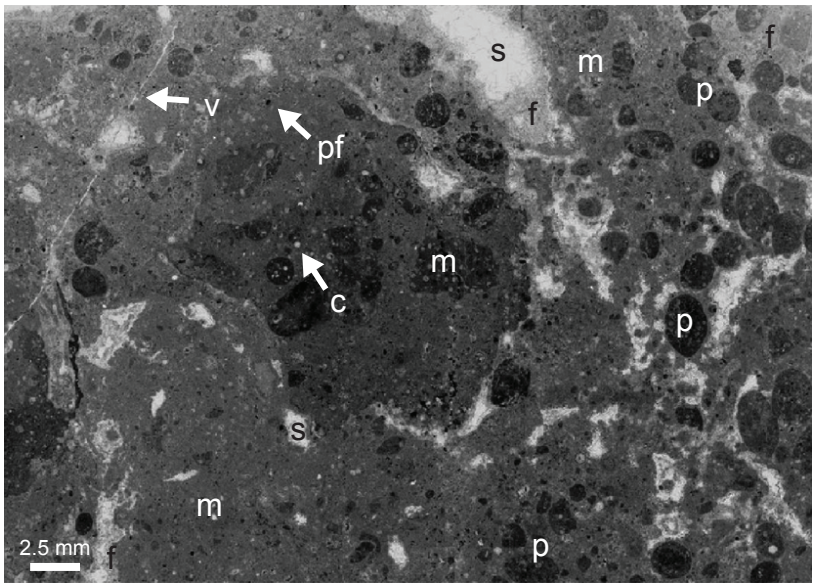

Figure 48. 2-SP2 13. Guenoc Ranch. Detrital-rich micarb (m) fills the bulk of this thin section, with the detritus including pyrite framboids (pf) and calcispheres (c). There are also vugs filled first with fibrous (f) calcite and then by sparry (s) calcite. Large peloids (p) are present and are surrounded by both detrital-rich micarb and fibrous calcite.

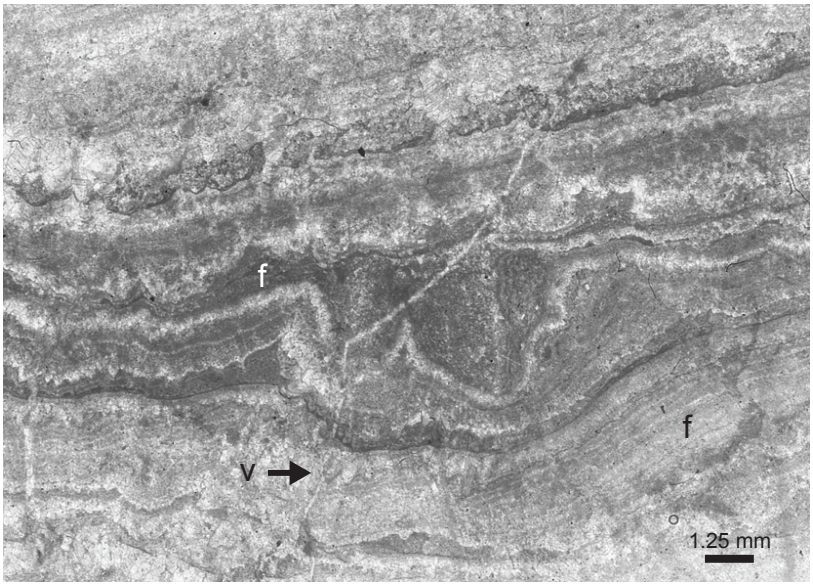

Figure 49. Rice Valley 1A. This entire thin section is comprised of multiple generations of fibrous (f) calcite with a late stage cross-cutting vein (v) cutting through the middle.

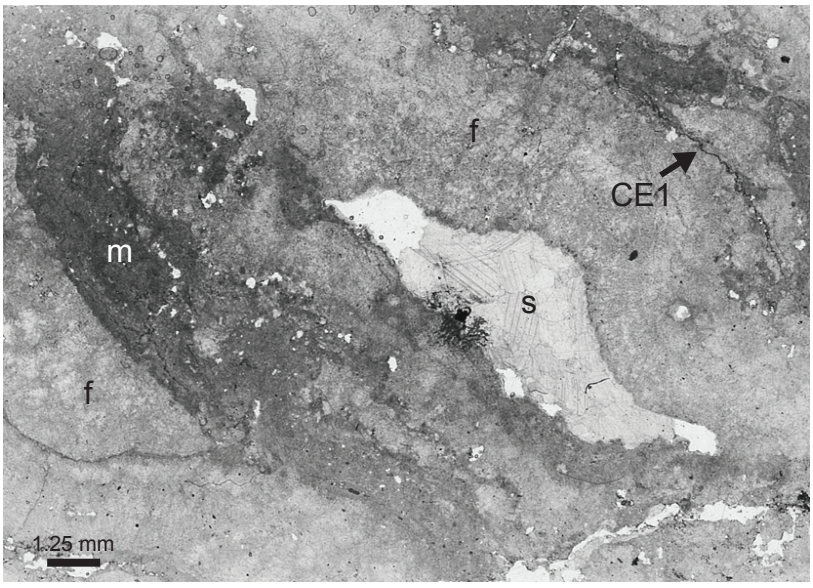

Figure 50. RV 2D. Rice Valley. The bulk of this thin section is comprised of fibrous (f) calcite, with some detrital-rich micarb (m) present as well. There is a large vug filled with sparry (s) calcite and evidence of a corrosion event lined with pyrite (CE1).

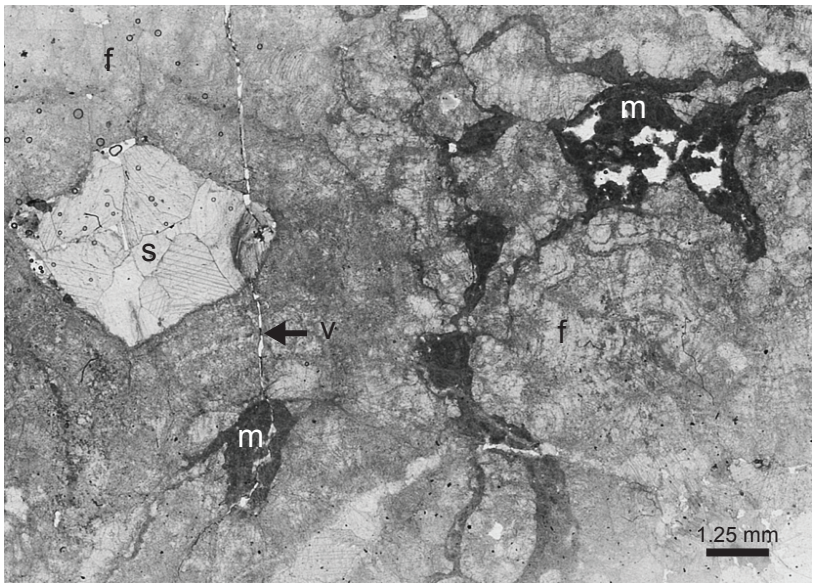

Figure 51. RV 2E. Rice Valley. The bulk of this section is comprised of multiple generations of fibrous (f) calcite with a late stage cross-cutting vein (v) cutting through the middle. There is a single vug filled with sparry (s) calcite, and a small amount of detrital-rich micarb (m).

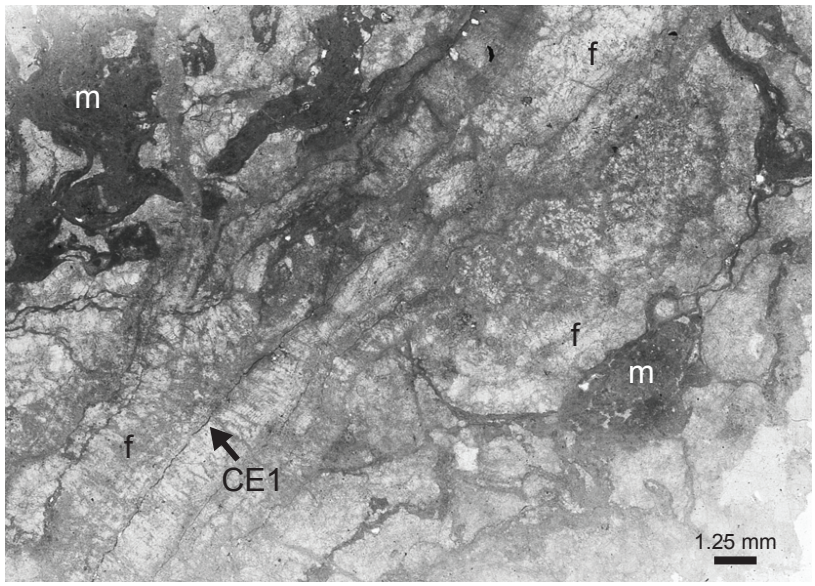

Figure 52. RV 2B. Rice Valley. The bulk of this section is comprised of multiple generations of fibrous (f) calcite with evidence of a corrosion event coated in pyrite (CE1) present and a small amount of detrital-rich micarb (m).

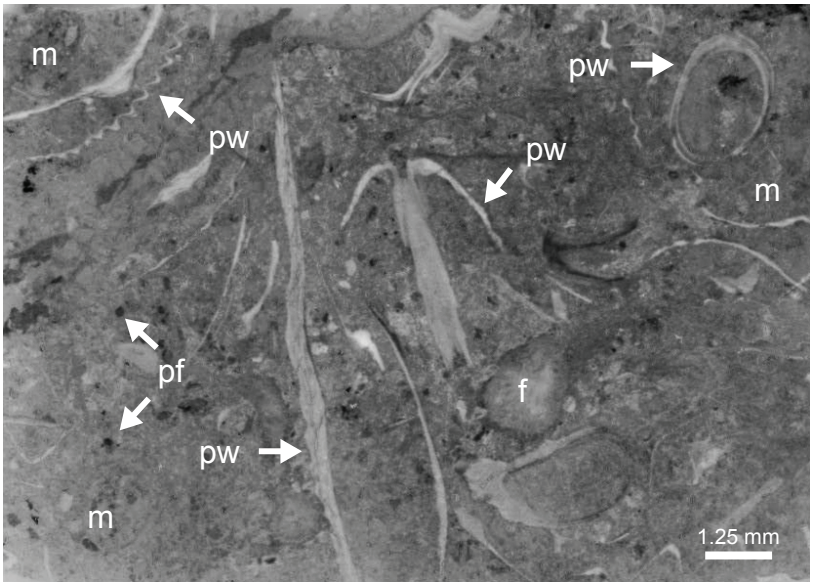

Figure 53. WAM 1D-3. Wide Awake Mine. Detrital-rich micarb (m) forms the bulk of the thin section, with the detritus including large pyrite framboids (pf) and numerous fragments of the brachiopod *Peregrinella whitneyi* (pw). There is also a small amount of fibrous (f) calcite.

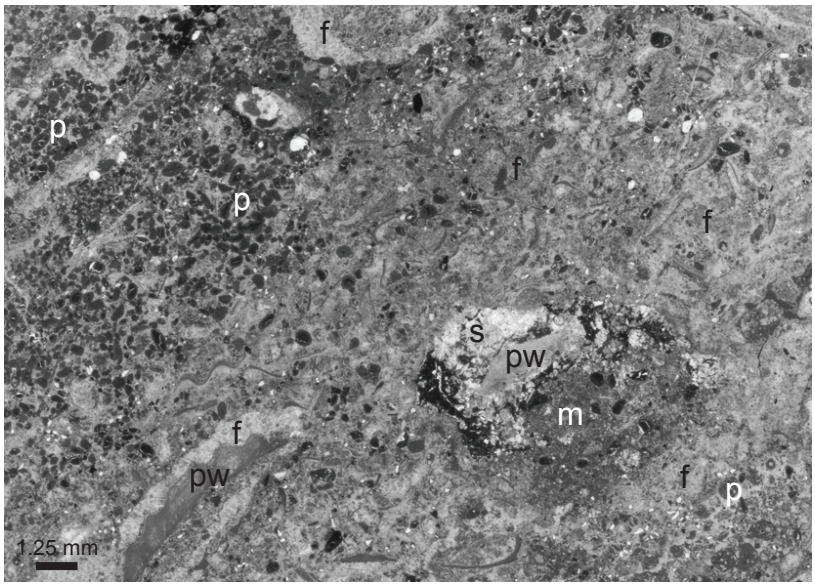

Figure 54. WAM 1C-2. Wide Awake Mine. This thin section is dominated by fibrous (f) calcite and by peloids (p) surrounded by the fibrous calcite. There are some fragments of the brachiopod *Peregrinella whitneyi* (pw) and a small amount of sparry (s) calcite and detrital-rich micarb (m).

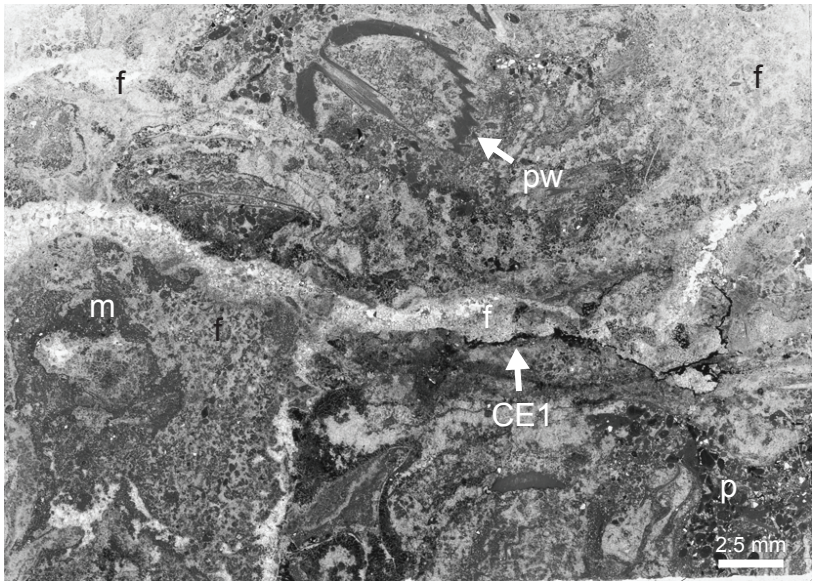

Figure 55. WAM 1F-3. Wide Awake Mine. The bulk of this thin section is dominated by detrital-rich micarb (m) or fibrous (f) calcite. There are also peloids (p) present, fragments of the brachiopod *Peregrinella whitneyi* present, and evidence of a corrosion event (CE1).

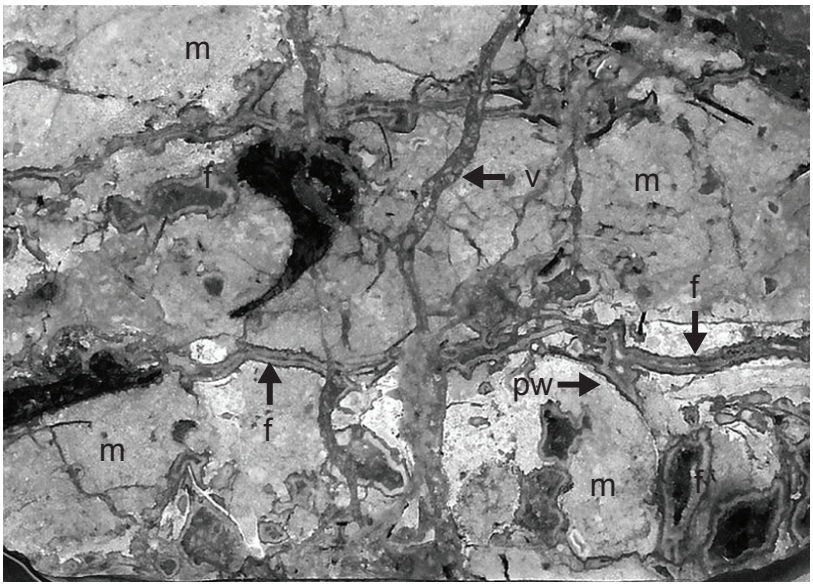

Figure 56. WAM 2B. Wide Awake Mine. 3 in x 2 in. This thin section is dominated by detrital-rich micarb (m) and is cross-cut numerous times by late stage veins (v) lined with either fibrous (f) or sparry (s) calcite. Fragments of the brachiopod *Peregrinella whitneyi* are also present.

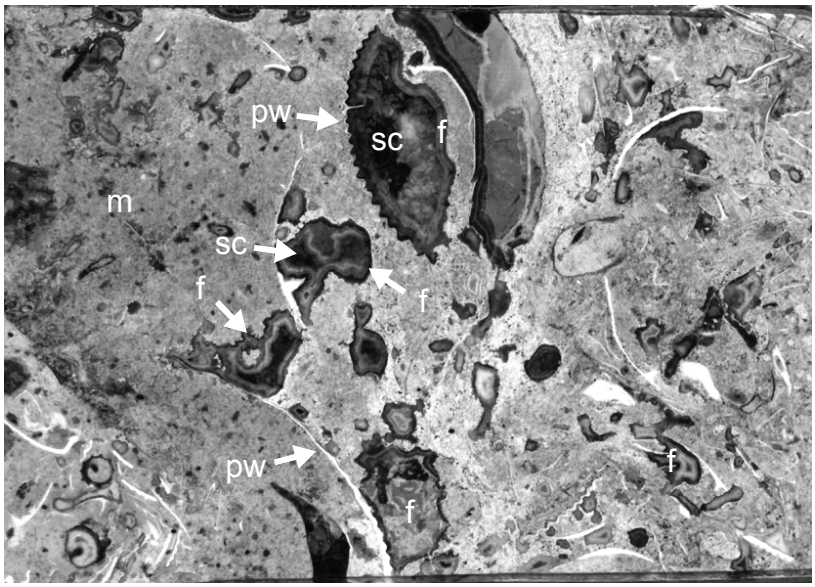

Figure 57. WAM 3B. Wide Awake Mine. 6.35 cm wide. The bulk of this thin section is comprised of detrital-rich micarb (m) and fragments of the brachiopod *Peregrinella whitneyi* (pw). Vugs filled with fibrous (f) calcite and silt-clay fill (sc) are also present.

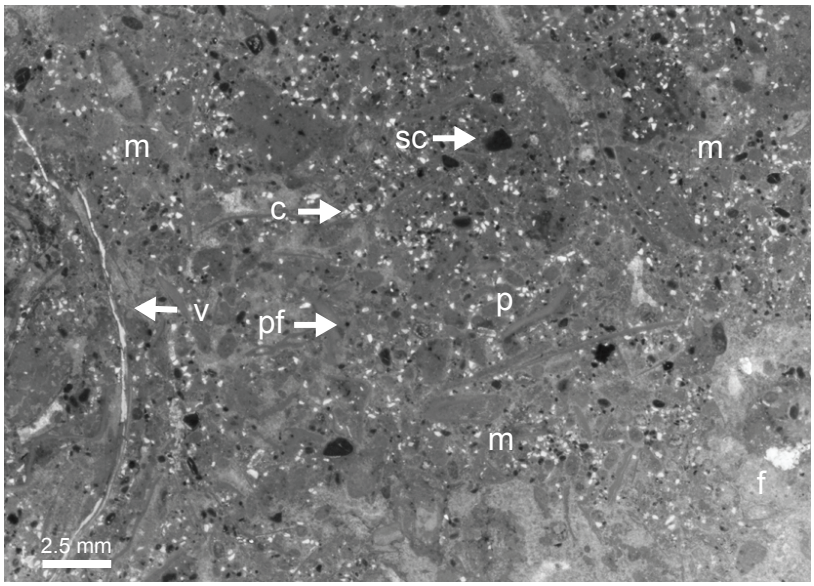

Figure 58. WAM 3F. Wide Awake Mine. The bulk of this thin section is comprised of detrital-rich micarb (m) with the detritus including silt-clay fill (sc), calcispheres (c), peloids (p), and pyrite framboids (pf). Some fibrous (f) calcite is also present as is a late stage cross-cutting vein (v) filled with sparry calcite.

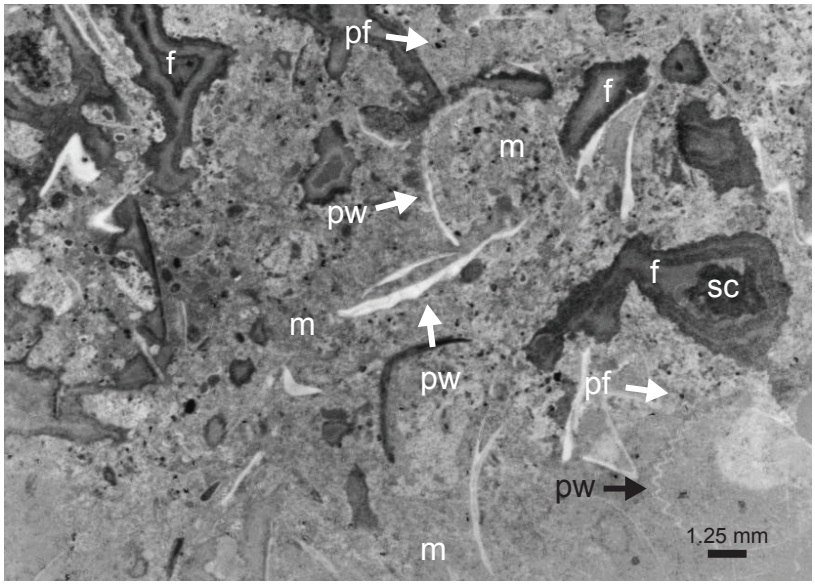

Figure 59. WAM 3E. Wide Awake Mine. The bulk of this thin section is comprised of detrital-rich micarb (m) and fragments of the brachiopod *Peregrinella whitneyi* (pw). Vugs filled with fibrous (f) calcite and silt-clay fill (sc) are also present.

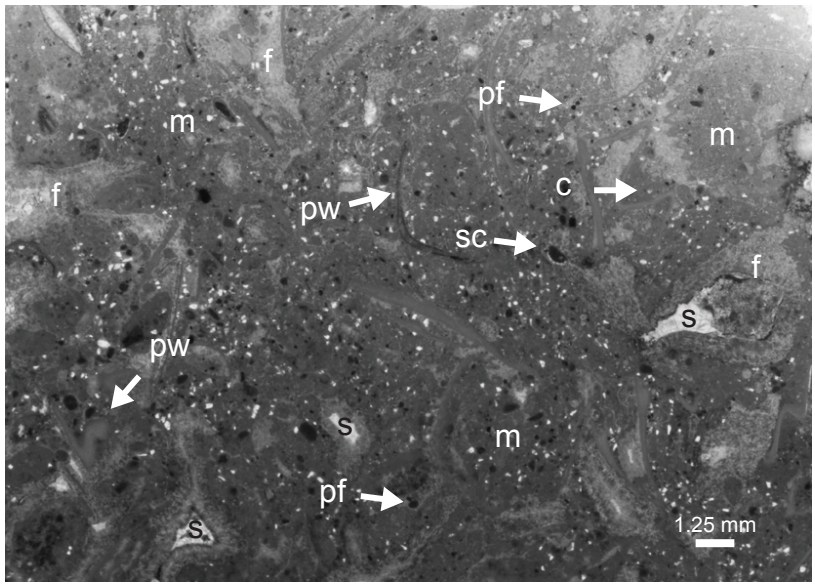

Figure 60. WAM 3EE. Wide Awake Mine. The bulk of this thin section is comprised of detrital-rich micarb (m) and fragments of the brachiopod *Peregrinella whitneyi* (pw). Vugs filled with fibrous (f) calcite and silt-clay fill (sc) are also present. The detritus includes calcispheres (c) and pyrite framboids (pf).

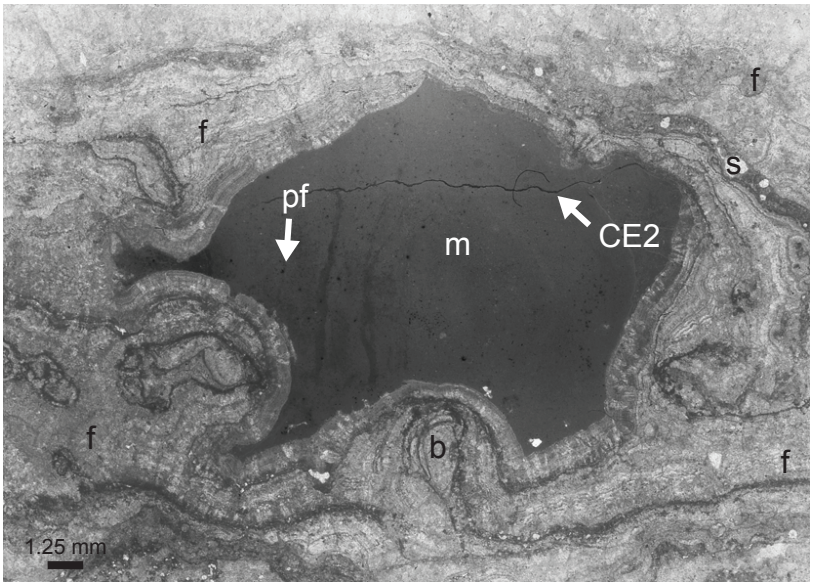

Figure 61. RC 1AA. Rocky Creek. The bulk of this thin section is dominated by multiple generations of both fibrous (f) and botryoidal (b) calcite and a small amount of sparry (s) calcite. There is some detrital-rich micarb (m) present, with the detritus including pyrite framboids (pf) and cross-cut by a non ferroan corrosion event (CE2).

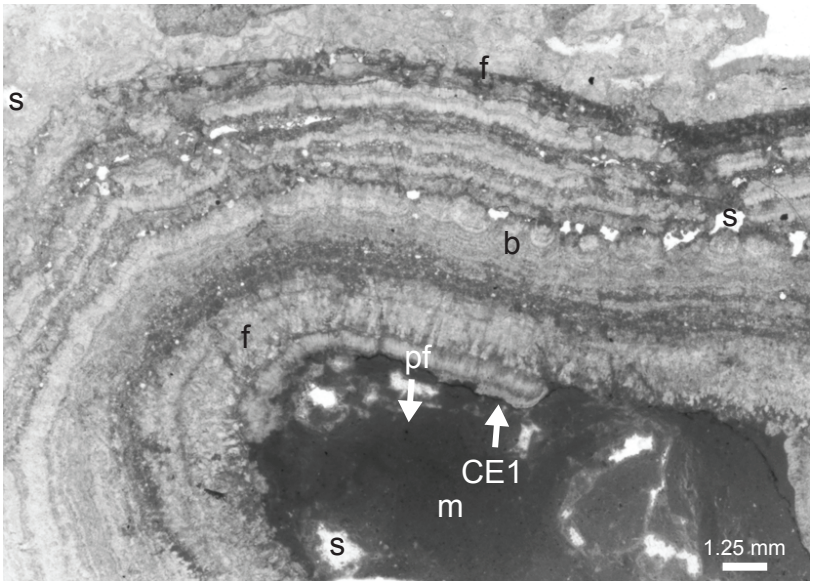

Figure 62. RC 1D. Rocky Creek. The bulk of this thin section is dominated by multiple generations of both fibrous (f) and botryoidal (b) calcite and a small amount of sparry (s) calcite. There is some detrital-rich micarb (m) present, with the detritus including pyrite framboids (pf) and cross-cut by a pyrite coated corrosion event (CE1).

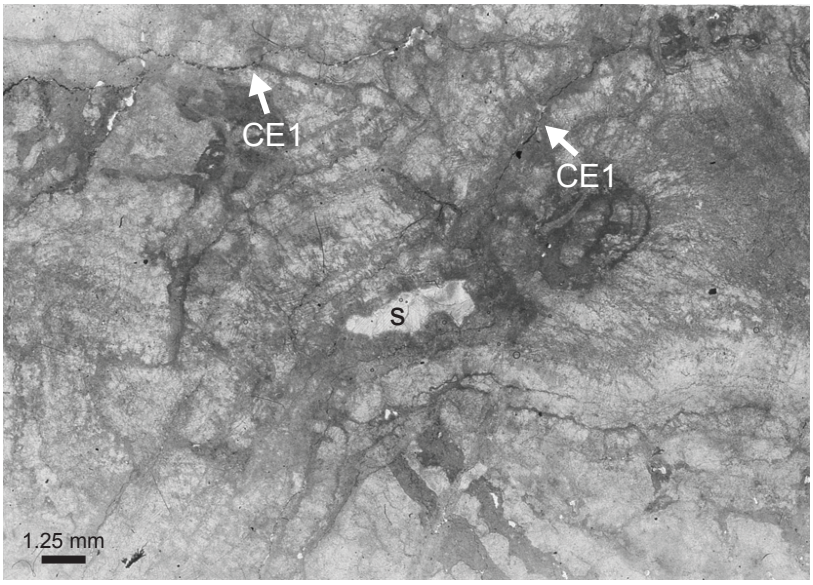

Figure 63. RC 2C. Rocky Creek. This thin section is almost entirely comprised of fibrous (f) calcite. There is also some botryoidal (b) calcite, as well as some sparry (s) calcite in vugs. There is evidence of a corrosion event (CE1), as well.

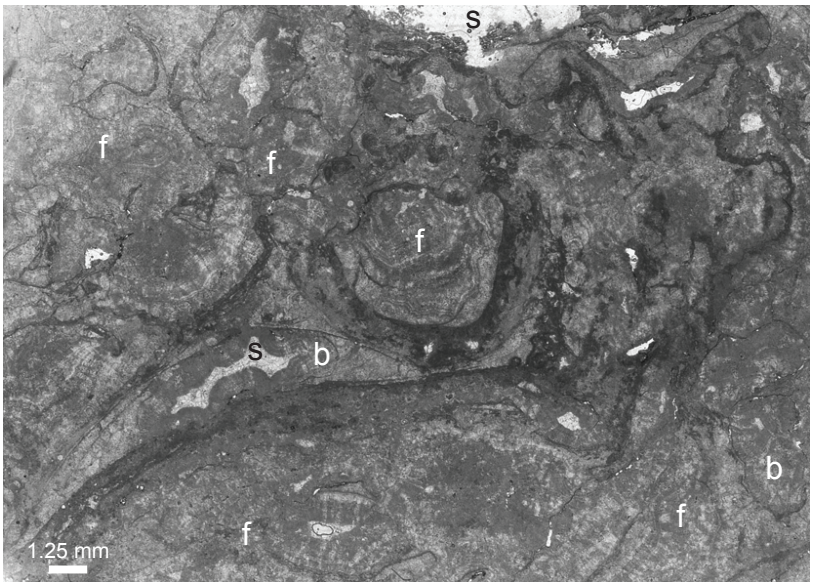

Figure 64. RC 3C. Rocky Creek. This thin section is almost entirely comprised of fibrous (f) calcite. There is also some botryoidal (b) calcite, as well as some sparry (s) calcite in vugs.

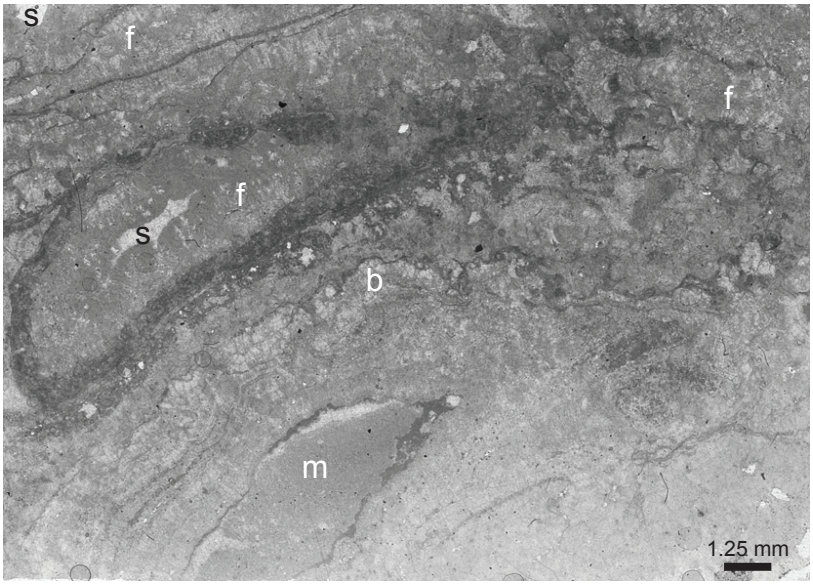

Figure 65. RC 3B. Rocky Creek. The bulk of this thin section is comprised of fibrous (f) calcite. There is also a small amount of detrital-rich micarb (m) present, botryoidal (b) calcite, and sparry (s) calcite.

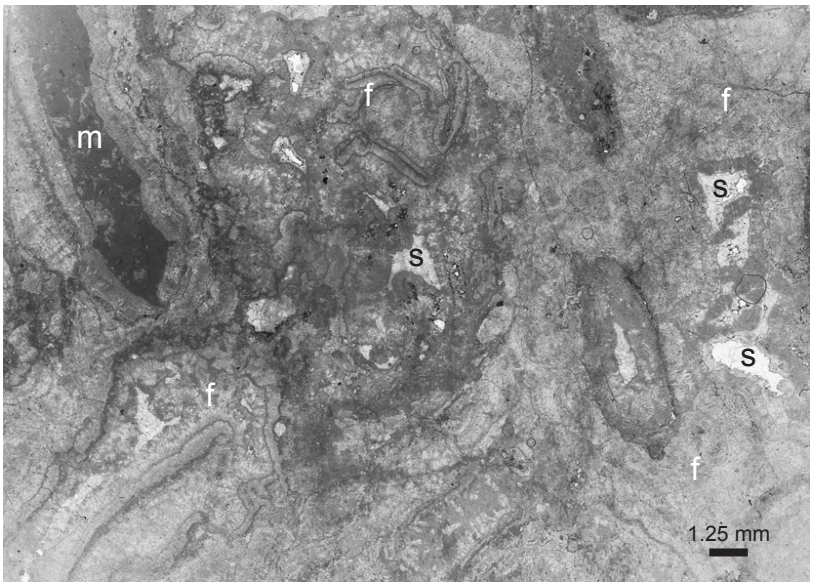

Figure 66. RC 1E. Rocky Creek. Figure 65. RC 3B. Rocky Creek. The bulk of this thin section is comprised of fibrous (f) calcite. There is also a small amount of detrital-rich micarb (m) present, botryoidal (b) calcite, and sparry (s) calcite.

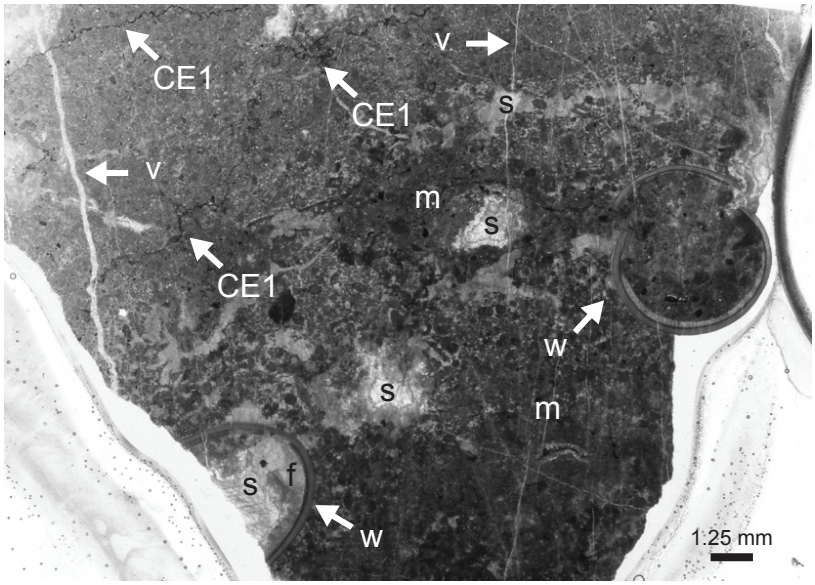

Figure 67. LIV WT. Little Indian Valley. Two well-preserved worm tubes (w) are prserved here and are filled with detrital-rich micarb (m), fibrous (f) calcite, and/or sparry (s) calcite. Evidence of corrosion events (CE1) and late stage cross-cutting veins (v) are present as well.

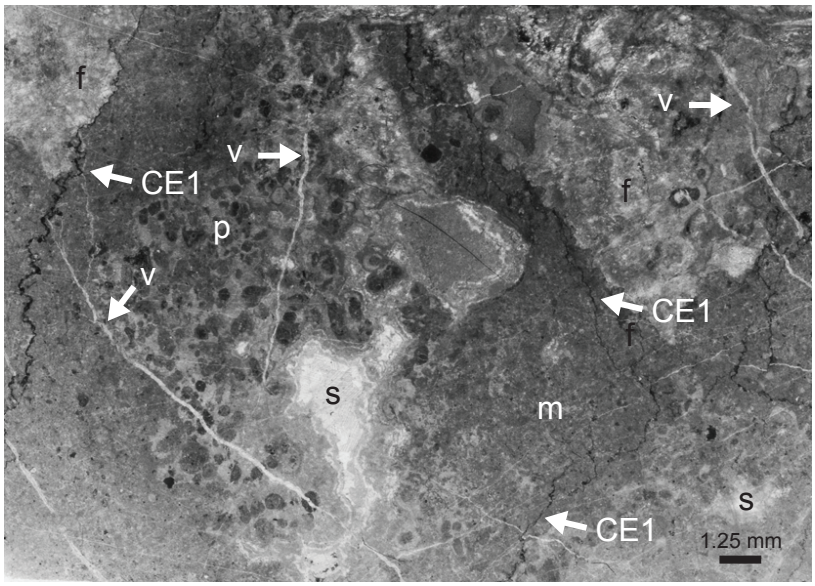

Figure 68. LIV 3C. Little Indian Valley. Detrital-rich micarb (m), fibrous (f) calcite, and/or sparry (s) calcite. Peloids (p) are also present. Evidence of corrosion events (CE1) and late stage cross-cutting veins (v) are present as well.

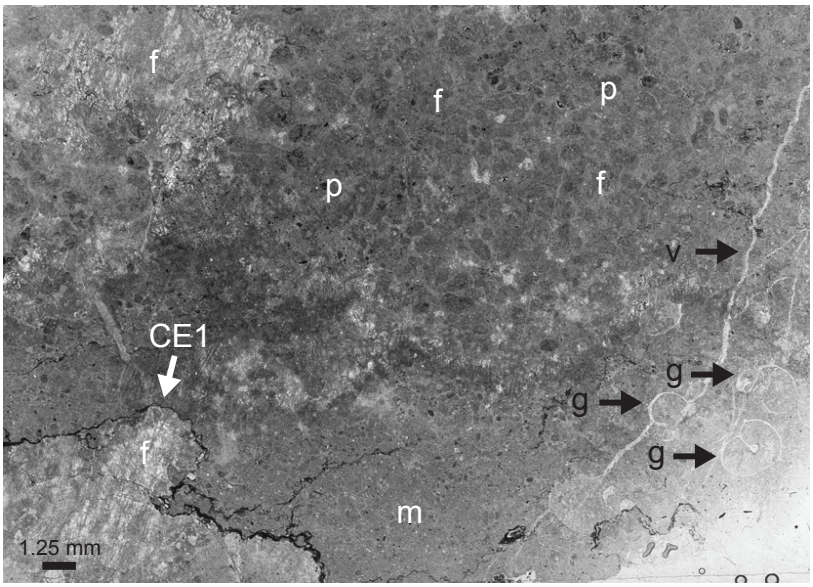

Figure 69. LIV 1CC. Little Indian Valley. Peloids (p) dominate this thin section and are surrounded by fibrous (f) calcite. There is a small amount of detrital-rich micarb (m) present, gastropods (g), evidence of a corrosion event (CE1) and late stage cross-cutting veins (v), as well.

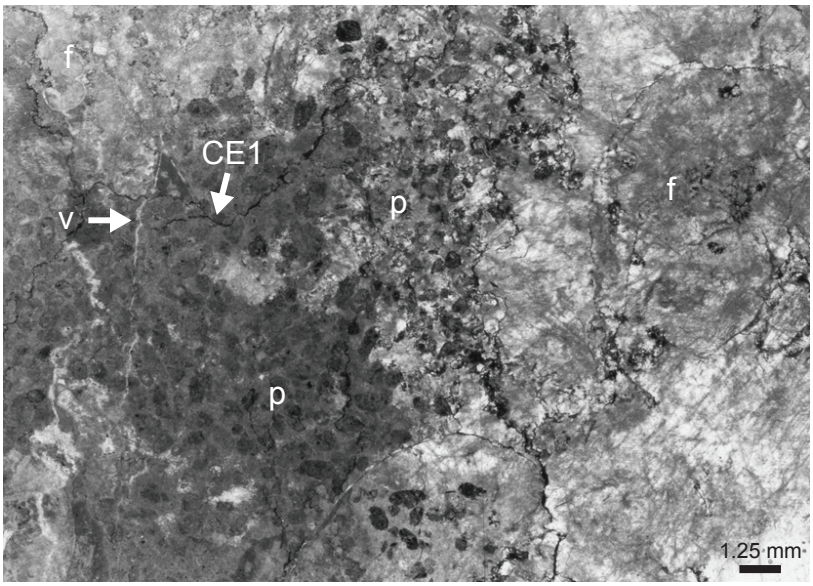

Figure 70. LIV 1DD. Little Indian Valley. Peloids (p) dominate this thin section and are surrounded by fibrous (f) calcite. There is also evidence of a corrosion event (CE1) and late stage cross-cutting veins (v), as well.

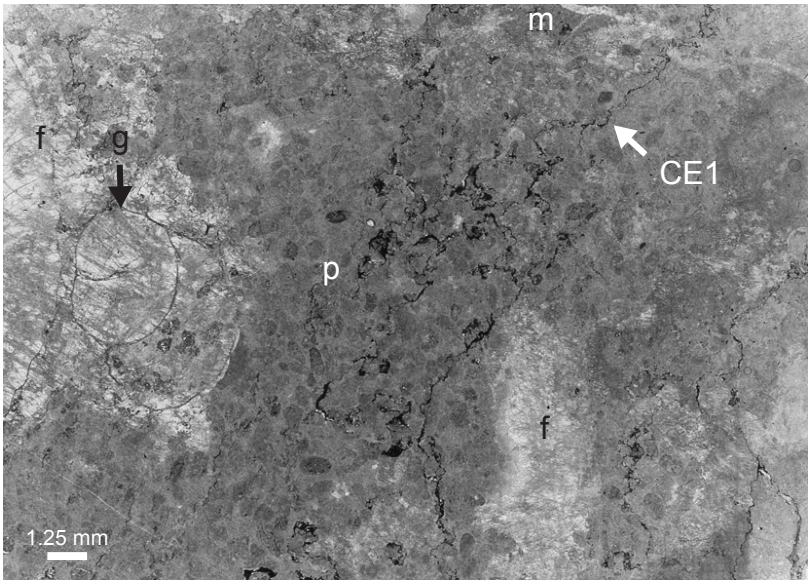

Figure 71. LIV 1EE. Little Indian Valley. The bulk of this thin section is comprised of fibrous (f) calcite and peloids (p) surrounded by fibrous calcite. There is a large gastropod (g), which is most likely *Paskentana paskentaensis*, there is a small amount of detrital-rich micarb (m) present as well, and there is evidence of a corrosion event (CE1).

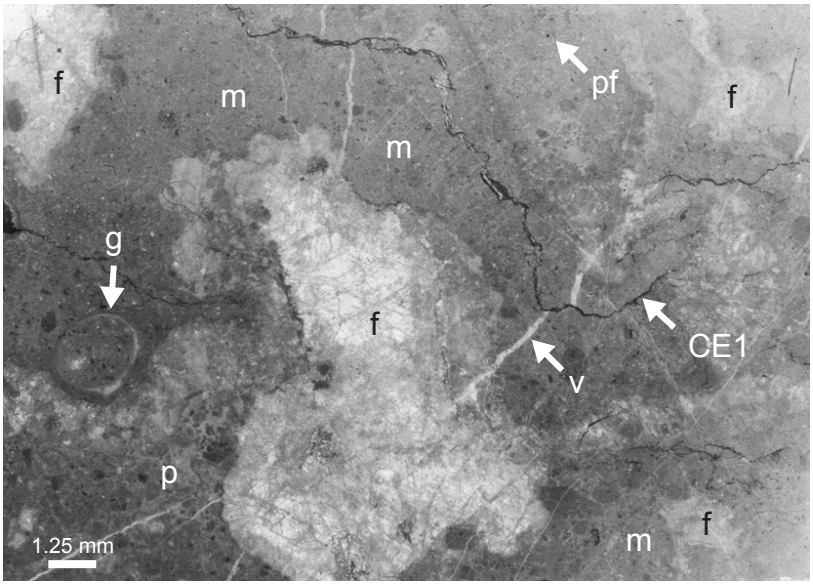

Figure 72. LIV 1B. Little Indian Valley. This thin section is dominated by detrital-rich micarb (m), with the detritus including peloids (p) and pyrite framboids. There is also a gastropod (g) present, fibrous (f) calcite present, evidence of a corrosion event (CE1), and late stage cross cutting veins (v) present.